Adhésifs nanostructurés en voie émulsion

Fanny Deplace

THÈSE DE DOCTORAT de
L'UNIVERSITÉ PIERRE ET MARIE CURIE

Spécialité
Chimie et Physico-chimie des Polymères
(ED 397)

Présentée par

M^lle Fanny DEPLACE

Pour obtenir le grade de
DOCTEUR de L'UNIVERSITÉ PIERRE ET MARIE CURIE

Sujet de la thèse :

ADHESIFS NANOSTRUCTURES EN VOIE EMULSION

WATERBORNE NANOSTRUCTURED ADHESIVES

Thèse dirigée par Costantino CRETON

Soutenue le : 11 avril 2008

Devant le jury composé de :

M^me Bernadette CHARLEUX,	Professeur, Université Pierre et Marie Curie,	Présidente du jury
M^me Catherine GAUTHIER,	Professeur, INSA de Lyon,	Rapporteur
M. Eric PAPON,	Professeur, ENSCPB,	Rapporteur
M. Jean-François TASSIN,	Professeur, Université du Maine,	Examinateur
M. Christophe DERAIL,	Maître de Conférences, Université de Pau,	Examinateur
M. Costantino CRETON,	Directeur de Recherche CNRS, ESPCI,	Directeur de thèse

à
Maman,
Becca et Lulu.

C'est soulagée mais aussi un peu émue que je commence ces remerciements. Soulagée car c'est la fin de plusieurs mois épuisants de rédaction. Emue car c'est la fin de plusieurs années fascinantes et enrichissantes au sein du laboratoire PPMD de l'ESPCI et c'est un peu attristée que je vais le quitter.

Je remercie en premier lieu Costantino Creton. Je me suis souvent rendue compte de la chance que j'avais de l'avoir comme directeur de thèse. Je lui suis entre autre reconnaissante de m'avoir fait profiter de son côté voyageur, ouvert sur le reste du monde et je le remercie de m'avoir permis de voyager dans le cadre de cette thèse, je ne serais peut-être jamais allée en Chine ! J'ai également beaucoup aimé sa petite initiation à la dégustation de vins alsaciens. Souvent parti, Costantino a néanmoins toujours été là pour me guider, résoudre des problèmes ou débloquer des situations quand j'en ai eu besoin.

Je tiens aussi à remercier Henri Van Damme et François Lequeux, directeurs successifs du laboratoire pour m'y avoir accueillie.

Je remercie aussi Antoine Chateauminois pour tous ses conseils utiles à la bonne manipulation du microrhéomètre et qui lui aussi était toujours présent pour me tirer d'affaires en cas de problème.

J'adresse évidemment mes sincères remerciements aux membres du jury : Bernadette Charleux d'avoir accepté de présider le jury, Catherine Gauthier et Eric Papon d'avoir bien voulu être rapporteurs et Jean-François Tassin et Christophe Derail d'avoir accepté de juger mon travail tout simplement.

Ce travail n'aurait bien sûr pu être effectué sans les autres membres du projet NsHAPe. Peter Lovell le coordinateur du projet, Andrew Foster, Mike Rabjohns, Joe Keddie, Chunhong Lei, Ismo Pietari, Tuija Helin, Olivier Dupont et Gwynfor Hughes. Bon, cette liste est bien entendue plus qu'incomplète sans Keltoum!
Je remercie aussi Haris, Sandrine, Clara, Aude et Jeanne du laboratoire qui ont eux aussi participé à ce projet et ont apporté leur contribution dans les résultats de cette thèse.

Je pense maintenant à toutes les personnes que j'ai côtoyées plus quotidiennement au laboratoire et qui m'ont accompagnée de près ou de loin. Merci d'abord à Gauthier, Sarah, Becca, Elise et Lars mes compagnons de bureau successifs. Ensuite à l'ensemble des étudiants et en particulier Karine, Julia, Antonella, Chaujean, Griffith, Sébastien et Samy et à ceux qui sont partis du laboratoire avant moi : Diane, Guillaume, Thomas, Marie-Hélène, Angélina, Nick, Tetsuo...
Et comment ne pas citer Eric, Ludovic, et Olivier qui m'ont tenu compagnie pendant des journées de manips de tack et Régis Schach avec toute l'aide qu'il m'a apportée lorsque je suis arrivée au laboratoire.
Les permanents aussi vont me manquer et je remercie Isabelle, Yvette, Alba, Anke, Ludo, Hélène et Freddy qui a toujours été là quand j'ai eu besoin de son aide et surtout aussi pour sa naturelle bonne humeur. Une petite pensée aussi pour Gilles et Flore qui est née le même jour que moi.

D'un point de vue plus personnel, je dis merci à Lulu, Fred et Sly qui resteront longtemps chers à mon cœur. Merci aussi à Vincent et Mathieu.
Je pense aussi bien entendu à toute l'équipe du DAPS : Gégé, Serge, Robert, David, Stéphen, Benoît, Isabelle, les Michèles, Dominique, Nicole, Omar, Pierre, Claude…

Je remercie enfin du fond du cœur toute ma famille, maman, papa, Benoit, Mathilde, Clément, Céline, Johan, Arthur et Léonie.

Et un dernier merci à ceux que j'aurais pu oublier.

Nous avons étudié les propriétés d'adhésion et de déformation de films de polymères adhésifs préparés à partir de particules de latex nanostructurées. Une méthodologie basée sur deux critères rhéologiques et applicable à tout type de PSA a été proposée pour optimiser les performances adhésives. Elle nous a permis d'identifier des stratégies permettant d'améliorer le compromis entre propriétés adhésives et cohésives dans le cas particulier de PSA préparés à partir de particules de latex ayant une morphologie cœur-écorce. Une stratégie intéressante est l'activation d'une réaction de réticulation interparticule pendant le séchage du latex. Nous avons fait varier l'hétérogénéité du réseau tout en gardant constante la composition en monomères. Nous avons montré l'effet remarquable de cette réaction de réticulation sur les propriétés en grandes déformations de nos matériaux. Ces propriétés sont assez bien décrites par un modèle non-linéaire combinant le modèle de Maxwell sur-convecté et le modèle de Gent. Les meilleurs résultats d'adhésion sont obtenus pour des matériaux caractérisés par un net ramollissement à déformations intermédiaires suivi d'un rhéodurcissement. Ce comportement est notamment obtenu pour des PSA préparés à partir de particules de latex ayant une fine écorce assez réticulée et un cœur très mou. Dans un registre plus industriel, des performances adhésives prometteuses ont été obtenues avec des PSA préparés à partir de latex tackifiés in situ synthétisés par polymérisation en miniémulsion.

Mots clés : Adhésion, PSA à base aqueuse, Particule de latex, Structure hétérogène, Viscoélasticité linéaire, Viscoélasticité et élasticité non-linéaires.

We studied adhesive and deformation properties of soft polymer films made from nanostructured latex particles. A methodology based on two rheological criteria and suitable for all kinds of PSA has been proposed to optimize adhesive performances. It allowed us to identify strategies to improve the balance between adhesion and cohesion of PSA prepared from core-shell latex particles. An interesting strategy is the activation of an interparticle crosslinking reaction during the drying of the film. The heterogeneity of the network has been varied without changing the monomer composition. This crosslinking reaction has a spectacular effect on nonlinear properties of the materials. These properties are well described by a nonlinear model constructed from the combination of the Upper-Convected Maxwell model and the Gent model. Best results are obtained with PSA prepared from latex particles with a fine and crosslinked shell and a soft only slightly crosslinked core. With a more empirical approach, promising adhesive performances have been obtained with PSA prepared from in situ tackified latexes synthesized by miniemulsion polymerization.

Keywords: Adhesion, waterborne PSA, Latex particle, Heterogeneous structure, Linear viscoelasticity, Nonlinear viscoelasticity, Nonlinear elasticity.

UPMC Univ Paris 06
Laboratoire PPMD UMR 7615 CNRS
ESPCI
10 Rue Vauquelin
F-75231 Paris Cedex 05

Table of Content

(1) This bibliography is an alphabetical list of all references used in this thesis. A numbered list of references is given at the end of each chapter.

List of abbreviations

This table provides abbreviations used in the present thesis.

AA	Acrylic Acid
ADH	Adipic Acid Dihydrazide
AFM	Atomic Force Microscopy
AIBN	2,2'-Azobisisobutyronitrile
ASTM	American Society for Testing and Materials
BA	Butyl Acrylate
CF	Cohesive Failure
CT	Cohesive Transfer
CTA	Chain Transfer Agent
DAAM	DiAcetone AcrylaMide
DSC	Differential Scanning Calorimetry
EA	Ethyl Acrylate
EGDMA	Ethylene Glycol DiMethylAcrylate
EHA	Ethy Hexyl Acrylate
FINAT	Fédération Internationale des fabricants et transformateurs d'Adhésifs et Thermocollants
FTM	FINAT Test Methods
GPC	Gel Permeation Chromatography
HDPE	High Density PolyEthylene
NsHAPe	designed NanoScale Heterogeneities for controlling waterborne Pressure-sensitive Adhesive Performance
MAA	Methacrylic Acid
MFFT	Minimum Film Formation Temperature
MMA	Methyl MethAcrylate
MOTT	Mechanical Optical Tack Test
MWD	Molecular Weight Distribution
OPP	Oriented PolyPropylene
PBA	Poly(Butyl Acrylate)
PBMA	Poly(Butyl MethAcrylate)
PEA	Poly(Ethyl Acrylate)
PEI	Poly(EthylenImide)
PEHMA	Poly(Ethylhexyl Acrylate)
PMMA	Poly(Methyl MethAcrylate)
PSA	Pressure Sensitve Adhesive
PSTC	Pressure Sensitive Tape Council
PVOH	Poly(Vinyl Alcohol)
QELS	Quasi Elastic Light Scattering
SC	Semi Continuous
SDS	Sodium Dodecyl Sulphate
SEC	Size Exclusion Chromatography
SFS	Sodium Formaldehyde Sulfoxylate

TBHP	Tert Butyl HydroPeroxide
TEM	Transmission Electron Microscopy
T_g	Glass transition Temperature
THF	TetraHydroFuran
TLMI	Tag & Label Manufacturers Institute
TM	Tapping Mode
UCM	Upper Convected Maxwell
wb-PSA	Waterborne PSA
1H-NMR	proton Nuclear Magnetic Resonance
2-EHA	2-EthyHexyl Acrylate

Introduction Générale

Déjà il y a trois millénaires se manifestait le besoin de coller, d'assembler différentes structures entre elles. On utilisait pour cela des produits naturels d'origines végétale, animale ou minérale : la glu tirée de l'écorce du houx, la gomme arabique extraite de certains acacias, le latex tiré de plusieurs espèces d'hévéa, le blanc d'œuf, la cire d'abeille, le bitume, etc.
Cependant, ce n'est que dans la première moitié du vingtième siècle que la forte croissance industrielle a eu un effet sur la technologie des adhésifs. De nombreuses résines synthétiques ont été développées en laboratoire pour remplacer l'utilisation des adhésifs naturels. Aujourd'hui pour répondre aux exigences d'application (fort pouvoir collant et bonne résistance à des conditions difficiles) de plus en plus fortes, des produits de haute performance ont été développés.

Dans le cadre de cette thèse nous nous sommes plus particulièrement intéressés aux adhésifs autocollants (en anglais pressure-sensitive-adhesives ou PSA[(1)]). Les adhésifs PSA adhèrent immédiatement à la surface d'application par simple contact sous faible pression. Ils ont commencé à être commercialisés à partir de l'après-guerre. Les premiers PSA étaient composés de caoutchouc naturel et de tackifiants en dispersion dans des solvants organiques.
Des produits de plus en plus innovants ont ensuite été créés grâce à la compréhension des mécanismes mis en jeu lors du décollement d'un film adhésif. Ces problèmes d'adhésion ont été appréhendés par différentes voies impliquant la chimie macromoléculaire, la physique de la matière molle et la mécanique des milieux continus.

Les adhésifs peuvent être répertoriés en fonction de leurs applications finales. Pour certaines applications on utilise des adhésifs dits « adhésifs permanents » qui sont conçus pour coller de façon définitive sur le support alors que dans d'autres il peut être nécessaire de décoller l'étiquette du produit, l'adhésif doit donc être enlevable, si possible sans laisser de résidus.

(1) Les abbréviations utilisées dans ce manuscrit sont reportées dans la liste d'abbréviations figurant page 15.

Quelle que soit l'application souhaitée, de bonnes propriétés adhésives sont obtenues par le contrôle fin, des propriétés viscoélastiques du matériau. Le collant serait majoritairement contrôlé par les propriétés dissipatives apportée par les chaînes de petites masses alors que les points de réticulation et les enchevêtrements donneraient la cohésion nécessaire au matériau pour qu'il puisse se décoller du support sans laisser de résidus.

Les adhésifs sont invariablement utilisés sous forme de films d'épaisseur variant entre 15 µm et quelques centaines de microns. En classant les PSA par méthode de mise en œuvre on trouve les trois grandes familles suivantes : les PSA hot-melt (autrement dit sans solvant ou dispersant), à base aqueuse (polymère dispersé dans l'eau) et en solvant (polymère dissous). Le développement de la réglementation environnementale a impliqué des évolutions importantes sur les répartitions de ces différentes familles de PSA. La conséquence directe est une augmentation de la production des adhésifs à base aqueuse et une diminution de ceux à base solvant.

Les adhésifs étudiés dans ce travail de thèse sont des adhésifs acryliques préparés par polymérisation en émulsion. Les films adhésifs sont obtenus par séchage de dispersions colloïdales de particules de latex dont le diamètre est de l'ordre de quelques centaines de nanomètres et dont la composition et les structures interne et de surface peuvent être contrôlées à l'échelle nanométrique pendant la synthèse. Cette étude a été motivée par le désir de surmonter les limitations de ces matériaux en termes de propriétés d'adhésion et d'obtenir d'aussi bonnes performances que celles des PSA hot-melt ou en solvant notamment sur des surfaces de faible énergie comme le polyéthylène.

Ce travail a été réalisé dans le cadre du projet européen NsHAPe (NsHAPe pour "designed Nanoscale Heterogeneities for controlling water-borne pressure-sensitive-Adhesive Performance"). L'objectif est de concevoir des stratégies de synthèse et de design des particules permettant de contrôler les propriétés adhésives.
Autour de ce projet ce sont rassemblées cinq équipes de recherche européenne ayant chacune son expertise dans des domaines assez variés.
Nous avons travaillé en collaboration avec deux laboratoires universitaires Anglais. Le premier est situé à l'Université de Manchester. La synthèse par polymérisation en émulsion de particules à composition et morphologie contrôlées a été réalisée dans le laboratoire des matériaux de l'université par Mike Rabjohns et Andrew Foster sous la direction du Profeeseur Peter Lovell. Les propriétés adhésives de ces matériaux ont également été caractérisées sur place par des tests industriels standard d'adhésion.
Le second, l'Université de Surrey se situe à proximité de Londres. Chunhong Lei sous la direction du Professeur Joe Keddie du département de physique de l'université a étudié les phénomènes mis en jeu lors de la formation des films et a caractérisé par microscopie à force atomique les structures des films adhésifs.
Deux industries leader des PSA ont également participé à ce projet: Cytec Surface Specialties, implantée à Bruxelles, qui fabrique des adhésifs en solvant ou à base aqueuse depuis plus de 40 ans et UPM Raflatac, situé à Tampere en Finlande, qui est l'une des premières sociétés à avoir développé et utilisé activement les adhésifs à base d'eau pour fabriquer des supports étiquettes. Alors que Keltoum Ouzineb a supervisé le travail de synthèse des latex et de caractérisations des films (par des tests industriels d'adhésion) chez Cytec, Tuija Helin et

Ismo Pietari de UPM Raflatac se sont attachés à évaluer les performances adhésives de reproductions à l'échelle industrielle de matériaux synthétisés au laboratoire.

Le bon déroulement de ce projet a sans doute été le fruit des multiples échanges et transferts des connaissances qui ont permis de considérer un très grand nombre de phénomènes ou de paramètres mis en jeu dans le problème d'adhésion des PSA préparés à partir de particules de latex : des structures et architectures moléculaires des polymères et nanométriques des particules aux propriétés mécaniques et adhésives des films adhésifs à l'échelle macroscopique en passant par les caractéristiques microscopiques de surface. L'obtention in fine d'un brevet et de films fabriqués à partir de latex à l'échelle industrielle ayant des propriétés adhésives prometteuses en est le résultat direct.

Nous nous sommes situés au cœur de ce projet et notre rôle était de caractériser les propriétés rhéologiques, mécaniques et adhésives des films adhésifs.
Les propriétés d'adhésion ont été caractérisées grâce au test du probe tack. Une meilleure compréhension des mécanismes de décollement observés a été obtenue par l'analyse des propriétés rhéologiques. Dans le domaine linéaire, les propriétés viscoélastiques ont été caractérisées à l'aide d'un nouveau microrhéomètre mis au point au laboratoire et permettant de mesurer quantitativement des films aussi minces que ceux utilisés pour les tests de probe tack. Si les propriétés à grandes déformations ont quant à elles été caractérisées par des tests de traction assez simples, leur interprétation a été très poussée dans ce travail et constitue une contribution originale.

Le premier chapitre de cette thèse sera consacré à une revue de quelques notions de chimie et physico-chimie des polymères préparés par polymérisation en émulsion. Ce chapitre est destiné à mieux appréhender les concepts théoriques à la base de ce travail.
Le deuxième chapitre résume et discute un certain nombre de travaux de la littérature réalisés sur des PSA préparés par polymérisation en émulsion. Il vise essentiellement à mettre en lumière les paramètres et caractéristiques inhérents aux systèmes aqueux pouvant influencer les propriétés d'adhésion et aussi à montrer la difficulté à contrôler indépendamment les propriétés d'adhésion et de cohésion.
Dans le troisième chapitre sont présentées les techniques expérimentales utilisées et en particulier le microrhéomètre dans son application PSA.

Nos résultats sont contenus dans les chapitres 4, 5 et 6.
Le chapitre 4 est une partie méthodologique consacrée à la démarche d'optimisation des propriétés d'adhésion de films adhésifs préparés à partir de particules de latex. Cette étude qui a été réalisée sur des films préparés à partir de particules ayant une morphologie cœur-écorce a permis d'identifier une stratégie permettant d'améliorer le compromis entre propriétés adhésives et cohésives et de définir un système modèle.

Dans le chapitre 5 nous nous sommes intéressés à un système modèle spécifique ayant déjà d'assez bonnes performances adhésives. De nouveau, la morphologie cœur-écorce a été choisie comme base mais ici dans le but précis de varier de façon contrôlée l'hétérogénéité du réseau de points de réticulation en gardant la composition monomère constante. Nous avons pour cela utilisé une méthode de réticulation interparticule pendant le séchage qui permet de

réaliser des réseaux de type nid d'abeille. Ce chapitre fait une large place aux propriétés en grandes déformations des matériaux.

Le chapitre 6 est quant à lui consacré au volet industriel de ma thèse à travers l'exemple de l'étude de latex tackifiés synthétisés par la technique de miniémulsion dans le but d'obtenir des prototypes industriels ayant des propriétés adhésives optimisées. La démarche y est par la force des choses plus empirique mais permet de faire le lien entre les concepts fondamentaux développés dans les deux chapitres précédents et leur implémentation industrielle.

Afin de permettre à l'ensemble des partenaires du consortium Européen de lire dans les meilleures conditions les résultats de ma thèse, la totalité de ce travail est rédigée en anglais à l'exception de cette introduction et de la conclusion générale. Nous nous excusons donc par avance auprès du lecteur francophone pour ce supplément d'effort à la lecture d'un anglais par la force des choses moins policé que ne l'aurait été le français.

1. Theoretical Concepts

In order to better follow the various aspects of the thesis it is useful to briefly remind the reader of the main basic scientific concepts that we used.
First, we will summarize some basic concepts of polymer synthesis. This chapter covers a non exhaustive range of fundamental aspects of polymer synthesis, of the free radical polymerization and of its application in the case of emulsion polymerization. Some polymer and latex characterization techniques are also presented.
Then, the transformation from the aqueous dispersion to dry polymer films is explained.
In the third part of this chapter, the mechanical properties of solid polymers are considered first from two phenomenological viewpoints and then with some physically based models, bridging the gap between the macroscopic and the molecular scale. This latter approach is complementary of a better understanding and control of polymer structure which was outlined in the first part.
Finally, some theoretical concepts of adhesion are presented.

1.1. Polymers

The core component of all pressure sensitive adhesives are high molecular weight low T_g *polymers*. This chapter provides some basic definitions related to the polymer world. The important topics of *average molecular weight* and *glass transition temperature* are introduced.

Polymers are macromolecules composed of repeating structural units, or *monomers*, connected by covalent chemical bonds. These units are repeated more than thousand times. When the monomer is repeated much less (only a few repeat units), the macromolecule is called *oligomer*. Figure 1-1 shows some common polymers and their corresponding monomers. (These monomers are typical monomers used in the copolymers of which PSA studied in this thesis are composed).

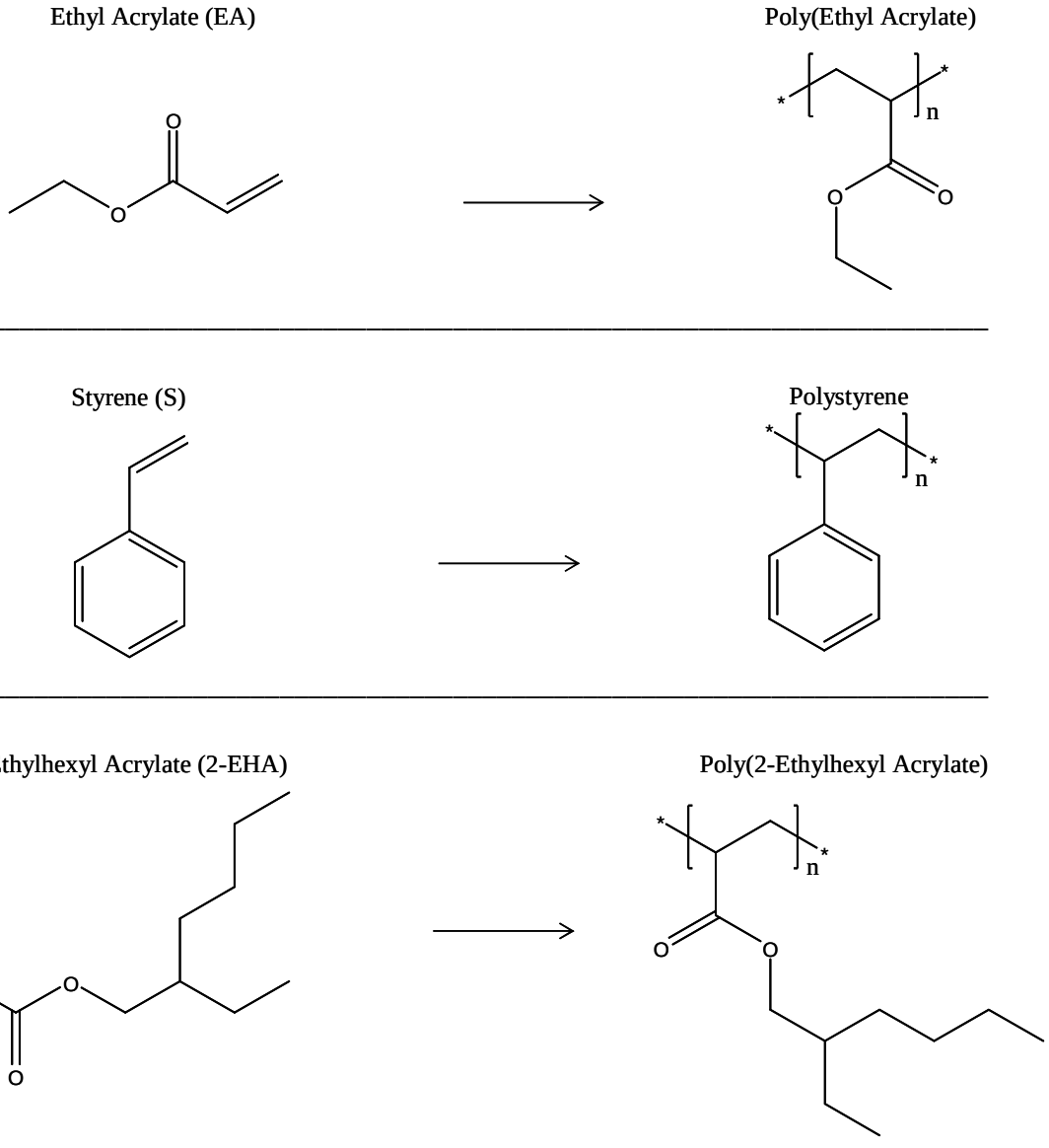

Figure 1-1. Some usual polymers and their monomers.

Some polymers are classified as *homopolymers* (Figure 1-2-a). They have very simple structure constituted of the same monomer.

Others containing more than one variety of monomer are called *copolymers*. Monomers within a copolymer may be organized along the backbone in a variety of ways:

- *Alternating copolymers* possess regularly alternating repeat units (Figure 1-2-b).
- *Periodic copolymers* have specific sequences of monomers arranged in a repeating fashion (Figure 1-2-c).
- *Random copolymers* have a random sequence of repeat units (Figure 1-2-d).
- *Statistical copolymers* have repeat units arranged according to a known statistical rule.
- *Block copolymers* have two or more homopolymer subunits linked by covalent bond. Block copolymers with two or three distinct blocks are called diblock copolymers and triblock copolymers, respectively (Figure 1-2-e).

Copolymers may also be described in terms of the existence of or arrangement of *branches* in the polymer structure. Linear copolymers consist of a single main chain whereas branched copolymers consist of a single main chain with one or more polymeric side chains.

Graft copolymers are a special type of branched copolymer in which the side chains are structurally distinct from the main chain. Figure 1-2-f depicts a special case where the main chain and side chains are composed of distinct homopolymers. However, the individual chains of a graft copolymer may be homopolymers or copolymers.

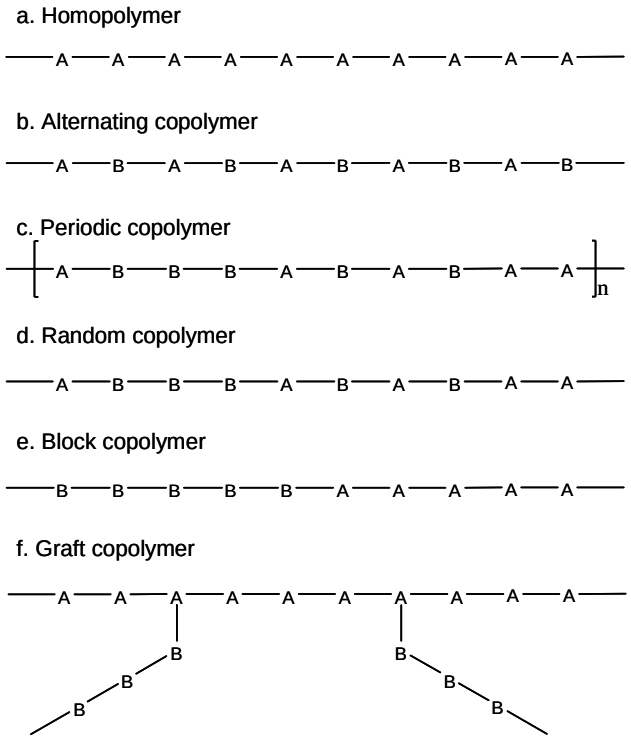

Figure 1-2. Types of copolymers.

Depending on the choice of the monomer and the polymerization process, polymer chains may be either linear, branched or crosslinked in a tridimensional network as illustrated in Figure 1-3.

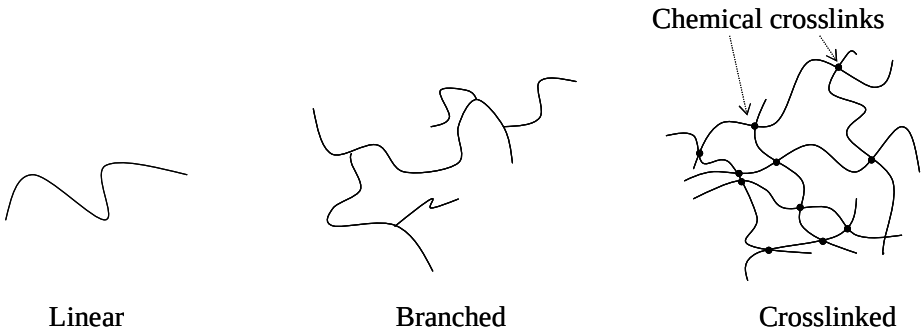

Figure 1-3. Schematics of linear, branched and crosslinked polymer chains.

1.2. Polymerization

The covalent linking of the monomers forming the polymeric chain is obtained through a reaction called polymerization. Different types of polymerization exist depending on the chemical reaction involved.

1.2.1. Free radical chain polymerization

Within this work, materials are synthesized using the well known *free radical chain polymerization.* Polyethylene, polystyrene, poly(vinyl chloride), three polymers of major economic importance are obtained by such processes. Poly(methyl methacrylate), poly(2-ethylhexyl acrylate) are also manufactured by using free radical processes, as well as many copolymers, which are the main components of the pressure sensitive adhesive formulations studied in the present work.

It is convenient to divide the polymerization process into *initiation*, *propagation* and *termination*.

Initiation

The whole process of a free radical chain polymerization starts off with a molecule called an *initiator*. This is a substance that generates radicals by hemolytic scission when heated or irradiated, or by any other means. The free radical initiators can be classified in several groups, of which the most important are:

- Peroxides, organic or inorganic like ammonium persulfate
- Hydroxoperoxides
- Peresters
- Aliphatic azocompounds

Two radicals, which are able to initiate free radical polymerization, are generated for each molecule of initiator (Figure 1-4-a1). The actual initiation reaction is the attack of a monomer molecule by a primary radical originating from the initiator (Figure 1-4-a2).

Propagation

The new radical formed during initiation reacts with another monomer molecule in the exact way as the initiator fragment did. The process, the adding of more and more monomer molecules to the growing chains, is called *propagation*. This reaction is repeated hundred to many thousands of times for each chain formed. It can be written as on Figure 1-4-b. It is generally assumed that the rate constant of this reaction remains the same, regardless of the length of the chain to which the radical site is attached.

One characteristic of the propagation step for multicomponent polymerizations is the difference in the tendency of monomers to enter the polymer chains (Figure 1-4-b2). The reactivity ratios characterize the reactivity of radicals ending in monomer unit A toward monomer A or monomer B in the reaction mixture.

$$r_A = \frac{k_{pAA}}{k_{pAB}} \qquad r_B = \frac{k_{pBB}}{k_{pBA}} \qquad \textbf{Eq. 1-1}$$

Depending on the values of these reactivity ratios, different types of copolymers are obtained. Let's consider some special cases.

- If $r_A = r_B = 0$: monomer A prefers to react with monomer B and monomer B with monomer A. In that case a perfectly *alternating copolymer* results.
- If $r_A = r_B = \infty$: monomer A prefers to react with monomer A and monomer B with monomer B. In that case *a mixture of homopolymer A and homopolymer B* is formed.
- If $r_A = r_B = 1$: There is no distinction between monomer A and monomer B. They are consumed without any preference. In that case a *completely random copolymer* is formed.
- If $r_A < 1$ and $r_B < 1$, both monomers do not homopolymerize. They react together to give alternating copolymers.
- If $r_A >> 1 >> r_B$: In the initial stage of the copolymerization monomer A is incorporated faster and the copolymer is rich in monomer A. When this monomer gets depleted, more monomer B segments are added. The greater the difference in the reactivity ratios, the greater is the possibility of the change in chemical composition of the polymer formed. Such a change is also commonly called "*composition drift*".

Termination

Radicals are unstable, and eventually they are going to find a way to become paired without generating a new radical. Growing radicals can react with each other in two different ways:

- By *recombination*, a homopolar bond is formed by pairing the single electrons of the free radical sites of two chains (Figure 1-4-c_1).
- By *dispropornation*, whereby a hydrogen atom is transferred from one chain to the other; two molecules of "dead" polymer are formed, one of them bearing a double bond at each chain end (Figure 1-4-c_2).

In both cases, the reaction involves mutual destruction of radicals, and kinetically these two processes cannot be distinguished. But their consequences as to what concerns the molecular weight distribution and polydispersity of the polymers formed are different.

a) Initiation

a_1: Radical decomposition

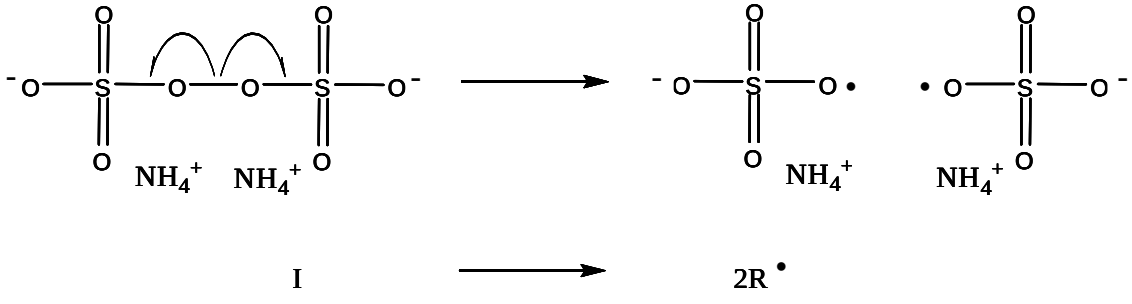

(Figure continued)

a2: Actual initiation reaction

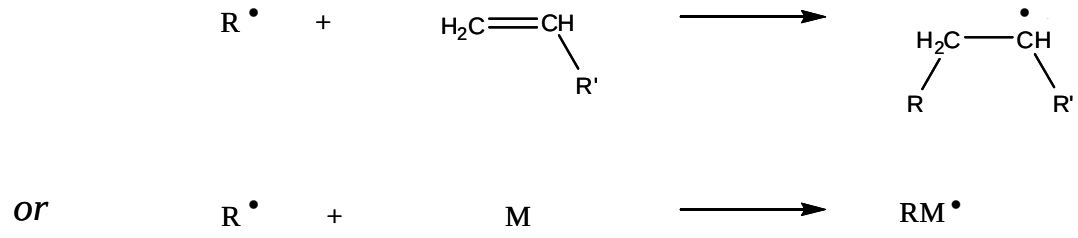

b) Propagation

b1) homopolymer

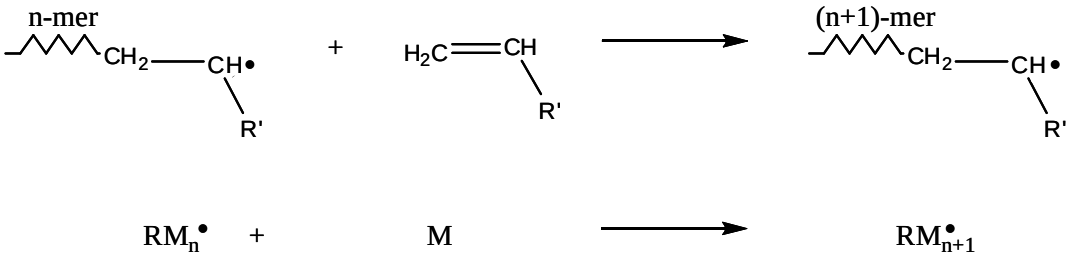

b2) copolymer

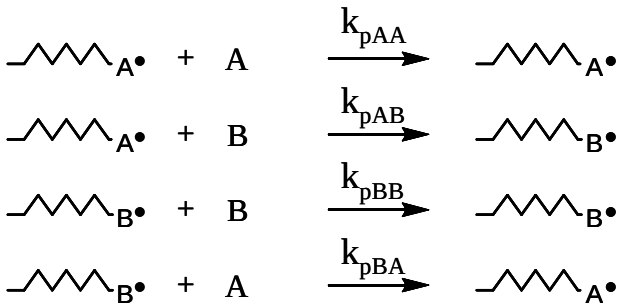

c) Termination

c1: Termination by recombination

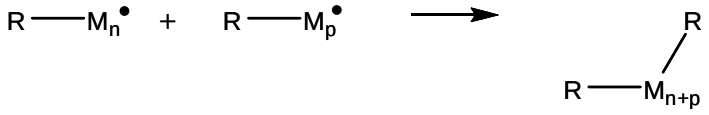

c2: Termination by dispropornation

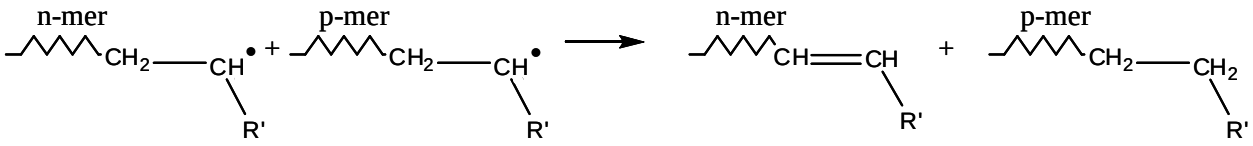

Figure 1-4. Mechanism of radical chain polymerization.

1.2.2. Branched and crosslinked polymer formation

1.2.2.1. Branched polymer formation

It can happen that a free radical site reacts with a molecular of initiator, or monomer, or chain transfer agent (such as a mercaptan Figure 1-5-a), even the polymer itself (Figure 1-5-b). This process is called *chain transfer reaction*. The result of such reactions is that the growing site at chain end is removed. A hydrogen atom or some labile group will saturate it; but another radical site arises from the molecule which has reacted, and if it is able to add monomer, it gives rise to the formation of a new macromolecule. For chain transfer to the polymer, branches are formed. Branches are long in the case of intermolecular chain transfer, branches are shorter for intramolecular chain transfer.

a) Chain transfer to a mercaptan

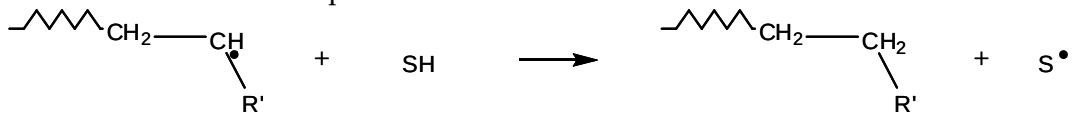

b) Chain transfer to the polymer leading to branching

Intermolecular chain transfer to polymer

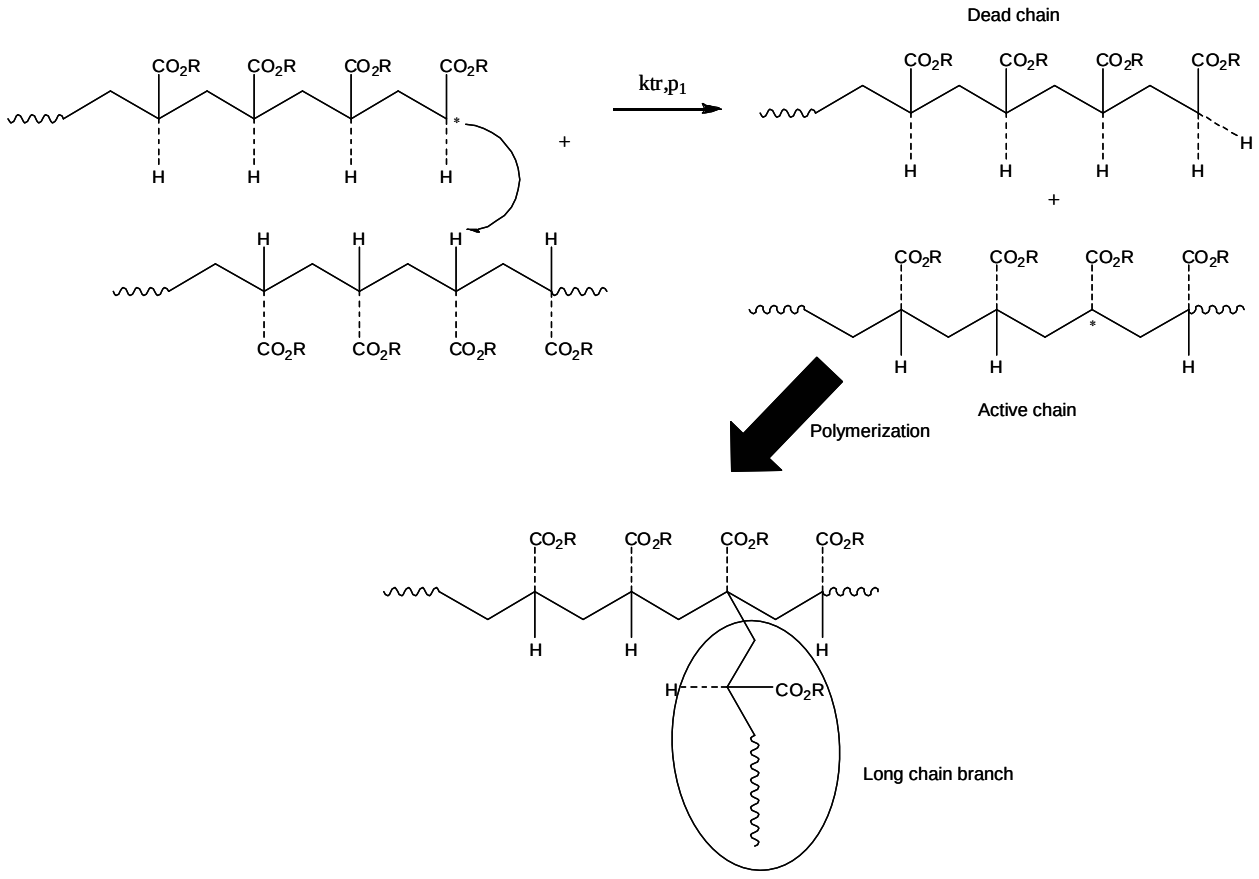

(Figure continued)

Intramolecular chain transfer to polymer, backbiting

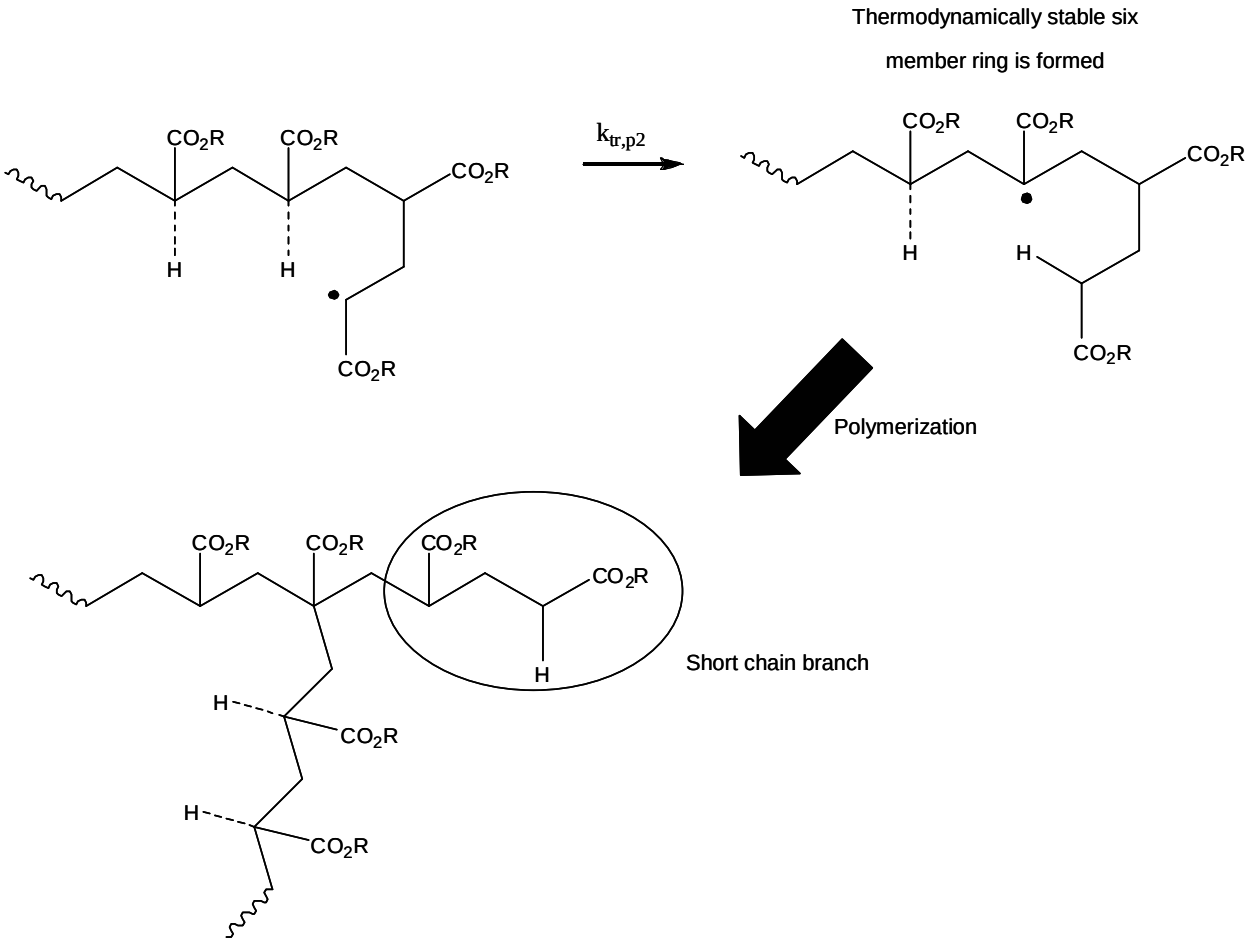

Figure 1-5. Mechanism of transfer reaction

The occurrence of transfer processes strongly influences the molecular weight of the polymer formed. Instead of building one polymer molecule (or ½ if termination occurs by recombination) a given radical site can produce several polymer molecules during its lifetime, if transfer is involved.

A few additional remarks have to be made:

- The probability for any given transfer reaction to occur is usually low. But since the growth process can involve 100 to 1 000 000 steps, the probability of transfer being the same at each stage, it is impossible to discard the possibility of transfer, even when no specific transfer agent have been added.
- Transfer reactions are sometimes used specifically to obtain short chain polymers. A well defined amount of transfer agent is then added on purpose, to "regulate" the molecular weight.
- Transfer to the polymer yields *branching* of the chain. The tendency to give rise to transfer reactions depends on the corresponding radicals of the monomer considered.

- The last but not the least important remark is that in starved monomer feed conditions, the occurrence of chain transfer to polymer is increased due to a low concentration of monomer. And in the absence of crosslinking agents, intermolecular chain transfer reactions lead to the formation of long branches, and gel structures form when the branch ends meet and terminate each other.[1]

The time needed for the creation of a macromolecule, even up to 10^4 units, is thus of the order of a few seconds.

1.2.2.2. Crosslinked polymer formation

Besides chain transfer reactions, crosslinking reaction generally occurs during free radical polymerization without the need of adding any specific crosslinker.

Basically, the free radical copolymerization of a monomer A and a di-unsaturated monomer D yields crosslinked species. Each time a D unit is added to a growing polymer chain, a pendant double bond results that exhibits its own reactivity. The system thus involves three different types of unsaturations, originating from A, from D and from the pendant double bonds. Moreover, when the latter species reacts in turn with a growing radical, a tetrafunctional branch point is formed as shown in Figure 1-6.

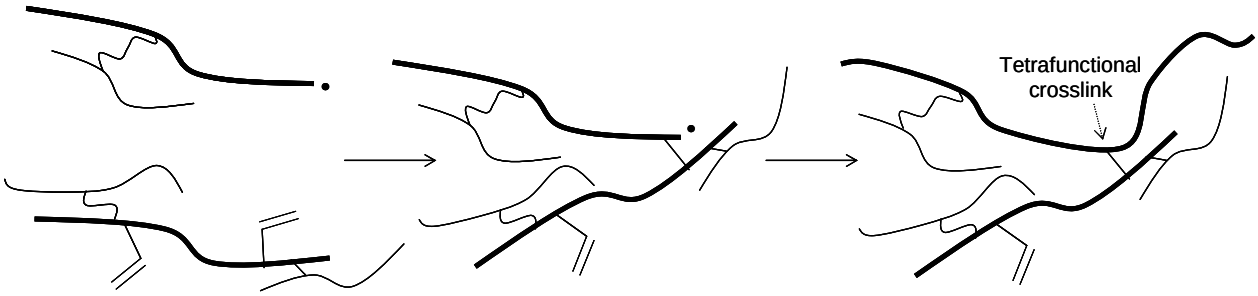

Figure 1-6. Crosslinking reaction.

1.3. Some polymer analytical characteristics

For the characterization of polymers used for adhesive applications, basically, we have to investigate and monitor three major characteristics. The first two are well-known and they are of course the average molecular weight and molecular weight distribution and the glass transition temperature. The third one is specific to the PSA application and is the gel fraction. Most PSA made from acrylic polymers contain both soluble and insoluble fractions. The insoluble fraction is constituted of connected or disconnected 3-D networks which can swell in a good solvent but not dissolve. This insoluble fraction due to crosslinking is called *gel fraction*. The procedure to measure gel content of a latex is detailed later.

1.3.1. Average molecular weight

Both the chemical nature of the repeated monomer and the total number of monomers will have a key role in the properties of the polymer chain.

Polymer molecular weight is important because it determines many physical properties. There are many ways to calculate an average molecular weight. The desired type of average molecular weight is determined by the type of property studied.

If we consider a property which is only sensitive to the number of molecules present and not to the size of the molecules in the material, the most relevant average molecular weight is the total weight of polymer divided by the number of polymer molecules. This average molecular weight is called the *number average molecular weight* M_n.

$$M_n = \frac{\sum_i N_i M_i}{\sum_i N_i} \qquad \textbf{Eq. 1-2}$$

where N_i is the number of molecules with the molar mass M_i.

Consider a polymer property which depends not just on the number of polymer molecules but on the size or weight of each polymer molecule. For such a property we need a weight average molecular weight. To derive the weight average molecular weight, we need to replace the appearance of the number of polymers of molecular weight M_i or N_i in the number average molecular weight formula with the weight of polymer having molecular weight M_i or $N_i M_i$. This average molecular weight is called the *weight average molecular weight* M_w.

$$M_w = \frac{\sum_i N_i M_i^{\,2}}{\sum_i N_i M_i} \qquad \textbf{Eq. 1-3}$$

Other average molecular weights are defined, like M_v and M_z.

Schematically, a typical molecular weight distribution might appear as in Figure 1-7. The various average molecular weights are indicated in their expected rank. The ratio

$I = M_w/M_n$ represents the polydispersity index of the material. When it is equal to one, the distribution is monodisperse. For all real polymers, it is greater than one and the amount that it is greater than one is a measure of the polydispersity of that polymer. This is an indication of the width of the molecular weight distribution.

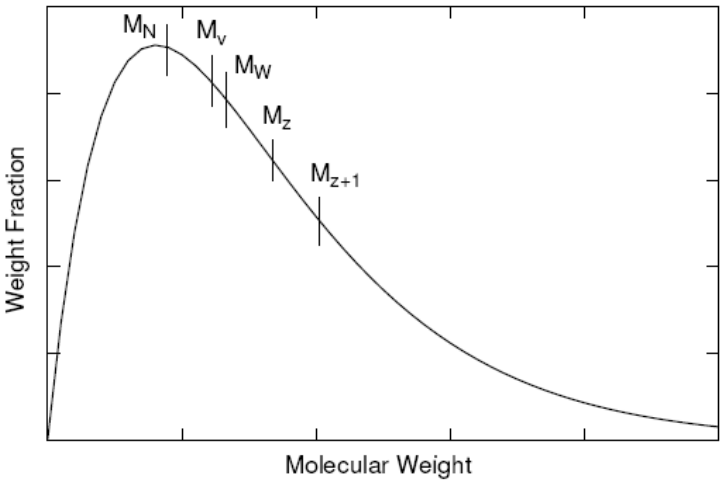

Figure 1-7. A schematic plot of a distribution of molecular weights along with the rankings of the various average molecular weights.

The *size exclusion chromatography (SEC)* also called *gel permeation chromatography (GPC)* is an extremely powerful method for determining the complete molar mass distribution of a polymer. In a GPC, a dilute polymer solution is injected into a solvent stream which then flows through a column packed with beads of a porous gel. The small solvent molecules pass both through and around the beads, carrying the polymer molecules with them where possible. The smallest polymer molecules are able to through most of the pores in the beads and so have a relatively long path-flow through the column. However, the largest polymer molecules are excluded from all but the largest of the pores because their greater molecular size and consequently have a much shorter flow-path.

However the molecule must be soluble to be characterized. Therefore insoluble fractions such as gels cannot be characterized in this way.

1.3.2. Fraction of gel

The *gel fraction* of a polymer is the fraction of polymer chains which are crosslinked while the uncrosslinked part is the soluble part and more commonly called *"sol"*. We have just seen how the M_w of linear polymer chains (i.e. the chains of the soluble part) is measured. We will now explain how the fraction of insoluble part is determined.

Different methods exist for the determination of the gel content. The most common consists in the extraction of a polymer foil with solvent in a Soxhlet apparatus.

A cartridge (weight W_1) is loaded with about 1 g of polymer (W_2) and the extraction is carried out under reflux (typically about 24 h). The cartridge is then dried and weighed (W_3) to calculate the gel fraction as follows:

$$\text{Gel content} = \frac{W_3 - W_1}{W_2 - W_1} \qquad \textbf{Eq. 1-4}$$

The extraction solvent is evaporated and the extracted sol polymer is recovered to measure the sol-weight-average molar mass by GPC as already seen (see section 1.3.1).

1.3.3. Glass transition temperature

A pure polymeric material can be either *amorphous* or *semi-crystalline* (Figure 1-8). In an amorphous material there is no order, the polymer chains form a big tangled mess. Monomers from different chains or from different part of a chain can overlap so as to form *entanglements*. A semi-crystalline polymeric material shows some highly ordered regions (*crystallites*) distributed in an amorphous matrix.

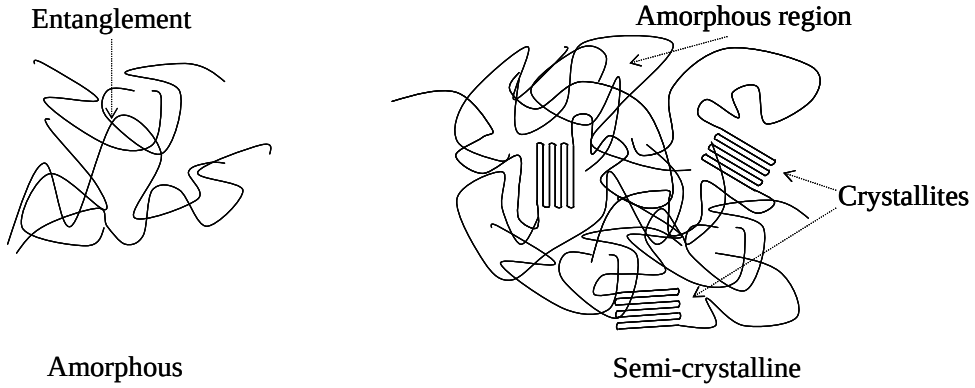

Figure 1-8. Schematic of entangled amorphous and semi-crystalline polymers.

Amorphous materials exhibit two different types of mechanical behavior. Some like polystyrene are hard, rigid, glassy (but not crystalline) plastics at room temperature while others like poly(ethyl acrylate) are soft, flexible rubbery materials at room temperature.

There is a temperature, or range of temperatures, below which an amorphous polymer is in a glassy state and above which it is rubbery. This temperature is called the *glass transition temperature*, T_g, and it characterizes the amorphous phase.

The glass transition temperature depends on the chemical nature of the monomers and on the structure of the main chain. Typically, everything that makes the chain stiffer will increase T_g (presence of phenyl group, conjugated double bond…). Large, bulky pendant groups usually raise the glass transition temperature by preventing the chains from sliding past each other easily. Short alkyl pendant groups may lower the T_g by a lubricant effect.

We can note that in cooling an amorphous material from the liquid state there is no abrupt change in volume such as occurs in the case of cooling a crystalline material through its freezing point T_f. Instead, at the glass transition temperature, there is a change in slope of the curve of specific volume vs. temperature, moving from a low value in the glassy state to a higher value in the rubbery state over a range of temperatures. This comparison between a crystalline material (1) and an amorphous material (2) is illustrated in Figure 1-9-a. Note that the intersection of the two straight line segments of curve (2) defines the quantity T_g. The determination of T_g is found to be rate dependent. This is schematically illustrated in Figure

1-9-b where the higher T_{g2} is obtained with a substantially higher cooling rate than for T_{g1}. We can understand this rate dependence in terms of relaxation processes.

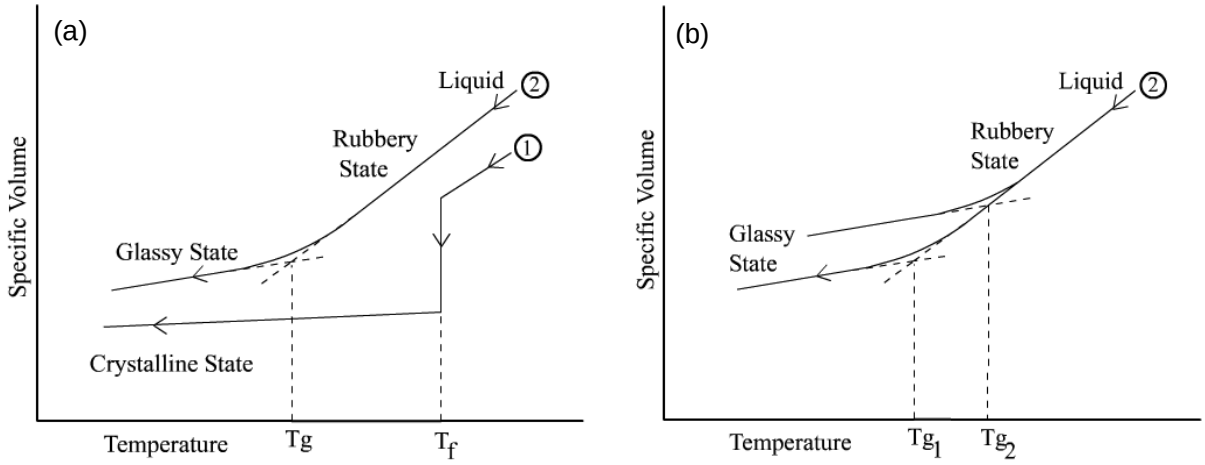

Figure 1-9. Specific volume as a function of temperature. (a) comparison between a crystalline polymeric material and an amorphous polymeric material (2). (b) rate dependence of T_g.

While the dilatometer method is the more precise method of determining the glass transition temperature, it is rather tedious experimental procedure and measurements of T_g are often made in a differential scanning calorimeter (DSC). In this instrument the heat flow into or out of a small sample is measured as the sample is subjected to a programmed linear temperature change. The glass transition process is illustrated in Figure 1-10 for a glassy polymer which does not crystallize and is being slowly heated from below T_g.

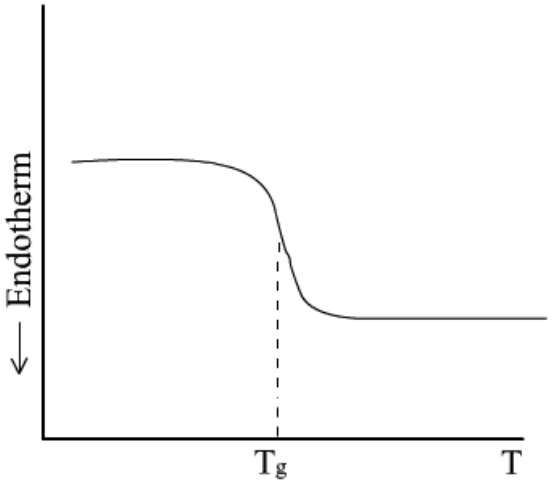

Figure 1-10. Typical DSC thermogram.

Another method to determine T_g is to take the point of inflection of the elastic modulus vs. temperature curve (this point will be discussed later in the section 1.6.2 about *viscoelasticity*).

Various other methods exist for the determination of T_g, but regardless of the method used T_g is defined at a given rate (rate of deformation, rate of cooling or heating…).

1.4. Waterborne polymers

We have described in details the free radical polymerization. This type of polymerization is used for bulk polymerization processes as well as for emulsion polymerization processes, by which waterborne polymers are produced. In this section, we will describe the emulsion polymerization process. Some variants of the conventional batch process will be discussed and some analytical properties of the products formed presented.

Emulsion polymerization leads to the production of fine dispersion of a polymer in a continuous medium which most often is water, called *latex* (the plural of latex is *lattices* or *latexes*, and in this paper, the latter word will be used). The aqueous liquid in which the latex particles are dispersed is referred to simply water. In reality, however, the water usually contains electrolytes, initiators, excess of emulsifiers, and other free species. This aqueous solution is referred to as the *latex serum*. Emulsion polymers are "products-by-process" whose main properties are determined during polymerization. Thus the process variables affect the final properties of the product and the term *emulsion polymerization* encompasses several processes:

1. Conventional emulsion polymerization
2. Inverse emulsion polymerization
3. Miniemulsion polymerization
4. Dispersion polymerization
5. Microemulsion polymerization

Conventional emulsion polymerization accounts for the majority of the world's production ($> 20.10^6$ tones/year).

Only conventional emulsion polymerization and miniemulsion polymerization have been used as processes for the production of the wb-PSA studied in the present research. We will start with a detailed description of the conventional emulsion process; the miniemulsion will be then introduced highlighting the differences between these two processes.

1.4.1. Conventional emulsion polymerization

Typically, emulsion polymerization is carried out in stirred tank reactors, which commonly operate in a semi-continuous mode, although both batch and continuous operations are also used. The synthesis process which has been effectively selected for the production of the wb-PSA is the semi-continuous one. However, for sake of clarity we will start with the description of the simpler batch process. The semi-continuous strategy will be then explained showing how the synthesis mechanisms are modified.

1.4.1.1. Batch emulsion polymerization

In a batch emulsion polymerization, the mixture of monomers is dispersed in water using emulsifiers. The monomer droplets are stabilized by the surfactant adsorbed on their

surface. The available surfactant partitions between the surface of the monomer droplets and the aqueous phase, and in most formulations, the amount of surfactants exceeds that needed to completely cover the monomer droplets and saturate the aqueous phase. The excess of surfactant forms micelles that are swollen with monomer (Figure 1-12-a).

The first successful theory to explain the distinct features of emulsion polymerization was largely developed by Smith and Ewart, and Harkins in the 1940s.[2,3] Smith and Ewart arbitrarily divided the mechanism of emulsion polymerization into three stages or intervals. Subsequently, it has been recognized that not all monomers or systems undergo these particular three intervals. Nevertheless, the Smith-Ewart description is a useful starting point to analyze emulsion polymerizations. A simplified interpretation is given in Table 1-1.

Interval	*Typical conversion range (%)*	*Micelles*	*Monomer droplets*	*Particle number*	*Particle size*
I	0-10	Present	Present	Increases	Increases
II	10-40	Absent	Present	Constant	Increases
III	40-100	Absent	Absent	Constant	~Constant

Table 1-1. Different intervals of an emulsion polymerization.[4]

Interval I: Particle Nucleation.

Polymerization is commonly initiated by water-soluble initiators (both thermal like potassium persulfate and redox like tert butyl hydroperoxide/ascorbic acid) although oil-soluble initiators (like 2,2'-Azobisisobutyronitrile called AIBN) may be also used. When a water soluble initiator such as potassium persulfate is added to the monomer dispersion, radicals are formed and these radicals are too hydrophilic to enter into the organic phase of the systems, they react with the monomer dissolved in the aqueous phase, forming oligoradicals (Figure 1-11). The growth rate of the oligoradicals is generally modest because of the low concentration of monomer in the aqueous phase. After adding some monomer units, the oligoradicals become hydrophobic enough to be able to enter into the small micelles (about 10 nm). Entry into the much less numerous large monomer droplets (about 1 μm) is not likely because their total surface area is about three orders of magnitude smaller than that of the micelles.

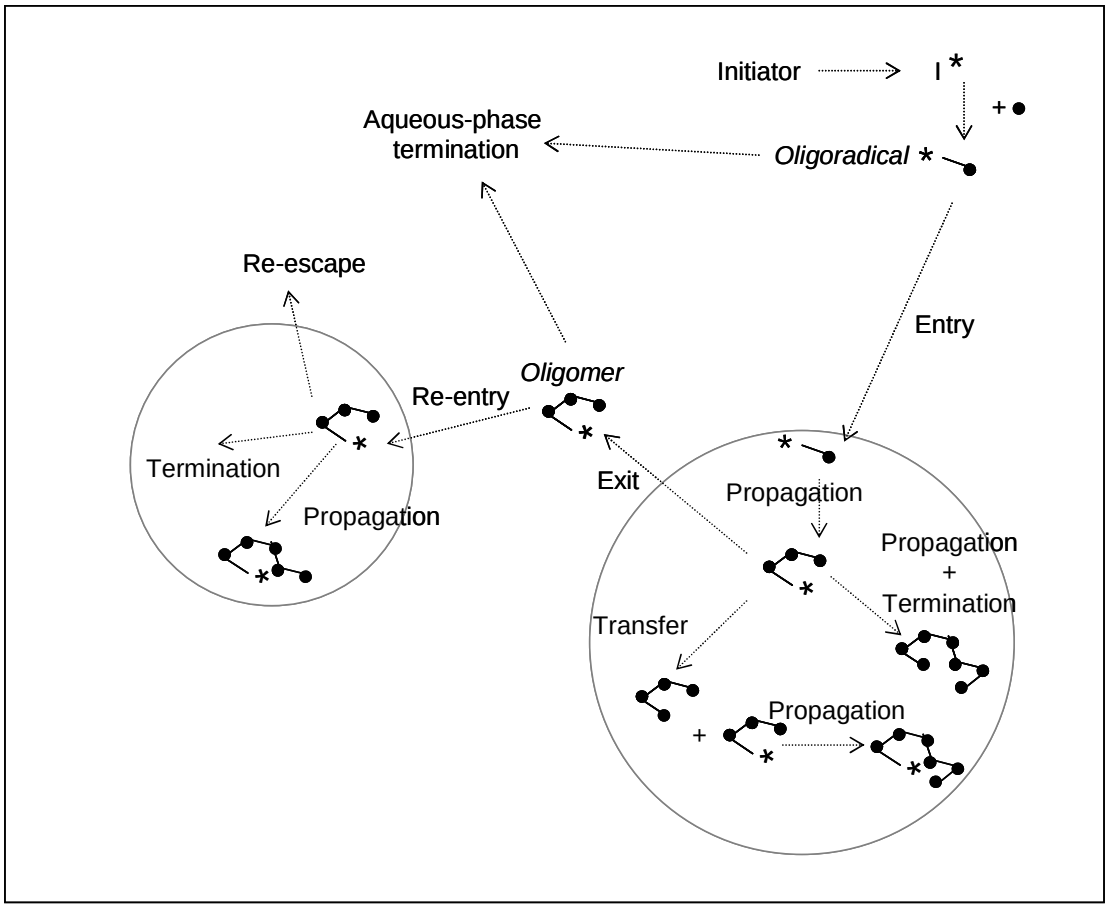

Figure 1-11. Mechanisms involved in emulsion polymerization.

Three major nucleation mechanisms are possible:

- In *heterogeneous nucleation*, initiator radicals enter the monomer-swollen micelles to initiate the polymerization. Those micelles that capture radicals will become *polymer particles* while others will serve as reservoir for the stabilization of formed particles.
- Common to monomers with higher water solubility is *homogeneous nucleation*, where radicals generated in the water phase continue to grow, adding the monomer molecules located in the aqueous phase. When the growing oligomeric radical reaches a particular size, it becomes water insoluble and precipitates. These precipitated oligomeric radicals form primary particles. These will adsorb stabilizer for stabilization and monomer for further growth.
- A radical may also be captured by a monomer droplet to form a particle. This is less likely due to the difference in the surface/volume ratio of monomer droplets and monomer swollen micelles. This mechanism can be induced under some conditions; for example *droplet nucleation* is the dominant mechanism of nucleation in miniemulsion polymerization (miniemulsion polymerization is presented later).

During nucleation, large monomer droplets, small and far greater in number monomer swollen micelles and monomer swollen polymer particles coexist in the reactor (Figure 1-12-b). Polymer particles efficiently compete for radical, and hence monomer is consumed by polymerization inside the polymer particles. The monomer that is consumed by polymerization in the polymer particles is replaced by monomer that diffuses from the

monomer droplets through the aqueous phase. Therefore, the size of the particles increases and that of the monomer droplets decreases. The number of micelles decreases because they become polymer particles upon entry of a radical and also because they are destroyed to provide surfactant to stabilize the increasing surface area of the growing polymer particles. After some time, all micelles disappear. This is considered to be the end of the nucleation and only limited formation of new particles may occur after this point because heterogeneous nucleation is not possible and there is no free surfactant available in the system to stabilize the particles formed by homogeneous nucleation.

At the end of Interval I, which typically occurs at a monomer conversion of about 5-10% (depending on the surfactant/monomer ratio), 10^{17}-10^{18} particles/L are formed. Unless coagulation occurs, the number of particles remains constant during the rest of the process.

Interval II: Polymer particle growth.

During Interval II (Figure 1-12-c), the system is composed of monomer droplets and polymer particles. The monomer diffuses from the monomer droplets through the aqueous phase and into the latex particles, to maintain saturation swelling and support the propagation reaction.

Because of the polymerization and monomer transport, the polymer particles grow in size and after some time, the monomer droplets disappear. This marks the end of Interval II. The monomer conversion at which Interval II ends depends on the capability of the polymer particle to be swollen by monomer. The higher the maximum swelling the earlier the monomer droplets disappear. In general, the more water-soluble the monomer the higher is the maximum swelling, and hence the lower the monomer conversion at the end of Interval II.

Thus, the transition from Interval II to Interval III occurs at about 40% conversion for styrene (solubility: 0.045 g / 100 g of water) and at about 15% conversion for vinyl actetate (solubility: 2.5 g / 100 g of water).

Interval III: Final stage.

Transition from Interval II to Interval III occurs at low conversion, this means that most monomer polymerizes in Interval III (Figure 1-12-d). In this interval, monomer concentration in the polymer particles decreases continuously. The final product is a waterborne concentrated (50-60 wt% solids) dispersion of tiny (80-500 nm in diameter) polymer particles called *latex*.

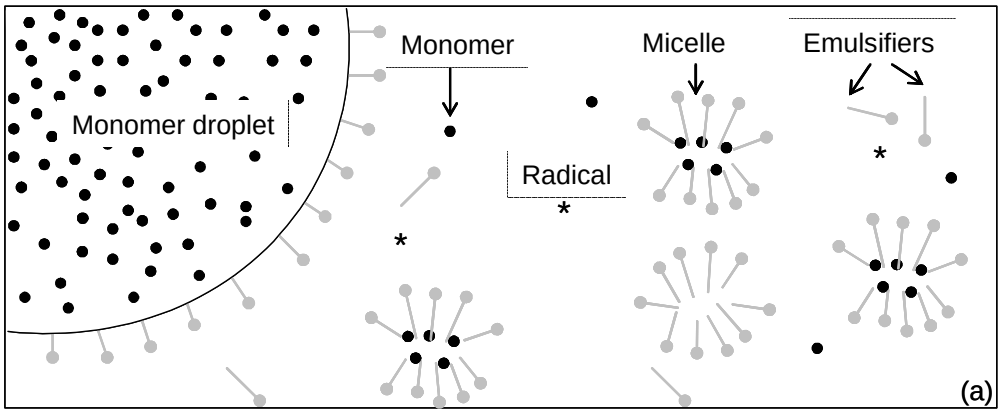

(Figure continued)

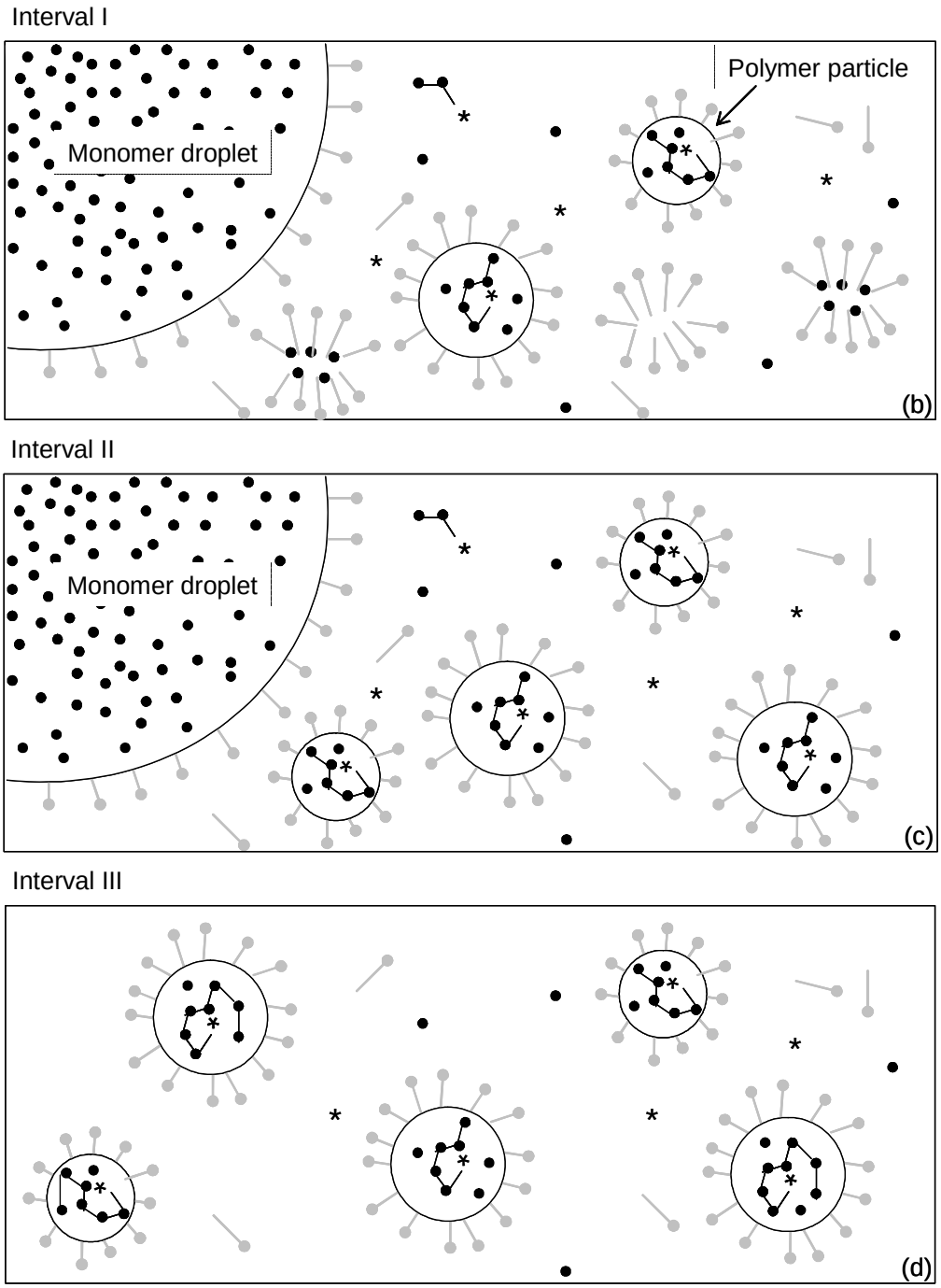

Figure 1-12. Intervals of the batch emulsion polymerization.

To summarize, the mechanism of free-radical emulsion polymerization is divided into the following steps:

- Monomer dispersed or emulsified in a solution of surfactant and water forming large monomer droplets.
- Excess surfactant creates micelles in water.
- A water soluble initiator is introduced into the water phase and hydrophobic oligoradicals are formed.

- Monomers diffuse from monomer droplets to micelles the oligoradicals that have entered into the micelles grow fast, forming a polymer chain. Micelles disappear and polymer particles are formed.

- The free monomer droplets disappear and all remaining monomer is located in the polymer particles.

1.4.1.2. Semi-continuous emulsion polymerization

In a semi-continuous reactor in which monomers, surfactants, initiator and water may be continuously fed into the reactor, emulsion polymerization does not follow the sequence of events described above. Thus, slow monomer feed and fast surfactant feed may lead to a system composed by polymer particles and micelles (Figure 1-13-a). The system will contain only monomer swollen polymer particles if both monomer and surfactant are fed slowly (Figure 1-13-b). On the other hand, a fast monomer feed and a low surfactant feed will lead to a system containing monomer droplets and polymer particles (Figure 1-13-c).

Slow monomer feed. Fast surfactant feed.

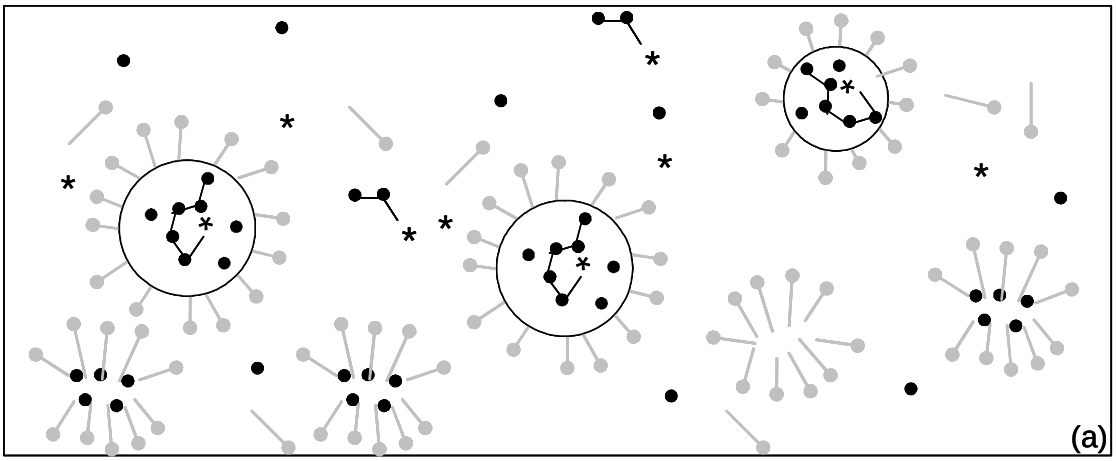

Slow monomer feed. Slow surfactant feed.

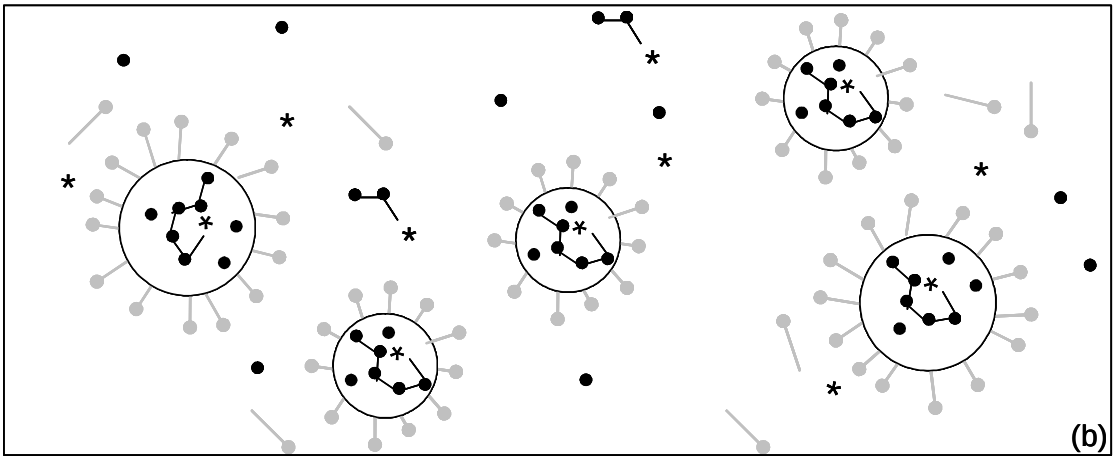

(Figure continued)

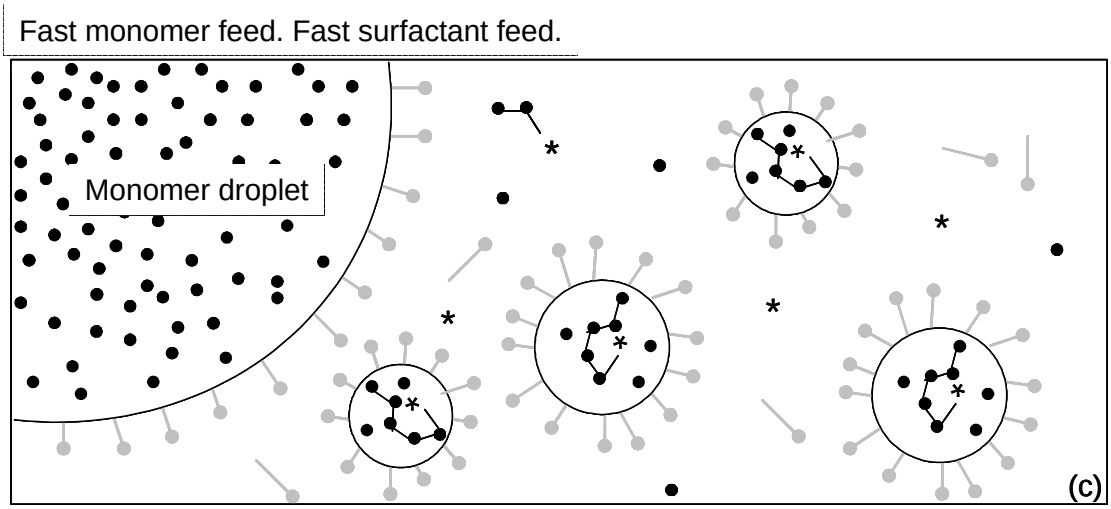

Figure 1-13. Species present in semi-continuous emulsion polymerization.

One of the advantages of the semi-continuous polymerization process compared to the batch is the possibility to work under *starved conditions*. More precisely, one way to address the issue of compositional drift in free radical batch copolymerization is to operate the reactor under this starved feed policy (slow monomer feed).[5] In this case, the monomer feed rate is automatically adjusted to maintain a constant rate of reaction. In this starved feed operation the reaction environment is maintained constant during the batch and therefore the monomer composition in the reactor feed is equal to the desired polymer composition.

Moreover, under starved conditions, the polymer/monomer ratio in the polymerization loci is very high and polymer chain transfer reactions are more likely to occur.[6] In addition, gel can be formed in systems in which there is chain transfer to polymer and termination mainly occurs through recombination.[6]

The comparison between batch and semi-batch starved emulsion polymerization made by do Amaral et Asua[7] showed that, because of the combined effect of the high polymer concentration and high average number of radicals per particle, the amount of gel formed in the starved process was higher than for the batch system. On the other hand, the molecular weights of the sol fraction produced in the starved process were lower than that of the batch process because the long chains were more easily swept up by the gel.

The possible control of the copolymer composition is for a part at the origin of the choice of this *semi-batch emulsion polymerization process operated under monomer-starved conditions* for the synthesis of wb-PSA within the NsHAPe project.

Besides the composition but related to, such processes provide great versatility for control of latex particles properties at larger scales than the molecular one, particularly particle size and size distribution and particle morphology. Figure 1-14 shows some examples of particle morphologies that can be achieved.

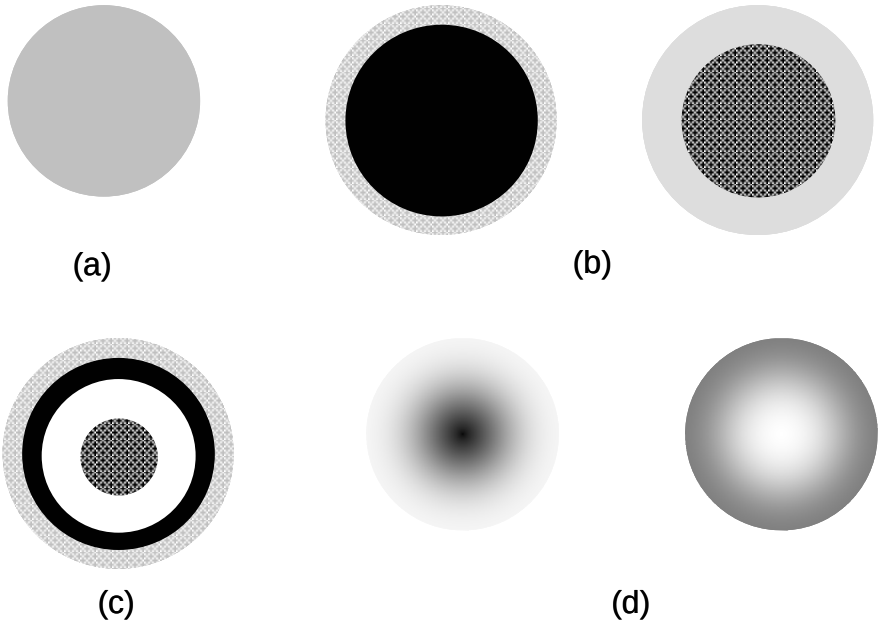

Figure 1-14. Examples of latex particle morphologies that can be synthesized by semi-continuous emulsion polymerization operated under monomer-starved conditions. (a) homogeneous, (b) core-shell, (c) multi-layer, and (d) radially-varying composition. Particle diameters are typically in the 100-400 nm range and layer thicknesses can be controlled to a few nanometers.

Finally, from an industrial point of view, this process is realistic in terms of its ability to be scaled-up for commercial production.

1.4.2. Miniemulsion polymerization

A second process, the *miniemulsion polymerization* process, has been selected for the synthesis of the materials. It has been used more specifically for the production of in-situ tackified waterborne PSA particles. A brief description of the miniemulsion process and some of its characteristics follow.

In conventional emulsion polymerization, nucleation mechanism arises most of the time in micelles or water. Less likely is the third mechanism where a radical may be captured by a monomer droplet to form a particle due to the difference in the surface/volume ratio of monomer droplets and monomer-swollen micelles. On the other hand, droplet nucleation is the dominant mechanism of nucleation in miniemulsion polymerizations.[8-10]

Miniemulsion is a system where small droplets with high stability in a continuous phase are created by using high shear. To create such a state, the droplets must be stabilized both against molecular diffusion degradation (Ostwald ripening, a monomolecular diffusion process) and against coalescence by collisions (a bimolecular process). In creating a miniemulsion, diffusional stabilization is achieved by adding a small quantity of a highly monomer-soluble and water-insoluble agent. This agent cannot diffuse from the droplet to the other and is trapped in each droplet, thus providing an osmotic pressure inside the

droplets, which counteracts the Laplace pressure. Coalescence can be controlled by the effective use of a surfactant.

For a typical oil-in-water miniemulsion, an oil, a hydrophobic agent (or several), an emulsifier, and water are homogenized by high shear to obtain homogeneous and monodisperse droplets in the size range of 30 to 500 nm. The idea of miniemulsion polymerization is to initiate the polymerization in each of the small stabilized monomer droplets meaning that polymerization takes place in small nanodroplets (Figure 1-15).

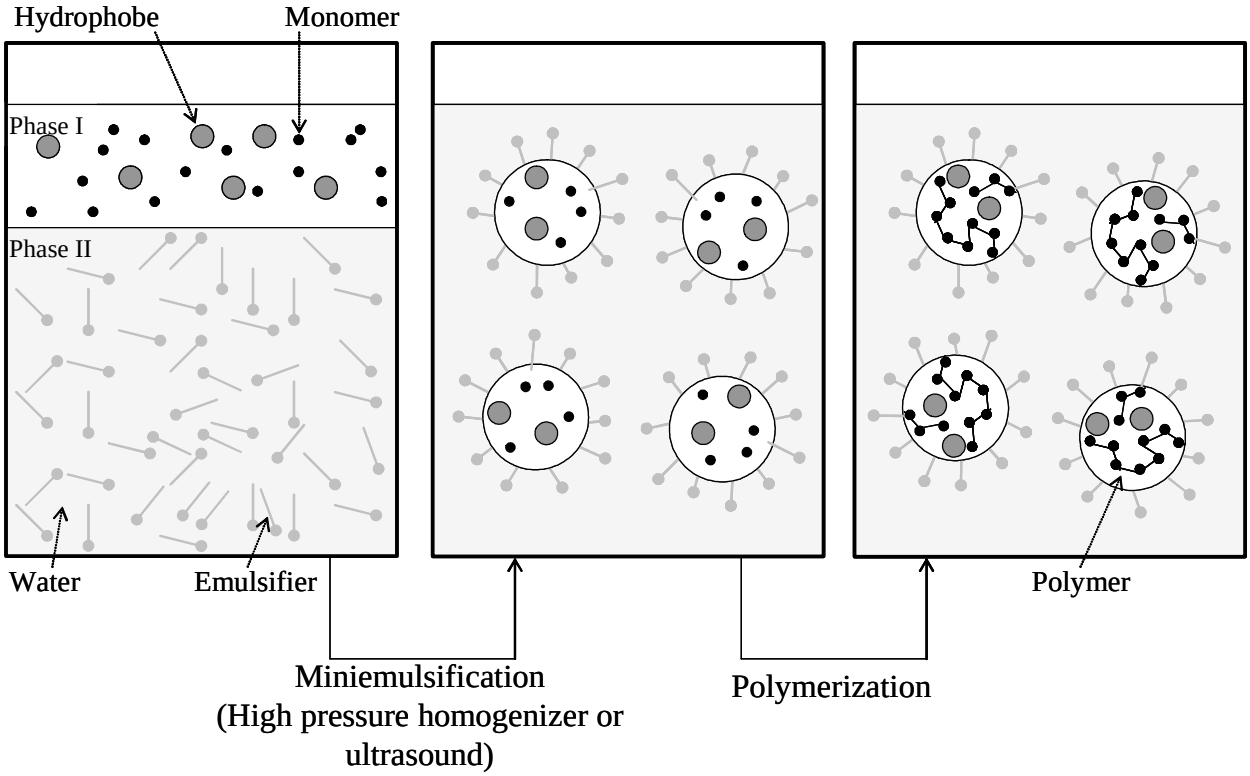

Figure 1-15. The principle of miniemulsion polymerization.

The differences between conventional emulsion (the simpler term "emulsion polymerization" is used later) polymerization and miniemulsion polymerization are obvious. In emulsion polymerization, the latex particle does not correspond to the primary emulsion droplet, and the size is established by kinetic processes where kinetic parameters, such as temperature or the amount or initiator play a fundamental role. These factors remain unseen in miniemulsion polymerization where the latexes are essentially a polymerized copy of the original droplets, the size of which is essentially given by dispersion process and droplet stability, not by polymerization parameters.

Miniemulsion polymerization enables to incorporate water-insoluble components such as tackifying resins. During the reaction, the resin can act as hydrophobe and stabilizes the stabilization of the miniemulsion. In miniemulsion polymerizations carried out with acrylic monomers in the presence of an alkyd resin, it was found that resin is grafted onto the polyacrylate.[11] Polymerizing acrylic monomers in the presence of reactive polyurethane also leads to a grafting onto the polyacrylics.[12] The presence of an unsaturated resin was found to favor chain transfer reactions.[13]

1.4.3. Latex characterization techniques

We already know how latex polymer particles are produced. At the end of the synthesis, a milky fluid is obtained. It is now useful to know how latex is characterized in its liquid state.

1.4.3.1. Particle size

The most important fundamental property of a latex, from the colloidal standpoint, is the particle size and its distribution. They can have a great effect on the physical properties of dispersions. Dynamic light scattering, also known as quasi-elastic light scattering (QELS), is usually used to determine the particle size and size distribution of colloidal particles. Particles that are dispersed in a liquid undergo random movement caused by their bombardment by liquid molecules, with smaller particles "diffusing" through fluid faster than larger particles. This phenomenon is termed *Brownian motion* after its discoverer Robert Brown, and can be used to determine the size of the constituent particles. If a coherent and vertically polarized source, such as a laser, shines on the latex, concentration fluctuations give rise to scattered intensity fluctuations. Variation in the intensity of the light scattered by the particles can be detected at any time by a single photon counting detector, and the size of the particles are derived using an autocorrelator and mathematical algorithms.

Typically, diameter of latex particles studied is about 250 nm.

1.4.3.2. Solid content and viscosity

A last latex characteristic of interest is its *solid content*. The solid content of latex is commonly measured gravimetrically. High solid content latexes offer numerous advantages for most in commercial applications, e.g. lower shipping costs and less water to be removed. Ideal solid content lies between 50 and 55 wt%.

The viscosity of a synthetic latex is ordinarily measured with a rotating cynlinders viscosimeter, such as the Brookfield model. Since latex is a non-Newtonian fluid, its viscosity is shear dependent.

Typical values of viscosity are about 200 mPa.s at 50 rpm and 5000 mPa.s at 0.5 rpm.

In practice, the solid content of a latex is limited by its viscosity. For a monodisperse latex, viscosity approaches infinity as the volume fraction of the polymer particles approaches 0.64. On the other hand, polydisperse latexes show a lower viscosity, because the small particles fit within the voids of the array of the big particles.[14]

1.5. Film formation from the colloidal particles of the latex

In the previous section we showed how polymer latexes are synthesized and we described some of their properties in the liquid state. In this part, we explain the mechanisms which occur during the drying and how these aqueous dispersions of polymer particles are transformed into a continuous dry material. We describe drying stages and outline how mechanisms can be affected by the characteristics of the polymer chains of which latex particles are made. Further information and details can be found in the review article of Keddie about *film formation process.*[15]

1.5.1. Film formation mechanism

When a latex dispersion is deposited on a substrate and evaporation is allowed to proceed, a continuous, homogeneous film is formed. This process is called *film formation*. During the synthesis, great effort is spent to keep particles separated and deflocculated in order to obtain a stable dispersion. During film formation, however, these same particles must overcome their mutual repulsion in order to form a continuous film.

There are three primary physical processes, or stages, that occur during film formation.

1. Evaporation of water and particle ordering.
2. Particle deformation.
3. Interdiffusion of polymers across particle-particle boundary.

These stages are schematized in Figure 1-16 and are described in the following.

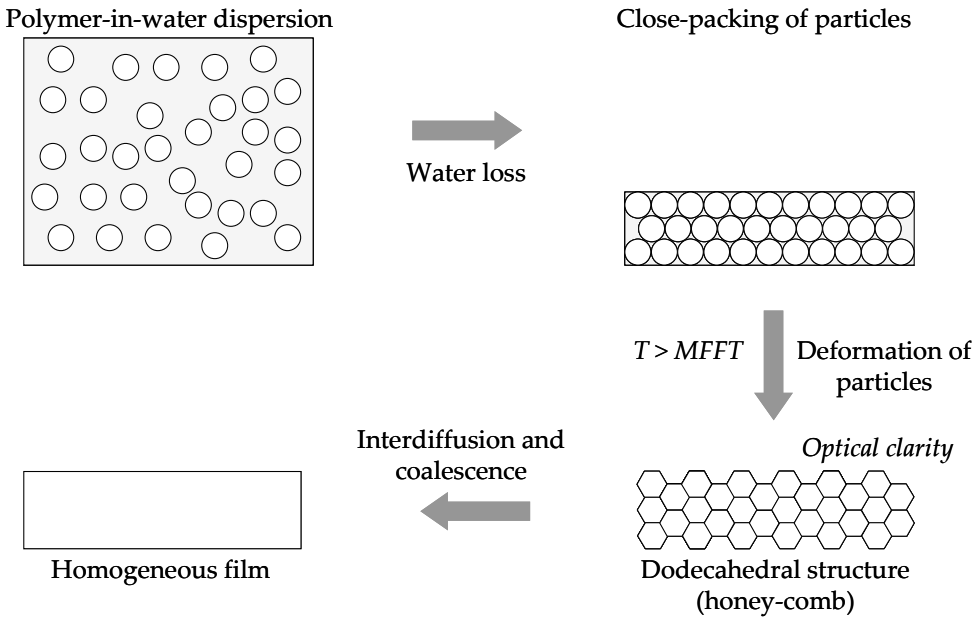

Figure 1-16. Idealized view of latex film formation.

Before detailing the stages, an important property of a latex is its *minimum film formation temperature* (MFFT). The formation of a continuous film (i.e. transparent and crack free) at a given temperature depends on this MFFT which in turns depends on the mechanical properties of the polymer. For a homogeneous polymer, it is typically within a few degrees

of the *glass transition* of the polymer. If the film is cast above its MFFT, then coalescence of the latex particles can occur. However, if the film is below its MFFT, then a friable discontinuous film or powder compact may form, which is optically opaque.

1. Evaporation of water and particle ordering

The first stage of the film formation process refers to the process of *evaporation of water* accompanied by *particle ordering*. The ordered arrays of particles are created by the convective particle transport. Two processes of drying have been reported. In a process referred to as *lateral drying*,[16] the solids fraction near the center remains close to the initial value while a region of high solids content develops at the edge. At later times, a drying front moves inward from the edges. Drying films of latexes have known values of thickness, particle size and surface tension which are encapsulated in an expression for the reduced capillary pressure, p_c. Capillary pressure can pin the water at the film edge, thus, higher p_c (larger particles, slower evaporation rates, and thinner films) encourages more uniform lateral drying.

In the *vertical drying*,[17] the fraction of solids increases relatively uniformly or to only a limit extent in the lateral direction. In that case, it has been shown that the vertical uniformity of water distribution depends on the *Peclet number Pe* defined for the system studied. There is a competition between Brownian diffusion that re-distributes particles and evaporation that causes particles to accumulate at the surface. The Peclet number in the case of the film formation from colloidal particles of latex is defined as:

$$P_e = \frac{HE}{D_0} \qquad \textbf{Eq. 1-5}$$

where H is the thickness of the wet film, E is the rate of evaporation and D0, the Brownian diffusion (Figure 1-17).

When *Pe*<<1 the water concentration tends to be uniform while when *Pe*>>1 a gradient develops, with less water near the interface with air. Cases where non uniform drying occurs are schematized in Figure 1-17.

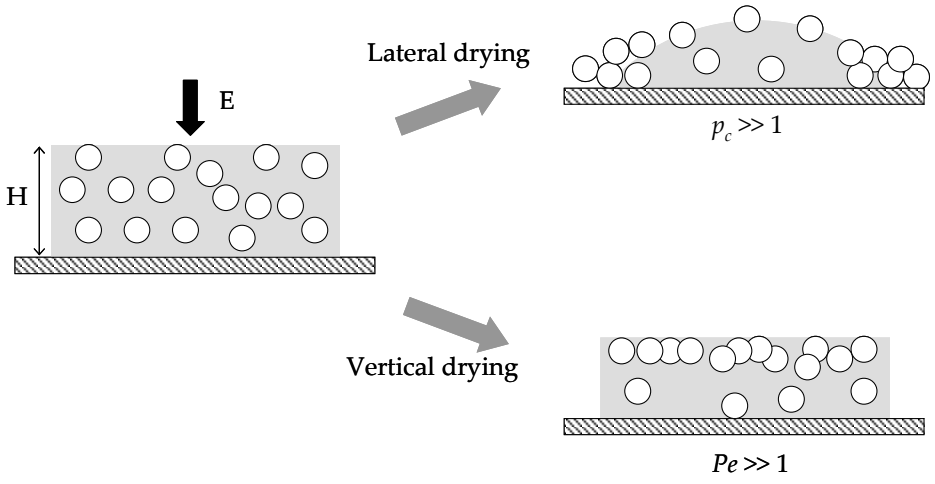

Figure 1-17. Two typical situations which can occur during water evaporation through lateral and vertical drying processes.

2. Particle deformation

We now consider the second stage which corresponds to *particle deformation*. From the various studies performed on this subject, it appears that possible causes of particle deformation include air/water, water/polymer, or polymer/air interfacial tensions, osmotic force or surface adhesive forces as shown on Figure 1-18. There exist three particle deformation mechanisms.[18] *Wet sintering* occurs when particles are deformed before water has evaporated and reduction of the polymer/water interfacial energy is the driving force. *Dry sintering* occurs when water recedes before particles are deformed and reduction of the polymer/air interfacial energy is the driving force. Another particle formation mechanism results from the *capillary forces*.

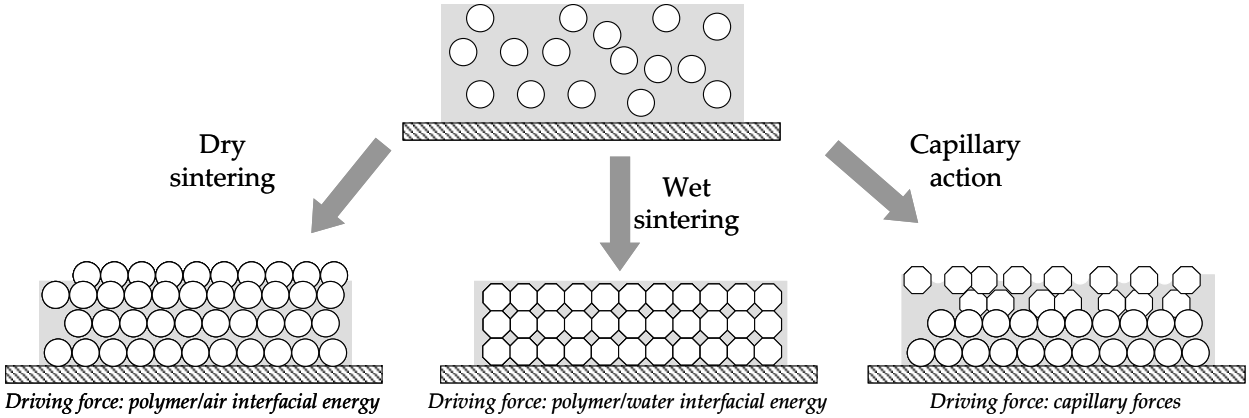

Figure 1-18. Particle deformation mechanisms: dry sintering, wet sintering and drying through the capillary action.

In cases in which the water distribution is non-uniform and in which *wet sintering* is favored, *skin formation* is predicted to occur as shown in Figure 1-19.

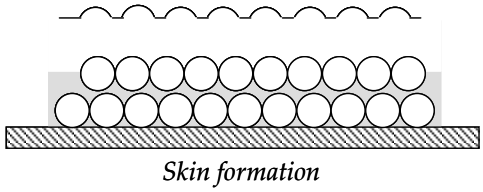

Figure 1-19. Skin formation.

We have described mechanisms which occur during the particle ordering and deformation. We have shown that depending on the drying system characteristics, drying non uniformities can occur. These non uniformities have some impact on the final quality of dried films. They can be at the origin of some crack defects or of the non transparency.

At the end of this second stage, the film is still mechanically weak. A reinforcement of the interfaces that give strength of the film occurs during the third stage presented below.

3. Interdiffusion of polymers across particle-particle boundary.

Coalescence means the union of two particles to reduce their surface area. After coalescence, the boundary between particles no longer exists. Therefore, to achieve coalescence, polymer molecules must diffuse across the boundary between particles. If the molecules entangle over a distance on the order of the *radius of gyration* of the polymer[(1)], then the film is strong. Otherwise, the boundaries can be weak.

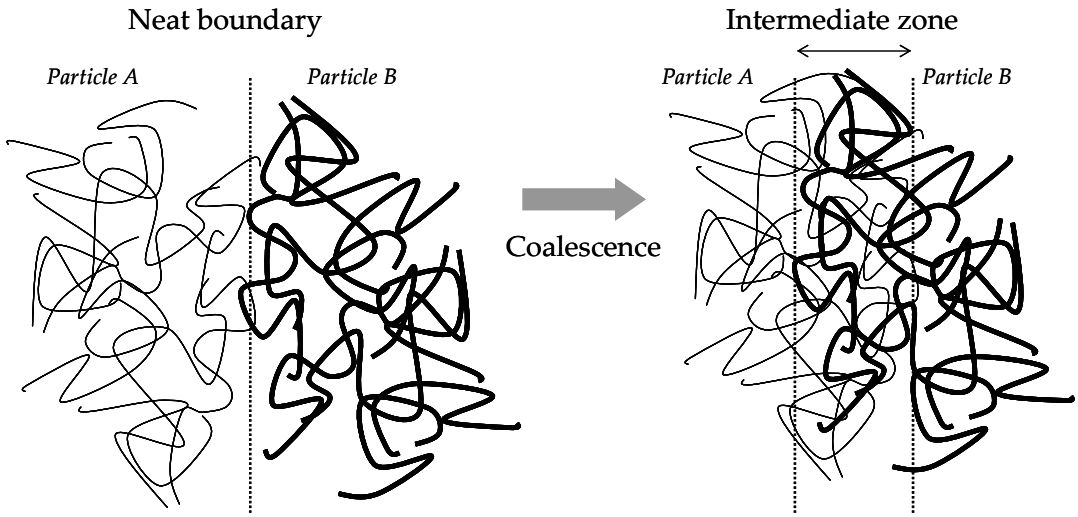

Figure 1-20. Entanglement formation at the polymer / polymer interface.

Coalescence of the particles is thus controlled by the *diffusivity* of polymer molecules. *Diffusivity D* depends on several factors like the molecular weight ($D \sim 1/M^2$), the temperature ($D = D_0 \exp(-E/RT)$[(2)]), the nature of the particle membranes (for instance the presence of hydrophilic acrylic acid[19]) since these membranes must break-up to enable interdiffusion.

Diffusion depends also on the gel content of polymer particles and branching of polymer chains. Crosslinking can entirely prevent diffusion and molecular branching slows down diffusion. While in the case of free chains, diffusion occurs easily making the interfaces disappear, diffusion is limited between gel particles as shown in Figure 1-21.

(1) The dimensions of linear chains are often characterized in terms of the root mean square of a chain segment from the center of mass of the molecule, which is known simply as the root mean square *radius of gyration*.

(2) D_0 is a constant, E is the activation energy, R is the constant gas and T is the temperature.

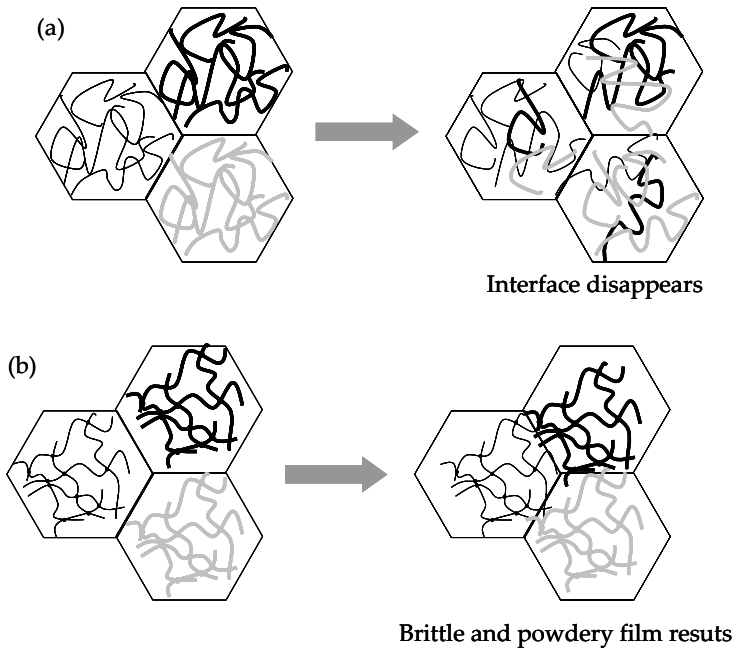

Figure 1-21. (a): Interdiffusion, mixing of polymer chains and disappearance of interface for free chains. (b): Limited interdiffusion between gel particles.

However, in some cases, interdiffusion can occur even for crosslinked particles. Some works demonstrated that the major parameter controlling interdiffusion is the polymer T_g. Zosel and Ley[20] examined the mechanical properties of films formed from lightly crosslinked poly(butyl methacrylate) (PBMA). They showed that unlike films prepared from linear PBMA, crosslinked films remained brittle and were unable to develop tensile strength. A rather different result was reported by Tamai et al.[21] who examined a series of P(BMA-BA) containing different amounts of ethylene glycol dimethylacrylate (EGDMA), a crosslinking agent. They found that tough elastomeric films were formed thanks to significant intercellular polymer diffusion even for latex particles containing 4 mol% crosslinker. The intercellular mixing is thought to be caused by diffusion of dangling polymer chains anchored in the crosslinked network. The major difference between the Zosel and Ley experiments and those of Tamai et al. is the T_g of the latex polymer. Tensile measurements were carried out below the T_g in the case of crosslinked PBMA and above the polymer T_g for P(BMA-BA-EGDMA).

To increase diffusivity, some coalescing aids exist. But in general, the use of *coalescing aids*[22] increases the volatile organic compounds (VOC) concentration of a waterborne system and should be minimized.

It has also be shown that surfactants and latex serum prevent particle coalescence.[23] Better coalescence is achieved when the latex has been "cleaned" via dialysis. However, surfactant transport mechanisms are still unclear. During the drying stage, surfactant must be either:

- Adsorbed on particle surfaces, where it moves along with the particles or…
- Diffusing in the latex serum or…
- Adsorbing on particles, described by adsorption isotherm or…
- Desorbing from particles, as particles compact together.

1.5.2. Drying of core-shell latex particles

An alternative solution to the use of coalescing aids and widely used for the drying of coatings is to use tailored core-shell particles with a soft shell having a better ability for film forming than the hard core.[24] This improvement of film forming is possible since core-shell particles maintain their structure during film formation. More generally, after drying, nanostructured particles form nanostructured polymer films. This has been observed by Schellenberg et al.[25] in the case of core-shell structured latexes consisting of poly(ethyl hexyl methacrylate) (PEHMA) for the core and crosslinked poly(n-butyl acrylate) (PnBA) for the shell. On Figure 1-22-a is shown a transmission electron microscopy (TEM) image obtained on the polymer film of the original undiluted core-shell latex with RuO_4 staining. The core-shell morphology is clearly resolved; the crosslinked shell is darker than the core because of staining of the crosslinker molecules. In addition the picture made by the cryo-TEM (Figure 1-22-b) confirms the structural uniformity of the original latexes.

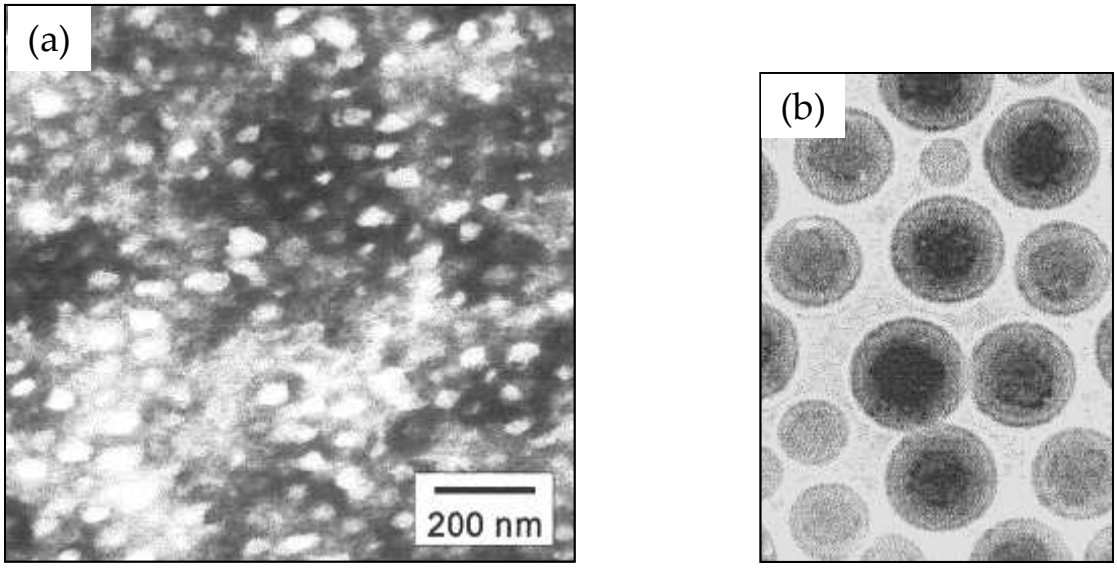

Figure 1-22. (a): TEM of ultrathin section of the polymer film made of PEHMA-crosslinked PnBA core-shell particles. (b): Cryo-TEM of a diluted latex (same original latex as (a)) (after [25]).

An important conclusion of this study is that it is possible to adjust mechanical properties when using a well defined nanostructured polymer networks. Mechanical properties are precisely the object of the part which follows.

1.6. Elasticity and Viscoelasticity

We have shown how a solid layer of polymer is obtained after the drying of an aqueous dispersion by evaporation of water. These latexes dry by evaporation of water, leaving behind a solid layer of polymer. For final adhesive applications, the properties of these dried films are the most important. Adhesive films are soft and highly deformable and can sustain a certain level of stress with limited or no flow. This type of behavior directly comes from the unique mechanical properties of the lightly crosslinked network of polymer chains. In this part, some basic mechanical properties of polymer are presented.

A polymer above its T_g displays *entropic elasticity*. If it deforms under stress, it then returns to its original shape when the stress is removed. Unlike purely elastic materials, a *viscoelastic* polymer has an elastic component and a viscous component. It loses energy when a load is applied, then removed and a hysteresis is observed in the stress-strain curve.

We start with some considerations about *elasticity*. We continue with the presentation of the more complicated *viscoelastic* behavior.

1.6.1. Elasticity

1.6.1.1. Thermodynamics of elastomer deformation

We have seen that most of the time crosslinking reaction inherently occurs during emulsion polymerization process. The presence of crosslinks is at the origin of the elastic behavior of the material produced. When extended to several times its original length, an elastic strip will return to that original length exhibiting little or no permanent deformation as a result of the extension. Its deformation is *reversible*. Without crosslinks, the applied stress would result in a permanent deformation. In such materials, chains between crosslinks are mobile but only over a distance of the order of the average distance between crosslinks. We have effectively a liquid at the local scale but a solid at the macroscopic scale. Such materials are called *elastomers*. Elastomers are crosslinked amorphous flexible polymers considered above their glass transition temperature.

At small strains, most solid polymers exhibit a "*linear elastic behavior*" which means that there is a linear relationship between the components of stress and strain. Linear elastic solids follow *Hooke's law*:

$$\sigma = E\varepsilon \qquad \textbf{Eq. 1-6}$$

where σ is the stress (force over the area), ε is the deformation (defined as $(L-L_0)/L_0$ with L_0 and L the initial and actual length of the sample respectively) and E is called the *Young's modulus*. The elasticity is internal energy-controlled and the potential energy stored is given by:

$$U = \frac{1}{2}kx^2 \qquad \textbf{Eq. 1-7}$$

where k is the spring constant and x the distance that the spring has been stretched away from the equilibrium position.

Behavior of elastomers which are able to stretch to several times their initial length is different. In the range of high deformations, energy controlled linear elastic properties are no more applicable. Properties of elastomeric materials are controlled by their molecular structure. And it was observed that an elastomer behaves essentially as an "entropic spring" and that elastomer deformation is particularly amenable to analysis using thermodynamics. Stretching a sample of rubber provides heat and a stretched sample of rubber contracts under heating.

The first law of thermodynamics establishes the relationship between the change in internal energy of the system dU and the heat đQ absorbed by the system and the work đW done by the system as:

$$\mathrm{d}U = đQ - đW \qquad \textbf{Eq. 1-8}$$

the bars of đ indicates that đQ and đW are inexact differentials because Q and W, unlike U are not macroscopic functions of the system.

If the length of an elastic specimen is increased a small amount dl by a tensile force f, then the amount of work fdl will be done on the system. There is also a change in volume dV during the elastic deformation and work PdV is done against the pressure, P. Since elastomers deform at roughly constant volume the contribution of PdV to đW at ambient pressure will be small and so the work done by the system when it is extended is $-f$dl.

The deformation of elastomers can be considered as a reversible process and so đQ can be evaluated from the second law of thermodynamics which states that for a reversible process:

$$đQ = T\mathrm{d}S \qquad \textbf{Eq. 1-9}$$

where T is the thermodynamic temperature and dS is the change in entropy of the system. This leads to:

$$f\mathrm{d}l = \mathrm{d}U - T\mathrm{d}S \qquad \textbf{Eq. 1-10}$$

For the free energy F:

$$\mathrm{d}F = \mathrm{d}U - T\mathrm{d}S = f\mathrm{d}l - S\mathrm{d}T \qquad \textbf{Eq. 1-11}$$

under conditions of constant temperature.

Combining Eq. 1-10 and Eq. 1-11 and taking into account the standard relation for partial differentiation one obtains:

$$\mathrm{f} = \left(\frac{\partial \mathrm{F}}{\partial \mathrm{l}}\right)_{\mathrm{T}} = \left(\frac{\partial \mathrm{U}}{\partial \mathrm{l}}\right)_{\mathrm{T}} - \mathrm{T}\left(\frac{\partial \mathrm{S}}{\partial \mathrm{l}}\right)_{\mathrm{T}} = \left(\frac{\partial \mathrm{U}}{\partial \mathrm{l}}\right)_{\mathrm{T}} - \mathrm{T}\left(\frac{\partial \mathrm{f}}{\partial \mathrm{T}}\right)_{\mathrm{l}} \qquad \textbf{Eq. 1-12}$$

To compare the ideal rubber with the ideal gas, we note that Eq. 1-12 resembles the relation:

$$-\mathrm{P} = \left(\frac{\partial \mathrm{U}}{\partial \mathrm{V}}\right)_{\mathrm{T}} - \mathrm{T}\left(\frac{\partial \mathrm{S}}{\partial \mathrm{V}}\right)_{\mathrm{T}} \qquad \textbf{Eq. 1-13}$$

For ideal gases, the internal energy is independent of volume. By analogy, the ideal rubber may be looked at in the same way and its internal energy is independent of elongation and the stress can be attributed to the configurational entropy alone.

1.6.1.2. Statistics of ideal rubber elasticity

From the molecular point of view, the simplest way to represent an isolated flexible polymer chain is the "*Brownian random walk*" of *n* steps in a periodic lattice. The simplest way to describe a polymer chain is the ideal (or *freely jointed chain*) chain model. It only assumes a polymer chain as a random walk and neglects interactions between monomers (Figure 1-23).

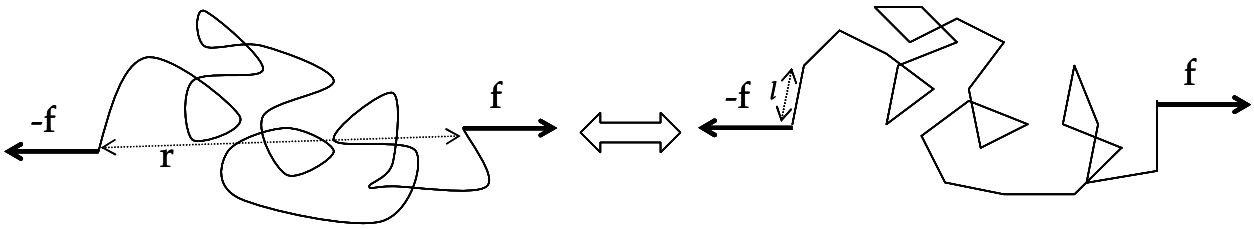

Figure 1-23. Representation of a real polymer chain as an assembly of n rigid rods of a fixed length *l*. K is the force applied to the chain at each end.

At each step, the probability for a segment to choose one of the neighboring sites is the same. Therefore, the average end-to-end distance $\langle r_0^2 \rangle$ is:

$$\langle r_0^2 \rangle = nl^2 \qquad \textbf{Eq. 1-14}$$

Where *n* is the number of monomers and *l* the size of each monomer, and < > indicates that the quantity is averaged over time.

The number of possible arrangements of segments within a random coil characterized by an end-to-end distance equal to r is:

$$\omega(r) = \omega_0 \exp\left(-\frac{3r^2}{2\langle r_0^2 \rangle}\right) \qquad \textbf{Eq. 1-15}$$

with ω_0 the number of arrangements when r = 0.
The entropy associated to all chains with the end-to-end distance r is:

$$S(r) = k\ln\omega(r) = k\ln\omega_0 - \left(\frac{3kr^2}{2\langle r_0^2 \rangle}\right) \qquad \textbf{Eq. 1-16}$$

with k the Boltzmann constant.
The free energy of the ideal chain is then:

$$F = F_0 + T\left(\frac{3kr^2}{2\langle r_0^2 \rangle}\right) \qquad \textbf{Eq. 1-17}$$

The simplest mechanical theory of rubber elasticity, the *affine model*, considers that each crosslink is deformed exactly in the same way as the macroscopic sample (Figure 1-24). Note that the polymer chains between behave like random coils and follow the Gaussian statistics.

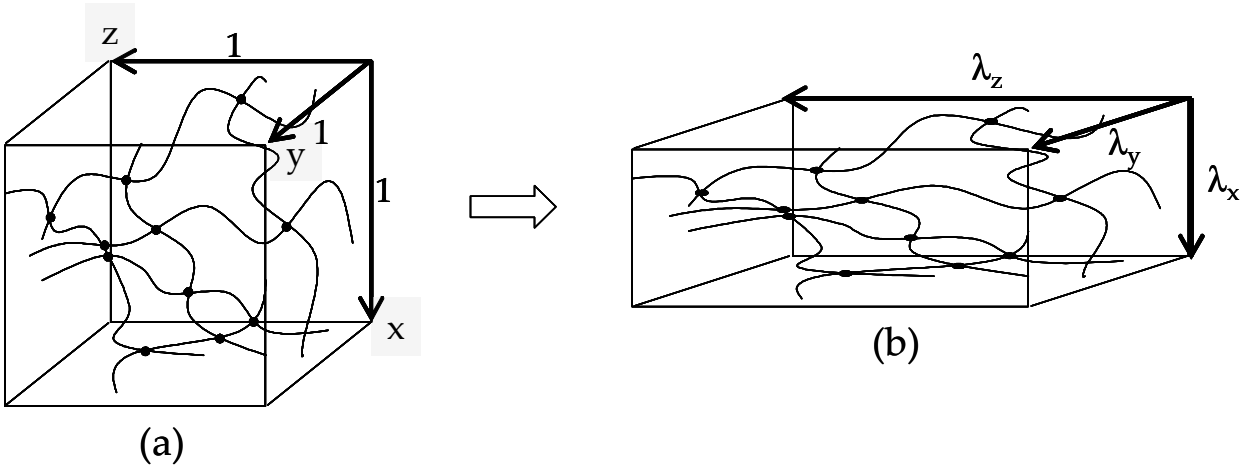

Figure 1-24. (a) Ideal representation of the non deformed crosslinked network. (b) Same network after deformation, stretching along direction z.

The affine model also assumes that the deformation occurs under constant volume. This means that $\lambda_x\lambda_y\lambda_z=1$ (where λi is the deformation along direction "i" and is defined as L_i/L_{i0} with L_i, the length of the sample along direction "i").
The force f (Figure 1-23) applied to each ideal network chain is derived from the entropy (Eq. 1-12 and internal energy is independent of elongation):

$$f = -T\left(\frac{dS}{dr}\right)_T \qquad \textbf{Eq. 1-18}$$

In a three-dimensional network, a network chain is defined as the polymer portion between two crosslinks. For a network constituted of N network chains per unit volume:

$$S_{network} = NS_{chain} \qquad \textbf{Eq. 1-19}$$

If the sample is submitted to the deformations λ_x, λ_y and λ_z in the three directions, the network chains are submitted to the same deformations and:

$$\Delta S = S_{stretched} - S_{at\ rest} = -\frac{1}{2}Nk(\lambda_x^2 + \lambda_y^2 + \lambda_z^2 - 3) \qquad \textbf{Eq. 1-20}$$

In the case of a uniaxial elongation along direction z and considering a constant volume:
$\lambda_z = \lambda$
$\lambda_x = \lambda_y = (1/\lambda)^{1/2}$

$$\Delta S = -\frac{1}{2}Nk(\lambda^2 + \frac{2}{\lambda} - 3) \qquad \textbf{Eq. 1-21}$$

From the above equation is derived the force f:

$$f = \frac{1}{2l_0}NkT(\lambda - \frac{1}{\lambda^2}) \qquad \textbf{Eq. 1-22}$$

with l_0 the initial length of the sample.

The nominal stress σ_N is the force per unit initial cross-sectional area A_0, and the true stress σ_T is defined as the force per the effective cross-sectional area $A=A_0/\lambda$. Thus expressions of σ_N and σ_T are as follows:

$$\sigma_N = \frac{1}{2V_0} NkT(\lambda - \frac{1}{\lambda^2})$$

$$\sigma_T = \frac{1}{2V_0} NkT(\lambda^2 - \frac{1}{\lambda}) \qquad \textbf{Eq. 1-23}$$

where V_0 is the initial volume of the sample.

Eq. 1-23 is known as the *neo-Hookean equation* from which the *shear modulus G* can be defined:

$$G = NkT/V_0 = \nu kT \qquad \textbf{Eq. 1-24}$$

Where ν is the number of cross-links per unit volume.

In the affine model, crosslinks are supposed to be fixed and are only allowed to deform exactly in the same way as the macroscopic sample. The *phantom network model* is a generalization of the affine model where crosslinks are allowed to fluctuate around average positions. If Φ is the functionality of the network,

$$\sigma_N = \nu kT\left(1 - \frac{2}{\Phi}\right)\left(\lambda - \frac{1}{\lambda^2}\right) \qquad \textbf{Eq. 1-25}$$

For a functionality of four, the shear modulus predicted by the phantom network is half that of the affine network.

This molecular model however does not take into account defects present in a real network like pendant chains, loops, entanglements…(Figure 1-25).

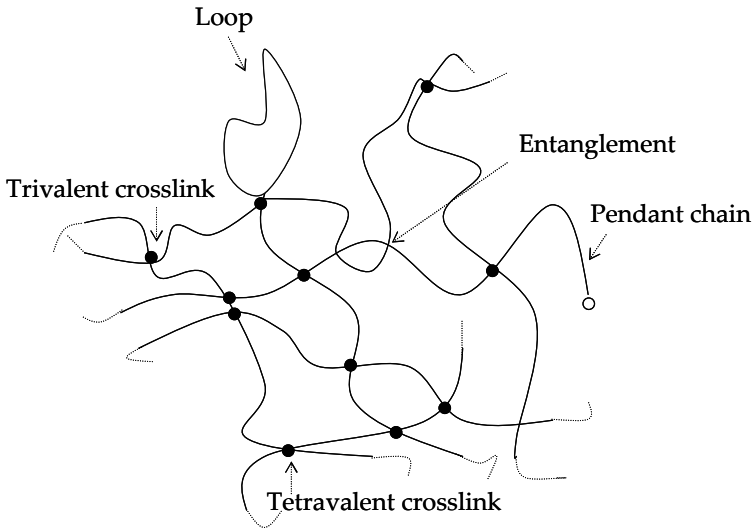

Figure 1-25. Molecular structure of a real network.

The approximations implicit in the use of the Gaussian network model for soft rubber were widely discussed by James and Guth.[26]

1.6.1.3. Mooney Rivlin phenomenological model

In practice, either the affine model or the phantom model is not well suited for the prediction of the behavior of real materials. In general, the affine model is well adapted for the small strain behavior description when fluctuations of crosslinks are hindered. At large strains, however, chains tend to disentangle and the phantom model is more adapted to describe this decrease in the modulus (Figure 1-26). Some phenomenological alternatives to the previous molecular models exist. The Mooney-Rivlin model is one of the models proposed and is described in more details in this part.

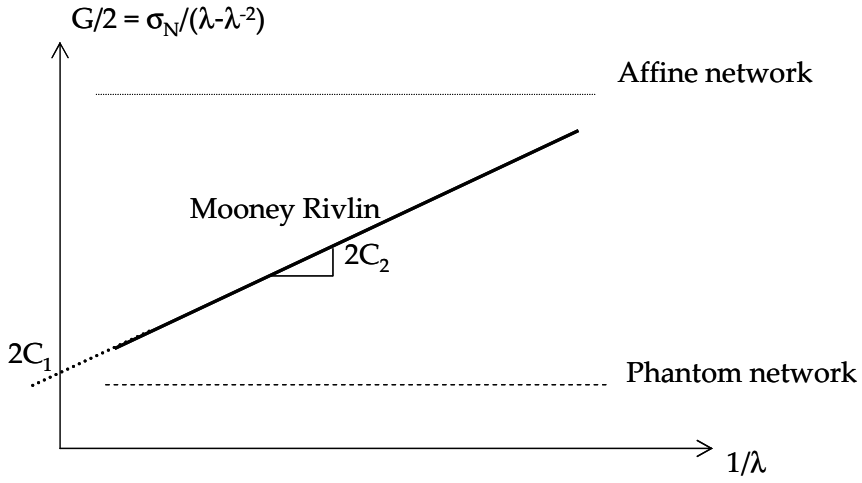

Figure 1-26. Affine and phantom network models and Mooney-Rivlin curve.

The Mooney Rivlin model is a phenomenological model first proposed by Mooney[27] and further developed by Rivlin which is based on the incompressibility and isotropic conditions and introduces a λ dependent term in the modulus.

The starting point of the Mooney Rivlin model is the three first invariants called I_1, I_2 and I_3.

$I_1 = \lambda_x^2+\lambda_y^2+\lambda_z^2$

$I_2 = \lambda_x^2\lambda_y^2+ \lambda_y^2\lambda_z^2+\lambda_z^2 \lambda_x^2$

$I_3 = \lambda_x^2\lambda_y^2\lambda_z^2$

The free energy density of the network $\Delta W/V = -T\Delta S/V$ is written as a power series of differences between these three invariants and their values at initial state:

$$\frac{\Delta W}{V} = C_0 + C_1(I_1 - 3) + C_2(I_2 - 3) + C_3(I_3 - 1) + \ldots \qquad \textbf{Eq. 1-26}$$

For uniaxial elongation along direction z, and if the power series is limited to the first three terms:

$$\frac{\Delta W}{V} = C_0 + C_1(\lambda^2 + \frac{2}{\lambda} - 3) + C_2(2\lambda + \frac{1}{\lambda^2} - 3) \qquad \textbf{Eq. 1-27}$$

This leads to the following expression of the nominal stress:

$$\sigma_N = 2\left(C_1 + \frac{C_2}{\lambda}\right)\left(\lambda - \frac{1}{\lambda^2}\right) \quad \textbf{Eq. 1-28}$$

C_1 and C_2 are two material constants.
The reduced stress σ_R is then defined as:

$$\sigma_R = \frac{\sigma_N}{\lambda - \frac{1}{\lambda^2}} = 2\left(C_1 + \frac{C_2}{\lambda}\right) \quad \textbf{Eq. 1-29}$$

The Mooney-Rivlin representation is commonly defined as the plot representing the reduced stress as a function of $1/\lambda$.
When $C_2=0$, the classical neo-hookean equation is retrieved and $2C_1$ corresponds to the shear modulus G.
When $C_2>0$, a decrease in the modulus as the deformation increases is observed. This is a signature of a softening experimentally observed for numerous real elastomers.

1.6.1.4. Gent phenomenological model

At high strain, the maximal deformation of the polymer network is limited by the finite extensibility of the polymer chains between crosslinks (Figure 1-27) and an increase in the stress also called *hardening* is observed.

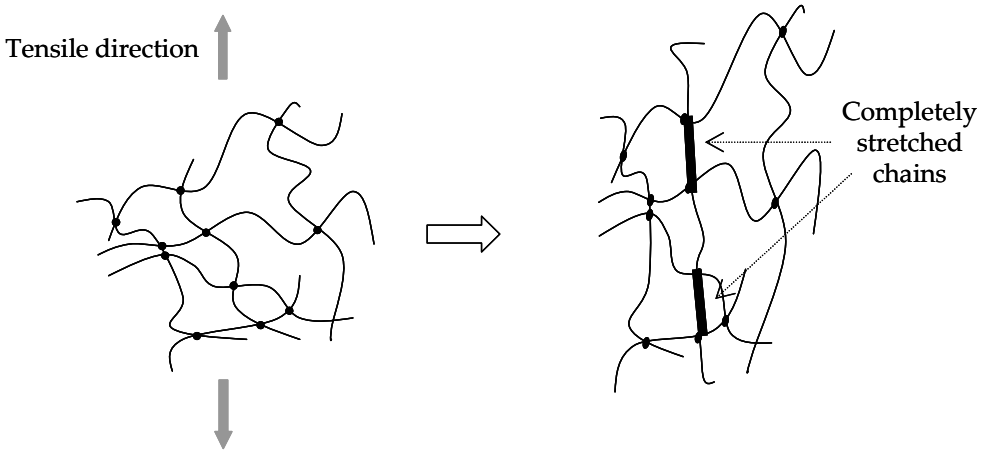

Figure 1-27. Schematics of the maximal extensibility of stretched polymer chains.

Neither the Neo-Hookean equation nor the Mooney-Rivlin equation is able to predict such behavior at ultimate strains as shown on Figure 1-28 (a comparison between experimental tensile stress-strain data from Treloar[28] is also shown in Figure b). An obvious limitation of the elementary statistical theory is the assumption of Gaussian chain statistics which does not predict any finite extensibility of polymer chains. At high strains, polymer chains are not organized as random coils and orient themselves along the direction of the elongation. The Gaussian assumption is not valid at large strains when the chains approach

their limiting stretched states. It is valid only for end-to-end distance much inferior to the maximal end-to-end distance R_{max} (i.e. $\langle r_0^2 \rangle \ll R_{max} = nl$).
The observed hardening results from the divergence at R_{max} of the force required to stretch the chain due to the finite extensibility of polymer chains.

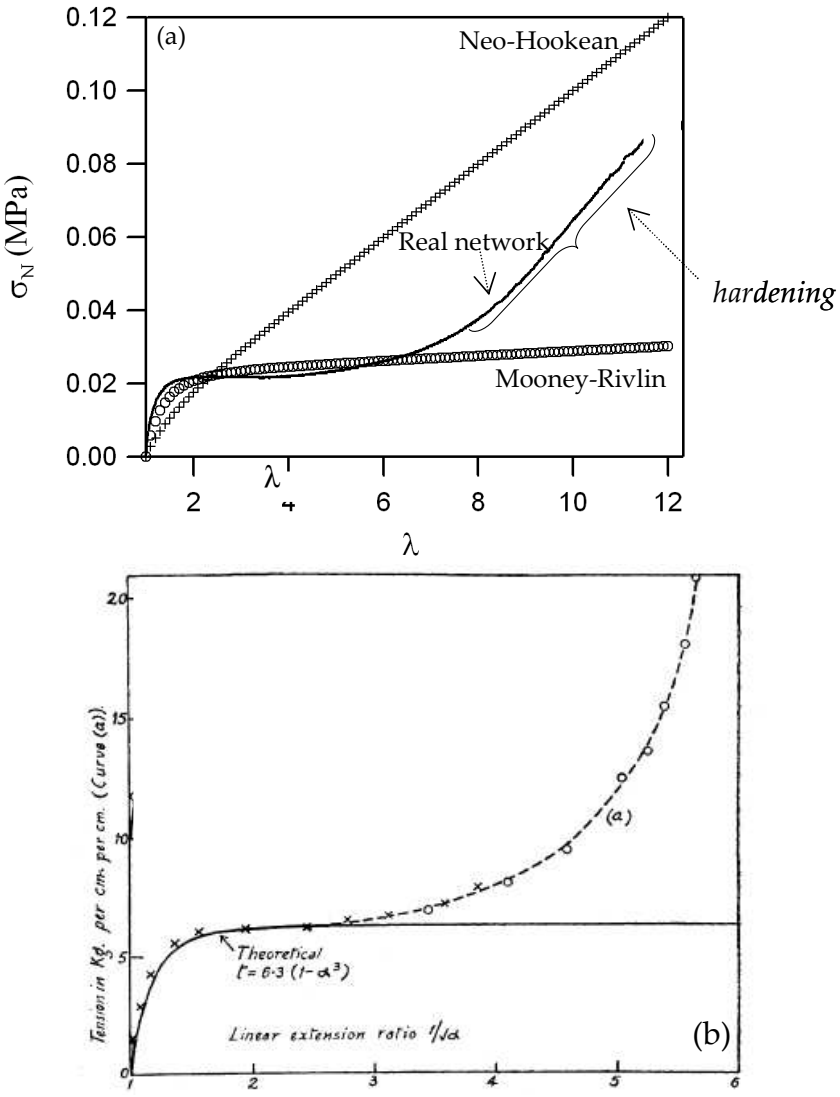

Figure 1-28. (a) Comparison between a typical stress-strain curve of a real network with the Neo-Hookean and Mooney-Rivlin equations. (b) 2-dimensional extension of a latex rubber at 50°C(after [28]).

A large number of models (molecular and phenomenological) have been proposed for the description of the hardening. Within the framework of the phenomenological theory similar models have been obtained on considering the idea of limiting chain extensibility, i.e. by considering strain-energy density functions that have a singularity when the first invariant I_1 reaches a finite value I_1^*. The simplest model with limiting chain extensibility is due to Gent[29-31] who proposed the strain-energy density:

$$W_I = -\frac{G}{2} J_m \ln\left(1 - \frac{I_1 - 3}{J_m}\right) \qquad \textbf{Eq. 1-30}$$

where G is the shear modulus for infinitesimal deformations and J_m is the constant limiting value for $J_1 = I_1-3$, taking into account limiting polymeric chain extensibility. When this polymer chain extensibility parameter tends to infinity, Eq. 1-30 reduces to the classical neo-Hookean form:

$$W = \frac{G}{2} J_1 \qquad \textbf{Eq. 1-31}$$

We can note that for a uniaxial elongation, $J_1 = \lambda^2+2/\lambda-3$ and $J_m = \lambda_m^2+2/\lambda_m-3$ with λ_m the maximal deformation equal to:

$$\lambda_m = \frac{R_{max}}{(< r_0^{\,2} >)^{1/2}} = n^{1/2} \qquad \textbf{Eq. 1-32}$$

where n is the number of monomers in the polymer chain.
From Eq. 1-31, the true stress ($\sigma_{Gent,T}$)-strain and nominal stress($\sigma_{Gent,N}$)-strain relations in the case of a unixial elongation are given by:

$$\sigma_{Gent,T} = G\frac{(\lambda^2 - 1/\lambda)}{\left(1-\frac{J_1}{J_m}\right)} \text{ and } \sigma_{Gent,N} = G\frac{(\lambda - 1/\lambda^2)}{\left(1-\frac{J_1}{J_m}\right)} \qquad \textbf{Eq. 1-33}$$

This simple relation describes well the experimental the high strain behavior of crosslinked networks using only two parameters *G* and J_m (Figure 1-29). As it is observed on Figure 1-29, if the large strain behavior is well predicted, the model fails for the description of the small strain behavior.

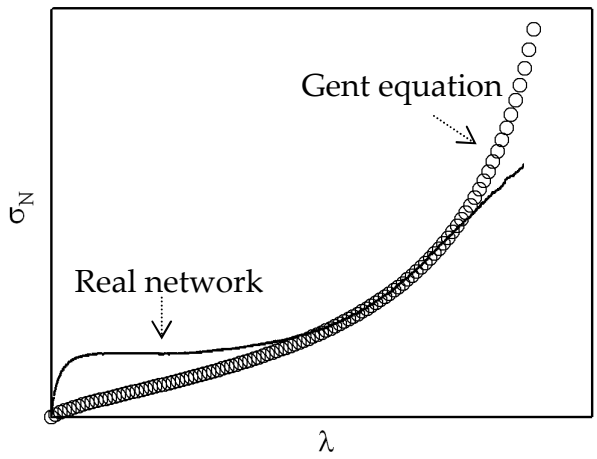

Figure 1-29. Comparison between the stress-strain curve of a real network and the curve obtained with the Gent equation.

1.6.2. Viscoelasticity

Up to now, we have discussed the origin of polymer elasticity and presented some of the models which can describe this behavior. However, in general, a polymeric material exhibits a behavior somewhere between that of a purely elastic solids (which obeys the *Hooke's law*, see Eq. 1-6) and a purely liquid. The behavior of viscous liquid will not be studied in detail: we just say that it is time dependent and that it can be represented by *Newton's law* whereby the stress is proportional to the strain-rate and independent of strain. *Newton's law* is given below:

$$\tau = \eta\dot{\gamma} \qquad \textbf{Eq.1-34}$$

where τ is the shear stress, η is the viscosity of the viscous liquid and $\dot{\gamma}$ is the strain rate.

At low temperatures and high strain rates, polymers display elastic behavior whereas at high temperatures and low strain rates they behave in a viscous manner. In between these extreme conditions, polymers are termed *viscoelastic* as it has both elastic (reversible) and viscous properties (dissipative).

A viscoelastic polymer which is quite solid does not maintain a constant deformation under constant stress but goes on slowly deforming with time or creeps (Figure 1-30-a). When such a material is constrained at constant deformation, the stress requires to hold it diminishes gradually, or *relaxes* (Figure 1-30-b).
On the other hand, a viscoelastic polymer which is quite liquid may, while flowing under constant stress, store some energy input, instead of dissipating it all as heat.

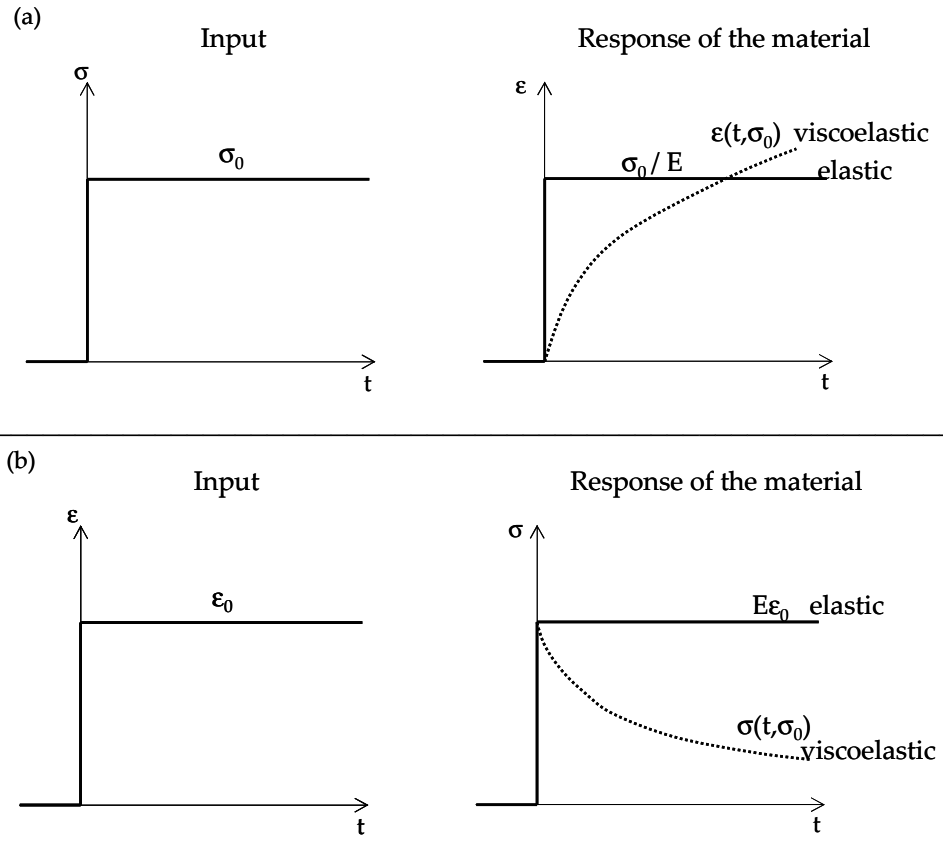

(Figure continued)

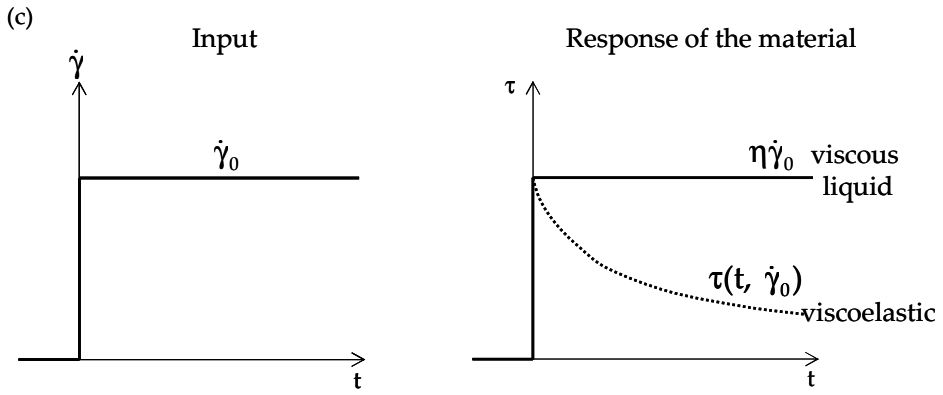

Figure 1-30. (a) Comparison of the creep at a constant applied stress of an elastic and a viscoelastic material. (b) Comparison of the relaxation of an elastic and a viscoelastic material submitted to a constant strain. (c) Comparison of the responses of a viscous liquid and a viscoelastic material after the application of a constant strain rate.

When such viscoelastic polymers (either more liquid-like or solid-like) are subjected to sinusoidally oscillating stress, the strain is neither exactly in phase with the stress (as it would be for a perfectly elastic solid) nor 90° out of phase (as it would be for a perfectly viscous liquid) but it is somewhere in between. Some of the energy input is stored and recovered in each cycle, and some is dissipated as heat.

1.6.2.1. Linear viscoelasticity

If strain is infinitesimal the time-dependent stress-strain relations can be described by linear differential equations with constant coefficients (independent on the strain for a relaxation tests or on the stress for a creep experiment), we have a *linear* viscoelastic behavior.

Some notions of l*inear viscoelasticity* are now described in more detail. The response of a viscoelastic polymer during creep or relaxation has been briefly discussed above. However, very often, polymers are subjected to variable loading at a moderately high frequency and viscoelastic properties are commonly estimated through dynamic experiments (Figure 1-31). An oscillating sinusoidal deformation γ is applied to a specimen at a particular frequency:

$$\gamma = \gamma_0 \cos(\omega t) \qquad \textbf{Eq. 1-35}$$

where ω is the angular frequency.
The resulting shear stress τ is given by:

$$\tau = \tau_0 \cos(\omega t + \delta) = \tau_0 (\cos(\omega t)\sin(\delta) + \sin(\omega t)\cos(\delta)) \qquad \textbf{Eq. 1-36}$$

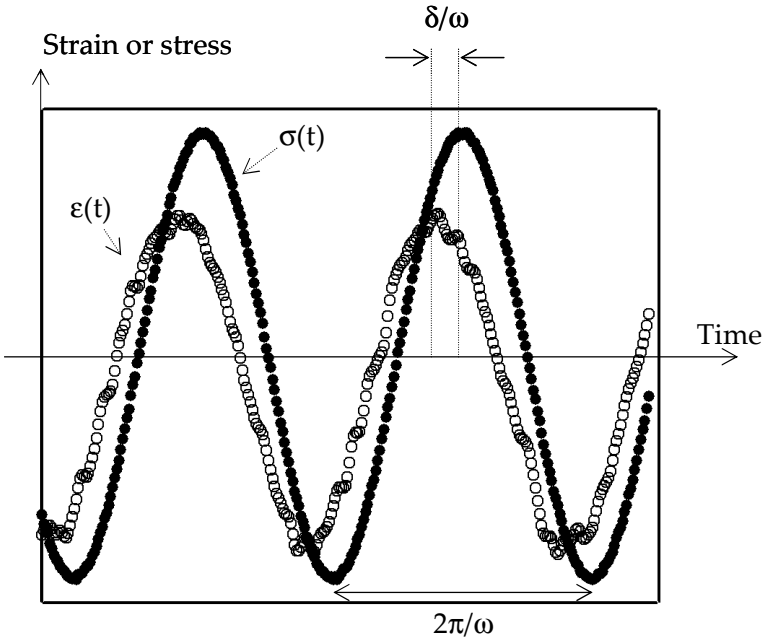

Figure 1-31. Oscillations in stress and deformation for a viscoelastic material.

The resulting stress presents a lag δ which depends on ω, δ is also commonly called the "*phase angle*" or the "*phase lag*".

The stress can be separated into two components: the stress in phase and the stress out of phase. The *storage modulus* (also called *shear elastic modulus*) G' is defined as the stress in phase with the strain divided by the strain. It is a measure of the energy stored and recovered per cycle. The *loss modulus* (also called *viscous modulus*) G" is defined as the stress 90° out of phase with the strain divided by the strain. Therefore, Eq. 1-36 can be rewritten as:

$$\tau = \gamma_0 (G'(\omega)\cos(\omega t) + G''(\omega)\sin(\omega t)) \qquad \textbf{Eq. 1-37}$$

A complex notation is often favored for the representation of the dynamic mechanical properties of viscoelastic materials, and the complex shear modulus is defined as:

$$G^*(\omega) = G'(\omega) + iG''(\omega) \qquad \textbf{Eq. 1-38}$$

Another useful parameter is the measure of the ratio of the energy lost or dissipated to energy stored in a cyclic deformation. This ratio is called the *loss tangent* and noted tan(δ):

$$\tan(\delta) = G''(\omega)/G'(\omega) \qquad \textbf{Eq. 1-39}$$

For a perfectly elastic material G" and tan(δ) are equal to zero and in the other hand, for a perfectly viscous material, G' is equal to zero and tan(δ) tends to infinity.

Typically, *rheological experiments in the linear regime* (experiments used to measure G' and G" and detailed in "Experimental Techniques" section) are performed at a given frequency and at various temperatures or at a given temperature and at various frequencies as shown on Figure 1-32. At low temperatures or high frequencies, the polymer is glassy. The modulus then falls through the glass transition regime where the material is viscoelastic[1] and the

[1] This regime will be the regime of interest when looking at properties of viscoelastic PSA.

modulus becomes very rate- and temperature-dependent. As already said in section 1.3.3 about the *glass transition temperature*, T_g can be determined by the point of inflection of the elastic modulus–temperature. At a sufficiently high temperature the polymer becomes a rubber. In the case of a crosslinked polymer, G′ stabilizes for further increase of the temperature or decrease of the frequency. This is not the case for uncrosslinked materials which behave like a liquid and flow irreversibly.

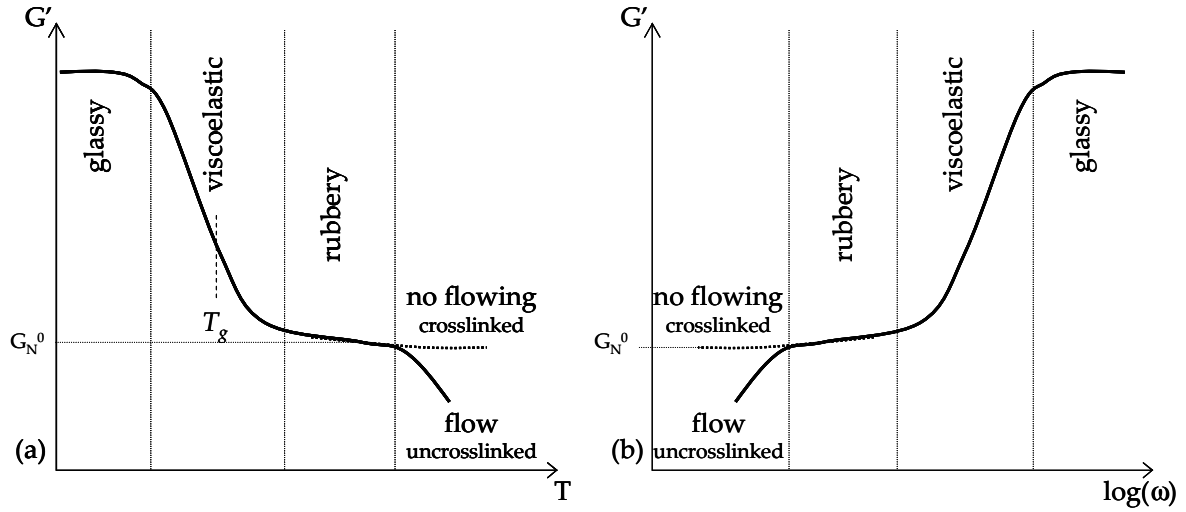

Figure 1-32. Variations of the elastic and loss moduli (a) with the temperature and (b) with the frequency.

We have shown how viscoelastic properties can be characterized. We will now look at the origin of such interesting properties.

Viscoelastic properties are controlled by the molecular structure of the polymers. In the glassy state, the molecular motions of the polymeric chains are frozen and the moduli are high. In the glass transition region, the relative motion of the monomers begins. On the rubbery plateau, the elastic modulus is kept constant thanks to the entanglement points that can exist between the polymeric chains provided that the total chain length of the polymer or the length of the chain between crosslinks (the corresponding molecular weight is called M_c) is higher than the so-called molecular weight between entanglements M_e (Figure 1-33).

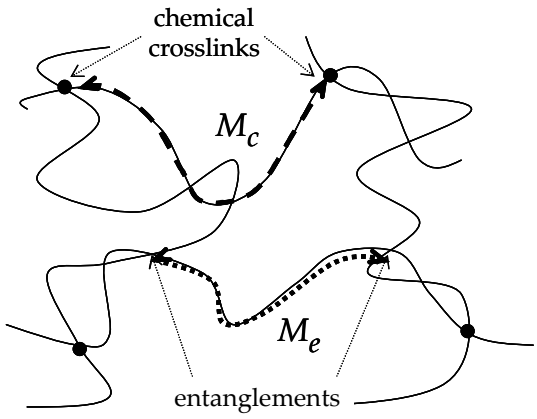

Figure 1-33. Schematic representation of a polymer crosslinked network to define M_c and M_e.

A relation exists between the value of the modulus of the rubbery plateau G_N^0 (Figure 1-32) and M_e:

$$G_N^0 = \frac{\rho RT}{M_e} \qquad \textbf{Eq. 1-40}$$

with ρ the polymer density and R the gas constant.

Finally, for uncrosslinked polymers, when the testing frequency becomes lower than the inverse of the characteristic time for a chain to completely lose the memory of its original position (also called the reptation time) the polymeric chains flow and behave increasingly like a Newtonian fluid. For crosslinked networks, the modulus remains approximately constant due to the presence of the crosslinks.

Note that in section concerning elasticity we used σ for the stress and ε for the strain, and we defined E as the Young's modulus. Here, we preferred τ for the stress and ε for the strain and polymers were characterized by their shear modulus G ($G^2=G'^2+G''^2$). In general, σ, ε and E are related to elongation or tensile experiment while τ, γ and G are more frequently used for shear test. However, there exists a relation between G and E, and for a polymer with a Poisson ratio[(1)] ν equal to 0.5, E=3G.

1.6.2.2. Linear viscoelastic phenomenological models

In practice, linear viscoelasticity of polymers is well described assuming that the material contains an elastic component and a viscous component and that the deformation of this material can be described by a combination of *Hooke's law* and *Newton's law.*

Various phenomenological models involving different combinations of these two basic components have been proposed. The most simple for the description of the behavior of a viscoelastic liquid is the so-called *Maxwell model*. In the other hand, the most simple for the description of the behavior of a viscoelastic solid is the so-called *Kelvin-Voigt model*. Both models consist of a spring and a dashpot, in series for the *Maxwell model* and in parallel for the *Kelvin-Voight model*. The elastic spring of modulus G obeys *Hooke's law* and the viscous dashpot of viscosity η obeys *Newton's law*.

[(1)] The Poisson ratio measures the tendency of a stretched polymer sample in one direction to be thinner in the other two directions.

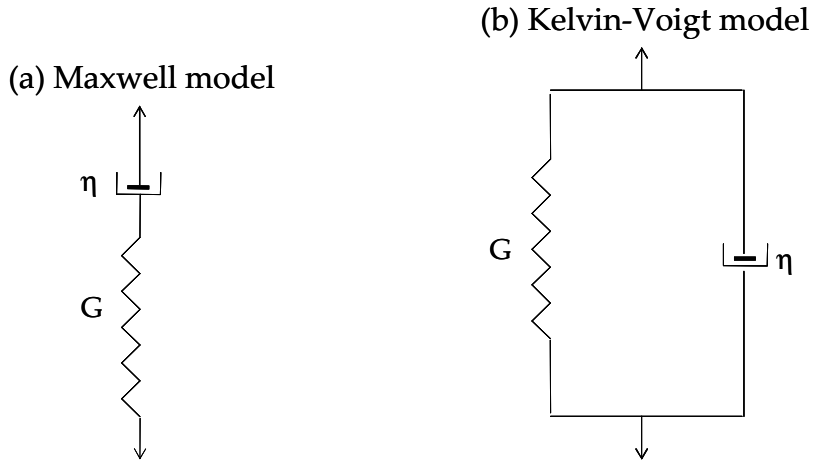

Figure 1-34. Two mechanical models used to represent the viscoelastic behavior of polymers. (a) Maxwell model, (b) Kelvin-Voight model.

We discuss now in more detail *Maxwell model*. Under the action of an overall stress τ there will be an overall strain γ in the system which is given by:

$$\gamma = \gamma_{spring} + \gamma_{dashpot} \qquad \textbf{Eq. 1-41}$$

where γ_{spring} is the strain in the spring and $\gamma_{dashpot}$ is the strain in the dashpot. Since the two elements are in series the stress is identical in each one and:

$$\tau = \tau_{spring} = \tau_{dashpot} \qquad \textbf{Eq. 1-42}$$

Hooke's law can be rewritten as:

$$\frac{d\tau}{dt} = G\frac{d\gamma_{spring}}{dt} \qquad \textbf{Eq. 1-43}$$

Newton's law gives:

$$\tau = \eta\frac{d\gamma_{dashpot}}{dt} \qquad \textbf{Eq. 1-44}$$

And so, the differential equation of the Maxwell model is:

$$\frac{1}{G}\frac{d\tau}{dt} + \frac{1}{\eta}\tau = \frac{d\gamma}{dt} \qquad \textbf{Eq. 1-45}$$

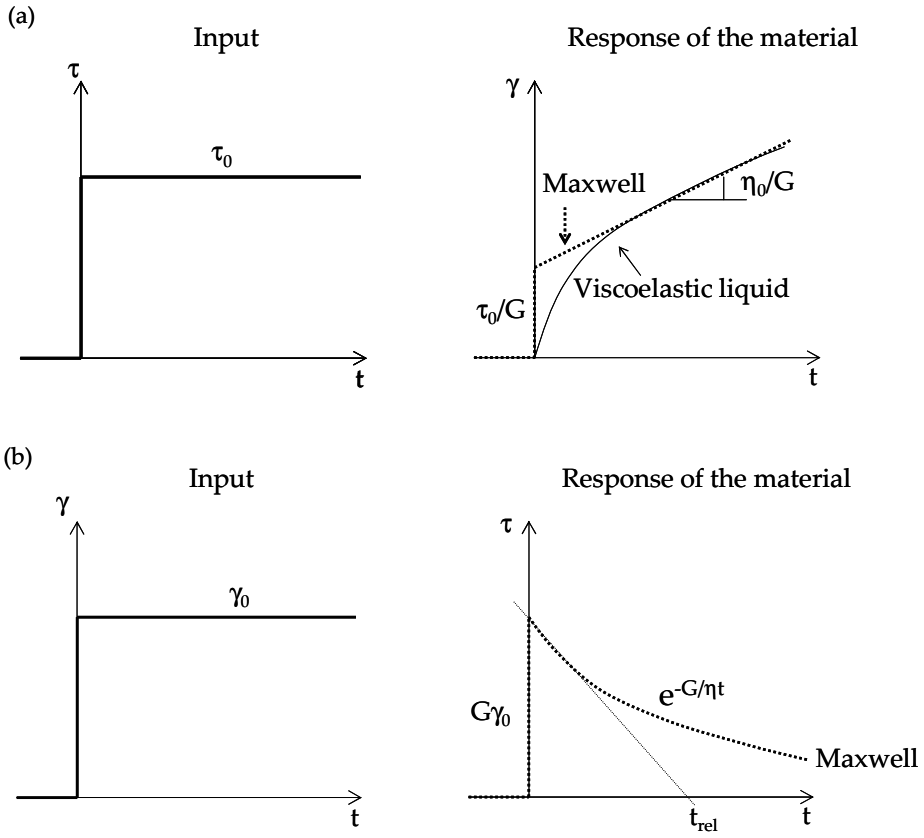

Figure 1-35. (a) Creep at a constant applied stress of "Maxwell material". Comparison with the response of a real viscoelastic liquid. (b) Relaxation of Maxwell material.

The response of the spring to the input is instantaneous while the response of the dashpot becomes important at longer time (Figure 1-35).

This model is widely used to predict the response of a polymer during relaxation. In this case, a constant deformation γ_0 is imposed. Eq. 1-45 can be readily integrated if at t = 0, $\tau = \tau_0$:

$$\tau(t) = \tau_0 \exp\left(-\frac{G}{\eta}t\right) = G\gamma_0 \exp\left(-\frac{G}{\eta}t\right) \qquad \textbf{Eq. 1-46}$$

and the evolution of the relaxation modulus G(t) as a function of time is given by:

$$G(t) = G\exp\left(-\frac{G}{\eta}t\right) \qquad \textbf{Eq. 1-47}$$

The decrease of the stress is even more rapid that G/η is high, i.e. when the viscous character dominates compared to the elastic one. This term is referred to as a "*relaxation time*" called "t_{rel}" here to avoid any ambiguity with the stress τ. A measure of it is possible from the relaxation curve as shown on Figure 1-35-b.

For a purely elastic material, t_{rel} tends to infinity while for a purely viscous liquid, t_{rel} is equal to zero. Real materials have of course a spectrum of relaxation times and various molecular models have been developed to attribute these relaxation times to specific molecular relaxations. Unfortunately our PSA have a very broad spectrum of relaxation times with a molecular structure not easy to be determined. Therefore, they are difficult to

model with a molecularly based model other than empirically. We thus decided to stick to phenomenological models but rather to explore nonlinear viscoelastic models.

1.6.2.3. Nonlinear differential model: Upper Convected Maxwell model

We have encountered different constitutive equations for the description of various material behaviors, from the *Newtonian fluid model* and the *Hooke elastic solid model* to the *Maxwell viscoelastic differential model*. These models are only valid in the linear regime and we have seen that linear viscoelastic properties are governed by the molecular motions of the polymers.

In this part, we seek for a more general constitutive equation that can be used for the description of a *nonlinear mechanical behavior* of a macroscopic sample. For that we use a generalization of the Maxwell model. We have chosen to use the well-know *Upper Convected Maxwell Model* (denoted UCM model) (Figure 1-36) which a generalization of the Maxwell model for the case of large deformations and is written in the three dimensional space. The UCM model is widely used for the description of the elongational flow of viscoelastic fluids.

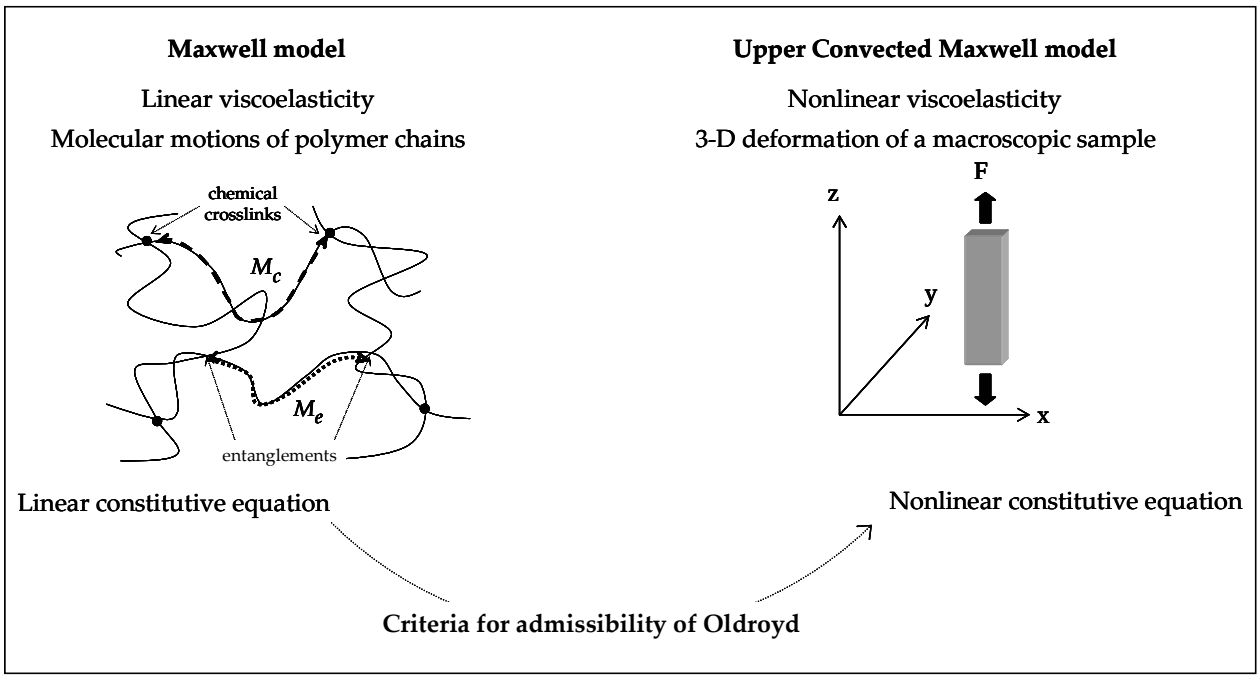

Figure 1-36. Establishment of the nonlinear constitutive equation of the UCM model from the linear constitutive equation of the Maxwell model using the criteria for admissibility of Oldroyd.

The objective here is not to construct the UCM constitutive equation, those wishing more on this subject should consult one of the many available textbooks or reference works ([32] for instance). This part is intended to define the term *"upper convected"* and to show that the UCM constitutive equation is *admissible*.

We begin with the rewriting of the Maxwell equation in a three dimensional space.

i) Maxwell model generalization in 3-D

The constitutive equation of the UCM is a generalization of Eq. 1-45 in a three dimensional space. For that, scalars are replaced by 3x3 tensors.
The *stress tensor* is defined as $\underline{\tau}$ with:

$$\underline{\tau} = \begin{pmatrix} \tau_{xx} & \tau_{xy} & \tau_{xz} \\ \tau_{yx} & \tau_{yy} & \tau_{yz} \\ \tau_{zx} & \tau_{zy} & \tau_{zz} \end{pmatrix}$$

The *gradient tensor velocity* $\underline{L}$ is defined as:

$$\underline{L} = \begin{pmatrix} \frac{\partial v_x}{\partial x} & \frac{\partial v_x}{\partial y} & \frac{\partial v_x}{\partial z} \\ \frac{\partial v_y}{\partial x} & \frac{\partial v_y}{\partial y} & \frac{\partial v_y}{\partial z} \\ \frac{\partial v_z}{\partial x} & \frac{\partial v_z}{\partial y} & \frac{\partial v_z}{\partial z} \end{pmatrix}$$

thus,

$$dv = \underline{L}\, dx \qquad \textbf{Eq. 1-48}$$

where dv is the velocity vector and dx the position vector.

If τ can be directly replaced by $\underline{\tau}$ this is not the case for $\frac{d\gamma}{dt}$, it cannot be replaced by $\underline{L}$.
Indeed, the generalization of the linear constitutive equation of a *Newtonian liquid* cannot be written as:

$$\underline{\tau} = \eta \underline{L} \qquad \textbf{Eq. 1-49}$$

because in the case of a simple shear, $\underline{\tau}$ is a symmetric tensor but not $\underline{L}$.

Thus we define $\underline{D}$ *the strain rate tensor* as:

$$\underline{D} = \frac{1}{2}(\underline{L} + \underline{L}^T) \qquad \textbf{Eq. 1-50}$$

Therefore, the generalization of the constitutive equation of a Newtonian liquid is written as:

$$\underline{\tau} = 2\eta \underline{D} \qquad \textbf{Eq. 1-51}$$

The same can be done for the Maxwell equation. The constitutive equation of the *Upper Convected Maxwell model* can thus be written as:

$$\frac{1}{G}\frac{\delta \underline{\tau}}{\delta t} + \frac{1}{\eta}\underline{\tau} = 2\underline{D} \qquad \textbf{Eq. 1-52}$$

where $\frac{\delta}{\delta t}$ is the *convected derivative* (we will see later that this is the derivative taken with respect to a coordinate system moving with velocity v. It is defined as:

$$\frac{\delta}{\delta t} = \frac{\partial}{\partial t} + v.\nabla \qquad \textbf{Eq. 1-53}$$

where $\frac{\partial}{\partial t}$ is the partial derivative with respect to t and $v.\nabla$ is the derivative relative to a mobile part of the fluid (∇ is the gradient operator).

In the case of polymer melts of high viscosity and of low Reynolds number, the conservation of momentum implies that:

$$v.\nabla = 0 \qquad \textbf{Eq. 1-54}$$

We will then briefly explain what "*convected*" stands for. For that we define the *convected coordinates*.

ii) Convected coordinates

In this section we consider a material element moving in an arbitrary way as a part of a flowing continuum.

The "*convected coordinate system*" has coordinate surfaces $\hat{x}^i$ = constant (independent on the time) (i = 1, 2, 3) embedded in the fluid and deforming with it; in this coordinate system, a fluid particle P has by definition the same coordinates ($\hat{x}^1$, $\hat{x}^2$, $\hat{x}^3$) for all times. In Figure 1-37 we show how a *convected coordinate system* which moves through space as it is swept along the moving fluid; for simplicity a two-dimensional flow is depicted.

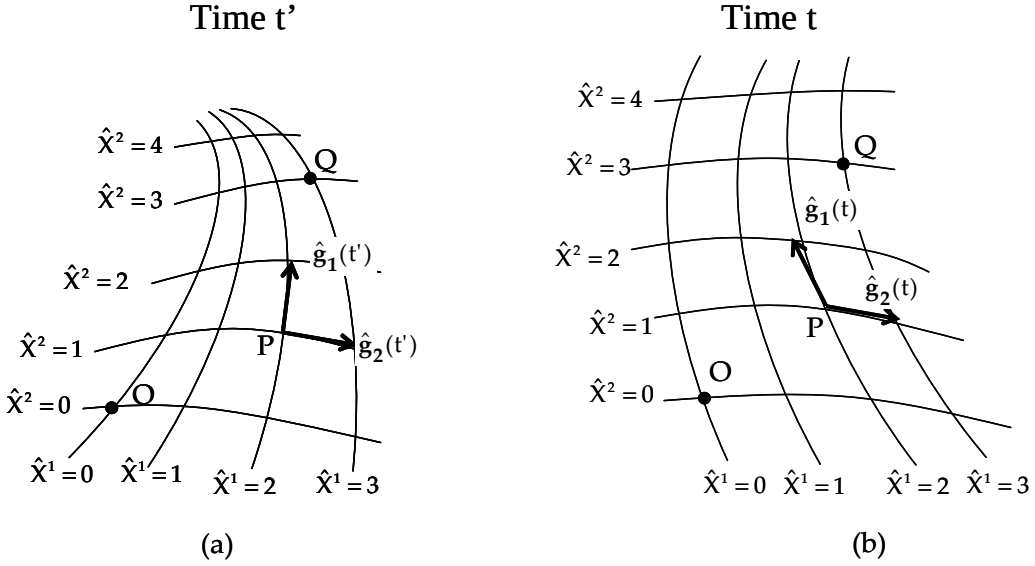

Figure 1-37. An arbitrarily chosen coordinate system, embedded in a flowing fluid, at two different times (a) t' and (b) t. Fluid particle P is located at $\hat{x}^1$=2, $\hat{x}^2$ = 1 at all times , fluid particle Q is located at $\hat{x}^1$=3, $\hat{x}^2$ = 3 at all times. The base vectors $\hat{g}_1$ and $\hat{g}_1$ at fluid particle P are also shown. (after [32]).

iii) Criteria for admissibility

We introduced the idea of a *convected coordinate system* embedded in a flowing fluid and deforming with it, no reference was made to any *coordinate system fixed* in space. In this section, we make a relation between the *convected coordinate system* and a *coordinate system fixed* in space.

The objective is to show that the constitutive equation of the UCM verifies the Oldroyd's criteria for admissibility which stipulates that the constitutive equations are:

- Form invariant under a change motion of coordinate system.
- Value invariant under a change of translational or rotational motion of the fluid element as it goes through space.
- Value invariant under the change of rheological history of neighboring fluid elements.

We do not investigate in details all these requirements, but we propose to simply look at each component of the UCM constitutive equation and to check if they are *invariant* under a change from the convected coordinate system to a specific Cartesian fixed coordinate system.

In the following, notations chosen are {e1, e2, e3} for the *fixed system* and {e1*, e2*, e3*} for the *convected* (or mobile) one (Figure 1-38).

For any position, the *mobile system* can be viewed as the image of the *fixed coordinate system* after a rotation θ and a translation $\vec{T}$ or inversely after first a translation $\vec{T}$ and then a rotation θ.

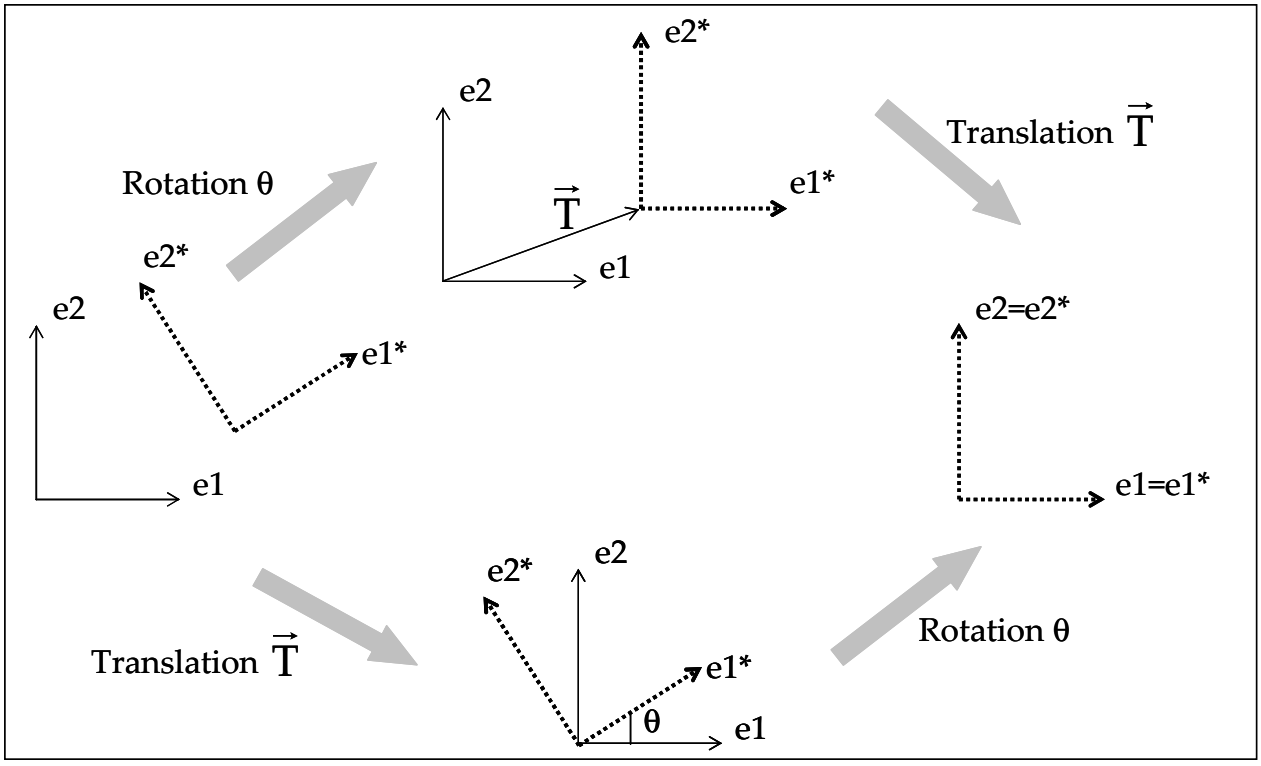

Figure 1-38. Mobile coordinate system {e1*, e2*, e3*} as the image of the fixed coordinate system {e1, e2, e3} after a rotation and a translation or inversely, after a translation and a rotation. (e3 and e3* are out of the plane).

The rotation matrix Q for a change from {e1, e2, e3} to {e1*, e2*, e3*} is:

$$Q = \begin{pmatrix} \cos\theta & \sin\theta & 0 \\ -\sin\theta & \cos\theta & 0 \\ 0 & 0 & 1 \end{pmatrix}$$

A scalar α, a vector $\vec{a}$ and a tensor $\underline{A}$ are said to be *invariant* if, their transforms (denoted α^*, $\vec{a}^*$ and $\underline{A}^*$) after a change of coordinate system are like:

$$\alpha^* = \alpha$$

$$\vec{a}^* = Q\vec{a}$$

$$\underline{A}^* = Q\ \underline{A}\ Q^T \qquad \textbf{Eq. 1-55}$$

where Q^T is the transpose of Q.
Coordinate components of $\underline{A}$ are written in the *fixed coordinate system*.
Coordinate components of $\underline{A}^*$ are written in the *convected coordinate system*.

The above definitions are used to know if components involved in the constitutive equation of the Upper Maxwell model are invariant or not.

- Let us start with the *stress tensor* $\underline{\tau}$. It is defined as:

$$df = \underline{\tau}\ n\ dS \qquad \textbf{Eq. 1-56}$$

with df the force applied on a part of the continuum fluid of surface dS characterized by its normal vector n.
df and n are invariant (their values are unchanged after a change of the coordinate system and $df^* = Qdf$ and $n^* = Qn$). Thus $\underline{\tau}^* = Q\underline{\tau}\ Q^T$ and $\underline{\tau}$ is invariant.

- For *the strain rate tensor* $\underline{D}$, we need first to look at $\underline{L}$.

We can demonstrate that:

$$dx^* = Qdx \text{ and } dv^* = \dot{Q}\,dx + Qdv \qquad \textbf{Eq. 1-57}$$

where $\dot{Q}$ is the time derivative of Q.
therefore

$$\underline{L}^* = \dot{Q}Q^T + Q\underline{L}Q^T$$

(One can remark that dx is invariant but dv and $\underline{L}$ are not).

Finally, after calculations, we find that:

$$\underline{D}^* = Q\underline{D}Q^T \qquad \textbf{Eq. 1-58}$$

which means that $\underline{D}$ is invariant.

- Invariance of the *stress time derivative* $\frac{\partial \underline{\tau}}{\partial t}$

We can demonstrate that $\frac{\partial}{\partial t}$ is not invariant. Therefore, the UCM model with such a derivative is not admissible. To overcome this problem, several forms of the time derivative have been proposed. At each kind of derivative is associated a type of model. The most important models are the *corotational time derivative* (defined by Jaumann) and the *covariant convected time derivative or contravariant convected time derivative (also called upper-convected time derivative* and defined by Oldroyd).

The *upper convected time derivative* is defined as:

$$\frac{\delta \underline{A}}{\delta t} = \dot{\underline{A}} - \underline{L}\underline{A} - \underline{A}\underline{L}^T \qquad \textbf{Eq. 1-59}$$

Here we can try to derive the upper-convected time derivative for a tensor $\underline{A}$. $\underline{A}$ has to satisfy the requirement of invariance. First we can write:

$$\underline{A}^* = Q^T \underline{A} Q \qquad \textbf{Eq. 1-60}$$

since
$QQ^T = I$ (indentity tensor) and

$$\frac{d(QQ^T)}{dt} = \dot{Q}Q^T + Q\dot{Q}^T = 0$$

The time derivative of $\underline{A}^*$ is given as:

$$\begin{aligned}\dot{\underline{A}}^* &= \dot{Q}^T \underline{A} Q + Q^T \dot{\underline{A}} Q + Q^T \underline{A} \dot{Q} \\ &= -(Q^T \dot{Q} Q^T)\underline{A}Q + Q^T \dot{\underline{A}} Q - Q^T \underline{A}(Q\dot{Q}^T Q) \\ &= Q^T(\dot{\underline{A}} - \dot{Q}Q^T \underline{A} - \underline{A}Q\dot{Q}^T)Q \qquad \textbf{Eq. 1-61}\end{aligned}$$

Since the time derivative of $\underline{A}$ should be invariant, we obtain the relation for the time derivative of $\underline{A}$, i.e. the upper-convected time derivative:

$$\begin{aligned}\frac{\delta \underline{A}}{\delta t} &= \dot{\underline{A}} - \dot{Q}Q^T \underline{A} - \underline{A}Q\dot{Q}^T \quad (\underline{L} = \dot{Q}Q^T \text{ by definition}) \\ &= \dot{\underline{A}} - \underline{L}\underline{A} - \underline{A}\underline{L}^T \qquad \textbf{Eq. 1-62}\end{aligned}$$

Finally, the Maxwell model satisfies the invariance and the model has admissibility.

In this section we have seen how the Maxwell model valid in the linear regime has to be modified to be also valid in the nonlinear regime. The main change is in the time derivative of the stress tensor which must be invariant under a change of the coordinate system and more specifically after a rotation.

Lots of constitutive equations not limited to small deformation gradients, as are the linear viscoelastic regime, are proposed. We have described one of them and briefly explained how it has been constructed. It is simple enough to allow analytical solutions to be obtained for

interesting flows. However, it has been shown that the price of simplicity in the constitutive equation is paid sometimes (depending on the type of experience) in the poor approximation to some of the material functions.

1.7. Theoretical concepts of adhesion

We have described very general aspects of chemical and physical properties of polymers. Most of the properties presented are fundamental well-known notions for several years now and can be used for in a wide range of polymer fields from the study of plastics and rubbers to the study of the dynamics of polymeric liquids.

Here, the newer concepts of the adhesion of pressure sensitive adhesive (PSA) polymers will be presented. These concepts are applicable to the special class of PSA, i.e. polymers which adhere instantaneously on a surface upon application of a light pressure. Most of the notions presented have been recently reviewed by Shull and Creton.[33]

The mechanisms involved during the debonding of a PSA layer from a solid surface observed during tack experiments are presented in the first section. Then, the prediction of these debonding mechanisms from rheological properties of the sticky material will be discussed.

1.7.1. Tack experiments

Debonding of a soft adhesive layer from a rigid substrate involves rather complex deformation mechanisms. These mechanisms, which have been mostly described using axisymetric probe tests, occur both at the interface between the polymer and the substrate and in the bulk of the material. One of advantages of the probe test, in particular of the flat probe test, compared to standard adhesive tests (peel, shear and loop tack) is the separation of the mechanisms as a function of time.[34]

Figure 1-39 showing a typical stress vs. strain tack curve can serve as a support for the following description of these events. Typically, first the adhesive layer is homogeneously deformed, and then some cavities nucleate at the interface between the probe and the adhesive layer. They grow until the stress reaches a well defined maximum (σ_{max}). This peak is followed either by a sharp decrease or by a stabilization of the stress at a nearly constant value. In the first case, the layer debonds rapidly from the probe and the adhesion energy is really low. On the contrary, a stabilization of the stress is a signature of the creation of a fibrillating structure; fibrils are the walls of the preexisting cavities. In that case, adhesion energy can reach very high values especially when the material is highly deformable.

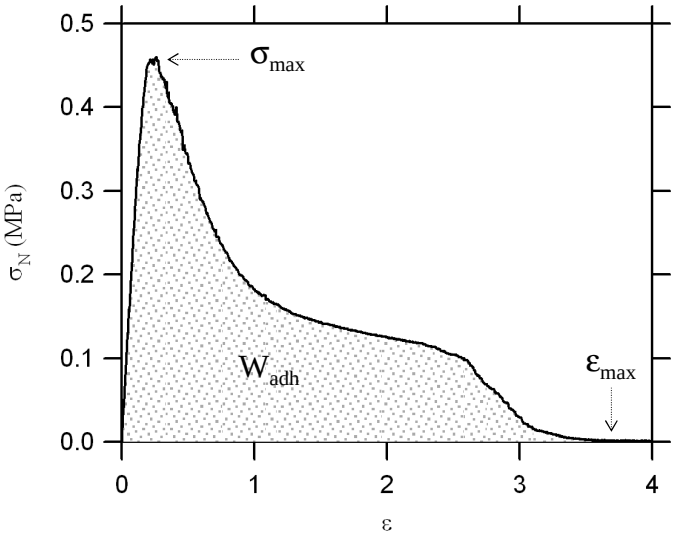

Figure 1-39. Definition of parameters used for a description of a tack curve.

The adhesive performance is typically evaluated quantitatively through three main parameters schematically defined in Figure 1-39: the *maximal nominal stress* σ_{max}, the *maximal strain* ε_{max} and the *adhesion energy* W_{adh} which is defined as the area under the stress vs. strain probe tack curve:

$$W_{adh} = h_0 \int_0^{\varepsilon_{max}} \sigma(\varepsilon)\, d\varepsilon \qquad \textbf{Eq. 1-63}$$

with h_0 the initial thickness of the adhesive layer and ε_{max} the failure deformation corresponding to the detachment of the adhesive from the probe or to the failure of the polymer in its bulk. Caution needs to be taken in the case of cohesive debonding when no failure occurs before the end of the test.

Figure 1-39 displays an example of tack curve but generally, four types of stress-strain curves have been observed from investigations of a great number of polymers.[33,35,36]

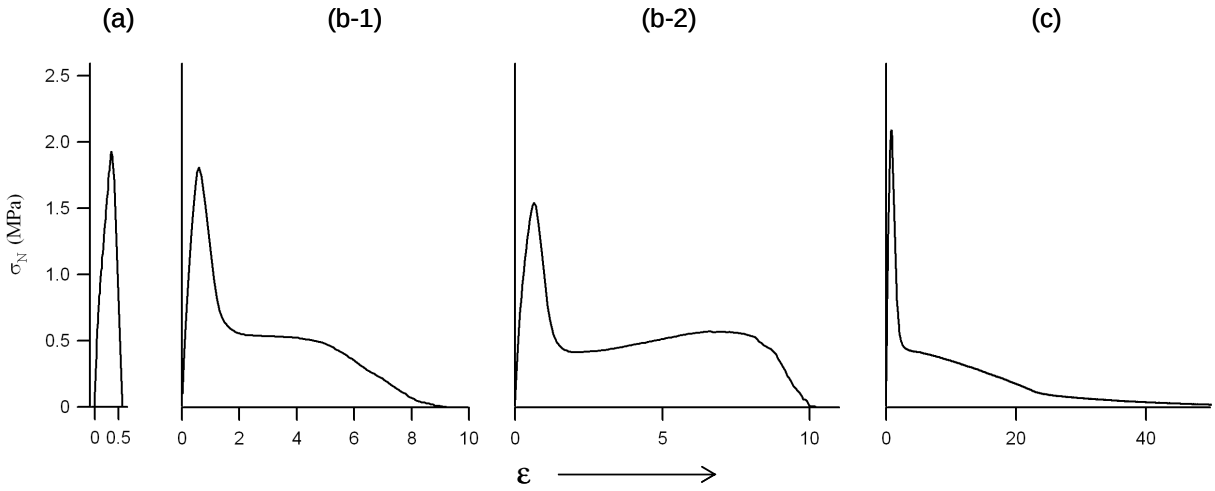

Figure 1-40. Different stress-strain tack curves. (a) brittle failure, (b) adhesive debonding, with hardening in the case of b-2, (c) cohesive debonding liquid-like behavior.

The first type of curve (Figure 1-40-a) is characterized by a sharp maximum at rather low strains and a very small area under the stress-strain curve. This type of behavior is commonly called "brittle failure" or "interfacial failure". A sequence of images taken during a probe experiments showing the horizontal shape of the cavities and schematic lateral profiles are shown on Figure 1-41. Video images correspond to the horizontal contact between the adhesive and the probe observed through the transparent glass slide. Cavities nucleate at the probe/adhesive interface and expand in the bulk of the adhesive layer (a). Then, the cavities expand laterally at the interface with a relatively small deformation of the adhesive layer (c). Video image at time t_4 shows that after the final debonding, the adhesive film is free of surface defects and appears undamaged.

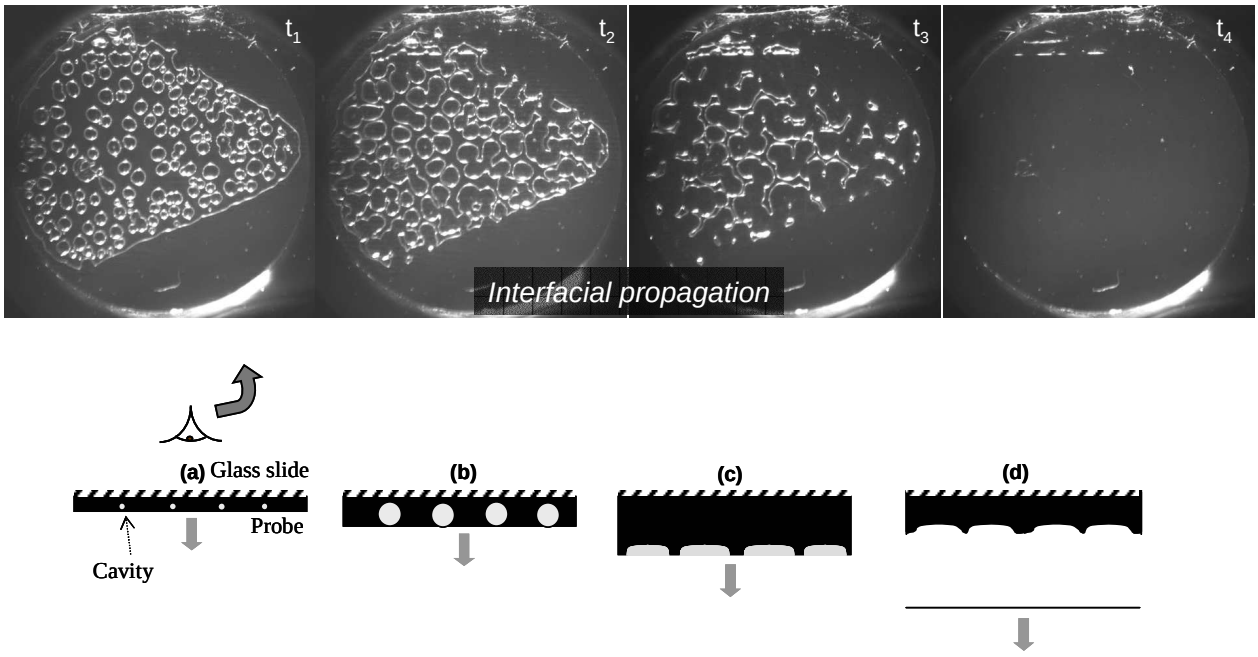

Figure 1-41. Sequence of images obtained during a tack experiment when interfacial propagation of the cavities occurs. Four images are depicted at four different times, $t_1 < t_2 < t_3 < t_4$. Below is shown the lateral profile of the cavities (note that we did not attempt to create a perfect correspondence between the real images and the schematics of the lateral profile).

At the other extreme (Figure 1-40-c) is displayed the case of a highly viscous liquid. The adhesive joint breaks by cohesive fracture within the adhesive and the debonding process is governed by viscous flow. The stress-strain curve is characterized by a peak stress followed by a double plateau. The decrease in the stress of about 0.1 MPa at a strain of 20 is due to the air penetration in the middle of the adhesive layer.[37] The force then plateaus at a non zero and constant value until the end of the test. This is a typical "liquid-like" debonding also called "cohesive" debonding (Figure 1-44) where some residues of adhesive are left on the probe at the end of the test. A typical sequence of images and a schematic lateral profile of this type of materials is shown on Figure 1-42. A sequence of images taken during a probe experiments showing the horizontal shape of the cavities and schematic lateral profiles are shown on Figure 1-42. At the beginning of the test the structure is made of more or less round cavities (t_1). Then one can follow the air which penetrates from the movement of fingers from the edges of the contact towards the centre (t_2 and t_3). At the end of the test, there are no cavities anymore but only fingers. Some highly deformable fibrils are present all

along the process. At the end of the tests, either there is a cohesive failure in the middle of these fibrils, or no failure occurs and the fibrils stay well attached to the probe.

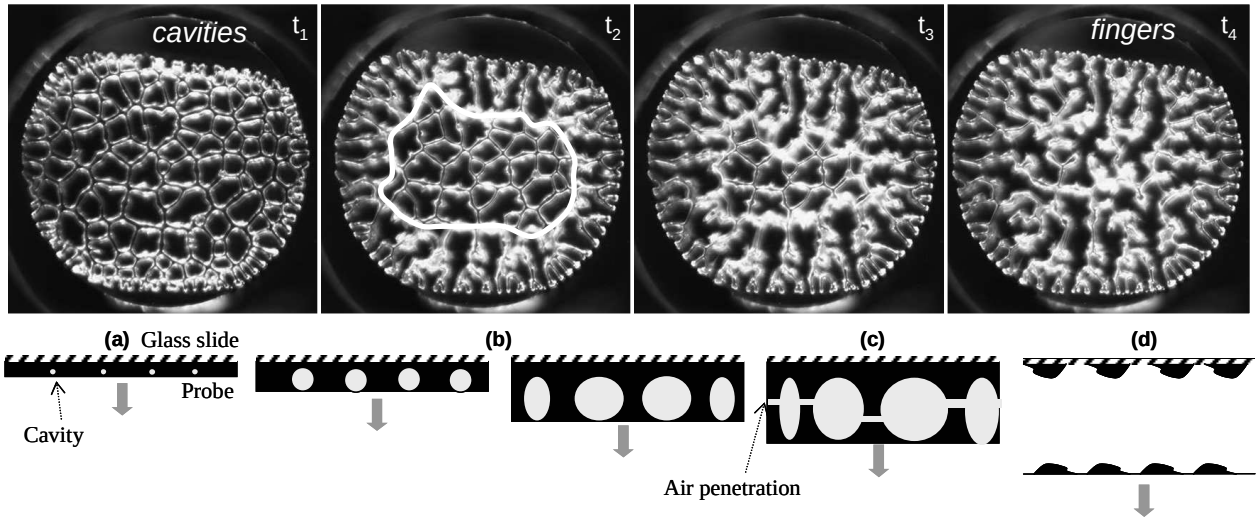

Figure 1-42. Sequence of images obtained during a tack experiment in the case of a liquid-like adhesive where the air penetration evolving from the edges to the centre is observed. Four images are depicted at four different times, $t_1 < t_2 < t_3 < t_4$. The white line on the second picture artificially materializes the frontier between the fingers and the zone made of cavities. Below is shown the lateral profile of the cavities.

In between these two cases, brittle fracture and cohesive liquid-like debonding, stress-strain curves are characterized by a maximum in the stress followed by a pronounced shoulder (Figure 1-40-b). The curve finally ends up by a decrease of the force to zero. Detachment in that case occurs at the interface between the probe and the adhesive layer. Such a debonding is called "adhesive debonding" (no residue on the probe at the end of the test) Figure 1-44. Figure 1-40-b-2 is observed when the material strain-hardens just before the final detachment. In that case a slight increase in stress is observed and a second peak is observed. A sequence of images taken during a probe experiments showing the horizontal shape of the cavities and schematic lateral profiles are shown on Figure 1-43. After cavitation, walls of the cavities deform vertically until the final detachment from the probe.

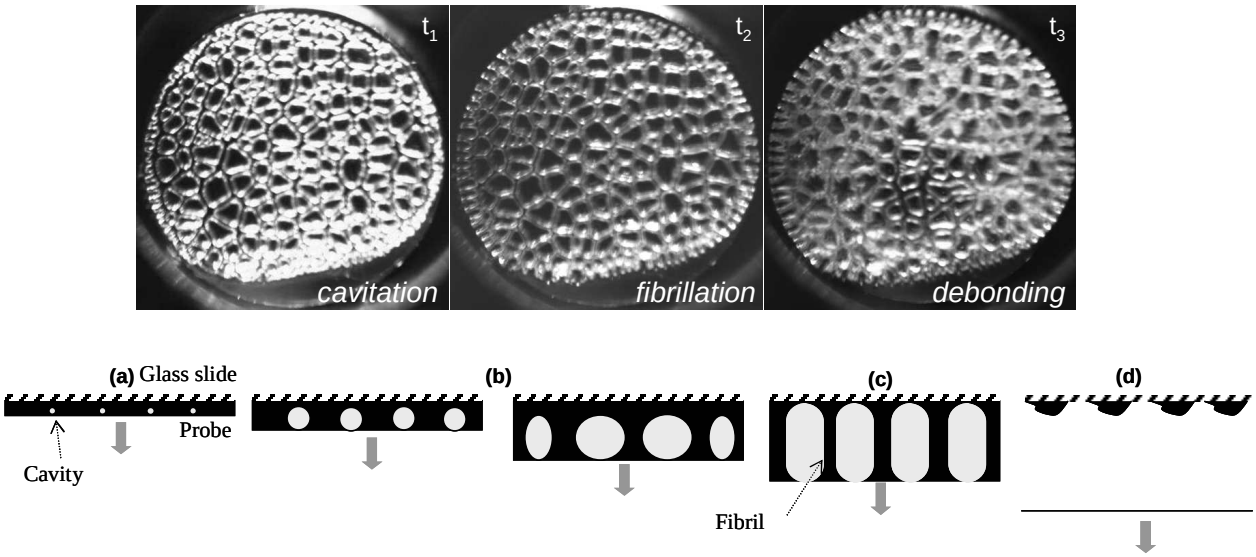

Figure 1-43. Sequence of images obtained during a tack experiment of a PSA characterized by cavitation, fibrillation processes and final debonding of the adhesive from the probe. Four images are depicted at four different times, $t_1 < t_2 < t_3 < t_4$. Below is shown the lateral profile of the cavities.

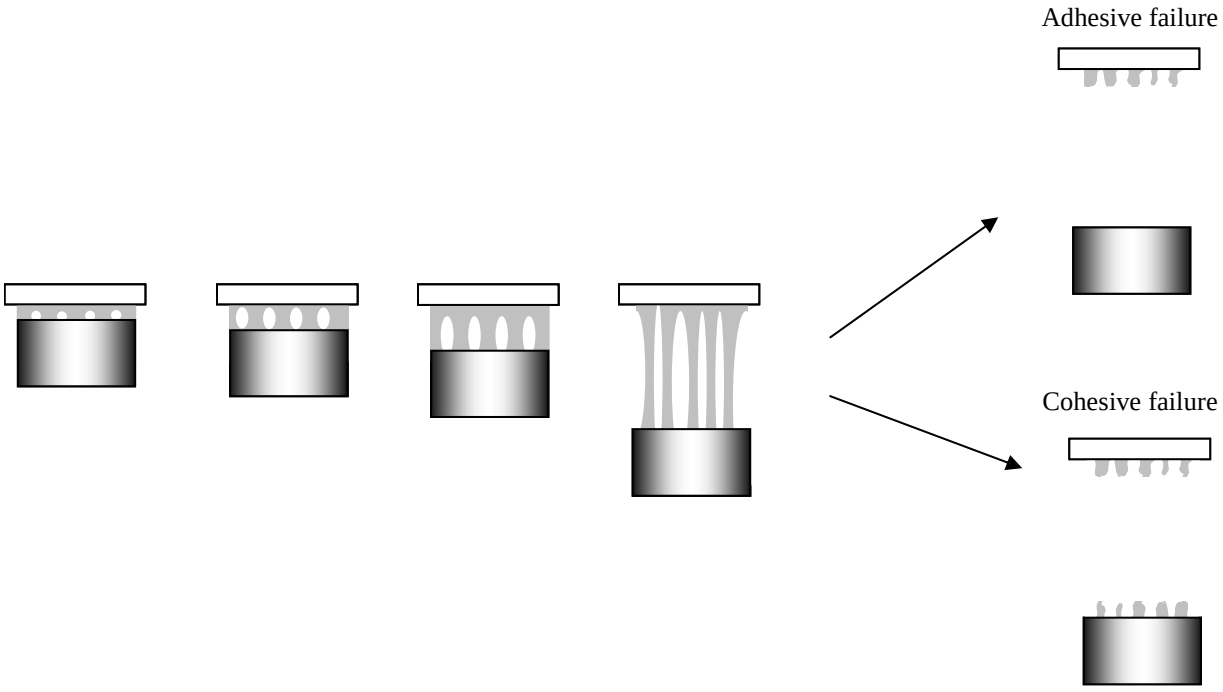

Figure 1-44. Schematics of the final stage of the debonding of soft and highly deformable material. Cohesive failure is observed when the material has a liquid-like behavior characterized by a low shear resistance.

1.7.2. Prediction of debonding mechanisms from linear rheological properties

For many scientists working in adhesion science, and in particular on PSA, it has been tempting to predict adhesive properties from linear viscoelastic properties[37] which are rather simple to characterize with a standard instrument. Yet, as just discussed, complex microscopic deformation mechanisms are observed during a debonding process from interfacial failure, where a crack propagates at the interface, to cavitation or bulk fingering followed by fibrillation, where larger deformations of the adhesive are achieved[33] and it is often not clear what can be predicted from linear viscoelasticity and what not. Two criteria based on linear viscoelastic properties are important necessary conditions to obtain PSA properties.

The first one is the so-called Dahlquist criterion: it stipulates that the shear elastic modulus (G') at the bonding frequency must be lower than 0.1 MPa for the layer to be able to form a good contact within the contact time.[38,39] Although the original Dahlquist argument may not always be the correct one, it is clear that when the modulus of the adhesive is too high, it becomes impossible to form a fibril structure for a short contact time and light bonding pressure and only interfacial failure is observed.

If the PSA has an elastic modulus which lies in the range defined by Dahlquist, the debonding process is then determined by the coupling of bulk and interfacial properties of the material. Within the framework of linear elasticity, the growth of a defect initially present at the interface is governed by the competition between two different mechanisms: the interfacial growth of a crack, which is governed by the critical energy-release rate, $\mathcal{G}_c$, and the bulk deformation, determined by the average stress within the layer, and essentially controlled by the elastic modulus of the adhesive, E.[40,41]

The physical principles for this analysis are based on the competition between linear elastic fracture mechanics and cavitation.[40,41] For a crack propagating at the interface between a rubbery material and a solid surface, $\mathcal{G}_c$ can be written as:[42]

$$\mathcal{G}_c = \mathcal{G}_0\left(1+\Phi\left(a_T V\right)\right) \qquad \textbf{Eq. 1-64}$$

where $\mathcal{G}_0$ is the resistance to crack propagation at vanishingly low crack velocity and $\Phi(a_T V)$ is the dissipative factor entering into $\mathcal{G}_c$. Previous studies on harder crosslinked rubbers simply relate this dissipative factor to the linear viscoelastic properties of the adhesive and in particular to either the dissipative part of the shear modulus G''[43]or to tan(δ), the ratio G''/G'[42]. However neither of these previous approaches considers large deformations of the material as it is observed for PSA. Based on the elastic analysis of the competition between interfacial crack propagation and cavitation in the layer a new analysis method has been proposed.

Webber et al. showed that for elastic layers, $\mathcal{G}_c$/E could be used as a predictor of the displacement applied to the adhesive before failure occurs (Figure 1-45).[41,44]

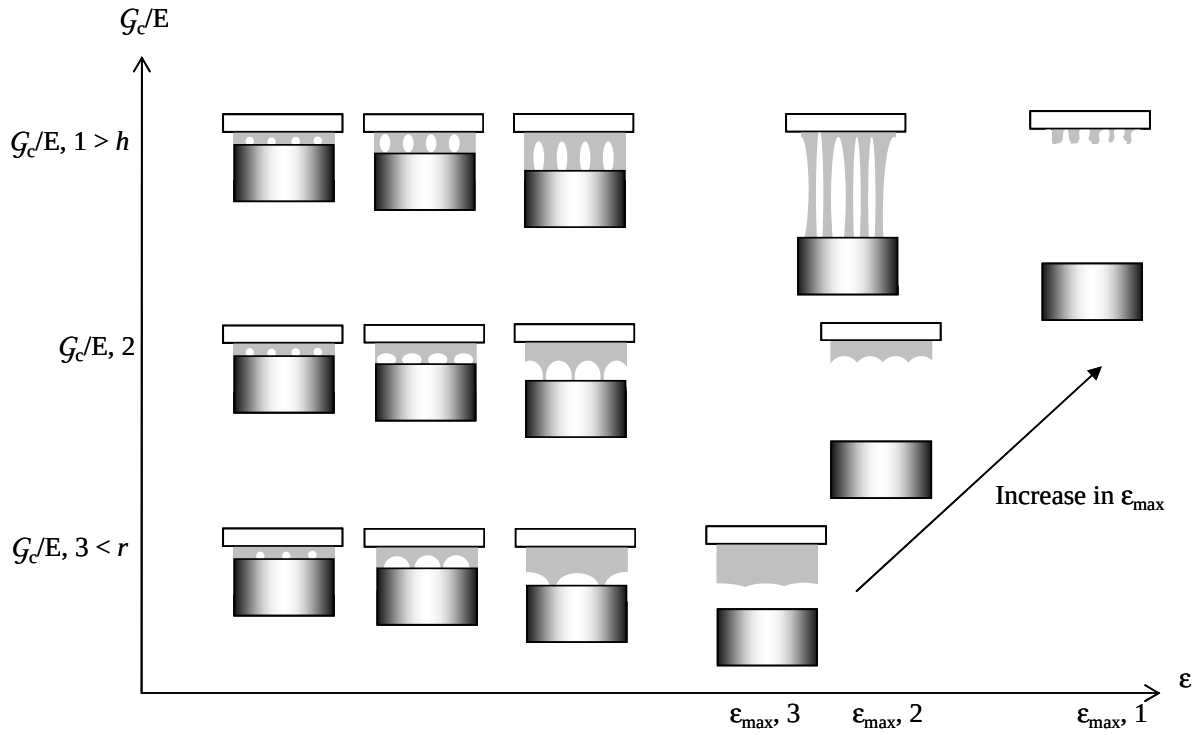

Figure 1-45. Schematics of the debonding process involved during probe tack test depending on the value of the ratio $\mathcal{G}_c$/E. Three different typical cases are displayed. For each value of $\mathcal{G}_c$/E four or five different steps observed during the test are displayed. (A test can be followed from the left to the right). The highest $\mathcal{G}_c$/E value ($\mathcal{G}_c$/E, 1) is higher than the thickness of the film h and the lowest $\mathcal{G}_c$/E value ($\mathcal{G}_c$/E, 3) is lower than the size of an initial defect r.

This elastic theory examines the growth of a small interfacial defect of size r at the interface between the elastic layer and the hard surface. It predicts that if $\mathcal{G}_c$/E is smaller than the initial defect size r (Figure 1-46-a), only interfacial crack propagation should be observed and the propagation of the interfacial crack should be controlled and limited by $\mathcal{G}_c$. At the other extreme if $\mathcal{G}_c$/E is larger than the thickness of the layer h (Figure 1-46-b), deformation in the bulk and a fibril structure should always be observed. The debonding in that case is limited by the stiffness of the material and depends on E, and it is less sensitive to $\mathcal{G}_c$. In the intermediate regime, as $\mathcal{G}_c$/E increases, a continuous transition is expected from interfacial crack propagation to bulk fibrillation.[33]

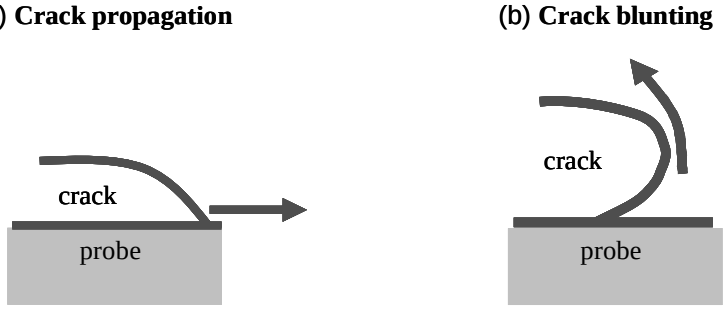

Figure 1-46. Schematics of a crack at the interface between the probe and the adhesive layer. (a) Case of a low value of $\mathcal{G}_c$/E, the propagation of the crack is controlled by $\mathcal{G}_c$. (b) Case of high value of $\mathcal{G}_c$/E, bulk debonding is limited by E.

An obvious question is the possible extension of these theoretical concepts developed for elastic layers to the more general case of viscoelastic materials. This development is one of the topics of this thesis and will be discussed in detail in chapter 4.

References

(1) Plessis, C.; Arzamendi, G.; Leiza, J. R.; Schoonbrood, H. A. S.; Charmot, D.; Asua, J. M. *Macromolecules* **2000**, *33*, 5041-5047.

(2) Blackley, D. C. *Emulsion Polymerisation*; Applied Science Publishers LTD: London, 1975.

(3) Smith, W. V.; Ewart, R. H. *Journal of Chemical Physics* **1948**, *16*, 592-599.

(4) Jovanovic, R.; Dube, M. A. *Journal of Macromolecular Science-Polymer Reviews* **2004**, *C44*, 1-51.

(5) Arzamendi, G.; Asua, J. M. *Journal of Applied Polymer Science* **1989**, *38*, 2019-2036.

(6) Arzamendi, G.; Asua, J. M. *Macromolecules* **1995**, *28*, 7479-7490.

(7) Do Amaral, M.; Asua, J. M. *Journal of Polymer Science Part a-Polymer Chemistry* **2004**, *42*, 4222-4227.

(8) Landfester, K. *Macromolecular Rapid Communications* **2001**, *22*, 896-936.

(9) Landfester, K. *Advanced Materials* **2001**, *13*, 765-768.

(10) Antonietti, M.; Landfester, K. *Progress in Polymer Science* **2002**, *27*, 689-757.

(11) Wang, S. T.; Schork, F. J.; Poehlein, G. W.; Gooch, J. W. *Journal of Applied Polymer Science* **1996**, *60*, 2069-2076.

(12) Gooch, J. W.; Dong, H.; Schork, F. J. *Journal of Applied Polymer Science* **2000**, *76*, 105-114.

(13) Tsavalas, J. G.; Gooch, J. W.; Schork, F. J. *Journal of Applied Polymer Science* **2000**, *75*, 916-927.

(14) Do Amaral, M.; Van Es, S.; Asua, J. M. *Journal of Polymer Science Part a-Polymer Chemistry* **2004**, *42*, 3936-3946.

(15) Keddie, J. L. *Materials Science & Engineering R-Reports* **1997**, *21*, 101-170.

(16) Salamanca, J. M.; Ciampi, E.; Faux, D. A.; Glover, P. M.; McDonald, P. J.; Routh, A. F.; Peters, A.; Satguru, R.; Keddie, J. L. *Langmuir* **2001**, *17*, 3202-3207.

(17) Gorce, J. P.; Bovey, D.; McDonald, P. J.; Palasz, P.; Taylor, D.; Keddie, J. L. *European Physical Journal E* **2002**, *8*, 421-429.

(18) Routh, A. F.; Russel, W. B. *Langmuir* **1999**, *15*, 7762-7773.

(19) Kim, H. B.; Winnik, M. A. *Macromolecules* **1995**, *28*, 2033-2041.

(20) Zosel, A.; Ley, G. *Macromolecules* **1993**, *26*, 2222-2227.

(21) Tamai, T.; Pinenq, P.; Winnik, M. A. *Macromolecules* **1999**, *32*, 6102-6110.

(22) Wang, Y. C.; Winnik, M. A. *Macromolecules* **1990**, *23*, 4731-4732.

(23) Mallegol, J.; Dupont, O.; Keddie, J. L. *Langmuir* **2001**, *17*, 7022-7031.

(24) Juhue, D.; Lang, J. *Macromolecules* **1995**, *28*, 1306-1308.

(25) Schellenberg, C.; Tauer, K.; Antonietti, M. *Macromolecular Symposia* **2000**, *151*, 465-471.

(26) James, H. M.; Guth, E. *Journal of Polymer Science* **1949**, *4*, 153-182.

(27) Mooney, M. *Journal of Applied Physics* **1940**, *11*, 582-592.

(28) Treloar, L. R. G. *Transactions of the Faraday Society* **1944**, *40*, 0059-0069.

(29) Horgan, C. O.; Saccomandi, G. *Journal of Elasticity* **2002**, *68*, 167-176.

(30) Gent, A. N. *Journal of Rheology* **2005**, *49*, 271-275.

(31) Gent, A. N. *Rubber Chemistry and Technology* **1996**, *69*, 59-61.

(32) Bird, R. B.; Armstrong, R. C.; Hassager, O. *Dynamics of Polymeric Liquids - Fluid Mechanics*; John Wiley & Sons second edition, 1987; Vol. 1.

(33) Shull, K. R.; Creton, C. *Journal of Polymer Science Part B-Polymer Physics* **2004**, *42*, 4023-4043.
(34) Lakrout, H.; Sergot, P.; Creton, C. *Journal of Adhesion* **1999**, *69*, 307-359.
(35) Zosel, A. *Journal of Adhesion* **1989**, *30*, 135-149.
(36) Zosel, A. *Adhesives Age* **1989**, 42-47.
(37) Poivet, S.; Nallet, F.; Gay, C.; Teisseire, J.; Fabre, P. *European Physical Journal E* **2004**, *15*, 97-116.
(38) Dahlquist, C. A. In *Treatise on Adhesion and Adhesives*; Patrick, R. L., Ed.; Dekker, 1969; pp 219-260.
(39) Creton, C.; Leibler, L. *Journal of Polymer Science Part B-Polymer Physics* **1996**, *34*, 545-554.
(40) Creton, C.; Lakrout, H. *Journal of Polymer Science Part B-Polymer Physics* **2000**, *38*, 965-979.
(41) Crosby, A. J.; Shull, K. R.; Lakrout, H.; Creton, C. *Journal of Applied Physics* **2000**, *88*, 2956-2966.
(42) Maugis, D.; Barquins, M. *Journal of Physics D-Applied Physics* **1978**, *11*, 1989-2023.
(43) Degennes, P. G. *Comptes Rendus De L Academie Des Sciences Serie Ii* **1988**, *307*, 1949-1953.
(44) Webber, R. E.; Shull, K. R.; Roos, A.; Creton, C. *Physical Review E* **2003**, *68*.

2. State of the Art

In previous years, our laboratory has carried out systematic investigations of adhesive performance on PSA based on hot melt styrene-isoprene-styrene block copolymers[1] and on solvent acrylic PSA.[2] Adhesion of PSA made from latexes has also been studied by Josse.[3] However, in this latter case, the objective was not to obtain PSA with optimized adhesive performance but to work on model systems to gain a better understanding of the physics of adhesive behavior on low-adhesion surfaces. In that case the waterborne PSA studied were simply made of homopolymers of PEHA and PnBA and were synthesized by Rhodia.

In this thesis, our goal is different. The objective is to use emulsion polymerization as a tool to finely control the polymer particle structure to finely control adhesive properties. Of course PSA made from latex particles have been around for quite some time and started to be widely used since the 1970s according to Jovanovic and Dubé.[4] However the systematic studies of their properties[5-10] as well as the recognition that the structure of the PSA and its properties will be different from a polymer made with an identical monomer composition but in solution, is only relatively recent.[11,12] This manufacturing process is attractive in terms of cost and is also environmentally friendly. However it has some significant drawbacks: the molecular structure of the individual particles cannot usually be controlled as well as in solution, surfactants must be used and remain in the dry film, altering properties and reducing water-whitening resistance, and finally because the final film is obtained from the coalescence of particles by molecular diffusion, the overall cohesion of the film is difficult to adjust without overcrosslinking the particle. The goal of the present work is to overcome some of these limitations and we have then to start with an overview of the current knowledge on such systems.

In the first part of this chapter, a review of the adjustable synthesis parameters during an emulsion polymerization is given. In the second part, results of adhesive performance of wb-PSA obtained by various research groups are reported. The impact of the synthesis parameters on the final molecular structure of the polymers is emphasized and finally the effect of these macromolecular properties on final adhesive properties is discussed.

2.1. Adjustable parameters during wb-PSA synthesis

To begin with, it is important to know what a typical waterborne acrylic PSA formulation is made of. The major components used in the production of waterborne PSA are listed in Table 2-1 with their approximate amounts. We can note how complex is a PSA formulation and the variability of the component amounts. There exists no unique recipe for the production of a wb-PSA with optimal adhesive performances but rather a collection of recipes, varying from one company to another and of course from an application to another.

Component	*Example*	*Amount*
Monomers		
"Soft"	Alkyl esters e.g. BA, 2-EHA, EA	50-90%
"Hard"	MMA, VAc, S	10-40%
Polar	AA,MAA	2-20%
Stabilizer(s)		
Electrostatic	Sodium Dodecyl Sulphate, sulfosuccinates	0-8%
Steric	Hydroxyethyl cellulose, PVOH, starches	
Surfmers	For example, allyl amine salts of (1) alkyl benzene sulfonate or (2) phosphate ester	
Buffer(s)	$CaCO_3$, $NaHCO_3$, Na_2CO_3	0-1%
Initiator(s)	Thermal (e.g. ammonium and potassium persulfate), Redox (persulfate/bisulfate systems)	up to 3%
Chain transfer agent(s)	Mercaptanes	0-3%
Water	Distilled de-ionized	40-70%
Additives	Not detailed here	0.5-2%

Table 2-1. Emulsion polymerization components for the production of wb-PSA (after [4]).

To tune adhesive properties, we can play with the reaction components but also with the synthesis process. As discussed in chapter 1, different emulsion polymerization processes exist, such as batch emulsion polymerization, semi-continuous emulsion polymerization and semi-continuous emulsion polymerization conducted under monomer starved conditions. Depending of the process used, the final macromolecular structure of the polymers formed is different.

Other synthesis parameters such as monomer feeding rate, temperature, initiator concentration… have also an effect on the final structure of the materials. These are however more challenging to be finely controlled.

The high number of adjustable parameters allows the production of emulsion based polymers with a large range of properties, from liquid (gel free) to solid (with gel or crosslinked), from soft (low T_g) to hard (high T_g), from dissipative (high tan(δ)) to more elastic... These rheological and mechanical properties are controlled by the macromolecular architecture of the polymer and they govern adhesive properties as schematically shown on Figure 2-1.

The optimization of adhesive performance requires first the adjustment of rheological properties through the design of the polymer structure.

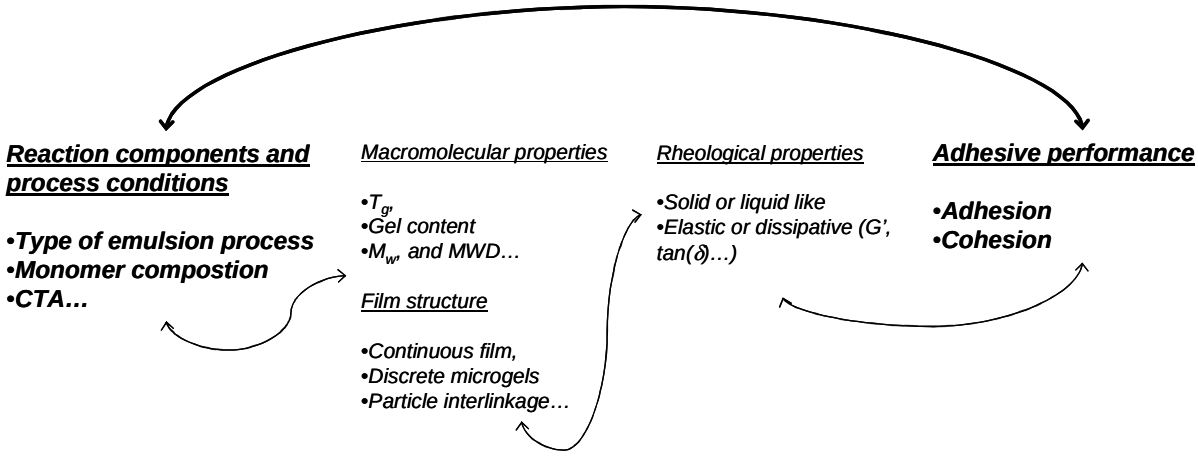

Figure 2-1. Schematic of the optimization of adhesive properties from the adjustment of synthesis factors and components. Importance of the macromolecular and rheological properties.

In the following part, general characteristics required for PSA applications are presented and their relation with rheological behavior is briefly discussed. Then, a review of previous works on adhesive performance of wb-PSA is made and we present results which have been found for the control of adhesion through the adjustment of factors and components of the emulsion polymerization.

2.2. Adhesive performance of wb-PSA

2.2.1. Adhesion characterization techniques

PSA adhere instantaneously to solid surfaces with the application of a light pressure and can be debonded without leaving a residue on the substrate. Thus PSA need to be sticky upon contact and to have a high viscoelastic character to dissipate energy through deformation during the debonding.[13] For the final detachment to be possible, PSA must also be able to strain-harden at high levels of strain. In the literature found about adhesive performance of wb-PSA, adhesion is most of the time characterized using three major tests. These are *tack*, *peel performance* and *resistance to shear.* After describing how these tests are carried out, rheological factors which are relevant to produce PSA with the required properties will be discussed.

- Peel Adhesion

The *peel adhesion* is defined as the force required to remove (adhesively or cohesively) the PSA from a standard test plate surface over the width of the tape at a given velocity and is expressed in *N/m.*

Different peel tests are suggested by various standards organizations (ASTM) or trade organizations (PSTC, TLMI, AFERA, FINAT). Differences are observed in the peel angle, the peeling rate, the time elapsed before the test is carried out and the type of the substrate surface.

The most common combinations[14] to test the resistance to peel are shown in Figure 2-2. For the first one, the angle between the adhesive strip and the backing is equal to 180° while for the second one, this angle is of 90°.

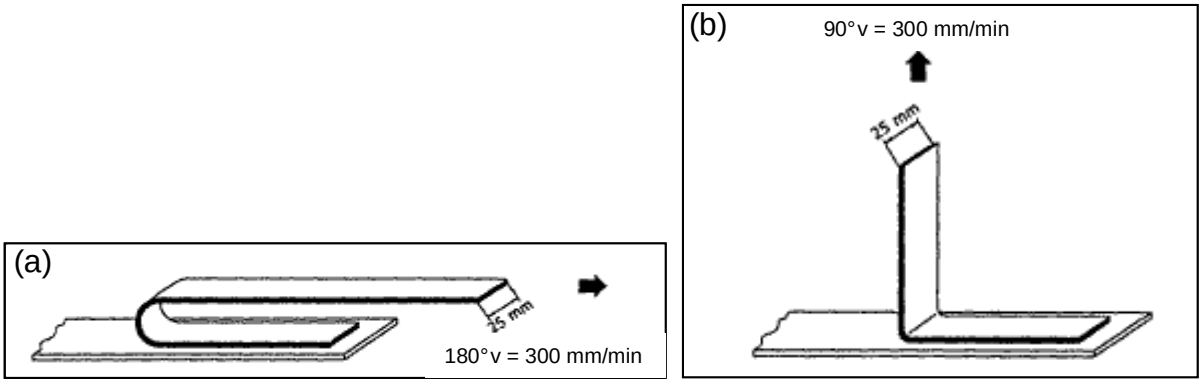

Figure 2-2. Two geometries to test the resistance to peel. (a): 180-degree peel test, (b): 90-degree peel test.

The relationship between viscoelastic and peeling properties has been extensively studied.[15-25] It was observed that during a *peel test*, two processes are taking place simultaneously. There is a lateral propagation of fractures at the interface and at the same time, vertical elongation of fibrils in the bulk (Figure 2-3). Thus, peel strength is governed by the dissipative properties at small and high strains and by the ability of the material to

deform. To obtain a high peel force while ensuring an adhesive debonding, a certain level of cohesion is also required.

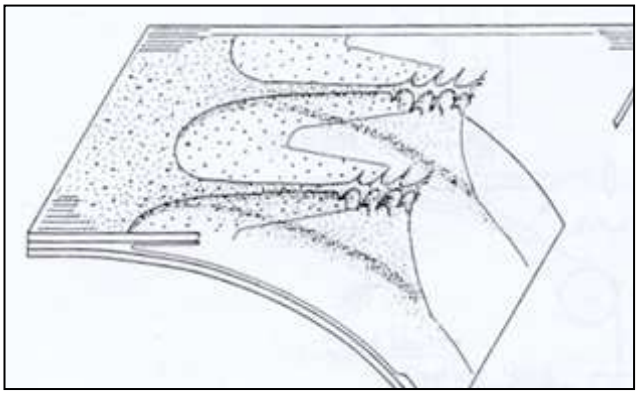

Figure 2-3. Schematics of the pattern observed during the peeling of an adhesive, (after [26]).

- Resistance to shear

The *resistance to shear* measures the time at which the adhesive bond fails (adhesively or cohesively) from a standard surface. Similar to peel, the determination of the *resistance to shear* can vary form one standards organization to another (different loads and areas of contact are recommended).

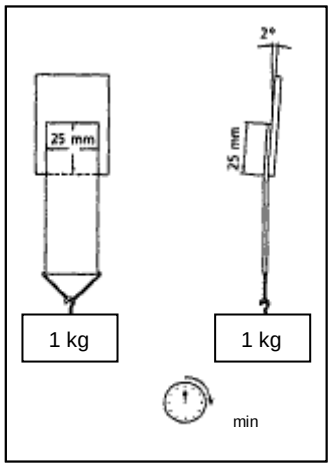

Figure 2-4. Geometry of the resistance to shear test.

The shear resistance is referred to as the PSA's cohesive strength or simply cohesion. There exists no predictive model of the shear strength from the mechanical properties of a material under a homogeneous stress, as typically measured with a classical rheological or tensile test.[27] But, a pressure sensitive adhesive must exhibit an elastic cohesiveness and a resistance to flow under stress[28] and the *shear resistance* is commonly defined a measure of the ability of the material to resist flow. This definition takes only into account the behavior of the adhesive at long times. Nonetheless, it is believable that behavior at shorter times plays also a role and that to reach acceptable resistance to shear, a PSA must also exhibit a certain level of cohesion at short time. Thus, a good shear resistance can be reached when the

material has an acceptable elastic modulus at small and intermediate strains and does not exhibit liquid like behavior but, on the contrary, is characterized by a hardening at high strains. It has been shown that long term creep can be greatly reduced[28] and thus resistance to shear can be greatly enhanced by cross-linking.

- Tack measurement

Different tack methods exist such as the loop tack test,[29] the *rolling ball*[30,31] and variations of these such as the mechanical optical tack test (*MOTT*).[32-36] We will not talk about the probe tack in this chapter since, in the literature we found, this technique was not much used to characterize adhesive performance of wb-PSA.

In a *loop tack test,* a loop of a coated facing material strip, with the adhesive surface facing the outside, is formed and brought into contact with a substrate at a defined rate (Figure 2-5). The loop tack value is expressed as the force required to remove at a defined rate the loop from the substrate. The loop tack value of a PSA is not typically very reproducible.

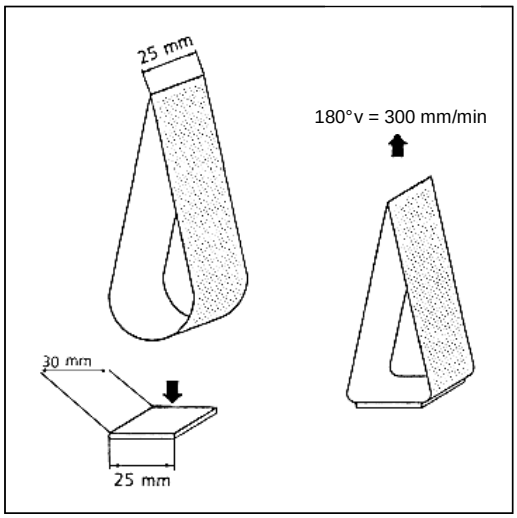

Figure 2-5. Geometry of the loop tack measurement.

Rolling ball is the Pressure Sensitive Tape Council's test method n°6 (PSTC-6).[30] In this procedure, an 11-mm diameter stainless-steel ball is rolled down an inclined ramp to come into contact at the bottom with a horizontal strip of PSA. The distance the ball travels out along the tape is taken as the measure of tack. The shorter the distance, the higher the tack.

In the *MOTT,* tack is measured by the force during the pulling up of a quartz probe, after contact with the adhesive film for a determined contact time, under a controlled contact stress. The tack stress σ_{tack} is defined as the ratio between this force and the actually wet probe area. The product of the area subtended by the curve $\sigma_{tack} = f(t)$ by the pulling rate gives the tack energy G_{tack}.

Regardless of the method used, t*ack,* measures the ability of the PSA to stick instantly and under a light pressure to the substrate. Rheological properties are important in controlling tack.[30,37] To ensure good tack performance adhesives have to be easily deformed in the time scale allowed for bond formation,[30] i.e. at low rate[38] and short times. Moreover, for good tack, it is essential to relax the stress created in the adhesive when it is made to conform to the topological irregularities of the adherent. Thus, for good tack, the adhesive deformation in the bonding stage has to be in large part viscous.[30] Moreover, since good tack involves the breaking of the bond, tack is enhanced by a low short time modulus and greater ultimate elongation at break and very viscoelastic behavior.

We have briefly discussed main rheological parameters which control tack, peel and shear performance. These desired rheological behaviors are obtained through a correct design of the macromolecular structure. For example, because, both tack and peel are governed by viscoelastic processes, they are directly related to M_w and M_e. On the other hand, gel content and network morphology are the major parameters which influence shear resistance.

Emulsion polymerization can be used of course to control this structure. The main difficulty is that PSA properties are not independent. Indeed, synthesis factors are correlated and affect tack, peel and shear strengths at the same time.

Most of studies found in the literature describe the influence of the most easily controllable synthesis parameters. These are:

- Monomer composition.
- Chain transfer agent level.
- Crosslinker level.
- Process conditions.

Tackifier is also used as an additive to improve tack performance. However, the role of the tackifier and its impact on adhesive performance is extensively discussed in chapter 6 of this thesis so we decided not to consider the tackifier amount as an adjustable parameter here.

Two different types of approach for the study of the adhesive performance of wb-PSA can be found in the literature. The first one is a knowledge based approach where effects of reaction components and type of process on adhesive behavior are studied in a systematic and controlled manner. With this approach however the final properties of the PSA investigated tend to remain very inferior to the performance of commercial systems and concepts cannot always readily be extrapolated.

The second approach is more used by industrial studies. It consists in an empirical optimization of adhesion; this means that from a material with optimized properties, some optimal reaction parameters or molecular structures are deduced. In this case of course the properties of the PSA are very close to those of real applications, but little knowledge can be extracted from the results other than practical optimization recipes.

2.2.2. Effect of reaction components

In general, works reported in the literature do not study the effect of T_g. It is most of the time kept as a constant value. The choice of monomers used in the copolymer composition is often made with the objective of reaching an acceptable value of T_g for PSA application. A maximum of adhesion is typically reached between 50°C and 70°C above the T_g.[39,40] Moreover, concerning the effect of reaction components, researches found in the literature are all made on materials synthesized using the semi-continuous emulsion polymerization process since a better control of the copolymer composition is achieved compared to the batch process.

A typical academic approach consisting in the construction of mathematical models based on the complex kinetic mechanisms has been found.[40-42] These models are interesting in the sense that they are able to predict molecular features which govern rheological properties which in turn control adhesion from parameters which depend on the monomer composition for example. Interesting features are gel fraction, sol molecular weight M_w and molecular weight distribution (*MWD*) and branching frequency. Results obtained from these models are discussed later.

Influence of a high T_g comonomer

Formulated PSA are made of soft monomers as the major components. However, the poor resistance to shear and low room temperature peel resistance of the soft homopolymers synthesized restrict their usefulness as polymers for PSA. Performances are however improved after raising the T_g by copolymerization with high T_g monomers. Plessis et al.[42] studied the effect of the addition of styrene as a high T_g comonomer. In the case of a seeded semibatch emulsion polymerization of nBA, they found that as the amount of S was increased, gel content was decreased and M_w slightly increased. One can note the inverse relationship between gel content and M_w of the sol. It has been noted by many authors.[40,43,44] This is attributed to the progressive transfer of high M_w fractions to gel fraction via transfer to large polymer chains followed by termination and combination when gel content increases. The latex with the lowest amount of S shows a weak shear resistance and this result was explained by the fact that particle interpenetration during film formation was precluded because of the large amount of gel. Concerning peel resistance, it increased first as the amount of gel increased, but further increasing gel led to a decrease in the peel performance due to a lack of mobility of polymer chains. However, for peel resistance as for shear, values stay very low. A maximum of 1662 s for the shear with 2.5% of S is reported this means that materials produced could not be used as effective PSA.

The effect of the secondary hard monomer has also been studied by Gower and Shanks[43] but using a different approach. A time temperature superposition was used to construct peel master curves in the objective to compare copolymers containing either styrene or MMA as high T_g monomers, and to reveal the influence of these molecular features on adhesion. Main differences between S and MMA appeared in the cohesive failure region (region where the cohesion is too low for the material to be used as a PSA) of the peel curve. Substituting MMA for S resulted in a decrease in the reduced peel adhesion. The construction of the super

master curves (which take into account the relative amount of the other two monomers BA and EHA present in the formulation) suggested differences in the relative mobility of S and MMA and this had been explained by the fact that chain branching and entanglement are more significant with MMA than with S. It has also been reported that S limited chain transfer more effectively than MMA leading to lower gel content and to higher M_w. Shear resistance results had been explained in terms of polymer viscosity (the relation used is the same as the definition of the long-term creep defined by Dahlquist[28]). Such reasoning is however valid only for low shear resistance and cannot be used anymore for high performance adhesive[27] where shear resistance is strongly governed by gel content .

Influence of the main monomers composition

Effect of the main monomers has also been experimentally studied.[44,45] Tobing and Klein[44] compared adhesive results obtained on model PSA based on P(2EHA-stat-AA) and P(nBA-stat-AA) at 97.5/2.5 wt% which were synthesized using semi-continuous emulsion polymerization (note that in these systems no high T_g comonomers were used). Results were explained in terms of M_w, M_e, and M_c. It has been found that the P(2EHA-stat-AA) composition showed a higher peel and loop tack than the P(nBA-stat-AA). This was explained by the higher M_e for P(2EHA). Moreover, P(nBA-stat-AA) compositions showed a lower gel content but a higher shear resistance compared with that of P(2EHA-stat-AA). In this situation where gel content is high, gel content has a detrimental effect to shear resistance since a discrete network morphology is formed. The observed increase in the shear holding is attributed to the possible formation of an interlinkage between particles. This is favored in the case of P(nBA-stat-AA) since it has a higher M_w/M_e ratio. The formation of an interlinkage between particles as a tool to increase the shear resistance has been reported in two other papers.[46,47] It has been shown that interconnection of the microgels can be produced through a crosslinking reaction where the role of the crosslinker was to graft the linear polymer chains of the sol with the microgels as depicted in Figure 2-6. However, for the reaction to be effective in creating interlinkages some conditions are required: the M_w of the linear polymer needs to be at least twice of M_e and the molecular weight between crosslinks of the gel, M_c, needs to be at least equal to M_e. These requirements can be reached by the adjustment of monomer composition (as it has just been discussed) and/or by the adjustment of content of the chain transfer agent (the effect of CTA level is discussed in more details later).

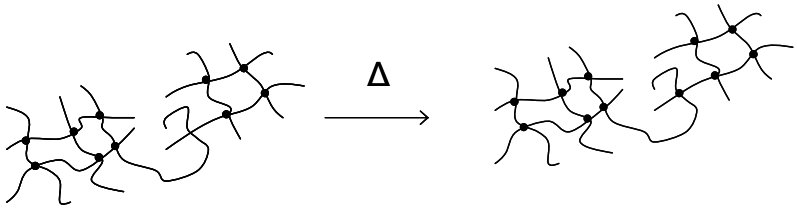

Figure 2-6. Network formation through the grafting of linear polymer chains (after [46]).

The work of Tobing and Klein was mainly focused on the film morphology obtained after the drying of latex particles and showed that the formation of a continuous film is an important requirement to achieve good cohesion. This study also revealed that, to significantly increase the shear resistance, only few crosslink points were needed. And in

contrast to building a whole network no detrimental effect on peel and tack had been observed.

Effect of the monomer composition and the influence of the relative amount of 2-EHA and BA has also been investigated by Gower and Shanks[45] but in a more complex system than the one studied by Tobing and Klein. 2-EHA and BA were copolymerized with high T_g monomers: MMA and AA. Similar to what Tobing and Klein had reported, an increase in gel content with increasing weight fraction of 2-EHA was observed. They however reported an increase in shear resistance due to this higher gel content. This shows the sensitivity of the adhesive properties on details of the molecular architecture.[44] Not surprisingly, the polymers showed a decreasing peel adhesion values with increasing copolymerized levels of EHA.

Influence of AA

The last but not the least important parameter in terms of monomer composition is the acrylic acid, AA, level. A considerable number of research works has been performed on the correlation between the acrylic acid level and the adhesive properties.[12,48-51] Lots of studies reported an increase in the adhesion as the AA level increases.[52,53] Effect of AA was explained by an increase in the interfacial interactions, particularly when using polar substrates and by a modification of the bulk rheological response of the material. The influence of the AA content in emulsion based systems have also been studied by Gower and Shanks.[54] The amount of AA was varied from 2 wt% to 6 wt% in copolymers made of EHA, BA, MMA and a CTA was added to lower the gel. An increase in the gel content as a function of AA level has been reported. This was explained by networks formation through hydrogen bonds formation. Not surprisingly, a decrease in M_w accompanied the increase in the gel. A higher shear resistance was obtained as a consequence of higher gel content. Some peel master curves have been constructed and increased AA content led to the shifting of the cohesive to adhesive failure transition to progressively lower reduced peel rates and an increase in the viscosity is suggested as responsible for this shift. This is in agreement with results of Ahn and Shull[55] who found that through hydrogen bonding, self association of acid groups resulted in a shift of curves of the elastic and dissipative modulus to lower reduced test frequencies. An interesting additional result from the study of Gower and Shanks[54] is that a maximum in loop tack value occurred as AA content varied. This suggests that from 2 wt% to 4 wt% the increase in interfacial interactions dominates compared to the increase in the rigidity as a result of the a network formation through hydrogen bonds while above 4 wt% the tendency is reversed.

The effect of AA content in a waterborne PSA is therefore a bit subtle. AA can be used to increase adhesive performance as soon as the creation of interfacial interactions dominated compared to the formation of a stiff network in the bulk. Effect of AA depends also on the rate at which test is performed. At low rates, hydrogen bonds are not effective in the formation of a stiff network while at higher strain rates hydrogen bonds can play the role of chemical crosslinks.

Effect of CTA level

When using the semi-continuous emulsion polymerization under monomer starved conditions as the synthesis process, chain transfer to polymer, leading to the formation of highly branched polymer structures and microgels inside latex particles is favored, and often the addition of a component to limit this gel formation is required. We have seen that some monomers have an inherent tendency to decrease the gel but most of the time a CTA is specifically added to play this role. With a similar approach used for the effect of the amount of styrene, Plessis et al.[40] investigated the effect of the amount of CTA. Again a mathematical model caught well the effect of the CTA content and it has been shown that an increase in the amount of CTA led to a decrease in gel content and had nearly no effect on M_w of the sol. Evolutions of gel content and M_w had been used as tools to understand shear resistance and peel performance. Plessis et al. found that an increase in the amount of CTA had nearly the same effect as the increase in styrene previously discussed. However, these materials have again very poor adhesive performance and therefore cannot be used for PSA applications.

The effect of CTA level has also been investigated by Gower and Shanks[56] through the construction of peel master curves. Not surprisingly an increase in the amount of CTA led to a decrease in gel content. This study also revealed that the presence of high levels of polymer gel tended to obscure the influence of monomer composition on the shear resistance. Decreasing the amount of gel, the influence of the presence of polymer gel on shear diminished and the influence of monomer composition began to dominate.

Influence of initiator concentration and monomer feeding time

Effects of less easily controlled parameters like initiator concentration and monomer feeding time have been studied.[57] Results showed that gel content was independent on initiator concentration and monomer feeding time. But the higher the initiator concentration and the monomer feeding time, the higher the level of branches and the lower the M_w. However, no adhesive tests have been carried out on this series.

We have reviewed some results of the influence of reaction components on adhesive performance. Plessis et al. constructed a mathematical model for the prediction of adhesive performance but a rheological study is lacking. Therefore, materials produced have only poor adhesive performance. Adhesive results were explained in terms of molecular parameters but no commercially viable PSA were obtained.

Empirical models for the influence of main monomer composition

In this part, we present results found in the literature and obtained when the second more industrial approach is adopted. The major objective of those research groups is to propose empirical models constructed after screening experiments. An example is given by Jovanovic et al.[58] where the influence of individual monomers BA, VAc and AA on the final adhesive performance of emulsion-based PSA was studied. For each adhesive characteristic, loop tack, peel and shear, an optimal operating region was proposed as shown on Figure 2-7. This example clearly shows that there was no single region where all responses were at their

maximum value. The final performance is a matter of trade-off where certain properties are favored at the expense of others.

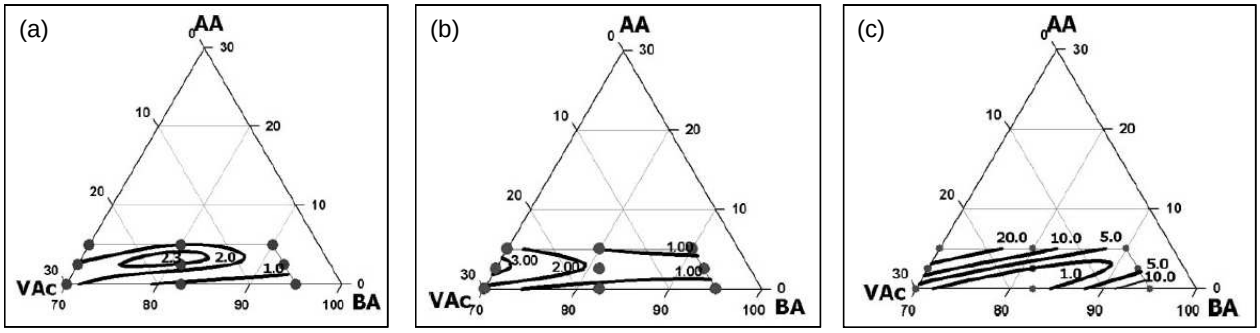

Figure 2-7. (a) loop tack contour lines, (b) peel strength contour lines, (c) shear strength contour lines (after[58]).

Even though the problem of the optimization of monomer composition to reach best adhesive performances (i.e. the best balance between adhesion and cohesion) is still unsolved, Jovanovic et al. proposed to complexify their system by adding lots of other variables like temperature, CTA content, stabilizer types, weight fraction of initiator, solids content and stabilizer type.[59] This is a typical case where screening experiments are conducted in order to achieve the best properties. However, from the huge number of parameters, it is a little bit difficult to look at the effect of each of them and we feel a bit lost when looking at the screening design (see Figure 2-8). It was there in black and white that "it is not possible to point out which of the investigated variables has the highest influence on any of the observed behaviors".

independent variable	level −	0	+
A = BA/VAc wt/wt ratio[a]	95/5	90/10	80/20
B = weight fraction of AA[a]	1	3	5
C = weight fraction of stabilizer[a]	2	4	6
D = weight fraction of CTA[a]	0.05	0.5	1
E = weight fraction of initiator[a]	0.2	0.3	0.4
F = temperature	60	70	80
G = solids content[b]	30	40	50
H = stabilizer type	SDS	PVOH	PVOH

[a] Weight fractions are based on the total weight of monomer mixture unless otherwise indicated. [b] Weight fraction of solids based on total weight of reaction mixture.

run	A	B	C	D	E = BCD	F = ACD	G = ABC	H = ABD
1	−	−	−	−	−	−	−	−
2	+	−	−	−	−	+	+	+
3	−	+	−	−	+	−	+	+
4	+	+	−	−	+	+	−	−
5	−	−	+	−	+	+	+	−
6	+	−	+	−	+	−	−	+
7	−	+	+	−	−	+	−	+
8	+	+	+	−	−	−	+	−
9	−	−	−	+	+	+	−	+
10	+	−	−	+	+	−	+	−
11	−	+	−	+	−	+	+	−
12	+	+	−	+	−	−	−	+
13	−	−	+	+	−	−	+	+
14	+	−	+	+	−	+	−	−
15	−	+	+	+	+	−	−	−
16	+	+	+	+	+	+	+	+
17	0	0	0	0	0	0	0	0
18	0	0	0	0	0	0	0	0
19	0	0	0	0	0	0	0	0
20	0	0	0	0	0	0	0	0

Figure 2-8. Example of a screening design (after [59]).

Empirical models could serve as a guideline for the choice of a recipe for the production of high-performance PSA. However, when using emulsion polymerization process, it is a real challenge to reproduce one system and a material with very different properties is most of the time finally obtained.

We have shown that the addition of a component to an emulsion formulation has a systematic effect on the molecular structure of polymers. Some mathematical models were proposed to predict such molecular features from parameters of the kinetics mechanism. They seem to work well but only studies on too simplified and non optimized systems have been reported. On the other hand, some empirical models taking into account the influence of a large number of parameters were constructed. However, the good adhesive performance obtained is in general really difficult to reproduce due to the complexity of the systems and to a lack of understanding of the influence of each parameter.

We have discussed the effect of the reaction components but emulsion polymerization is also an excellent tool to produce materials with a well defined structure giving rise to a heterogeneous structure of the dried film. The effect of the polymerization process on the particle morphology and film structure is the object of the next part.

2.2.3. Effect of the polymerization process and structure

Structure of a PSA made from latexes is different from a polymer made in solution.[11] And the emulsion process is attractive in the sense that a particular tailoring of PSA properties by selection of the polymerization process is possible.[60] Aymonier et al.[32,36] studied the effect of the polymerization process, batch, versus starved semi-continuous (SC), on the tack of emulsion copolymers of 2-EHA and MMA of a 50/50 molar composition. The batch process led to the formation of heterogeneous particles due to a kinetic control of the particle morphology. This process provides the formation of polymer particles with MMA-rich cores surrounded by increasingly rich concentric outer layers of 2-EHA as shown on Figure 2-9-b.

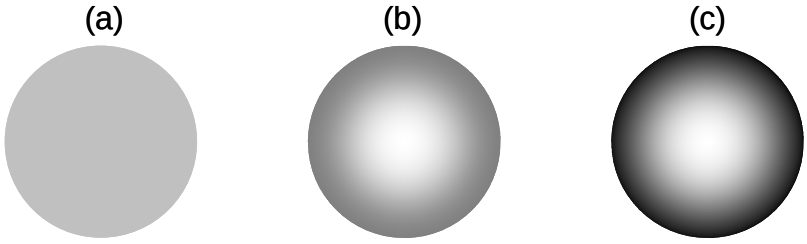

Figure 2-9. Assumed polymer particles structures induced by (a) SC mixture, (b) batch and (c) SC gradient polymerizations (after [32]).

Semi-continuous process under starved monomer conditions led to the formation of homogeneous particles (Figure 2-9-a) when the feed was a blend of EHA and MMA with the same composition during the whole process and core-shell like particles (Figure 2-9-c) were obtained when feeding was inversely varying with both monomers. 2-EHA content increased from the center to the outer of the particle.

They found that the heterogeneous structure showed a lack of adhesion and cohesion. They speculated that high adhesive energy of the homogeneous structure was reached because these materials were composed of long flexible and strongly entangled polymer

chains. On the contrary, low of adhesion and cohesion of the heterogeneous structure was explained by a lack of compatibility between the hard and the soft phase. The preceding part highlighted some effects EHA and MMA have on the kinetics mechanism of the emulsion polymerization and the important roles they have in controlling gel content and M_w of polymer chains. However, here, Aymonier et al. did not report any results of either the M_w or the gel content. Not much improvement had been obtained here with the heterogeneous structure probably because the overall composition would have needed to be adjusted when changing the particle morphology.

The effect of the composition profile of 2EHA-MMA latexes on adhesive performance has also been studied by Laureau et al..[61] In this study, the molecular weight was controlled to produce latexes of similar MWDs. Homogeneous particle morphology was obtained using a semi-continuous process with a feeding monomer composition made of an 85/15 mixture of 2EHA/MMA. Gradient particles with a molar cumulative composition of 2EHA/MMA varying from 75/25 at overall conversion zero to 85/15 at overall conversion one or varying from 95/5 to 85/15 are synthesized. Heterogeneous morphology is obtained using the batch process with an overall 85/15 composition of 2EHA/MMA. Adhesive results were unfortunately unclear and this was attributed to the fact that the differences between the different composition profiles were modest. Here again, gel content was not reported.

These two examples prove that emulsion polymerization can be used to finely tailor particle morphology. What has however not been done is the simultaneous fine adjustment of gel content and MWD required to reach good adhesive performance.

2.3. Conclusion

Different groups have investigated adhesive properties of wb-PSA. Each of them had their own way of approaching the problem, through the development of mathematical or empirical model for instance. However, in all cases, it seems that the effects of some synthesis parameters were investigated in the objective to give some tools for the tailoring of wb-PSA but not in the objective to target optimal adhesive properties. Nonetheless these results can serve as useful guidelines, and in the present work we take advantage of all of them.

The general trends of the effect of each adjustable parameter which result from previous studies can be summarized as follows:

- The main factor which affects the T_g is the monomer composition.
- The main factor that affects the amount of gel and M_w is the CTA level. A secondary factor that affects the amount of gel and M_w is the monomer composition since gel content is governed by the ability of the monomer to chain transfer.
- The main factor that affects the branching and entanglement is the monomer composition.
- The main factor affecting the hydrogen bonding formation if the amount of AA.
- The main factor favoring the formation of a continuous film is the activation of an interparticle crosslinking reaction.

These trends are however not sufficient to produce high performance wb-PSA from knowledgde-based methods and several reasons can be proposed.

First, some groups worked on simple model systems for a better control. However, it appears difficult to transpose results obtained on such systems on more complex formulations containing all components required in a typical waterborne PSA formulation (Table 2-1). Thus we decided to take as a starting point of our research an industrial non optimized PSA formulation.

Secondly, adhesive properties are a matter of trade-off, i.e. an improvement in the cohesion (or shear) is most of the time accompanied with a decrease in the adhesion (or tack and peel). And a good balance of adhesion and cohesion is difficult to reach through a single change of one synthesis variable. We tried to overcome this problem decoupling adhesion and cohesion. For that, we took advantage of the capability of emulsion polymerization to create heterogeneous particles with well controlled morphology as shown by Aymonier et al, but we took special care to control gel content and M_w.

Finally, rheological characterizations of the materials produced were rarely found in the literature even though adhesive performance is directly related to rheological behavior. In the present work, we decided to use rheological properties in addition to adhesive measurements to tune and finely characterize adhesive performance of our materials. Of particular interest for us will be the large strain behavior of the PSA, which contains two features, barely visible in linear rheology, i.e.:

- The nonlinear dissipative properties occurring at large strains due to the change in structure of the material and its nonlinear relaxation behavior.

- The finite extensibility of the polymer network which controls both the resistance to creep (and shear resistance) and the adhesive detachment without residues.

References

(1) Roos, A.; Université Paris VI, 2004.
(2) Lakrout, H.; Creton, C.; Ahn, D. C.; Shull, K. R. *Macromolecules* **2001**, *34*, 7448-7458.
(3) Josse, G.; Université Paris VI, 2001.
(4) Jovanovic, R.; Dube, M. A. *Journal of Macromolecular Science-Polymer Reviews* **2004**, *C44*, 1-51.
(5) Donkus, L. J. *Adhesives Age* **1997**, *40*, 32-37.
(6) Zawilinski, A. *Adhesives Age* **1984**, *27*, 29-32.
(7) Yang, H. W. H. *Journal of Applied Polymer Science* **1995**, *55*, 645-652.
(8) Zosel, A.; Schuler, B. *Journal of Adhesion* **1999**, *70*, 179-195.
(9) Dehnke, M. K. *Adhesives Age* **1994**, *37*, 12-13.
(10) Horwat, D. W. *Adhesives Age* **1999**, *42*, 20-+.
(11) Charmeau, J. Y.; Berthet, R.; Gringreau, C.; Holl, Y.; Kientz, E. *International Journal of Adhesion and Adhesives* **1997**, *17*, 169-176.
(12) Garrett, J.; Lovell, P. A.; Shea, A. J.; Viney, R. D. *Macromolecular Symposia* **2000**, *151*, 487-496.
(13) Creton, C. *Mrs Bulletin* **2003**, *28*, 434-439.
(14) Satas, D. *Handbook of Pressure Sensitive Adhesive Technology*; Van Nostrand Reinhold Book: New York, 1989.
(15) Marin, G.; Derail, C. *Journal of Adhesion* **2006**, *82*, 469-485.
(16) Derail, C.; Allal, A.; Marin, G.; Tordjeman, P. *Journal of Adhesion* **1997**, *61*, 123-157.
(17) Kaelble, D. H. *Transactions of the Society of Rheology* **1965**, *9*, 135-163.
(18) Benyahia, L.; Verdier, C.; Piau, J. M. *Journal of Adhesion* **1997**, *62*, 45-73.
(19) Gibert, F. X.; Marin, G.; Derail, C.; Allal, A.; Lechat, J. *Journal of Adhesion* **2003**, *79*, 825-852.
(20) Verdier, C.; Ravilly, G. *Journal of Polymer Science Part B-Polymer Physics* **2007**, *45*, 2113-2122.
(21) Piau, J. M.; Ravilly, G.; Verdier, C. *Journal of Polymer Science Part B-Polymer Physics* **2005**, *43*, 145-157.
(22) Yarusso, D. J. *Journal of Adhesion* **1999**, *70*, 299-320.
(23) Derail, C.; Allal, A.; Marin, G.; Tordjeman, P. *Journal of Adhesion* **1999**, *68*, 203-228.
(24) Verdier, C.; Piau, J. M.; Benyahia, L. *Journal of Adhesion* **1998**, *68*, 93-116.
(25) Christensen, S. F.; McKinley, G. H. *International Journal of Adhesion and Adhesives* **1998**, *18*, 333-343.
(26) Urahama, Y. *Journal of Adhesion* **1989**, *31*, 47-58.
(27) Zosel, A. *Journal of Adhesion* **1994**, *44*, 1-16.
(28) Dahlquist, C. A. In *Handbook of pressure sensitive adhesive technology*, 2nd ed.; Satas, D., Ed.; Van Nostrand Reinhold: New York, 1989; Vol. 1, pp 97-114.
(29) *FINAT Technical Handbook*, 7th ed., 2005.
(30) Hammond, F. H. In *Handbook of pressure sensitive adhesive technology*, 2nd ed.; Satas, D., Ed.; Van Nostrand Reinhold: New York, 1989; Vol. 1, pp 38-60.
(31) Kamagata, K.; Saito, T.; Toyama, M. *Journal of Adhesion* **1970**, *2*, 279-291.
(32) Aymonier, A.; Ledercq, D.; Tordjeman, P.; Papon, E.; Villenave, J. J. *Journal of Applied Polymer Science* **2003**, *89*, 2749-2756.
(33) Tordjeman, P.; Papon, E.; Villenave, J. J. *Journal of Polymer Science Part B-Polymer Physics* **2000**, *38*, 1201-1208.

(34) Aymonier, A.; Papon, E.; Villenave, J. J.; Tordjeman, P.; Pirri, R.; Gerard, P. *Chemistry of Materials* **2001**, *13*, 2562-2566.
(35) Marcais, A.; Papon, E.; Villenave, J. J.; Tordjeman, P.; Pirri, R.; Gerard, P. *Macromolecular Symposia* **2000**, *151*, 497-502.
(36) Aymonier, A.; Papon, E.; Castelein, G.; Brogly, A.; Tordjeman, P. *Journal of Colloid and Interface Science* **2003**, *268*, 341-347.
(37) Tse, M. F.; Jacob, L. *Journal of Adhesion* **1996**, *56*, 79-95.
(38) Chu, S. G. In *Handbook of pressure sensitive adhesive technology*, 2nd ed.; Satas, D., Ed.; Van Nostrand Reinhold: New York, 1989; Vol. 1, pp 158-203.
(39) Zosel, A. *Colloid and Polymer Science* **1985**, *263*, 541-553.
(40) Plessis, C.; Arzamendi, G.; Leiza, J. R.; Alberdi, J. M.; Schoonbrood, H. A. S.; Charmot, D.; Asua, J. M. *Journal of Polymer Science Part a-Polymer Chemistry* **2001**, *39*, 1106-1119.
(41) Plessis, C.; Arzamendi, G.; Leiza, J. R.; Schoonbrood, H. A. S.; Charmot, D.; Asua, J. M. *Industrial & Engineering Chemistry Research* **2001**, *40*, 3883-3894.
(42) Plessis, C.; Arzamendi, G.; Leiza, J. R.; Schoonbrood, H. A. S.; Charmot, D.; Asua, J. M. *Macromolecules* **2001**, *34*, 5147-5157.
(43) Gower, M. D.; Shanks, R. A. *Macromolecular Chemistry and Physics* **2005**, *206*, 1015-1027.
(44) Tobing, S. D.; Klein, A. *Journal of Applied Polymer Science* **2001**, *79*, 2230-2244.
(45) Gower, M. D.; Shanks, R. A. *Journal of Applied Polymer Science* **2004**, *93*, 2909-2917.
(46) Tobing, S. D.; Klein, A. *Journal of Applied Polymer Science* **2001**, *79*, 2558-2564.
(47) Tobing, S.; Klein, A.; Sperling, L. H.; Petrasko, B. *Journal of Applied Polymer Science* **2001**, *81*, 2109-2117.
(48) Novikov, M. B.; Roos, A.; Creton, C.; Feldstein, M. M. *Polymer* **2003**, *44*, 3561-3578.
(49) Aubrey, D. W.; Ginosatis, S. *Journal of Adhesion* **1981**, *12*, 189-198.
(50) Lindner, A.; Lestriez, B.; Mariot, S.; Creton, C.; Maevis, T.; Luhmann, B.; Brummer, R. *Journal of Adhesion* **2006**, *82*, 267-310.
(51) Lakrout, H.; Sergot, P.; Creton, C. *Journal of Adhesion* **1999**, *69*, 307-359.
(52) Chan, H. K.; Howard, G. J. *Journal of Adhesion* **1978**, *9*, 279-304.
(53) Aubrey, D. W.; Sherriff, M. *Journal of Polymer Science Part a-Polymer Chemistry* **1980**, *18*, 2597-2608.
(54) Gower, M. D.; Shanks, R. A. *Journal of Polymer Science Part B-Polymer Physics* **2006**, *44*, 1237-1252.
(55) Ahn, D.; Shull, K. R. *Langmuir* **1998**, *14*, 3637-3645.
(56) Gower, M. D.; Shanks, R. A. *Macromolecular Chemistry and Physics* **2004**, *205*, 2139-2150.
(57) Plessis, C.; Arzamendi, G.; Leiza, J. R.; Schoonbrood, H. A. S.; Charmot, D.; Asua, J. M. *Macromolecules* **2000**, *33*, 5041-5047.
(58) Jovanovic, R.; McKenna, T. F.; Dube, M. A. *Macromolecular Materials and Engineering* **2004**, *289*, 467-474.
(59) Jovanovic, R.; Dube, M. A. *Industrial & Engineering Chemistry Research* **2005**, *44*, 6668-6675.
(60) Jovanovic, R.; Ouzineb, K.; McKenna, T. F.; Dube, M. A. *Macromolecular Symposia* **2004**, *206*, 43-56.
(61) Laureau, C.; Vicente, M.; Barandiaran, M. J.; Leiza, J. R.; Asua, J. M. *Journal of Applied Polymer Science* **2001**, *81*, 1258-1265.

3. Experimental Techniques

Experimental techniques used for the characterization of the adhesive layer surface and for the investigation of adhesive and mechanical properties are presented in this chapter.

A short introduction to the *AFM technique* is given simply to inform the reader on how AFM images, shown later, were effectively obtained.

Then, tests used for the characterization of adhesive properties are presented. The conditions used to perform *standard adhesive tests* (principles have already been explained in chapter 2) in the present work are described while the principle of *the probe test* experiment we effectively used to test the adhesive performances is detailed.

Some experimental techniques are also used for the investigation of linear and nonlinear rheological properties of the adhesives. In this thesis, linear viscoelastic properties are obtained using a home made *microrheometer.* We describe the set-up and we explain how rheological data are obtained. At high deformations, nonlinear elongation properties are characterized using *tensile experiments*.

3.1. Adhesive layer characterization: AFM technique

The structure of the surface of the adhesive layer and of the particle morphology have been characterized using the atomic force microscopy (AFM) technique. This technique has been employed at the University of Surrey by Dr. Chunhong Lei and Dr. Joseph L. Keddie.

The AFM technique has been used for several years for the study of films formed from latex dispersions. However, most studies have been performed on nontacky surfaces with a T_g higher than or near room temperature. Before the work of Mallégol et al.[1] there were no published AFM images of acrylic PSA nor of freshly cast waterborne PSA surfaces and this is mainly due to the difficulty to perform AFM measurements on sticky surfaces. In the present work, these difficulties have been eliminated after the optimization of some experimental parameters.

All AFM measurements have been performed with *intermittent contact*, i.e. in the *tapping mode* (TM). The set-up for AFM tapping mode is shown in Figure 3-1. In this mode, the tip is oscillated (around an equilibrium position) by a piezocrystal near the resonant frequency of the cantilever and is brought into contact with the surface of the sample when reaching the lower point of its oscillation. This mode has the advantage to limit damage of the surface especially in the case of soft materials. Moreover, in the case of PSA, a potential problem is that the tip can be trapped by the adhesive surface. To overcome the sticking of the tip, the tapping AFM is usually carried out with stiff cantilevers (in the present work, k = 46 N/m) and relatively large oscillation amplitudes which provide enough energy to pull the tip away from the surface.

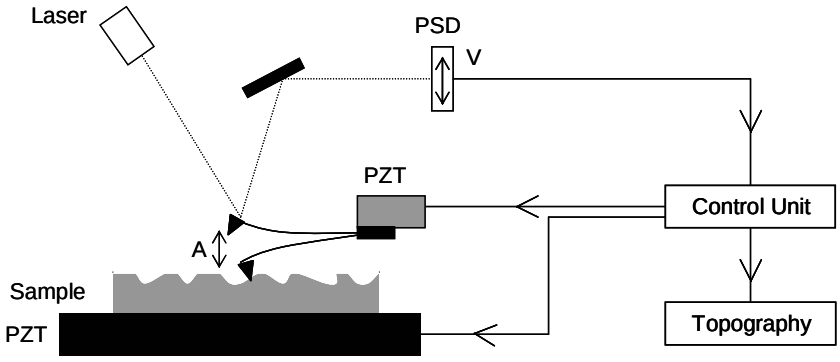

Figure 3-1. Set-up for AFM tapping mode.

The amplitudes of oscillation are not directly recorded during AFM imaging. The position of the cantilever is determined from the reflection of laser light from the top of the cantilever and detection of the light by a photodiode array. The output voltage is proportional to the amplitude. The two most important parameters in obtaining an image are the cantilever's free oscillation A_0 (where there is no interaction with the surface sample) and its setpoint A_{sp}. At the start of an AFM measurement, the cantilever's tip approaches the sample surface. When the tip makes contact, the amplitude of its oscillation decreases from A_0 to the pre-defined amplitude, A_{sp}. Thereafter the amplitude is maintained constant during the scan by adjusting the relative position of the tip with respect to the sample. The difficulty

with a soft material is that A_{sp} needs to be corrected by the indentation depth of the tip inside the sample.

In tapping mode, two images are obtained simultaneously. A *topographical image* is obtained by measuring how much the sample surface must be adjusted in the vertical direction to maintain A_{sp} at a constant value while scanning. A *phase image* represents the phase lag of the photodiode output signal from the signal in the piezoelectric that oscillates the cantilever. Phase images reflect changes in the mechanical properties of the sample surface such as viscoelasticity as the cantilever tip is moving laterally across the surface.

In a *topographical image*, darker areas correspond to deeper zones.

In a *phase contrast image*, lighter areas correspond to low dissipative zones while darker areas correspond to highly dissipative zones.

For AFM measurements of the surface structure of the adhesive layers, latex dispersions were cast on a polyethylene terephtalate (PET) sheet or on an oriented polypropylene (OPP) sheet using a 30 µm or 40 µm spiral bar coater (Figure 3-2). Latexes were dried either at 110°C during 3 min or at room temperature. The drying conditions have an impact on the film morphologies. In the following, when AFM images will be shown, we will indicate at which temperature films were dried. All images shown in the present work were obtained from the air-interface.

Figure 3-2. Spiral bar coater.

Not only the surface but also the bulk structure has been investigated using the AFM technique. For that, some cross-sectional images have been taken. For these experiments, latexes were cast on a release liner and then transferred to OPP film for cryo-microtoming.

Additionally, after diluting the latex and spin coating it onto a mica surface, individual particles have been imaged. Since most of the latexes, do not wet the mica surface, poly(ethylenimide) (PEI) was used to modify the mica surface and obtain a good wetting.

3.2. Adhesive properties

Standard industrial adhesive tests and the more fundamental *probe tack test* have been used for the investigation of adhesive properties. We start with the industrial tests.

3.2.1. Standard industrial adhesive tests

Materials studied were tested for their adhesive properties by Dr. Andrew Foster under the supervision of Pr. Peter Lovell from UMIST, Dr. Keltoum Ouzineb and Dr. Olivier Dupont from Cytec and Ms. Tuija Helin from Raflatac.

They performed a series of standard adhesive tests: 180° and 90 ° peel tests, shear tests and loop tack. These techniques have been already detailed in chapter 2. However, conditions under which tests are conducted can differ. Here, the conditions used by our partners for this thesis are described.

The preparation of the samples was the same for all standard adhesive tests. Films were prepared either via direct coating onto OPP sheets using a spiral bar coater (Figure 3-2) or by transfer coating (Figure 3-3).

In the latter case, the adhesive was first cast on a siliconized release liner or backing. An OPP facestock is placed on the upper surface. The laminate was dried in a fan assisted oven either at 110°C for 3 min (drying conditions used by Cytec and UMan) or at 100°C for 90 s (drying conditions used by Raflactac). A final thickness of about 19 µm was obtained. The release sheet was removed before performing the test. Tests were performed on the release paper/adhesive interface.

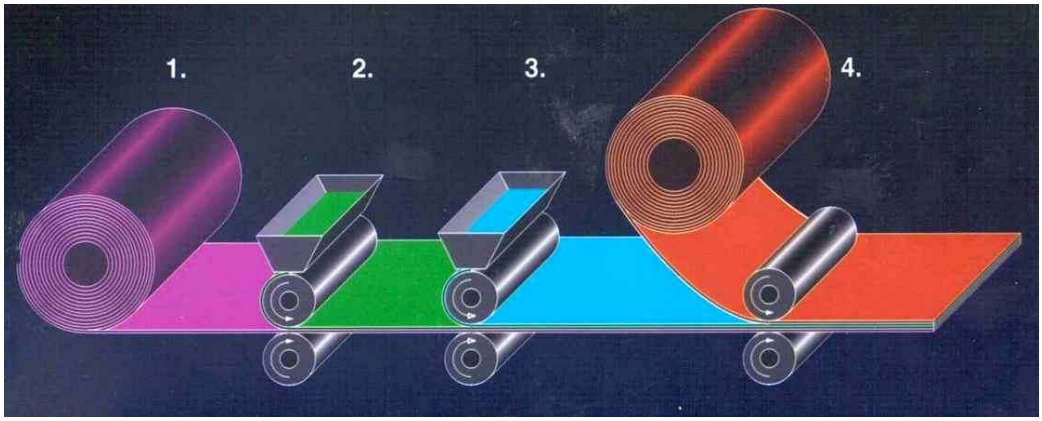

Figure 3-3. Transfer coating. 1. Release liner or backing. 2. Silicone release coating. 3. Adhesive coating. 4. Face material lamination.

Conditions used to perform the tests were those defined by FINAT[(1)] test methods (FTM)[2]:

[(1)] FINAT is an abbreviation of the French title: **F**éderation **IN**ternationale des fabricants et transformateurs d'**A**dhésifs et **T**hermocollants sur papiers et autres supports.

- Peel adhesion (FTM1, 180° and FTM2, 90°) tests were performed on glass, on stainless steel and on high density polyethylene (HDPE) at v = 300 mm.min^{-1}. Adhesion was measured 20 min and 24 hours after application.
- Shear tests (FTM8) were performed on stainless steel.
- Loop tack measurements (FTM9) were performed on glass and HDPE.

All these tests were conducted under external conditions imposed by the FINAT test conditions i.e. T = 23°C and RH = 50%.

3.2.2. Probe Tack Test

i. Description of the set-up

The more fundamental studies of adhesive performances have been made using the well-known p*robe tack test*. In this test a flat ended probe (of a diameter a = 10 mm) is brought into contact with a thin adhesive layer (with a thickness of h ~ 100 μm) lying on a glass slide and is then removed at a fixed velocity. A schematic of the test geometry is shown in Figure 3-4.

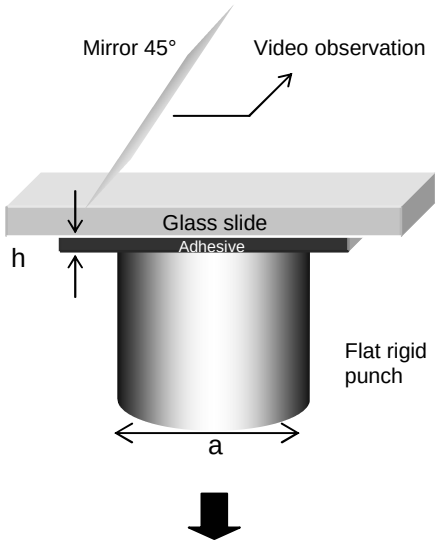

Figure 3-4. Geometry of the probe tack test.

With standard industrial FINAT tests like peel, results are given by a unique value of force. Here, the entire process is taken into account; the debonding mechanism is followed from the contact establishment to the final detachment. During a peel test the whole process can also be studied.[3] However, the great advantage of the probe-tack compared to the peel test is the decoupling of events occurring during the debonding. This is schematized in Figure 3-5.

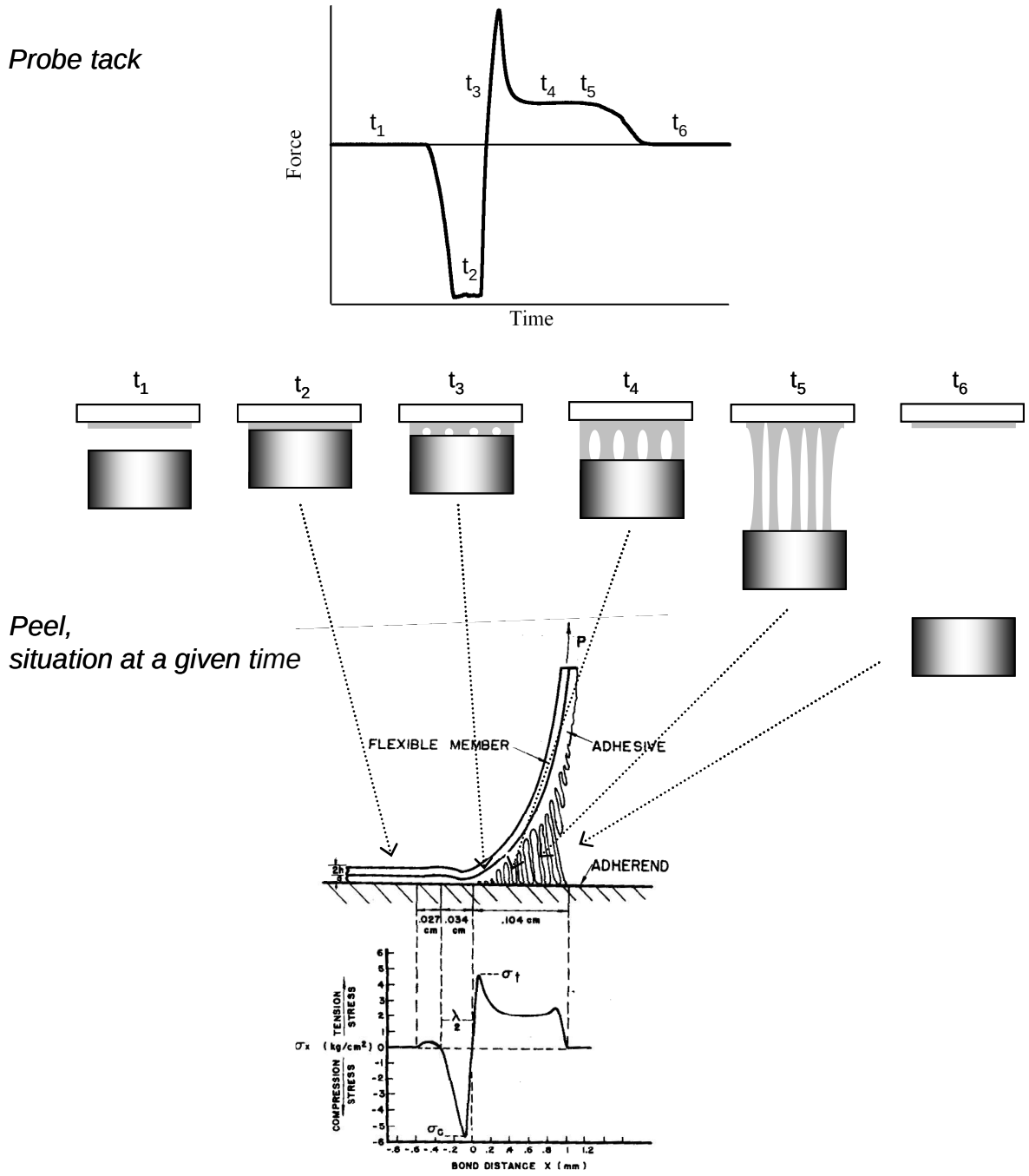

Figure 3-5. Force vs. time tack curve and schematics of lateral views of fibrils created between the probe and the adhesive layer during a probe tack experiment. The six pictures drawn correspond to six different times of the test. And below is shown a schematic representation of a peel profile and its experimental boundary distribution of nominal stresses (after [3]).

The shape of the force vs. time tack curve is highly similar to the force (or stress) distribution along a peel profile. Moreover, vertical fibrils observed between the probe and the adhesive layer resembles a lot that observed on a peel front.

Apart from the decoupling of events another advantage of the flat cylindrical probe tack geometry is that the imposed displacement of the probe is the same over all the contact area stretched in the tensile direction.

These probe tack experiments were performed on our custom-designed probe tester allowing the simultaneous observation of the debonding process through the transparent glass substrate. A schematic of the test geometry is shown in Figure 3-6, and further details on the experimental setup can be found elsewhere.[4] This set-up is made of several components. The force is measured with a load cell of a 250 N full scale (resolution 0.5 N). The displacement is measured by a displacement sensor whose maximal displacement is of 5 mm (resolution 0.5 μm). The deformation mechanisms of the adhesive layer are observed through the glass slide with the help of a 45-degree mirror and a video camera. Additionally, the surface of the adhesive and the surface of the probe are precisely aligned adjusting the position of the tripod system.

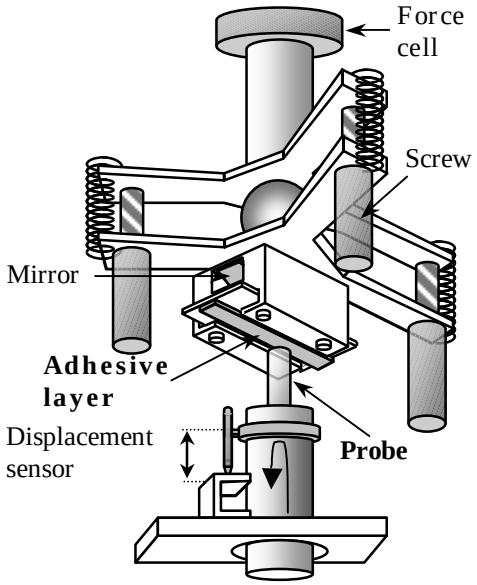

Figure 3-6. Schematic of the probe tack experimental set-up.

For the probe, the choice of the stainless steel as a standard probe surface was dictated by convenience. To test different surfaces, a probe coated with polyethylene (PE) was also used. The degree of surface roughness was well controlled. The flat ends of the probes were polished with several grades of abrasive paper until that a final average roughness of 0.1 μm was measured with an optical profilometer. PE and stainless steel probes were polished at the same time but PE probes have a surface a little bit rougher. The same probe was used throughout a series of tests and its flat end was cleaned with water and acetone in the case of stainless steel and ethyl acetate in the case of PE.

In the part which follows, the procedure used for the preparation of the adhesive samples is explained. For films made from aqueous dispersion, final nanostructure and also macroscopic structure of the film are dependent on the drying step. So, different drying conditions were examined.

ii. Preparation of the adhesive samples

For tack experiments a small amount of latex was deposited at one end of a precleaned microscope glass slide. A doctor blade with a gap of 300 µm or 400 µm (Figure 3-7) was used to spread the emulsion. Once the films were spread they were allowed to dry in air at room temperature and ambient humidity during about ten hours. At the end of this first drying step, the layers were transparent. These films were then dried in an oven at 110°C for 5 min at atmospheric pressure. The resulting films had thicknesses *h* of about 100 µm.

Figure 3-7. Doctor blade.

These drying conditions have been chosen after a study of the influence of the drying conditions on tack experiments. In Figure 3-8 are shown tack curves obtained on the same material but dried with different drying conditions (tack experiments have been performed the day following the drying).

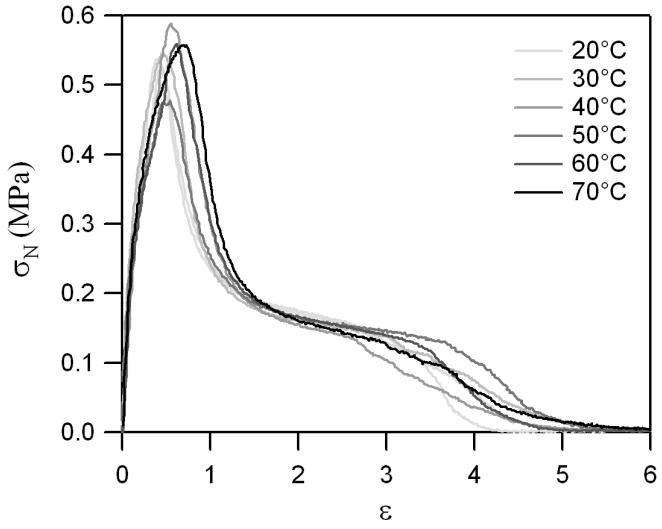

Figure 3-8. Nominal stress vs. strain tack curves of adhesive films made of the same latex formulation but dried in different conditions. Tests were performed at 10 µm.s^{-1} on stainless steel probes.

All samples were placed in the oven but the temperature inside was different. Since the time required for the film to become transparent (signature of a complete drying) decreases as a function of drying temperature, samples were left drying for shorter times as the temperature increases.

Drying conditions were as follows:

- At T = 20 °C during t > 15 min
- At T = 30 °C during t = 12 min 30s
- At T = 40°C during t = 6 min
- At T = 50°C during t = 4 min 30s
- At T = 60°C during t = 2 min 30s
- At T = 70°C during t = 2 min

Results showed that the drying temperature had no influence on tack results.

Moreover, during the drying process, the drying front was easily followed from the evolution of the white zone (which corresponds to the wet latex). The drying front evolved from the edges towards the middle of the glass slide as shown on Figure 3-9-a. Besides, at temperatures higher than 60°C, a crack defect appeared in the middle of the latex during the drying. Such crack defect was not observed when latexes are slowly dried at room temperature.

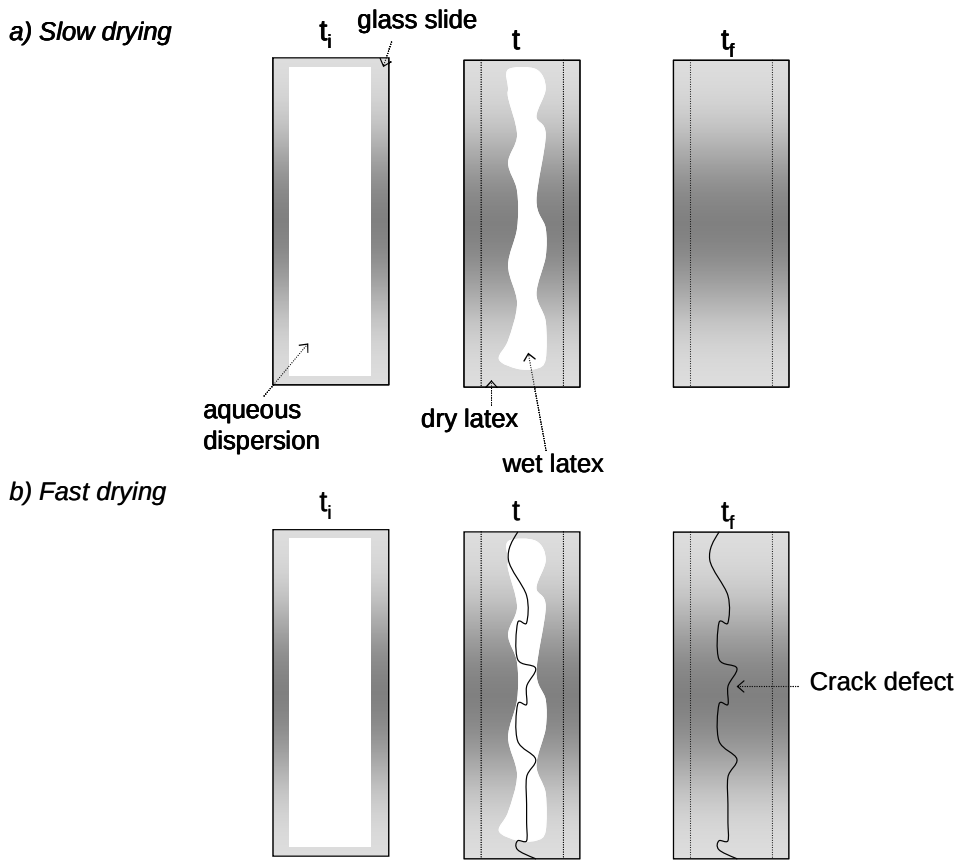

Figure 3-9. Schematics of the evolution of the drying front from the edges to the center. a) Case of a slow drying at low temperature. b) Case of a faster drying at higher temperature and formation of a crack defect.

A photo of a latex film drying at 70°C in the oven is shown on Figure 3-10. One clearly observes a surface crack both during the drying and on the dry adhesive film. When dried at room temperature, such cracks are no longer observed (Figure 3-9-a).

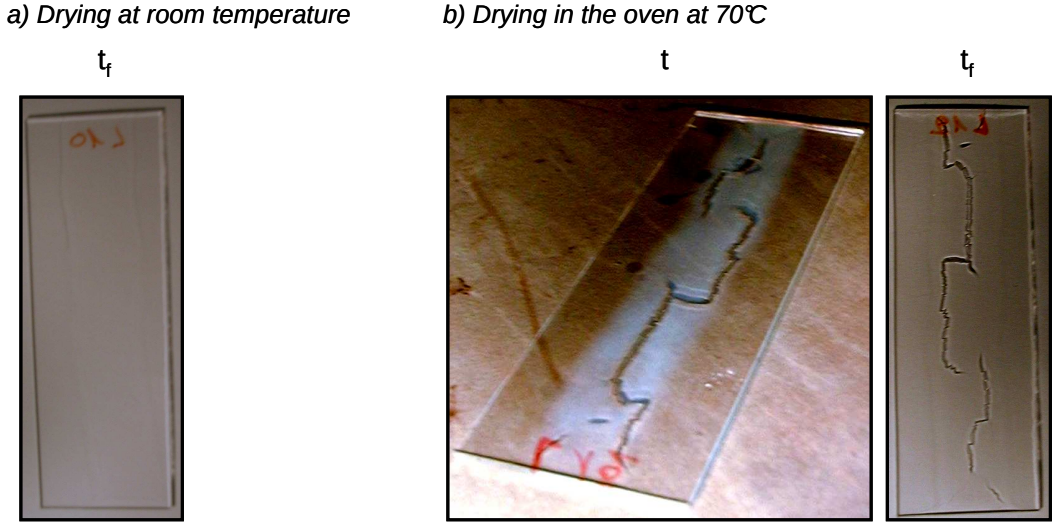

Figure 3-10. a) Picture of a dry adhesive film dried at room temperature. b) Pictures of wet and dry films dried in the oven at 70°C.

Such defects can be due to the non uniformity of the water distribution during the drying as already discussed in section 1.5. These non uniformities are even more favored in the case of thick films and this is in agreement with our observations: surface cracks were more easily formed for thicker films. For AFM and standard adhesive tests, films were thinner (about 20 µm) and they were dried directly during 5 min in the oven at 110°C. In that case no defects were observed on their surfaces.

iii. Nominal stress vs. strain tack curves

A typical experiment was carried out as follows: the flat-ended probe was brought in contact with the adhesive layer at a constant probe velocity until a set compressive force was reached, kept at a fixed position for a given time and subsequently removed at a constant probe velocity.

For each experiment the maximum area of contact during the compression stage was determined from the video observation. The experimental force-displacement curve was transformed into a nominal stress (σ_N) – strain (ε) curve by dividing the force F by the maximum contact, i.e. the initial contact area A_{c0}, and the displacement d by the initial thickness of the adhesive layer h_0 (by convention the displacement is zero when the force becomes tensile).

$$\sigma_N(t) = \frac{F(t)}{A_{c0}} \text{ and } \varepsilon(t) = \frac{d(t)}{h_0} \qquad \textbf{Eq. 3-1}$$

In addition, strain calculations take into account the compliance of the experimental setup[(1)], which includes the bending of the glass slide, so that the stress-strain curve reflects solely the deformation of the adhesive layer.

Certain parameters were kept constant for the present study. Tack experiments were all performed at room temperature and with a compressive force of 70 N (corresponding to an average pressure of 1 MPa for a probe fully in contact). The contact time was set at 1 s, and the approach velocity (compressive stage) was set at 30 $\mu m.s^{-1}$. The debonding velocity was varied between 10 and 1000 $\mu m.s^{-1}$. If a sufficient constant compressive pressure is applied on the layer and if the storage modulus of the layer at 1 Hz is below about 0.1 MPa, the compressive stage has little effect on the tensile results.[5] However, the conditions of the compression stage were kept constant when testing a series of adhesives.

For each experimental condition, i.e. for each material, debonding velocity and type of probe, three to five tests were performed. Results are highly reproducible as shown in Figure 3-11. Slight differences are observed on the peak stress σ_{max}, the stress level of the fibrillation plateau at intermediate strains is perfectly reproducible and values of the maximal deformation ε_{max} are a little more scattered.

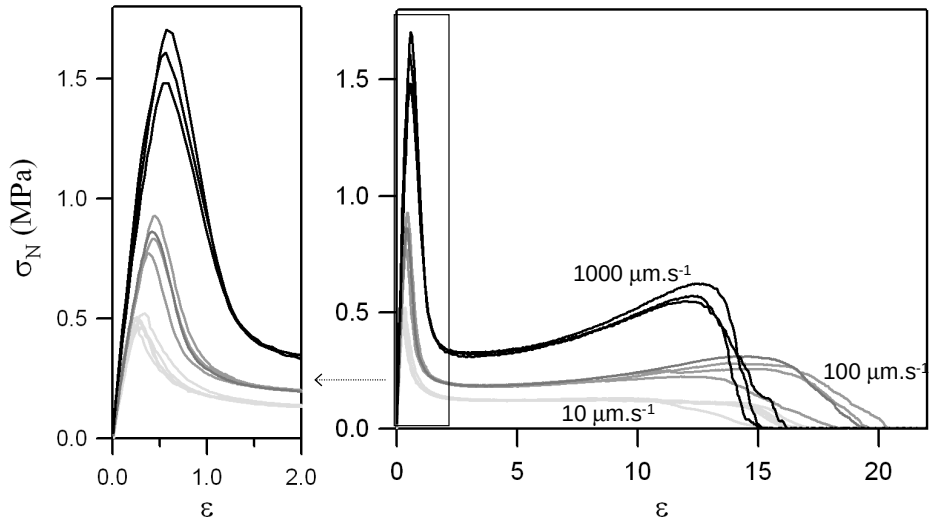

Figure 3-11. Nominal stress vs. strain curves obtained on stainless steel at three different debonding velocities and on stainless steel probes. Three to five tests are represented for each debonding velocity. A magnification of the small strain part of the curves is given on the left.

Therefore, all the nominal stress vs. strain curves we present in this study are representative curves, which were carefully chosen among three to five curves.

3.2.3. Possible predictions of peel and shear from tack results

Adhesive performance has been systematically characterized using both standard industrial tests and the probe tack test. We have shown (here and also in the previous chapter) that the probe tack results give more information than standard adhesive test

(1) This compliance has been precisely measured applying a ramp of displacement of a probe glued to the glass slide with a Loctite® glassy adhesive and the resulting force was measured.

results. Thus it is reasonable to think that tack curves contain the information obtained from peel and shear experiments. This part is just aimed at showing how peel performance and shear resistance can be approximately predicted from tack results. No systematic study about this relation has been made and we do not claim to give universal relations valid in all cases.

Peel tests are performed at a velocity v_{peel} of 300 mm/min, i.e. v_{peel} = 5000 µm/s. The strain rate $\dot{\varepsilon}_{peel}$ can be calculated using the thickness of the adhesive layer h_{peel} as:

$$\dot{\varepsilon}_{peel} = \frac{V_{peel}}{h_{peel}} \qquad \textbf{Eq. 3-2}$$

Therefore, for a film 20 µm thick, the strain rate is found to be equal to 250 s^{-1}. Peel tests are thus performed at a strain rate considerably higher than the maximal strain rate of a tack experiment performed at a debonding velocity of V_{deb} = 1000 µm.s^{-1} on an adhesive film 100 µm thick which is equal to 10 s^{-1}.(1)

Nonetheless, we proposed a correlation between tack results of tests performed at the highest debonding velocity (V_{deb} = 1000 µm.s^{-1}) and peel results.

Peel is expressed in N/m which is equivalent to J.m^{-2}. We have already seen in the previous chapter that the adhesive energy is also expressed in J.m^{-2}.

Thus we were tempted to relate peel results to adhesive energies obtained at a debonding velocity of 1000 µm.s^{-1}. Some comparisons are made in chapter 5 and both results are in agreement one with each other.

Concerning shear resistance, the result corresponds to a characteristic time where the adhesive layer fails usually cohesively. The higher the cohesion of the adhesive, the higher is the shear resistance.

Concerning tack experiments, let us first consider the case where a well defined fibrillation plateau is observed. At this stage of the test, the stress measured corresponds to the response of fibrils stretched in the vertical direction. Thus this parameter characterizes the cohesion of the material. For materials with a high capability to fibrillate, the higher stress level of the fibrillation plateau, the more cohesive is the sample and thus the shear resistance.

If there is no fibrillation stage, we have seen in the previous chapter that, either the material is very stiff and debonds rapidly after the interfacial propagation of the cavities or it is too liquid and debonds very rapidly in a cohesive manner. In the former case, the material is highly cohesive and a high shear resistance is predicted while in the latter case, the material is liquid-like and a very low shear resistance with a cohesive failure is predicted.

The lowest shear resistance values obtained in the present study was about ten minutes, which is a very low value in the standardized conditions used in these tests. This means that the sample deforms very slowly after the application of the load.

We have thus suggested that the stress level of the fibrillation at low debonding velocities (this is V_{deb} = 10 µm.s^{-1} in the present work but tests can also be performed at lower debonding velocities) could be a good predictor of the shear resistance.

(1) The maximal strain rate corresponds to the initial strain rate during a tack experiment. After, strain rate decreases as the deformation increases.

3.3. Linear rheological properties

Dynamic mechanical properties have been investigated using a newly designed *microrheometer* which was developed in our laboratory by Dr. Antoine Chateauminois and Philippe Sergot.[6]

The system is based on a sphere-on-flat contact configuration (Figure 3-12). This particular geometry has been originally chosen with the objective to test linear viscoelastic properties of thin waterborne PSA layers dried exactly in the same conditions as samples used for the tack experiments to avoid any effect of a change in the structure of the dried film. This was not possible using a standard rheometer.

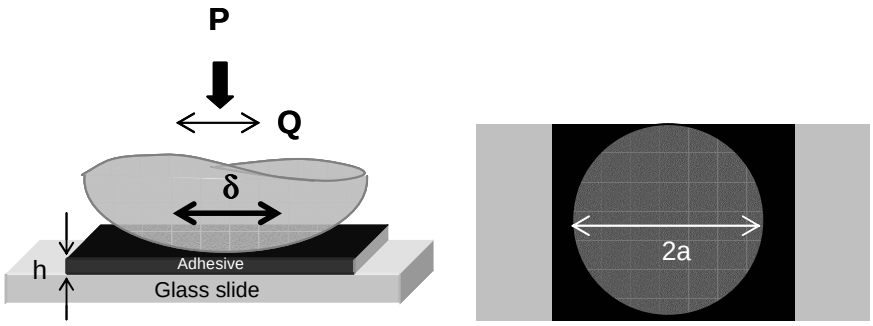

Figure 3-12. Left: sphere on flat configuration of the microrheometer used to measure linear viscoelastic properties of thin adhesive layer. Right: top view of the contact between the sphere and the layer.

Viscoelastic properties are measured from the determination of the lateral response of a macroscopic contact between a thin and confined ($h \ll a$) adhesive layer and a rigid lens. The experiments consist in applying small amplitude lateral sinusoidal micro-motions to the adhesive layer under a constant normal force. Moreover, the displacement amplitude was kept very low (in the range of few microns) in order to avoid any potential effects of micro-slip of the contact lateral response. A lateral contact loading has been preferred to a normal indentation since it has been shown that the lateral contact experiments are much more insensitive than the indentation ones to the incompressibility of the layer.[7]

Using a combination of flexible springs, a sapphire lens (radius = 25 mm) in normal contact with the adhesive film is allowed to rotate about an axis parallel to the specimen surface. The lens used is a convex-concave (or meniscus) lens (Figure 3-13). This shape has been preferred to the plano-convex shape since it reduces the diopter effect and thus error in the measure of the contact area.

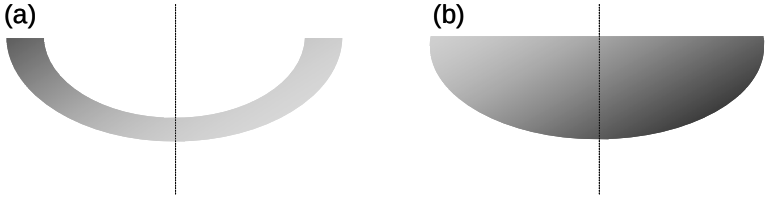

Figure 3-13. (a) Lateral view of a meniscus lens. (b) Lateral view of a plano-convex lens.

The rotation axis passes through the center of the virtual sphere defined by the lens, so that the tangential movement can be assimilated to a lateral displacement of the sphere. The tangential stiffness associated with the flexible springs is 0.25 mN/μm and was negligible compared to the stiffness of the samples studied.

During the tests, the contact between the lens and the layer is made by applying a normal displacement to the lens. A normal force *P* in the range of 0-2 N results from this contact. The lens is then actuated by a piezoelectric actuator (maximal displacement = 90 μm) which is operated in closed loop control using the signal of a non contact displacement transducer (optical fibre) as an input. The tangential load is continuously monitored using a piezoelectric load cell (with a maximal load of 50 N and a resolution of few millinewtons) with an extended dynamics (from 10^{-2} Hz to 10^{3} Hz).

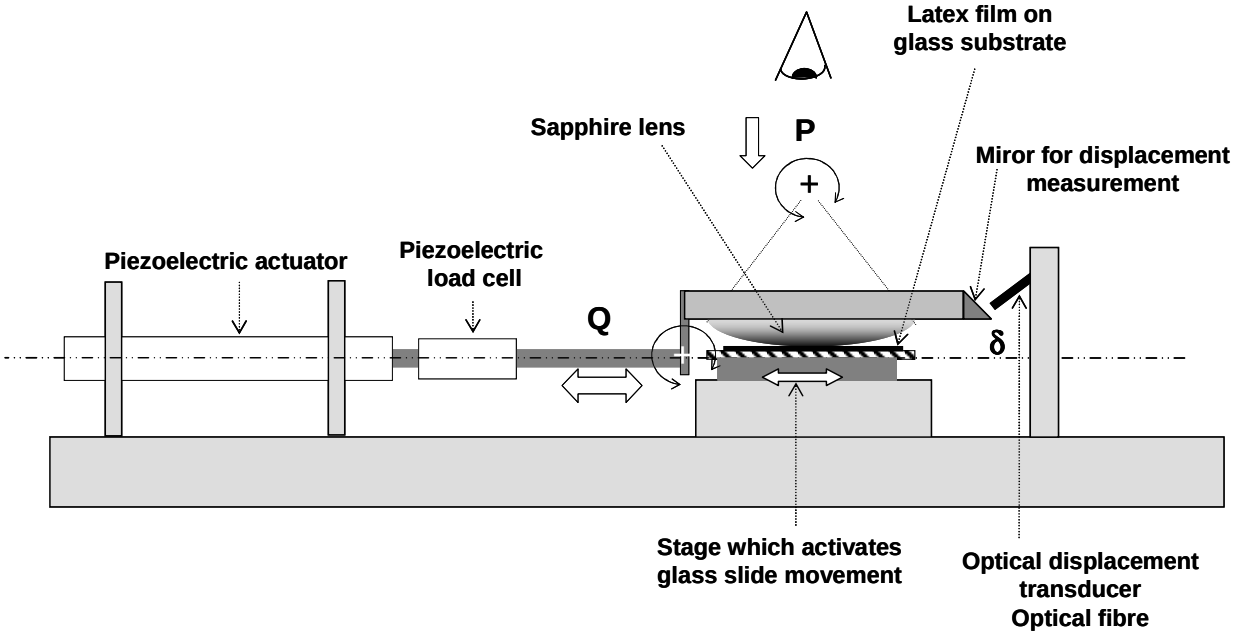

Figure 3-14. Schematic description of the microrheometer made of a piezoelectric actuator; a tangential load transducer; a displacement transducer. P is the normal load, Q is the tangential load.

Each test begins with the application of the lens on the adhesive layer. Since our soft films are adhesive, the contact area tends to increase a little at the beginning before stabilizing. The time required for this adhesive equilibrium depends on the material tested but it is always of few minutes. For a viscoelastic measure to be valid the most important is that no detectable change in the contact radius occurs within the time of the measure. When measurements are started 15 min after making the contact, I observed that the contact area did not change during a measurement. So, for each test, I decided to start measurements 15 min after making the contact.

The domain of strains where the response of the samples is in the linear regime has been explored for two samples. Values of storage (G') and loss (G") moduli obtained at 1 Hz are shown in Figure 3-15. A good linearity was obtained within the range of deformations between 2% and 15%. At lower deformations data were noisy. No tests have been performed at deformations higher than 8%.

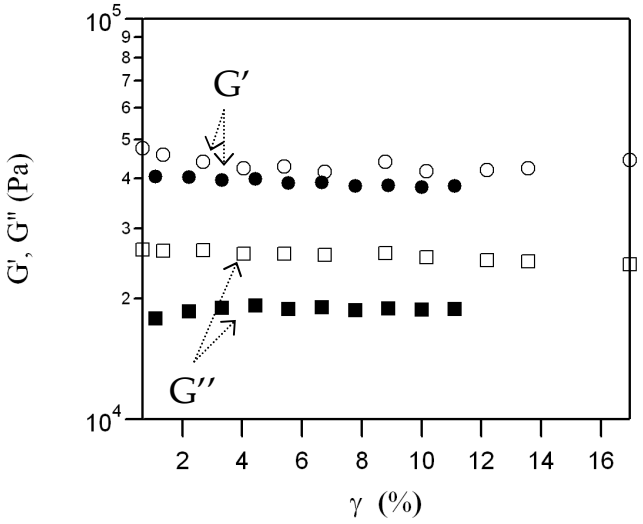

Figure 3-15. Linearity tests. Strain sweep at a given frequency (1 Hz). Empty values are from one sample, filled values from another one.

The linearity of the contact response confirms that no micro-slip occurs at the contact interface.[6] Within the investigated displacement domain, the magnitude of the tangential response was strictly proportional to the amplitude of the applied displacement, which would not be the case in the event of substantial micro-slip effects.

We have defined the deformation range where the response is linear when tests are performed at a frequency of 1 Hz. At lower frequencies, the displacement amplitude has been optimized to reduce the noise as much as possible. But no tests were performed at displacement amplitude above 8% which ensured that we stayed in the linear regime.

Increasing the frequency above 10 Hz, some irregularities were sometimes observed in sinusoids of the tangential load as shown on Figure 3-16. These defects in the curves were attributed to the fact that we drew nearer to the resonant frequency of the system. This resonant frequency has been measured and is of 50 Hz. This problem has been avoided through a decrease in the displacement amplitude. If such irregularities appeared, the test was considered as not valid.

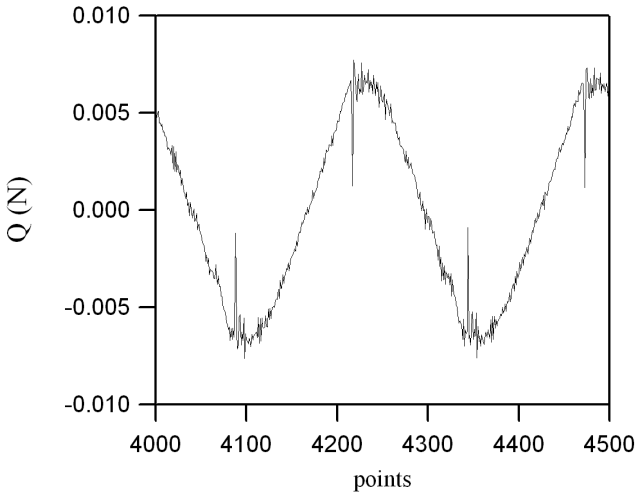

Figure 3-16. Irregularities observed at 10 Hz.

In practice, the microrheometer is used to provide the commonly used rheological properties (storage modulus G', dissipative modulus G'' and loss tangent $\tan(\delta)$) of the adhesive layer from the measurement of the dynamic contact stiffness K. Using this configuration, results are valid only if no substantial micro-slip is induced within the contact, and this condition has been verified from the linearity of the contact response within the investigated displacement domain.

How the elastic G' and dissipative G'' moduli are obtained from the contact stiffness is now described. The complex value of the stiffness K^* is defined as the ratio between the complex value of the tangential load Q^* and the complex value of the displacement δ^*.

$$K^* = \frac{Q^*}{\delta^*} \qquad \textbf{Eq. 3-3}$$

In our situation where a coated elastic substrate is in contact with a rigid sphere the contact stiffness K[(1)] includes the responses of both the coating and the rigid substrate. In our situation where the adhesive layer is confined we can adopt the approximation proposed by Gacoin et al.[7] where the lateral load applied to the surface is assumed to be integrally transmitted to the substrate over a constant contact area. In that case, the film and the substrate can be assumed to behave as stiffnesses in series[8] i.e.:

$$\frac{1}{K} = \frac{1}{K_F} + \frac{1}{K_S} \qquad \textbf{Eq. 3-4}$$

where K is the contact stiffness of the coated system, K_F, the stiffness of the film and K_S, the stiffness of the substrate.

For the film:

$$K_F = \frac{Q}{\pi a^2}\frac{h}{\delta}\frac{\pi a^2}{h} = G_F\frac{\pi a^2}{h} \qquad \textbf{Eq. 3- 5}$$

where δ is the actual displacement imposed by the sphere and h the thickness of the adhesive layer.

In the other hand, one has also to consider the lateral response of the contact deformation of the substrate. The associated stiffness is given by the classical Mindlin's theory.[9]

$$K_s = 8\, G^*_0\, a \qquad \textbf{Eq. 3-6}$$

where a is the contact radius and G^*_0 the reduced shear modulus of the substrate defined by:

$$G^*_0 = \frac{G_0}{2-\nu_0} \qquad \textbf{Eq. 3-7}$$

where G_0 denotes the shear modulus of the substrate and ν_0 the Poisson's ratio of the substrate (note that " * " is not related to a complex value here).

(1) In the following part which aims at determining the expressions of the stiffness of the film and of the stiffness of the glass slide as a function of their respective modulus, we decided to use real quantities to simplify notations. We will come back to complex quantities afterwards.

The shear modulus of our soft adhesive layers, G_F, in the range of few kPa is much lower than that of the glass substrate G_0 ($G_0 \approx 20$ GPa). Thus, in the case of a soft adhesive layer confined between a sapphire sphere and the glass slide, the response of the glass substrate can be neglected compared to that of the film in the calculation of the contact stiffness.

Therefore, if we come back to complex quantities, we obtain:

$$G_F^* \approx \frac{K^* h}{\pi a^2} \qquad \textbf{Eq. 3-8}$$

Using a fast Fourier transform (FFT), the in-phase, K', and out-of-phase, K'', components of the stiffness are obtained from which the elastic modulus, G', and dissipative modulus, G'', are calculated.

Such a measurement and calculations were repeated for each frequency of interest within the same contact. For each material, at least two series of measurements have been performed and results are highly reproducible as shown in Figure 3-17.

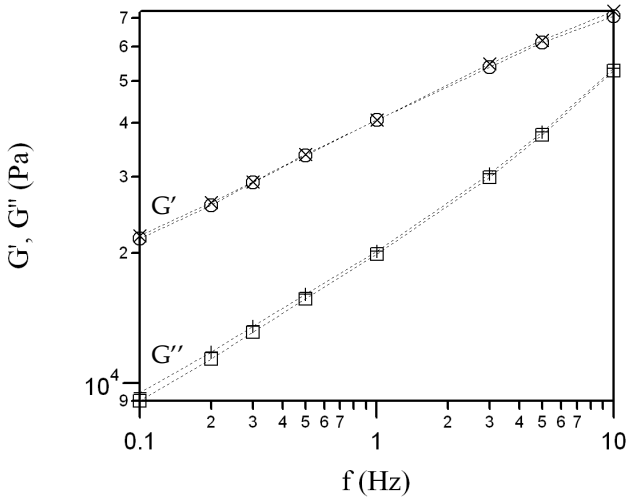

Figure 3-17. Elastic and dissipative moduli as a function of the frequency obtained on the same adhesive film but with two different contacts and two different displacement amplitudes (crosses: $\gamma = 8\%$ while circles and squares: $\gamma = 2\%$)

To validate experimental data obtained with the microrheometer, we compared some results with that given by a more standard Rheometrics RDA II parallel plates rheometer. Measurements were performed under torsional shear conditions. Adhesive samples were left drying during several days, the resulting film has a thickness of about 500 µm. Disks with a diameter of 8 mm were then cut and placed between the two disk plates of the rheometer. Tests have been carried out at a fixed temperature of 20°C while frequencies have been varied between 0.1 and 50 Hz. Results are shown on Figure 3-18. The contact mechanical data and the parallel plate data nearly overlay except at high strain rates (f > 10 Hz) where $G'_{\mu rheo}$ seems to drop down compared to $G'_{standard}$. Thus we can confidently use the contact

mechanical technique to measure rheological properties of thin adhesive layers in a range of frequencies between 0.1 and 10 Hz.

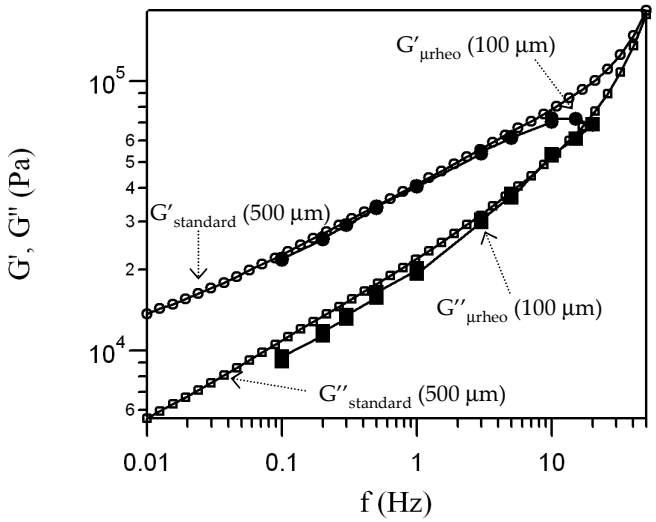

Figure 3-18. Frequency dependence of the storage moduli (G', circles) and loss moduli (G", squares) for the PSA based on latex particles made of random copolymers of 2-EHA, EA, MMA and S (control sample). Filled symbols correspond to data obtained from our contact mechanical test ($G'_{\mu rheo}$ and $G''_{\mu rheo}$), and open symbols correspond to data obtained from conventional shear rheometry ($G'_{standard}$ and $G''_{standard}$).

Therefore all rheological tests using the microrheometer are performed in the range of frequencies between 0.1 and 10 Hz.

Apart from confirming that data obtained from the microrheometer were accurate, more interestingly, this example showed that viscoelastic properties of this adhesive layer were not influenced by the thickness of the film. As already discussed in chapter 1, the film formation process and water distribution during the drying process depends on the thickness of the film. Therefore, in that case, we are confident in saying that the film formation process had no effect on the viscoelastic properties of the layer.

The fact that the viscoelastic behavior is independent on the layer thickness was confirmed by another series of experiments where *G′* and *G″* of thin industrial films with a thickness of about 20 µm are measured. These films were prepared from two adhesive formulations with the same monomer composition but different amounts of anti foam and wetting agent. Comparison was made with results obtained on a thicker adhesive film (~ 100 µm) prepared from the same latex formulation except that it does not contain any additives (neither anti foam nor wetting agent). Results of the thicker film lied in between that of the thinner ones (Figure 3-19). This shows again that the thickness of the layer had no obvious influence on viscoelastic properties of the material tested.

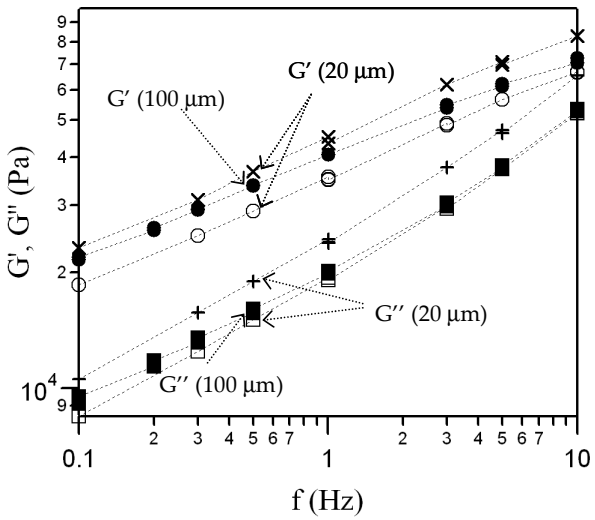

Figure 3-19. Crosses and empty symbols: elastic and dissipative moduli obtained on adhesive films with a thickness of about 20 µm. Filled symbols: Elastic and dissipative moduli of the same material but measurements are made on a thicker film with a thickness of about 100 µm.

This last example highlights another interesting advantage of this special set-up: it allows measurements of *G′* and *G″* of thin supported films down to thicknesses of about 20 µm, which is the standard thickness used for PSA in industrial applications.

Even though no obvious effect of the drying process on viscoelastic properties has been observed, all rheological measurements in this thesis have been carried out with the microrheometer. And for these viscoelastic measurements, films were dried exactly in the same conditions as samples prepared for tack experiments.

All rheological tests were performed at a frequency between 0.1 and 10 Hz at a small displacement amplitude (imposed shear strain $\gamma < 8\%$). Moreover all linear rheological measurements have been performed at room temperature.

3.4. Tensile tests

Tensile tests were performed on a standard tensile testing machine (JFC TC3) equipped with a Hounsfield non-contacting laser extensometer (Tinius Olsen H500L) allowing an accurate measurement of the strain even when the sample slips slightly between the clamps. The maximal displacement of the crosshead is of 400 mm with a maximal resolution of the extensometer of 0.02%. The machine uses a 10 N load cell with a resolution of 16 mN. A schematic of the tensile set-up is shown in Figure 3-20.

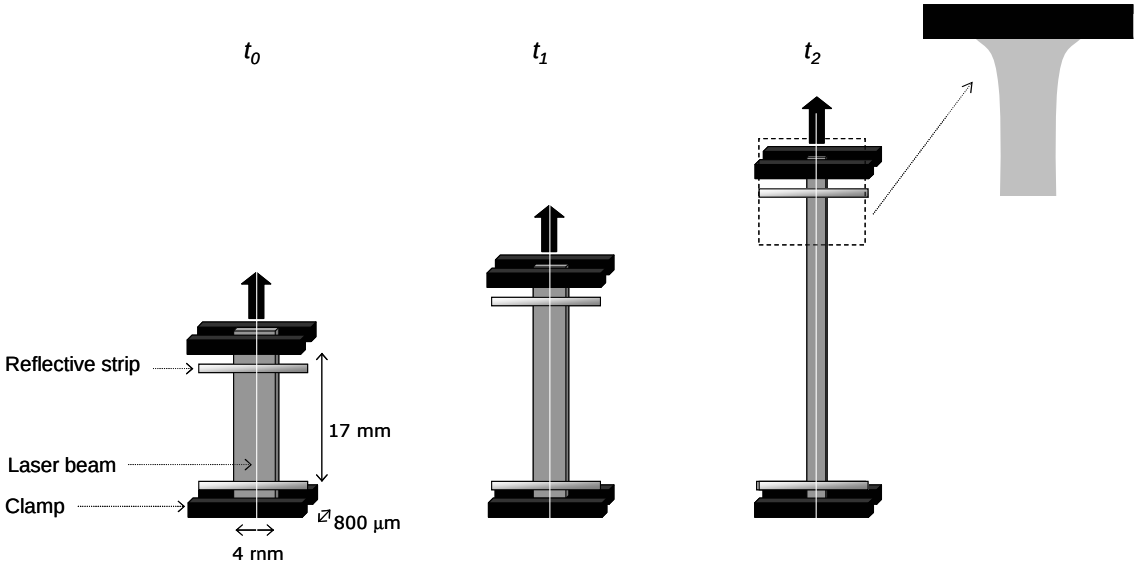

Figure 3-20. Schematics of the tensile set up at three different times of a tensile experiment. Magnification of the sample near the upper grip is shown.

The adhesive films were prepared from aqueous dispersions of latex cast on silicone molds. They were dried 10 days at room temperature and 5 min at 110 °C in the oven to ensure a complete drying. Our samples being very soft and tacky they can be removed from the molds only after sprinkling with talcum powder. They were then placed between two sheets of low release paper. Films were cut with a dog-bone punch, but only the central part was used. Samples tested were rectangular. They were 4 mm in width, about 800 µm thick and the initial length between the clamps was 17 mm. We did not use the entire dog-bone shape specimen since the maximal deformation would have been lowered (initial length between clamps would have been increased). Indeed, in our case since samples are very deformable and in several cases, the maximal displacement of the clamps is reached before the tensile specimen breaks. One drawback of the use of a rectangular shape is however the inhomogeneous strain near the grips as shown in Figure 3-20 (see the magnification on Figure 3-20). But, we have considered that errors resulting from this effect were negligible.

The crosshead velocity V_t was chosen between 50 and 500 mm.min^{-1} corresponding to initial strain rates varying from about 0.05 to 0.5 s^{-1}.

All tests were carried out at room temperature. The force (F) and displacement (L) data were directly obtained from the tensile machine. Nominal stress (σ_N) and strain (ε or λ) were

then calculated using the initial value of the width w_0, the thickness e_0 and the height L_0 of the sample (initial distance between clamps).

If the *nominal strain rate* $\dot{\varepsilon}$ is defined as:

$$\dot{\varepsilon}_N = \frac{dL(t)/dt}{L_0} = \frac{V_t}{L_0} \qquad \textbf{Eq. 3-9}$$

and the *Hencky's strain rate* as:

$$\dot{\varepsilon}_H = \frac{V_t}{L(t)} \qquad \textbf{Eq. 3-10}$$

our tensile experiments are performed at a constant *nominal strain rate* but at a decreasing *Hencky's strain rate*. A constant Hencky's strain rate is reached when the crosshead velocity increases exponentially.

For each material three to five tests were performed. Reproducibility is good as shown in Figure 3-21. The beginning of the curves is perfectly reproducible slight differences are observed at higher strains.

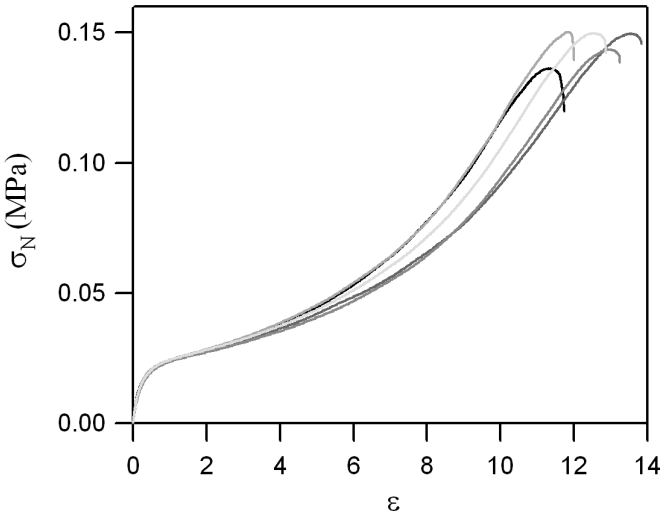

Figure 3-21. Five nominal stress vs. strain tensile curves obtained on the same material.

References

(1) Mallegol, J.; Dupont, O.; Keddie, J. L. *Langmuir* **2001**, *17*, 7022-7031.
(2) *FINAT Technical Handbook*, 7th ed., 2005.
(3) Kaelble, D. H. *Transactions of the Society of Rheology* **1965**, *9*, 135-163.
(4) Lakrout, H.; Sergot, P.; Creton, C. *Journal of Adhesion* **1999**, *69*, 307-359.
(5) Josse, G.; Sergot, P.; Creton, C.; Dorget, M. *Journal of Adhesion* **2004**, *80*, 87-118.
(6) Gacoin, E.; Chateauminois, A.; Fretigny, C. *Polymer* **2004**, *45*, 3789-3796.
(7) Gacoin, E.; Fretigny, C.; Chateauminois, A.; Perriot, A.; Barthel, E. *Tribology Letters* **2006**, *21*, 245-252.
(8) Tonck, A.; Sabot, J.; Georges, J. M. *Journal of Tribology-Transactions of the Asme* **1984**, *106*, 35-42.
(9) Mindlin, R. D.; Deresiewicz, H. *Journal of Applied Mechanics-Transactions of the Asme* **1953**, *20*, 327-344.

4. From Structure to Properties

This part contains the most general results of this thesis. The major objective here was to develop a reliable methodology to optimize adhesive performance of a PSA.

To be used for PSA applications a material needs to have a low enough elastic modulus and hence fulfill the so-called Dahlquist criterion.[1,2] Here we propose two additional rheological predictors of the adhesive properties.

The first one derived from the description of the detachment of linear elastic layer from a rigid substrate.[3,4] We made an approximate extension of this analysis to the viscoelastic regime and showed that the transition from interfacial cracks to cavitation and fibrillation can be quantitatively predicted from the easily measurable ratio $G''(\omega)/G'^{2}(\omega)$.

If a fibrillar structure is formed, the nonlinear large strain properties become important. We showed that the ability of the fibrils to be stretched in the vertical direction can be predicted from the softening which occurs at intermediate strains. Besides, tensile results can be used to predict the mode of failure. If a hardening occurs at large strains an adhesive debonding is expected.

This methodology has been used in the special case of wb-PSA made of core-shell particles and improved adhesive properties have been obtained.

4.1. Introduction

Pressure-sensitive adhesives (PSA) are soft materials characterized by instantaneous adhesion upon application of a light pressure. The core component of a PSA is always a polymer of low glass transition temperature which is highly deformable at room temperature. Although the function appears relatively simple, the design of proper PSA's is complex and relies heavily either on polymer chemistry (for acrylic polymers and silicone polymers) or on formulation (for block copolymers and natural rubber).

Although specific requirements for different applications vary, generally speaking, three basic properties have to be optimized for each PSA: peel adhesion which is the force required to remove a pressure sensitive adhesive from a standard test plate, shear strength which is the ability to sustain a certain level of stress and tack which is the force to break a bond after short contact time and low contact pressure. An optimal balance between peel strength and shear holding power is in particular required. This balance means that the PSA must be able to dissipate energy during the peeling process (a property optimized for a highly viscous liquid) but be resistant to creep in shear (optimum for solids). As discussed in chapter 2, in the family of acrylic polymers widely used for PSA, striking this balance means choosing the right monomer composition and the right molecular weight distribution and level of crosslinking.

The effect of several molecular parameters of the core polymer such as monomer composition, molecular weight (M_w), molecular weight distribution, molecular weight between entanglements (M_e) and molecular weight between crosslinks (M_c) on adhesive performance of PSA's have been studied.[5-9]

The results of these investigations show that the optimization of a PSA is crucially dependent on the balance between crosslinking (imparting cohesive strength) and viscoelastic dissipation (providing a high peel force). For the specific case of an acrylic core polymer, PSA are generally weakly crosslinked copolymers of a blend of monomers chosen to adjust the T_g which have an insoluble fraction (gel) and soluble fraction (sol). Increasing the gel fraction, reducing its M_c and reducing the M_e or increasing the M_w of the sol fraction leads to an increase in resistance to shear. However, peel strength is controlled by the formation and growth of fibrils and is mainly influenced by dissipative processes and flow of polymer chains. Energy dissipation is favored by a low gel content, a sol fraction containing a larger proportion of short chains and network with dangling ends.[10,11] Thus, contradictory requirements have to be covered to optimize both shear resistance and peel strength. A very broad molecular weight distribution combined with a highly dissipative sol fraction and a cohesive network formed by the gel is a good and relatively easy way to achieve practical solution, but has limitations due to the impossibility to independently control sol and gel parameters during the synthesis.

Recent environmental concerns have pushed many industries particularly in Europe to develop PSA's made from polymer no longer synthesized in solution but in emulsion in water. In this case individual particles are being synthesized and the material is then formed by the coalescence of these particles into homogeneous film. Since the particle grows during the synthesis by absorbing more monomer, its radial composition can be controlled and core-shell particle can be synthesized. This particular structure is used in number of industrial applications of polymers. In the particular case of paints, a soft shell around a hard core is

used to decrease the film forming temperature of the hard coating. In the case of PSA applications, coalescence of the soft particles is not the major issue and a core-shell structure is more used to adjust mechanical properties.[12] The objective is here to control shear resistance with a cohesive shell and peel performance with a soft and dissipative core. Thus shear and peel can be independently tuned since core and shell are synthesized in two distinct steps.

The influence of particle morphology on adhesive performance has already been studied by Aymonier et al..[13-15] However no special effort to control molecular weight and gel fraction of both phase was made and in that case, not much improvement is obtained using a heterogeneous morphology or a gradient composition compared to a homogeneous one. The heterogeneous structure of Aymonier et al.[13] shows for example a lack of adhesion and cohesion probably because the composition of each phase, outer and within the particle, is not optimized for this type of structure.

Our research started from the same idea as the Aymonier-Papon study but we focused on the synergy between particle structure and polymer structure which needs to be optimized globally in order to see an improvement in macroscopic adhesive properties. Linear viscoelastic properties and nonlinear properties both play fundamental roles in the debonding of the flat probe from the adhesive layer during probe tack experiments. Therefore our hypothesis was that only a thorough characterization of the mechanical properties in both the linear and the nonlinear regime can provide the proper guidelines to design and optimize particle and polymer structures. It is clearly very difficult to directly interpret adhesion tests (involving complex and heterogeneous deformations) in term of molecular structure. Therefore we have proceeded in a two step fashion. We have developed first a new and detailed rheological interpretation of the observed adhesive properties and the corresponding state of the art is summarized in part 2 and we have then used existing molecular models of the rheological properties to guide the design of the PSA for the required application. Part 3 contains the materials description and part 4 contains our analyzed experimental results for several core-shell structures of particles.

4.2. Theoretical background

4.2.1. Prediction of debonding mechanisms from linear rheological properties

In chapter 1 we have presented an elastic approach to predict debonding mechanisms from small strain properties which assumes that the layer is linearly elastic and that dissipative properties are confined in a small volume very close to the propagating interfacial crack. For soft and viscoelastic PSA this is clearly incorrect. However an extension of the model to linear viscoelasticity can be considered.

As discussed earlier, within a linear viscoelastic approximation G_c should be mainly related to the dissipative properties of the adhesive and scale with tan(δ). The Young's modulus E varies as the shear elastic modulus G'(ω). So, we decided to use the ratio $G''(\omega)/G'(\omega)^2$ experimentally obtained from linear rheological measurements as an approximation of G_c/E. Saulnier et al.[16] theoretically studied the adhesion of a linear viscoelastic material on a solid surface and demonstrated that the energy dissipation in such a linear viscoelastic body under time-dependent stress varies as:

$$\int_{\omega_{min}}^{\omega_{max}} \frac{G''}{G''^2+G'^2}\frac{d\omega}{\omega} \qquad \textbf{Eq. 4-1}$$

where $\omega_{min} = V/L$ and $\omega_{max} = V/l$, with V the crack velocity, L the layer thickness and l the size of the process zone directly ahead of the crack tip where local dissipative processes take place in the nonlinear regime. In this one relaxation time model, near the crack tip, the material is a stiff solid while far away from the fracture head it is a soft solid.

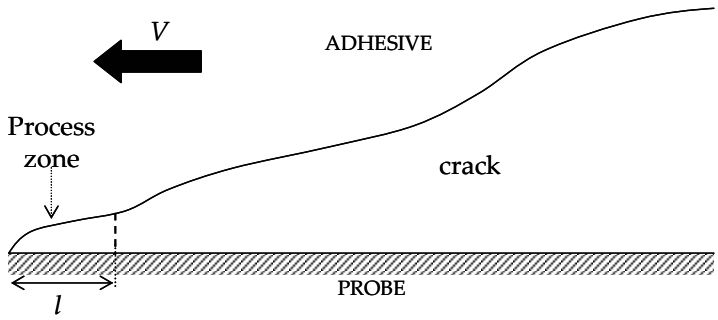

Figure 4-1. Crack shape between an adhesive and a hard solid. V is the crack velocity and l the process zone size (after [16]).

While this model is exact, it is difficult to use with real materials having a spectrum of relaxation times and the short length scale is difficult to identify precisely. However the expression inside the integral gives a good idea of the dissipation due to the propagating crack.

Using G''/G'^2 is clearly an approximation and requires an assumption on the value of ω but it has the advantage to be easily measured by widely used techniques. In real probe tack experiments the strain rates in the adhesive layer are heterogeneous spatially and temporally so ω can only be an approximate value and we propose to use the value $2\pi V_{deb}/h_0$, where V_{deb} is the velocity of the probe and h_0 is the initial thickness of the layer, as an estimate of ω.

From this approach, one can establish a quantitative criterion for the debonding mechanism using only results obtained from rheological measurements in the linear regime. The theory predicts that a transition from interfacial propagation of a crack to cavitation will occur at a given value of G''/G'^2. However, since $\mathcal{G}_c$ is also related to $\mathcal{G}_0$, which is the limiting value for the work of adhesion for vanishing crack velocity, the surface plays an important role in defining $\mathcal{G}_c$. The value of G''/G'^2 at which the transition occurs will depend on $\mathcal{G}_0$ of the probe-adhesive interface, and typically increases as $\mathcal{G}_0$ decreases. As it is shown on Figure 4-2, one can for example predict a lower critical value on stainless steel surface $(G''/G'^2)_{c,\,steel}$ than on polyethylene (PE) surface, $(G''/G'^2)_{c,\,PE}$.

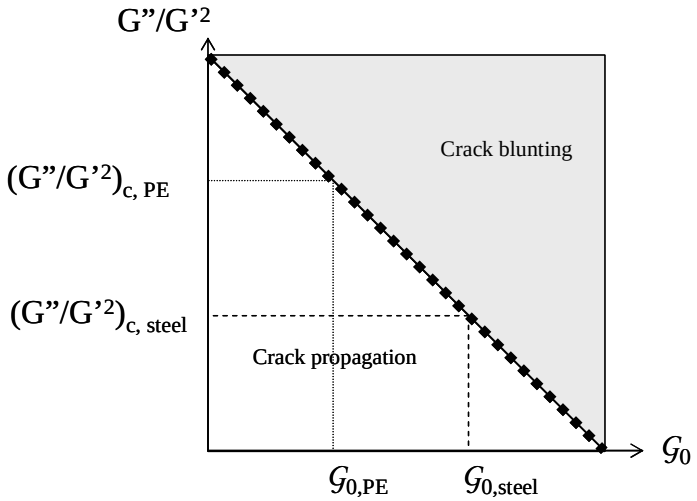

Figure 4-2. Prediction of a transition from interfacial propagation of a crack to cavitation from G''/G'^2 values. Critical value of G''/G'^2 depends on work of adhesion of the probe-adhesive interface $\mathcal{G}_0$.

The limits of the linear viscoelastic approximation to design PSA is obvious if one considers larger values of G''/G'^2. If the PSA becomes a liquid, dissipation increases dramatically and of course the modulus G' decreases well beyond the Dahlquist criterion. This leads to the prediction that viscous fluids will be tacky on almost any surface and is borne out by experiments. However PSA are required to resist creep and as such cannot be liquids. A third criterion addressing this aspect must therefore be defined.

4.2.2. Prediction of debonding mechanisms from nonlinear rheological properties

As discussed previously, if $\mathcal{G}_c/E$ is larger than the initial thickness of the layer or if G''/G'^2 is larger than a critical value (value which will be defined more precisely after the analysis of experimental results in section 4.4, bulk growth of the cavities is favored and foam is formed as the walls between cavities are extended into fibrils. At higher strains corresponding to the fibrillation regime, the behavior of the adhesive is dominated by a competition between viscoelastic extension of the cavity walls and the detachment of the fibrils from the probe.

During the fibrillation process, once the fibrils are formed, the only possible option in the absence of strain hardening is the thinning of the central section of the fibril, which results in

eventual cohesive failure.[17] This kind of behavior is for example foreseeable in the case of a viscoelastic liquid characterized by the progressive decrease of its reduced stress as the deformation increases.

If the material is crosslinked even slightly, a part of external work energy is elastically stored in the fibrils.[18] An adhesive failure is expected and the fibrils will peel off from the probe as soon as either the stored energy in the filaments is high enough to overcome the adhesion energy[19] or the stress in the fibril is high enough to overcome the surface forces (the two cases are not easy to distinguish experimentally). The higher is the amount of elastic energy stored the earlier the detachment occurs. High adhesion energy and high maximal deformation can be reached only if elongation of the fibrils is accompanied by some energy dissipation. Energy can be dissipated for example through the relaxation of polymer chains during the extension. Stress vs. strain and reduced stress vs. $1/\lambda$ tensile curves are useful in that case since for a weakly entangled system a pronounced softening is an indication of a pronounced viscoelastic behavior.[20]

Tensile experiments can then be used as a tool to investigate the large strain behavior of the material. An example of nonlinear behavior is shown on the stress-strain tensile curve displayed on Figure 4-3. One can observe a pronounced softening at intermediate strains followed by a hardening at large strains.

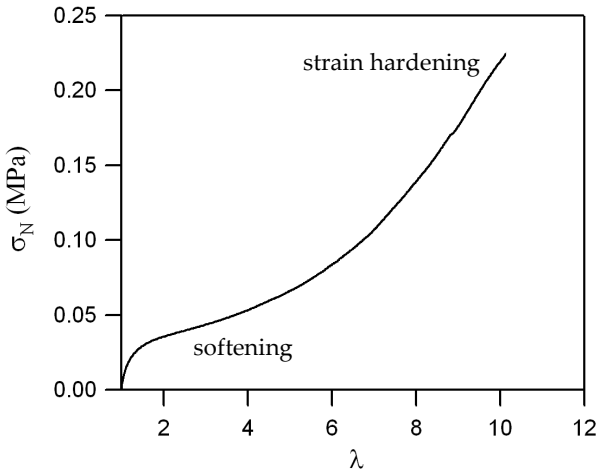

Figure 4-3. Stress-strain curve. Example of a PSA with nonlinear elastic properties.

The intrinsic nonlinear behavior of PSA appears more clearly using the Mooney stress σ_R defined as:

$$\sigma_R = \frac{\sigma_N}{\lambda - 1/\lambda^2} \qquad \textbf{Eq. 4-2}$$

This representation normalizes the measured stress by the predicted behavior of a neo-Hookean rubber in uniaxial extension and is usually plotted as a function of $1/\lambda$. On Figure 4-4-a, σ_R of two nonlinear elastic solids and a neo-Hookean rubber are displayed. The deviation of the behavior of a material from rubber-like elasticity is quantitatively predicted by the slope of the intermediate part of the reduced stress versus $1/\lambda$ curve. On Figure 4-4-b, the reduced stress of a viscoelastic solid and the reduced stress of a viscoelastic liquid are displayed. A liquid-like behavior is characterized by the absence of well defined minimum in

this 1/λ representation and of a strain hardening at the end of tensile test (the end of the test corresponds to the left side part of the curve).

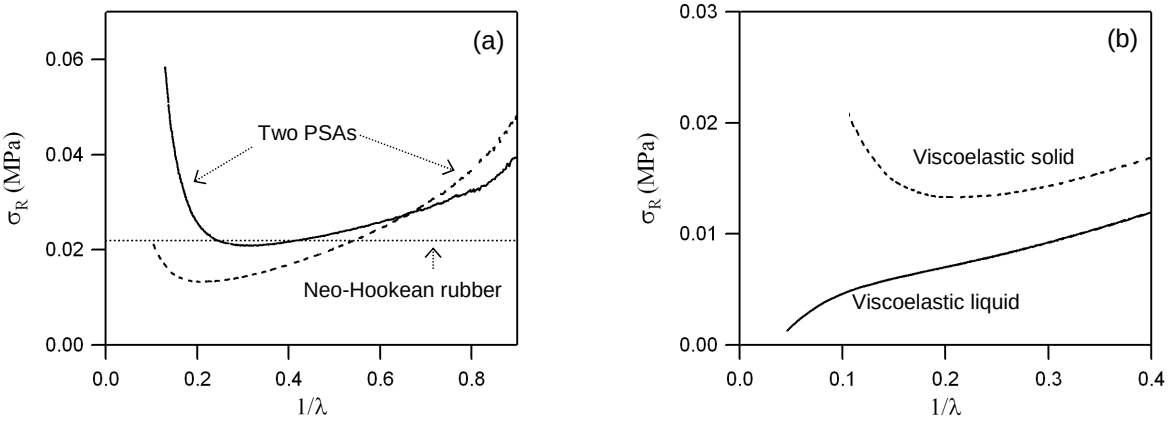

Figure 4-4. Mooney-Rivlin representations of tensile results. (a): comparison of two PSA (dashed and solid curves) with result of a neo-Hookean rubber (dotted curve), (b): comparison between a viscoelastic solid (dashed line) and a viscoelastic liquid (solid line).

If experimental data is fitted using the empirical Mooney-Rivlin model which in uniaxial tension predicts:

$$\sigma_N = 2\left(C_1 + \frac{C_2}{\lambda}\right)\left(\lambda - \frac{1}{\lambda^2}\right) \qquad \textbf{Eq. 4-3}$$

two characteristics material's parameters (C_1 and C_2) can be extracted (Figure 4-5). C_1 and C_2 can be approximately interpreted as the contribution due to permanent and temporary crosslinks to the modulus respectively[21].

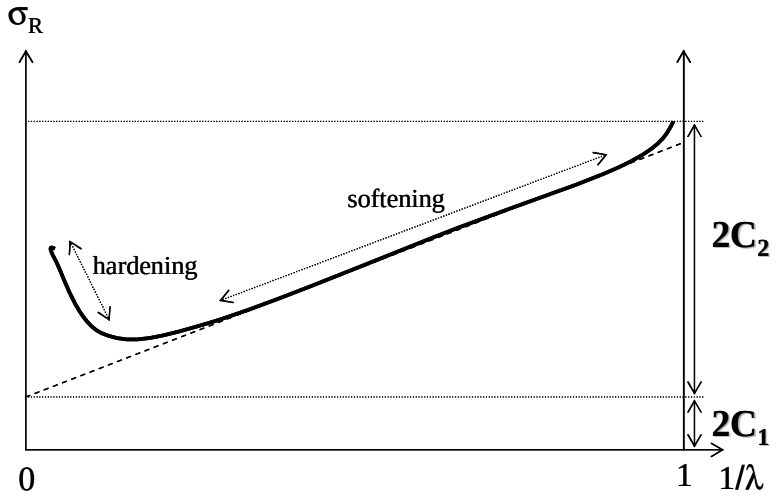

Figure 4-5. Mooney-Rivlin representations of tensile results of a typical PSA. Quantitative estimation of coefficients C_1 and C_2.

C_2/C_1 can be used to estimate the contribution of temporary crosslinks compared to that of permanent crosslinks. Very high values of C_2/C_1 are a signature of an under-crosslinked material while very low values of C_2/C_1 are obtained for highly crosslinked materials. For homogeneous acrylic copolymers synthesized in solution, a value of $C_2/C_1 \sim 5$ was close to

the optimum.[7] Lower values typically gave too elastic and well crosslinked materials. At the high end of the spectrum however some PSA have even negative values of C_1. The upper bound here is that the σ_R vs. $1/\lambda$ curve should have a well-defined minimum for the approach to be meaningful.

As a conclusion, the third criterion for the PSA design is the existence of a well-defined minimum in the σ_R vs. $1/\lambda$ curve and a ratio of $C_2/C_1 > 5$ with exact values depending on applications.

Let us now discuss these theoretical concepts with specific examples of PSA design based on the general idea of a waterborne PSA made from core-shell latex particles.

4.3. Materials

The model PSA latexes used in this study were synthesized by a semi-continuous emulsion polymerization process initiated by ammonium persulfate. Latex particle stability is controlled by a mixture of anionic surfactants (2wt% of the total monomer charged). Na_2CO_3 is used as a buffer. Polymerizations were carried out in a 3-l glass reactor equipped with a reflux condenser and anchor stirrer. The temperature was controlled through the circulation of water from a thermostatic bath in the reactor jacket. The latex solid content was determined gravimetrically and lied between 50 and 55 wt%. The average particle diameter was found to be equal to about 250 nm (measurements were performed with quasi-elastic light scattering, Nicomp™, 380 ZLS).

The latexes are made from random copolymers of butyl acrylate (BA) (glass transition temperature of the homopolymer, T_g = -54°C[22]), 2-ethyl hexyl acrylate (2-EHA) (T_g = -50°C[22]), ethyl acrylate (EA) (T_g = -24°C[22]), methyl methacylate (MMA) (T_g = 105°C, for the atactic[22]), acrylic acid (AA) (T_g = 106°C[22]) and styrene (S) (T_g = 100°C[22,23]) as the main monomers. The monomer composition varies from one latex to another and is used to adjust the glass transition temperature. Since this paper focuses more on the relationship between rheological properties and adhesive properties, we will not disclose the exact monomer composition for each latex but simply the details necessary to follow the arguments.

The syntheses were either performed at the University of Manchester by Dr. Andrew Foster and Dr. Michael Rabjohns both working under the supervision, of Prof. Peter Lovell, or at Cytec Surface Specialties in Drogenbos, under the supervision of Dr. Keltoum Ouzineb.

Experimental results have been obtained on particles with a core-shell morphology. This particular morphology of the particles has been chosen in order to create a stiff and elastic connected network of shells in a soft and dissipative matrix in the fully dry film.

The structure of the film can be characterized by Atomic Force Microscopy (AFM) in tapping mode following the methodology developed by Mallégol et al..[24] On this topic we collaborated with the Unviersity of Surrey and all AFM images were obtained by Dr. Chunghong Lei under the supervision of Dr. Joe Keddie at the University of Surrey.

Although, for all films, AFM pictures clearly show that the memory of the shape of the particle is retained and an example is shown in Figure 4-6, it is difficult to prove that a real core-shell structure, as depicted in Figure 4-7, actually exists in the film.

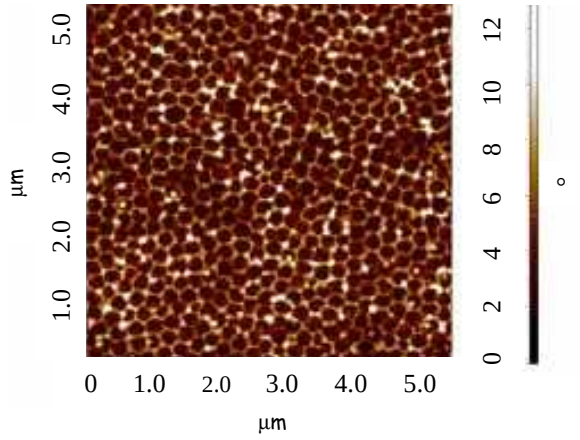

Figure 4-6. Phase AFM image of a hard shell - soft core particle.

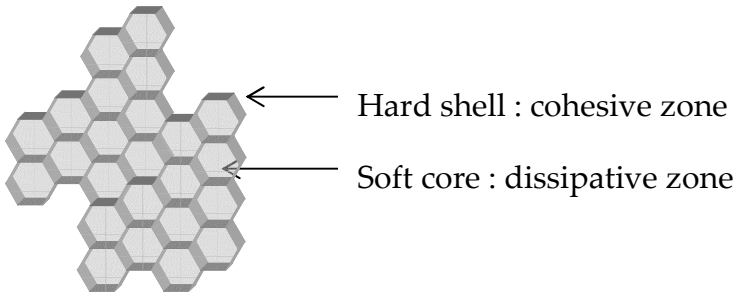

Figure 4-7. Theoretical 3D-honeycomb like structure obtained after the drying of soft core-hard shell particles.

The theoretical honeycomb like structure is displayed on Figure 4-7. Ideally, the cohesion and shear resistance should then be controlled by properties of the shell while tackiness should be adjusted by the properties of the core.

The first part of the experimental result section, will focus on a series of hard (high T_g) shell – soft (low T_g) core particles. Within the present work, mainly, two parameters will be varied: T_gs (of both the shell and the core) and the amount of chain transfer agent (CTA) in the core. T_gs have been changed through the monomer composition. Specific values of variable parameters are summarized in Table 4-1. Adhesive performance of these heterogeneous materials will be compared to that of a film made from homogeneous particles which will be considered as a benchmark and called WB. It should be noted that WB as well retains the memory of the shape of the particles.

All these particles have a thin shell and are characterized by a core/shell ratio equals to 91/9 (wt%). The diameter of the particles lies between 205 nm and 275 nm, the solid content is about 50%. A single particle with the corresponding thickness of the shell is represented on Figure 4-8-a.

With the first set from HS1[(1)] to HS3, we will show how the elastic modulus G' is important in controlling adhesive performance. G' has been adjusted with the T_gs of the shell and the core and with the amount of CTA in the core. Variations from -60°C to -45°C and from 98°C to 34°C for the core and shell T_g respectively have been studied. At the same time the CTA content in the core has been increased from 0 to 0.03 wt%/total monomer. This choice to simultaneously change the T_gs and the CTA content has been motivated by the desire to effectively reach acceptable adhesive performance.

Keeping T_gs constant, viscoelastic dissipation can be increased by decreasing the gel content, and the molecular weight of the sol. One can also decrease the crosslinking density of the gel network and increase its amount of free branches. Experimentally, we decided to use a chain transfer agent as a synthetic tool to adjust these molecular parameters. Decrease in the gel content (from 4% to 0%) and in the M_w of the sol (from M_w = 233,600 g.mol^{-1} to M_w = 112,500 g.mol^{-1}) have been obtained by increasing the amount of chain transfer agent (CTA) from 0.03 wt% (/ total monomer) to 0.1 wt%. Note that in such cases the gel content was low, an increase in the CTA amount led to the simultaneous decreases in gel content and in M_w. The molecular weight distribution of the sol does not appear to be very affected by the

(1) H for Hard shell and S for Soft core.

amount of chain transfer agent. The T_g of the core of HS5 is a bit lower due to a slight change in core monomer composition.

Note that HS3 and HS4 are the same in terms of their T_gs and CTA contents in the core but their different rheological and adhesive behaviors are due to the fact that HS3 is synthesized using the inverse process where the shell is polymerized during the first step of the synthesis and the core afterwards, while HS4 is synthesized using the direct process where the core is produced during the first step and the shell is added afterwards. Latexes from the first set (HS1, HS2 and HS3) are synthesized using the inverse process while HS4 and HS5 are produced using the direct process. This change in the synthesis process, while important in terms of structure and properties is however outside the scope of the present work.

	WB	HS1	HS2	HS3	HS4	HS5
Shell T_g (°C)[1]	-	98	93	34	34	34
Core T_g (°C)	-50	-60[2]	-45[2]	-45[3]	-47[3]	-38[3]
%CTA$_{core}$ (%wt / total monomer)	TA1[4]	0	0.013	0.03	0.03	0.1

[1] shell T_g is measured by differential scanning calorimetry.
[2] core T_gs of HS1 and HS2 are assumed to be close to the final T_gs of the particle which are measured by DSC.
[3] core T_gs of HS3, HS4 and HS5 are calculated using the Fox equation.
[4] value not reported here since it is a Cytec proprietary information.

Table 4-1. Some characteristics of hard shell-soft core particles studied.

The second part of the experimental result section will be more focused on soft shell-soft core particles with a core/shell ratio of 80/20 (Table 4-2). A single particle with the corresponding thickness of the shell is represented on Figure 4-8-b. They are characterized by almost the same monomer composition in both the shell and the core except that the amount of chain transfer agent added is a little lower (0.037 wt% / total monomer of the shell) in the shell and that the shell contains some diacetone acrylamide (DAAM) groups (0.4 wt% total monomer). The crosslinking reaction of these groups can be activated if adipic acid dihydrazide (ADH) is added to the water phase just prior to the drying of the latex. The two materials studied (SS1[(1)] and SS2 in Table 4-2) are nearly the same. In both cases, the gel content of the core is equal to zero as a consequence of the high amount of CTA. The amount of CTA is however slightly lower in SS2.

	WB	SS1	SS2
Shell T_g (°C)[1]	-	-41	-41
Core T_g (°C)[1]	-50	-41	-41
% CTA$_{core}$ (%wt / total monomer)	TA1	0.12	0.08
Gel content %	58.3	0	0

[1] T_gs are calculated using the Fox equation.

Table 4-2. Some characteristics of soft shell-soft core particles studied.

[(1)] SS for Soft shell and Soft core.

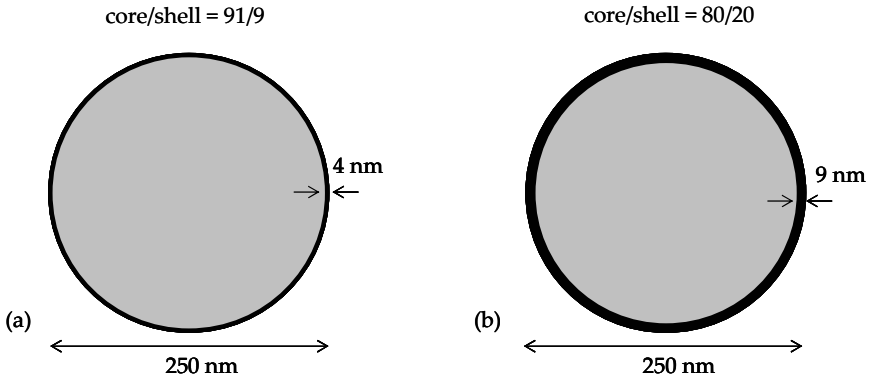

Figure 4-8. Representation of two single particles with the corresponding shell thickness. (a): core/shell ratio = 91/9. (b): core/shell ratio = 80/20.

These two series of latexes have been chosen as examples to illustrate the methodology used to design the best particle structure.

4.4. Particle and polymer design for adhesive properties

4.4.1. Linear viscoelastic properties and adhesive properties

As discussed in the introduction, adhesive tests are complex and difficult to interpret directly in terms of microstructure or molecular structure of the polymer. As stand-alone they can only provide some guidance to the expert or within a given family of materials in the final optimization stage. We present here some examples where the careful analysis of the linear viscoelastic properties can be used to direct the synthesis in the right direction.

4.4.1.1. Influence of the elastic modulus: the PSA must be soft enough

The first example, where results obtained on HS1 and HS2 are presented, shows how a change in the modulus of the material, obtained here mainly through a change of the T_gs of the core (the increase in the CTA content in the core from 0 to 0.013 wt% has probably a negligible effect compared to the change in T_g) can have a profound influence on adhesive properties.

On Figure 4-9 are shown both the evolution of the shear elastic modulus as a function of frequency in the linear regime (Figure 4-9-a) and stress-strain tack curves of the corresponding materials (Figure 4-9-b). Behavior of core-shell particles characterized by a low core T_g and a high shell T_g is compared to that of a benchmark PSA (WB) made of homogeneous low T_g particles.

As discussed in chapter 1, the first requirement for a PSA in terms of linear rheological properties is that the elastic component of the shear modulus should be below 100 kPa. On Figure 4-9-a, one can observe that G'(ω) of HS1 is higher than this defined boundary and nearly constant around 2 MPa between 0.1 and 10 Hz. This is clearly too hard to conform to a rough surface and the stress-strain curve of such an adhesive layer in probe tack is characterized by a sharp decrease of the stress without fibrillation plateau and a very low adhesive energy.

On the other hand the elastic modulus of WB lies well below 0.1 MPa in the overall range of frequencies studied and that of HS2 does not exceed 0.25 MPa. In these cases, interfacial failure proceeds by cavitation and a fibril structure is formed.

The increase in the T_g of the core from -60°C to -45°C leads to a significant decrease in the shear elastic modulus G'. Intuitively, we would expect an increase in G' with an increase in T_g. The inverse tendency observed here is not easily explained. It may be due to different organizations of the core-shell structure depending on the difference between the T_gs of both phases. In the case of HS1, the resulting modulus is too high for the material to be spontaneously sticky. A careful adjustment of the T_g of the core is clearly necessary.

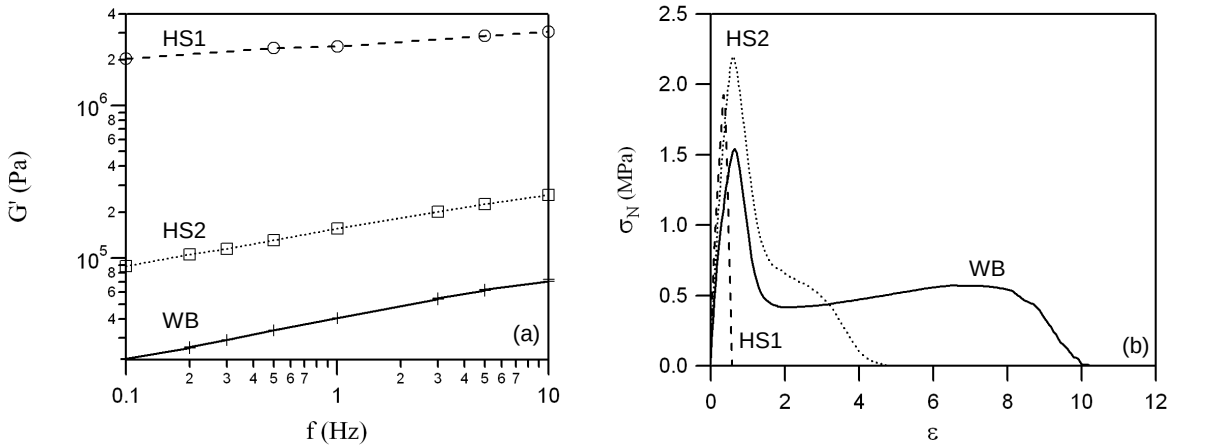

Figure 4-9. (a): Evolution of the elastic modulus with frequency for two hard shell-soft core particles. (b): Stress-strain tack curves. Tests were performed on stainless steel probe at 1000 µm.s^{-1}. (dashed line: HS1, dotted line: HS2, solid line: WB).

Our second example is given on Figure 4-10. The synthetic strategy was here to decrease the elastic modulus playing with both the T_g of the shell and with the CTA amount in the core. A decrease of the T_g of the shell from 93°C (HS2) to 34°C (HS3) was accompanied with an increase in the CTA amount in the core from 0.013 to 0.03 wt%.

In this case, the elastic modulus values of the materials are in the suitable range for the cavitation process to be complete and the fibrillation process to be activated. Lakrout et al.[7,25] observed that $\sigma_{max} \sim 10\ G'$ for acrylic systems. Even if this is not exactly verified with our experimental results, one can be confident in saying that the observed difference in σ_{max} is controlled by G′ in this case since the probe used has a comparable level of roughness.

To understand the differences in adhesive properties of Figure 4-10-d, it is necessary to examine this time the dissipative properties of the latexes and more specifically the parameter G_c/E. Once cavities are formed at the interface between the probe and the adhesive film, their rate of propagation is dependent on tan(δ). The more difficult is the crack propagation the smaller are the cavities and the higher is the value of tan(δ).

As discussed in section 4.2.1, once cavities are fully formed (on the right side of the peak) G''/G'^2 can be used as an approximation of G_c/E for a given surface. The lower is G''/G'^2 the more crack propagation is favored compared to crack blunting and the sooner the detachment is expected to occur. This is what is experimentally observed (Figure 4-10-c and Figure 4-10-d). Much shorter fibrillation plateaus are obtained on the probe tests in the case of low values of G''/G'^2 ($G''/G'^2 < 0.5.10^{-5}$ Pa^{-1}).

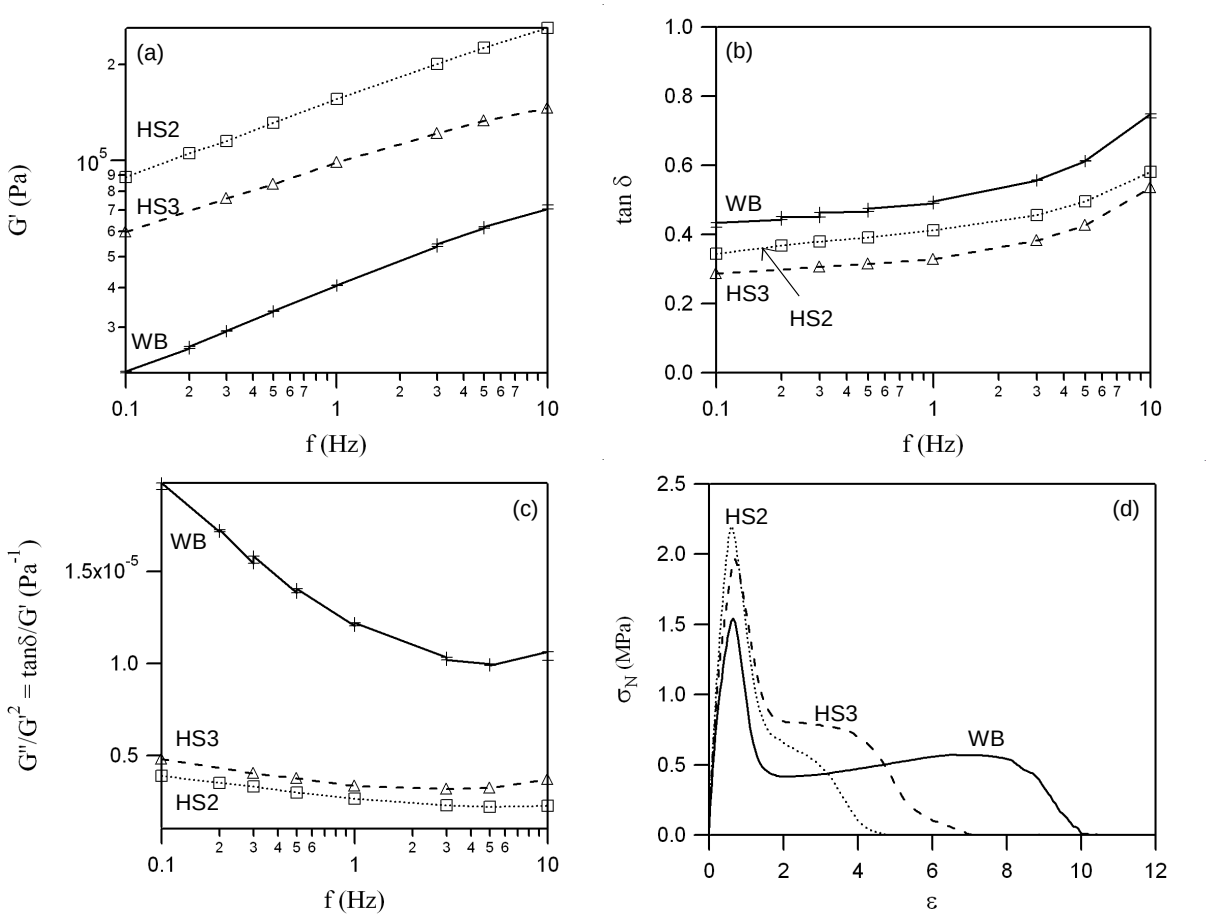

Figure 4-10. Evolution of the elastic modulus (a), tan(δ) (b) and of the ratio G″/G′² (c) with frequency for two hard shell-soft core particles. Stress-strain tack curves (d), tack experiments were performed on stainless steel at 1000 μm.s^{-1}. (Dotted line: HS2, dashed line: HS3, solid line: WB)

Let us finally examine a third example where different surfaces are used. Figure 4-11 shows tack results of HS3 on a stainless steel and a polyethylene surface. One can observe a large decrease in adhesion energy when tests are performed on a low energy surface such as PE. If values of G″/G′² are high enough for acceptable adhesion energy on stainless steel, a higher value is probably required for better performance on PE. This can be explained by the dependence of G_c on the surface energy and by the higher critical value of $(G''/G'^2)_c$ for crack blunting on PE (Figure 4-2) than on stainless steel. Such a result clearly demonstrates the need to adapt the linear viscoelastic properties of the PSA to the substrate as discussed recently.[26] This shortcoming requires then a change in synthesis strategy.

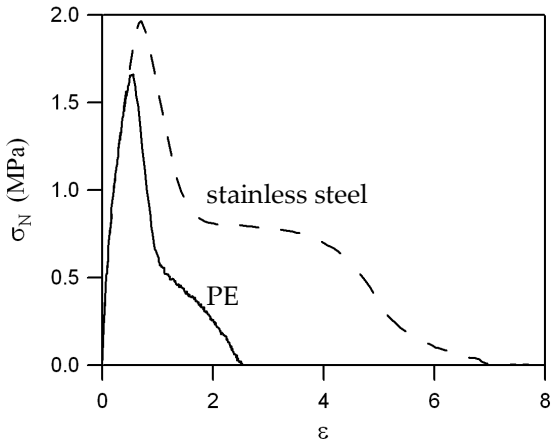

Figure 4-11. Tack stress-strain curves of a HS3. Dashed line: on stainless steel. Solid line: on PE. Experiments were performed at 1000 μm.s^{-1}.

To conclude, the absolute values of T_g of the soft core and of the hard shell and the amount of CTA in the core have an obvious influence on rheological and adhesive properties of the material. It is also clear that these properties depend on how the two phases are matched. A good compromise in terms of adhesive properties seems to be reached when the T_g of the core equals -45°C and the T_g of the shell equals 34°C with a CTA content in the core of 0.03 wt%. However, Figure 4-11 shows that adhesive energy on PE is still very low. In order to further improve adhesive properties, the strategy examined in the following section is to try to enhance tan(δ) by increasing the amount of CTA in the core.

4.4.1.2. Influence of the dissipative properties: how to further increase the adhesive energy

Linear rheological properties of hard shell-soft core particles differing both by their amount of CTA in the core and by their core T_g are displayed in Figure 4-12-[1]. Tack experiments have been also performed on these materials on stainless steel and PE at two speeds of debonding (V_{deb} = 10 and 1000 μm.s^{-1}) (Figure 4-12-[2]).

As a result of the changes in chemistry it is obvious that HS5 has a higher elastic modulus G′ and is more dissipative while HS4 is softer and more elastic. Values of G″/G′^{2} can be used to estimate $\mathcal{G}_c$/E. Comparing HS4 and HS5 a crossover of the curves representing values of G″/G′^{2} as a function of the frequency is observed at about 2 Hz. This means that at small frequencies, dissipation seems to dominate, while at higher frequencies, this is most probably bulk properties characterized by elastic modulus which play the major role. Figure 4-12-[2], illustrates the fact that the competition between the interfacial propagation of the crack and the vertical extension of the fibrils is governed by G″/G′^{2}. For example, at 10 μm.s^{-1}, on stainless steel as on PE, the lower value of G″/G′^{2} in the case of HS4 results in a debonding of the layer at a lower nominal strain. At 1000 μm.s^{-1}, on stainless steel, a longer fibrillation plateau is obtained for HS5 but on PE the tendency is reversed and is more in agreement with the frequency dependence of linear rheological parameters. The high elastic modulus of HS5 is responsible for the low value of G″/G′^{2} at high frequencies and leads to the brittle fracture characterized by the sharp decrease in stress after the initial peak.

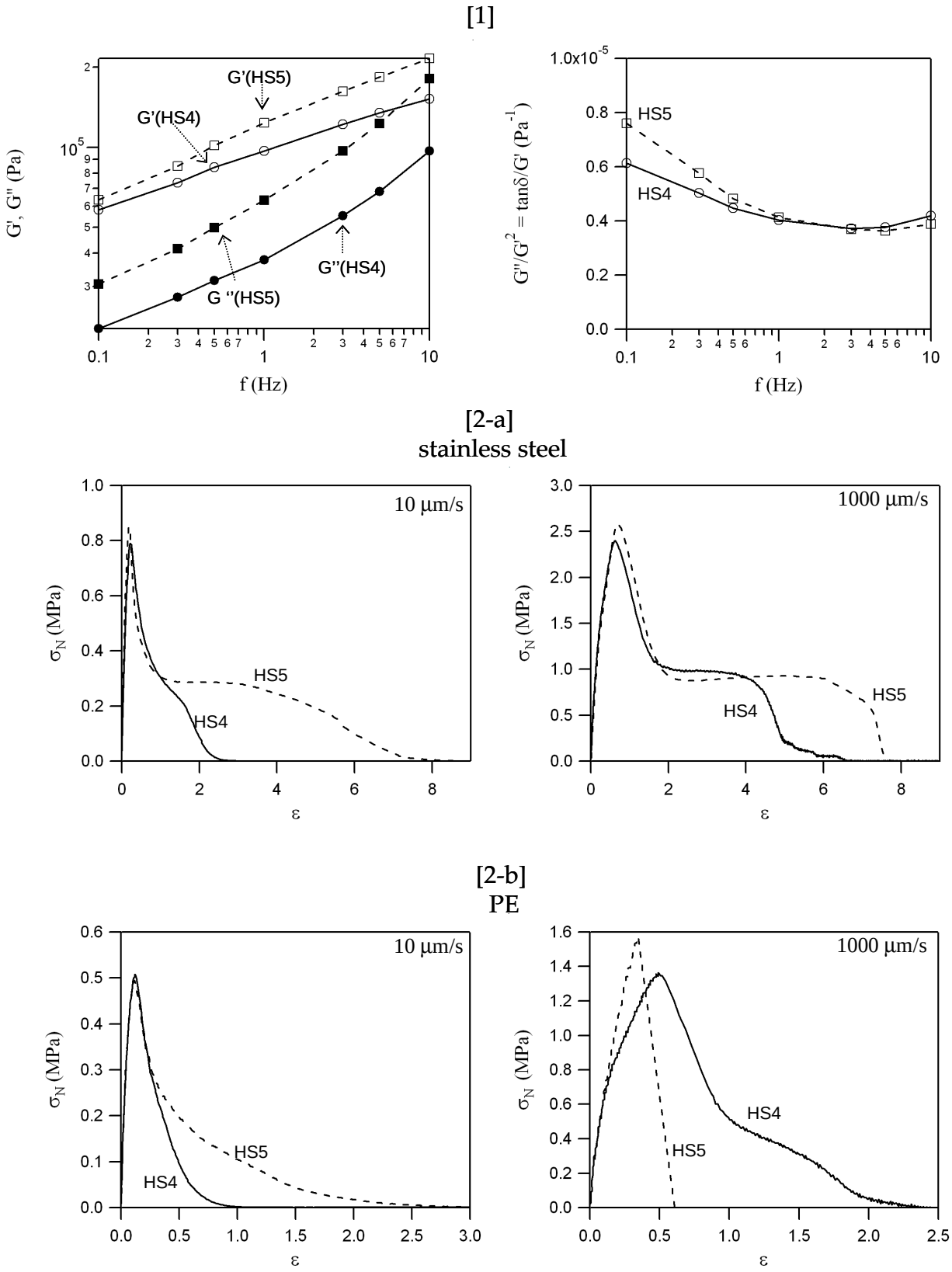

Figure 4-12. [1] Linear rheological results of two hard shell-soft core particles with different core T_gs and different amounts of CTA in their core. Left: evolution of elastic G′ (empty symbols) and dissipative G″ (filled symbols) moduli as a function of the frequency, right: evolution of the ratio G''/G'^2. [2] Stress-strain tack curves. [2-a]: stainless steel probe, [2-a]: PE probe (tests on PE on HS4 and HS5 were performed by Haris Retsos). Solid line: HS4, dashed line: HS5.

As a conclusion for this section concerning the use of linear rheological properties, we showed that trends in tack experiments can be predicted using linear rheology. A criterion for adhesion can be extracted from experimental results. One can assume that a good adhesion on PE is possible if $G''/G'^2 > 10^{-5}$ Pa^{-1} while a lower value (about $0.5.10^{-5}$ Pa^{-1}) is acceptable for adhesion on stainless steel.

Probe tack results are consistent with peel and shear results obtained with standard tests (Table 4-3). The higher shear resistance of HS4 has to be related to its earlier debonding during probe tack experiments at low debonding velocity (10 $\mu m.s^{-1}$). Here, the increase in the cohesion does not result in an increase in the level of the fibrillation plateau but in a change of the debonding mechanism from a bulk mechanism with fibrillation to an interfacial mechanism where cavities prefer to propagate at the interface between the probe and the adhesive layer.

The peel force of HS5 is higher than that of HS4 on a high energy surface such as glass while the opposite result is found on a lower energy surface such as PE. This in agreement with tack results obtained at high debonding velocity (1000 $\mu m.s^{-1}$) where the adhesive energy (area under the stress vs. strain curve) of HS5 was higher than that of HS4 on stainless steel and lower on PE.

		HS4	HS5
Peel 24h 180° (FTM1) (N/25mm)	**glass**	12.5 (10% CT[a])	14.65 (80% CT)
	HDPE plate	2.5	1.6
Shear (FTM8) (min)	**Stainless steel (1kg, 1 inch^2)**	4448 CF[b]	1579 CF

a-Cohesive transfer
b-Cohesive failure

Table 4-3. Standard adhesive tests results of HS4 and HS5.

From a more molecular design point of view, adhesive properties can be enhanced by an increase in the amount of CTA in the core (increasing dissipation). But then improvement in shear resistance requires an increase in the T_g of the shell.

However varying the T_g of an acrylic waterborne polymer by changing the copolymer composition also affects the gel fraction, the average molecular weights, and the level of branching as what has been already extensively discussed in chapter 2.

An alternative strategy is to activate an interfacial crosslinking reaction between the particles after the synthesis process, just prior to the drying of the film. This strategy is really interesting to adjust cohesion without having any major effect on the composition of the particles and thus to obtain a well controlled structure of the dry film.

Such a change in crosslinking is much more apparent in large strains than in small strains and in the next section we will focus on the importance of nonlinear deformation properties to predict adhesive properties.

4.4.2. Use of large strain deformation to further refine particle design for adhesive properties

Since the deformation of PSA is highly strain rate dependent, their large strain properties have to be studied at strain rates that are relevant for tack tests. The instantaneous strain rate in a tack test is defined as $\dot{\varepsilon} = V_{deb}/h_0(1+\varepsilon)$ where V_{deb} and h_0 are the debonding speed and the initial thickness of the adhesive layer respectively. During tensile experiments, $\dot{\varepsilon} = V_t/L_0(1+\varepsilon)$ with V_t and L_0 the stretching velocity and the initial distance between clamps respectively. Films for adhesive tests being about 100 µm thick and for an initial distance between tensile clamps equals to 17 mm, we find that tensile experiments performed at a fixed velocity equal to V_t = 50 mm.min^{-1} have to be compared with tack tests performed at V_{deb} = 10 µm.s^{-1}. Only results on stainless steel will be presented even though performance on PE is also highly controlled by high strain behavior and mainly by the softening at intermediate strains.

4.4.2.1. Activation of crosslinking at the interface of soft and dissipative particles: from a viscoelastic liquid to a viscoelastic solid

Maybe the most spectacular example of the relevance of the nonlinear properties is seen in the effect of the interparticle crosslinking process and this point will be addressed in much more detail in chapter 5. Figure 4-13 displays results obtained on uncrosslinked and crosslinked SS1 (in the latter case all DAAM groups of the shell are crosslinked). From Figure 4-13-a, linear rheological properties do not seem to be much affected by the activation of the interfacial crosslinking. The elastic modulus stays well below the Dahlquist critical value. Peak stresses of both materials are similar as a consequence of similar values of G'. G''/G'^{2} is in both cases superior to 10^{-5} Pa^{-1} and detachment never occurs through the interfacial propagation of the cavities.

However, clear differences are observable in the shape of tack stress-strain curves at higher strains (Figure 4-13-b) and these can only be explained by large strain tensile results. Indeed, contrary to small strain properties, nonlinear rheological properties seem to be significantly affected by the activation of the interfacial crosslinking. In the case of uncrosslinked particles, no local minimum in the reduced stress curve is observed (Figure 4-13-c). This is a signature of a liquid-like behavior: the tensile specimen does not break but flows at the end of the test. On the contrary, in the case of interfacially crosslinked particles, strain hardening appears and is responsible for the fracture of the tensile sample (no flow). Activating an interfacial crosslinking triggers a transition from a viscoelastic liquid behavior to a viscoelastic solid.

In an adhesion test, the liquid-like behavior of uncrosslinked core-shell particles leads to a cohesive debonding. This is visible since tack curves present a double fibrillation plateau and end up at a non null stress.[5,27] Activating interfacial crosslinking, a progressive transition from a cohesive to adhesive debonding is observed.

It is at this stage interesting to note that crosslinked particles keep the same value of C_2 indicating a similar density of temporary crosslinks while C_1, the density of permanent crosslinks, increases. This finally leads to a relatively high adhesion energy and an adhesive debonding rather than cohesive failure.

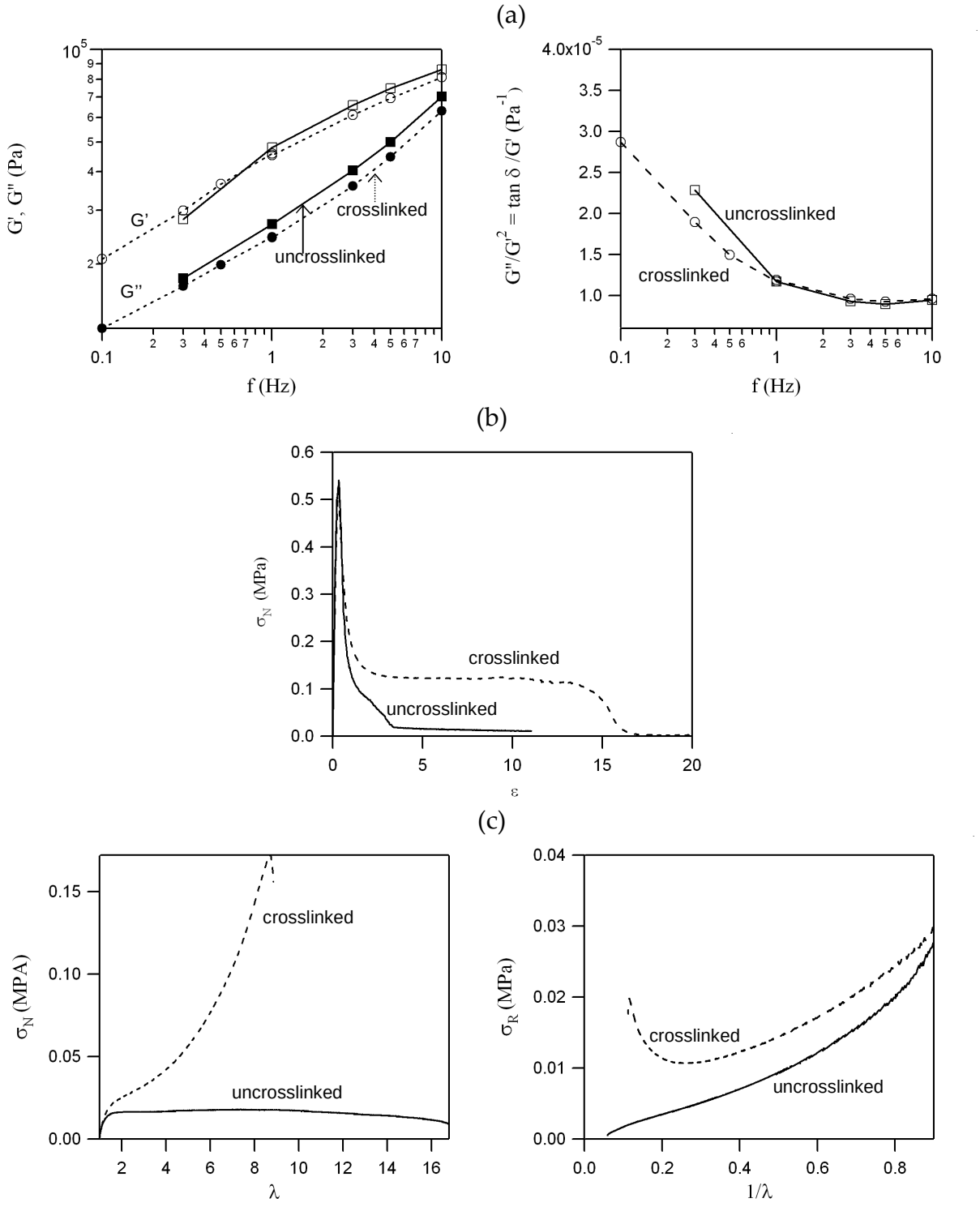

Figure 4-13. Effect of the activation of interfacial crosslinking of SS1 particles. Solid line: uncrosslinked particles (no ADH added), dashed line: interfacially crosslinked particles. (a) Linear rheology. Left: evolution of the elastic G′ (empty symbols) and dissipative G″ (filled symbols) moduli as a function of the frequency. Right: evolution of the ratio G″/G′². (b) stress-strain tack curves. Tack experiments were performed at 10 μm.s^{-1} on stainless steel. (c) Nonlinear rheology. Left: nominal stress vs. strain tensile curves. Right: Mooney Rivlin representations of tensile results.

4.4.2.2. Influence of gel content and M_w of the sol of the core

In the previous example it is clear that the introduction of a crosslinking chemistry in the shell has a profound effect on the large strain properties of the adhesive film. It is now interesting to investigate a change in the molecular architecture of the polymer in the core at a fixed degree of crosslinking of the shell. The first material studied with 0.12 wt%/total polymer of CTA in the core was compared to a similar core-shell particle with 0.08 wt% of CTA where all DAAM groups in the shell have been crosslinked by the ADH. The large strain behaviors of these two materials are displayed on Figure 4-14. The overall shape of the curves is very similar. The cavitation stress is reached and the fibrillation process is initiated. From reduced stress curves, strain hardening appears nearly at the same level of deformation indicating that the finite extensibility of the crosslinked network of shells is the same.

The parameter C_2 in the Mooney-Rivlin model is nearly the same for both materials, indicating that the density of non permanent crosslinks is nearly the same. However C_1 increases without significant change in the position of the minimum along the $1/\lambda$ axis. This indicates a difference in the density of permanent crosslinks without any change in the percolating network determining the finite extensibility of the material.

An increase in CTA amount in the core decreases the gel content and the M_w of the sol fraction (again M_w decreases since the gel content is really low) of the core and therefore decreases the density of permanent crosslinks. This loss of cohesion is confirmed by the decrease in fibrillation plateau level on stress-strain tack curves both on stainless steel and on PE (Figure 4-14-[2]). This could also be at the origin of the large increase in the length of the fibrillation plateau of SS1 compared to SS2. A more detailed explanation is proposed in the following paragraph.

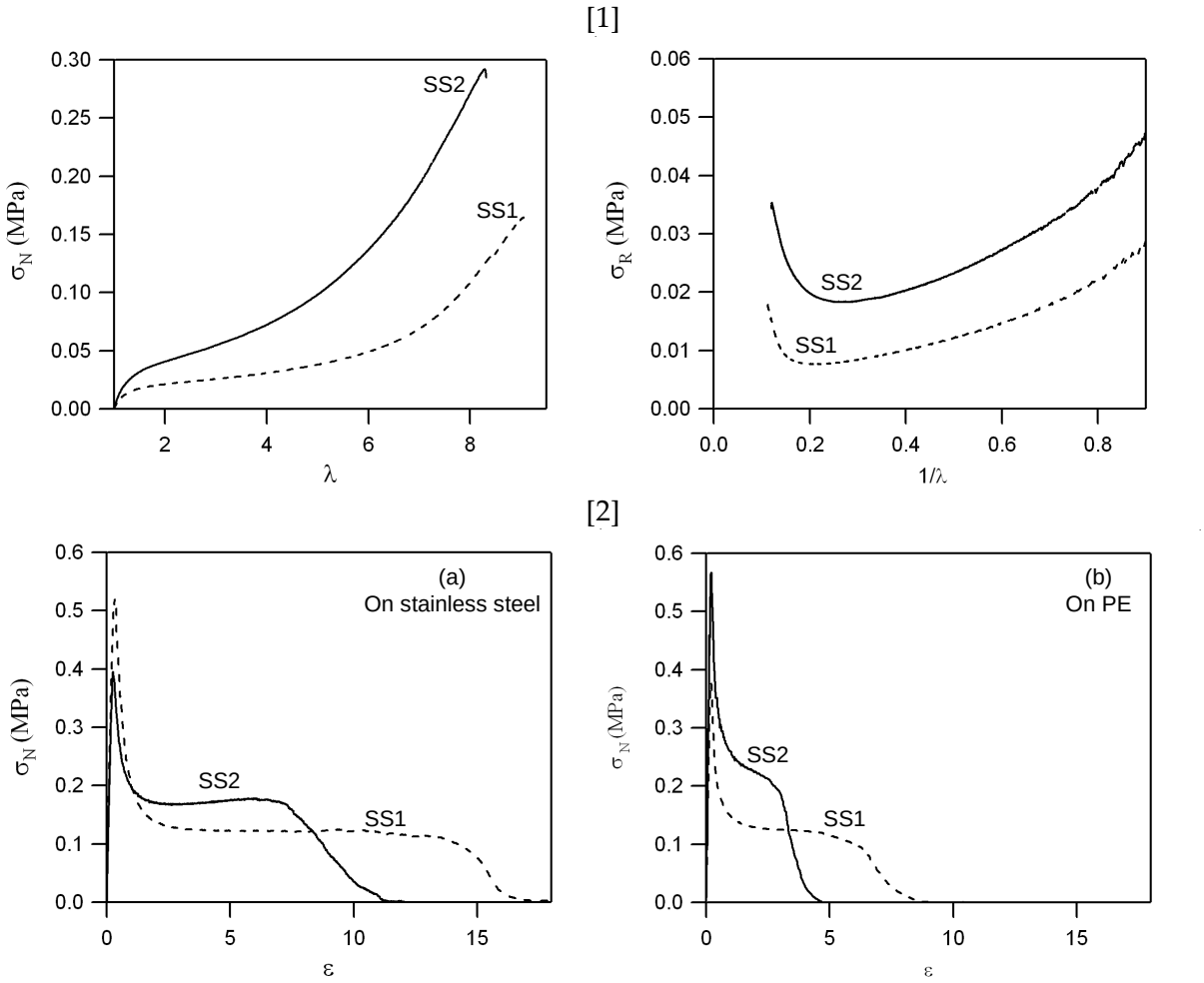

Figure 4-14. Effect of the amount of CTA in the core. Dashed line: crosslinked SS1, solid line: crosslinked SS2. [1] nonlinear rheological results. Left: nominal stress vs. strain tensile curves. Right: Mooney Rivlin representations of tensile results. [2] stress-strain tack curves. Tack experiments were performed on stainless steel (a) and on PE (b) at 10 μm.s^{-1}.

As can be observed on Figure 4-15, very often, the reduced stress vs. 1/λ curves cannot be easily fitted using the Mooney-Rivlin elastic model because there is no clear linear region of softening. To overcome this limitation, we decided to use the following methodology to evaluate the softening in the Mooney representation: we took the slope of the line defined by the experimental points at 1/λ = 0.8 and at the point where σ_R goes through a minimum and strain hardening starts ($1/\lambda = (1/\lambda)_{hard}$). For each material, three to five tests were performed and as can be seen on Figure 4-15-b, the results are highly reproducible except at low strains corresponding to the range of 1/λ values above 0.8. That is why 1/λ = 0.8 was chosen as the higher limit for the calculation of the slope. For an estimate of the contribution of the permanent crosslinks, we decided to take the value of the reduced stress when strain hardening starts and define it as C_{hard}. The crossover between the previously defined slope and y-axis (C_1) has not been chosen since it lies sometimes in the negative range values. The slope between 1/λ = 0.8 and the minimum in reduced stress will be called C_{soft}. In the case where no local minimum exists, C_{hard} is not defined and C_{soft} is calculated between (0.8;σ_R(0.8)) and (0.2;σ_R(0.2)).

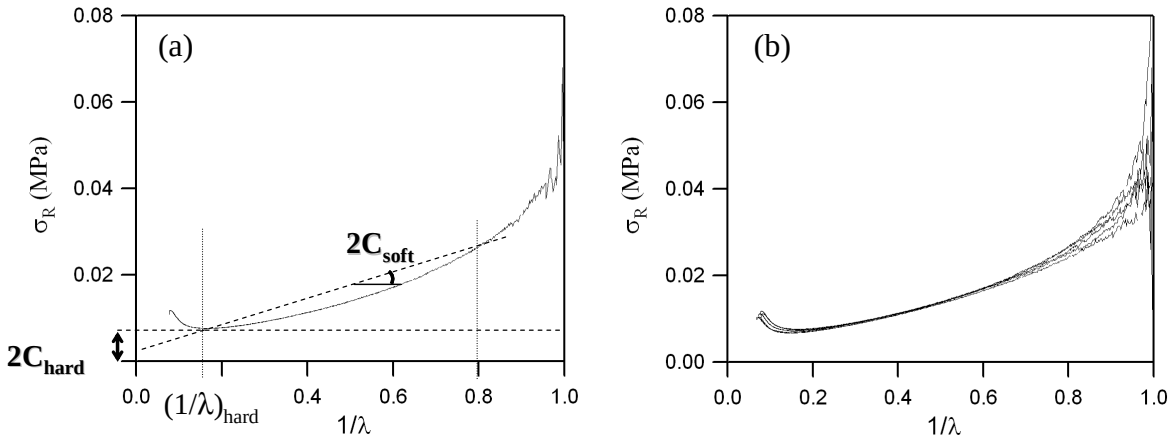

Figure 4-15. (a): Estimate of permanent and temporary crosslinks through C_{soft} and C_{hard} respectively. (b): Five curves obtained on the same material are represented.

Usually a more dissipative material has many temporary crosslinks (that can relax) and much fewer permanent crosslinks, resulting in a high ratio C_{soft}/C_{hard} and a long fibrillation plateau. Low values of C_{soft}/C_{hard} are on the contrary obtained in the case of more permanently crosslinked materials. In that case, the storage of elastic energy during elongation of the material is favored and leads to a rapid debonding of the adhesive layer when this energy is released.

Comparing SS1 and SS2, the maximal extension of the fibrils can effectively be predicted from this ratio C_{soft}/C_{hard}. An increase in the amount of CTA leads mainly to a decrease in C_{hard} without having much influence on C_{soft}.

Precise guidelines on the values of C_{soft}/C_{hard} clearly depend on the application. For the application that was considered with these interfacially crosslinked PSA, which was adhesion on PE, a relatively high value of 3 was optimal.

4.4.2.3. Comparison between a viscoelastic material and a more elastic one

In our next example we compare nonlinear properties of a highly dissipative material made of interfacially crosslinked soft core-soft shell particles (SS2) with that of a more elastic adhesive film made of soft and independently crosslinked particles (WB). The more elastic is the material and the less pronounced is the softening. This is experimentally observed by the less steep slope of the reduced stress versus 1/λ curve at intermediate strains (Figure 4-16-a).

If we consider again the ratio C_{soft}/C_{hard}, the longer fibrillation plateau of the core-shell particle is a consequence of both a decrease in the cohesion governed by permanent crosslinks and measurable by C_{hard} (decrease from 0.021 MPa to 0.019 MPa) and an increase in the dissipation measurable by C_{soft} (increase from 0.022 MPa to 0.040 MPa). This finally leads to an increase in C_{soft}/C_{hard} from 1.05 to 2.11.

For adhesion on stainless steel (the application considered here), a value of 2.11 for C_{soft}/C_{hard} was optimal. As discussed just above, for adhesion on PE, better adhesive properties can be obtained with higher values of C_{soft}/C_{hard}. This is an example of the coupling between surface and rheological properties.

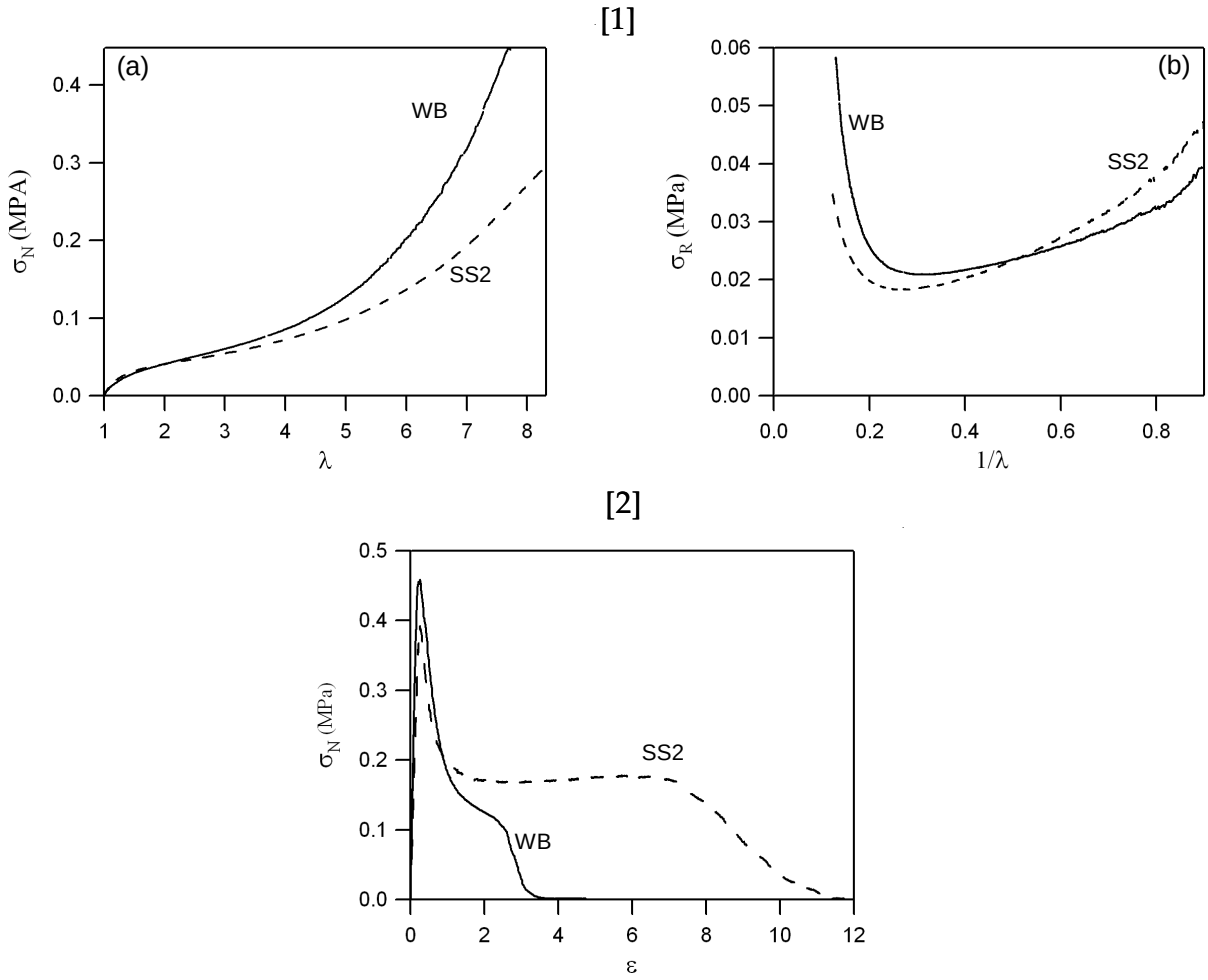

Figure 4-16. Comparison between an elastic material and a more viscoelastic one. Solid line: WB, dashed line: crosslinked SS2 [1] Nonlinear rheological results. (a): stress-strain tensile curves, (b) Mooney-Rivlin representations of tensile results. [2] Stress-strain tack curves. Tack experiments were performed on stainless steel at 10 µm.s^{-1}.

4.4.3. A more complex example

When using linear rheology for the prediction of adhesive performance, some caution is sometimes needed and Figure 4-17 is an example where adhesive properties cannot be easily correlated to the properties measured in the linear regime. One of the latex is made of homogeneously crosslinked particles (WB) while the second latex consists of hard shell–soft core particles (HS5).

The higher cohesion of the core-shell particle at small and intermediate strains can be easily explained by its higher elastic modulus (values not displayed here).

One can however observe that G''/G'^2 of the heterogeneous material made of core-shell particles is very close to the criterion, which stipulates that G''/G'^2 needs to be higher than $0.5.10^{-5}$ Pa^{-1} for good adhesion on steel, and that G''/G'^2 of the homogeneous latex is significantly higher. In principle this means that the core-shell system is not very dissipative relative to its modulus and would lead to a tack curve with a higher but shorter plateau for HS5. The adhesion energy on steel at 10 µm.s^{-1} in the case of the homogeneous particle is

however significantly lower due to an earlier detachment from the probe. As a consequence, it is clear that G″/G′² can not be used as a sole predictor for adhesive performance.

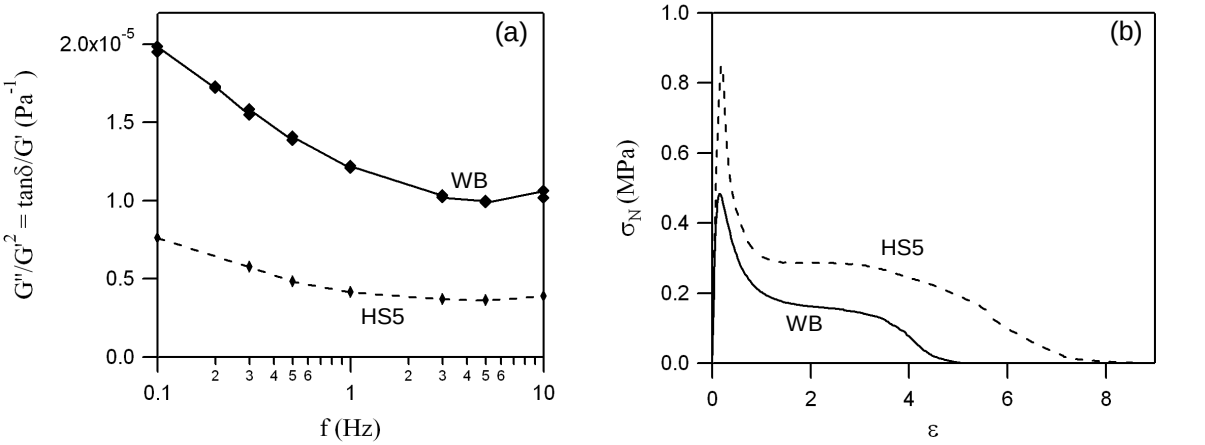

Figure 4-17. Evolution of the ratio G″/G′² of two waterborne PSA (dashed line: HS5, solid line: WB) on the left, and their corresponding tack behavior on steel at 10 μm.s^{-1} on the right.

Results of tensile experiments are shown on Figure 4-18. Nominal stress versus strain curves (left) and Mooney-Rivlin representations (right) are displayed. For both materials, a strain hardening is observed as well as a local minimum, but it is followed by an additional decrease in the reduced stress in the case of HS5 (this final decrease is more pronounced when stretching is performed at 500 mm.min^{-1} than at 50 mm.min^{-1}, that is why we decided to show results obtained at this stretching velocity). Thus, the longer fibrillation plateau of the core-shell is due to its flow behavior at high strain. In other words although the particles are crosslinked and cohesive and the linear viscoelastic properties of the film shown on Figure 4-18 are consistent with this, the strength of the interfaces between particles is probably weak. Although this is not apparent from the tack curves a cohesive debonding was effectively observed for HS5.

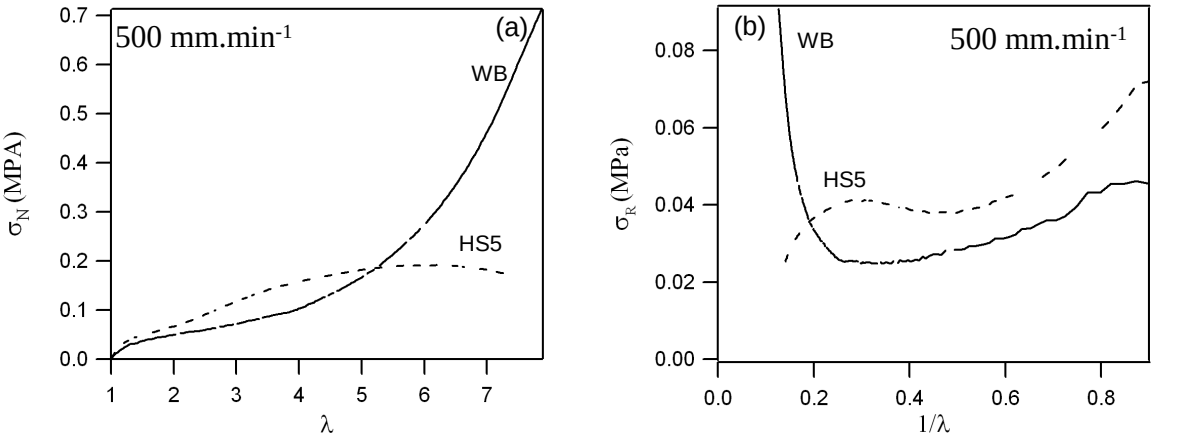

Figure 4-18. (a): stress-strain tensile curves of HS5 (dashed line) and WB (solid line). (b): Corresponding Mooney-Rivlin representation. Tests were performed at V_t=500 mm.min^{-1}. (tensile tests on HS5 were performed by Sandrine Mariot)

Combination of linear and nonlinear rheological results has led us to propose a mechanism for the deformation of this particular hard shell - soft particle (HS5) during a uniaxial elongation (Figure 4-19). The structure could be first homogeneously deformed. At intermediate strains, stress is probably mainly sustained by the hard shell and a strain hardening of the material can be observed. At a given higher strain, the thin and fragile shell could break. If so, behavior is then controlled by the core.

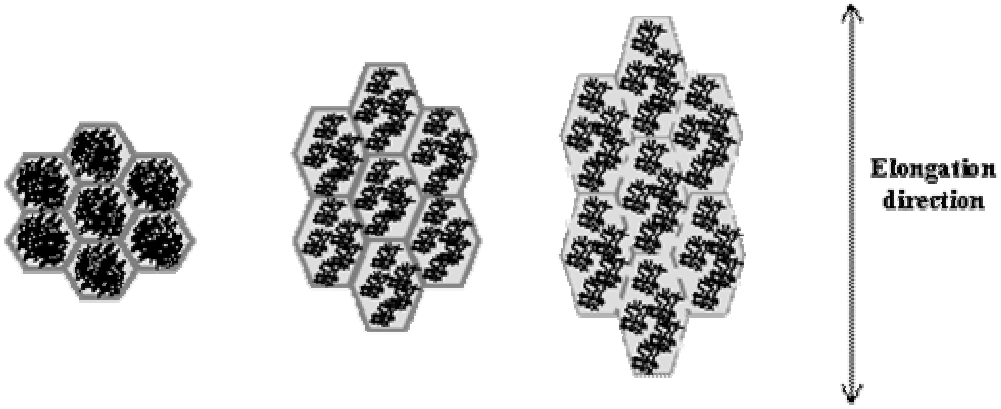

Figure 4-19. Expected evolution of the structured core/shell particles when stretched during a uniaxial elongation test.

To conclude, nonlinear properties are really useful for the fine tuning of adhesive properties when the linear viscoelastic criteria are met. This has been already demonstrated by Roos et al.[21] but what is especially new in the present study is that softening at intermediate strain is probably not much due to the elastic slippage of entanglements but rather to their viscous relaxation. This is due to the low entanglement density of acrylic polymers due to their high M_e (M_e of P(2EHA) varies between 35,000 to 130,000 g.mol^{-1} and M_e of P(BA) varies between 17,000 to 26,000 g.mol^{-1}[28]) and to the much more heterogeneous crosslinking of these acrylic systems relative to the physically crosslinked block copolymer based PSA. Softening is then due to viscoelastic process such as relaxation leading to viscous dissipation.

We have shown that the tensile tests can predict cohesive or adhesive debonding at the end of tack experiment, as well as the level of stress at which a plateau in fibrillation is formed. The quantitative prediction of the detachment strain of the fibrils remains a difficult problem as it involves both nonlinear elasticity and linear viscoelasticity. An attempt to discuss this process has been recently proposed by Glassmaker et al.[29]

Further modeling of the nonlinear viscoelastic behavior of the PSA requires tools able to specifically incorporate the viscoelastic behavior at small strains and the elastic hardening at large strain. This point will be addressed in more detail in the following chapter.

4.5. Conclusion

A new methodology can be proposed for the optimization of the adhesive properties of PSA and is illustrated with examples taken from the particular case of core-shell particle morphology with a thin shell (core/shell ratio typically equals to 80/20).

- First, the overall monomer composition of each phase has to be chosen in order to reach a T_g in the target for the adhesive application. Adhesion strongly depends on T_g and a maximum is reached between 50°C and 70°C above the T_g.[6]
A high shell T_g and a low core T_g can be obtained increasing the concentration of hard monomers (such as styrene or MMA) in the shell and increasing the concentration of soft monomers (such as 2-EHA, EA or BA) in the core.

- Linear rheological measurements should then be used to have a first idea of adhesive performance. Concerning the absolute value of G', a sticky material is obtained only if the Dahlquist criterion is fulfilled and G' < 100 kPa. Higher values of G' lead to premature adhesive debonding due to a poor or incomplete contact during the bonding phase.
Then, one has to look at the ratio G''/G'^2. If $G''/G'^2 < 10^{-5}$ Pa^{-1}, crack propagation accompanied with a low adhesion energy is expected and this is either due to a too high elastic modulus or to a very low energy dissipation. It is important to optimize these coupled linear viscoelastic parameters before examining the large strain behavior.
For our acrylic systems, an increase in the dissipation can be obtained through the addition of CTA in the core, specifically in the core since the objective is to control adhesion and dissipation by the core. A concentration about equal to 0.1 wt% / total monomer seems to be an acceptable value which can be further optimized if necessary. However other synthesis or formulation strategies can be used for the same purpose with other families of PSA.

- The large strain behavior can then be refined and optimized for adhesion using tensile test results. If the material already behaves as a solid at high strain, the dry film is probably made of a connected network. An improvement of peel performance can be obtained by increasing dissipative properties of the core. This can be, for example, adjusted through the amount of CTA. The level of stress and shear performance can finally be refined with gel content of the shell, a higher cohesion is obtained with a higher gel content.
If the material tends to flow at high strain, an interfacial crosslinking between particles during the drying of the films proves to be a good way to increase cohesion without damaging peel performance. A crosslinking reaction between DAAM (in the polymer) and ADH groups can for example be activated. Further increase in the cohesion can be finally achieved by increasing the gel content or the T_g of the shell. These adjustments need to be made carefully in order to avoid any dramatic effect on the ability of the particles to coalesce during the drying of the film. In more general terms a synthesis strategy leading to a very dilute but percolating network of crosslinks will have little effect on the linear viscoelastic properties but ensure resistance to creep and adhesive debonding of the PSA. This strategy will now be investigated more systematically in the next chapter.

References

(1) Dahlquist, C. A. In *Treatise on Adhesion and Adhesives*; Patrick, R. L., Ed.; Dekker, 1969; pp 219-260.

(2) Creton, C.; Leibler, L. *Journal of Polymer Science Part B-Polymer Physics* **1996**, *34*, 545-554.

(3) Webber, R. E.; Shull, K. R.; Roos, A.; Creton, C. *Physical Review E* **2003**, *68*.

(4) Crosby, A. J.; Shull, K. R.; Lakrout, H.; Creton, C. *Journal of Applied Physics* **2000**, *88*, 2956-2966.

(5) Lakrout, H.; Creton, C.; Ahn, D. C.; Shull, K. R. *Macromolecules* **2001**, *34*, 7448-7458.

(6) Zosel, A. *Colloid and Polymer Science* **1985**, *263*, 541-553.

(7) Lindner, A.; Lestriez, B.; Mariot, S.; Creton, C.; Maevis, T.; Luhmann, B.; Brummer, R. *Journal of Adhesion* **2006**, *82*, 267-310.

(8) Creton, C.; Fabre, P. In *The mechanics of adhesion*; Dillard, D. A.; Pocius, A. V., Eds.; Elsevier: Amsterdam, 2002; Vol. 1, pp 535-576.

(9) Zosel, A. *Advances in Pressure Sensitive Adhesive Technology* **1992**, *1*, 92-127.

(10) Satas, D. *Handbook of Pressure Sensitive Adhesive Technology*; Van Nostrand Reinhold Book: New York, 1989.

(11) Jovanovic, R.; Dube, M. A. *Journal of Macromolecular Science-Polymer Reviews* **2004**, *C44*, 1-51.

(12) Dos Santos, F. D.; Leibler, L. *Journal of Polymer Science Part B-Polymer Physics* **2003**, *41*, 224-234.

(13) Aymonier, A.; Ledercq, D.; Tordjeman, P.; Papon, E.; Villenave, J. J. *Journal of Applied Polymer Science* **2003**, *89*, 2749-2756.

(14) Aymonier, A.; Papon, E.; Villenave, J. J.; Tordjeman, P.; Pirri, R.; Gerard, P. *Chemistry of Materials* **2001**, *13*, 2562-2566.

(15) Aymonier, A.; Papon, E.; Castelein, G.; Brogly, A.; Tordjeman, P. *Journal of Colloid and Interface Science* **2003**, *268*, 341-347.

(16) Saulnier, F.; Ondarcuhu, T.; Aradian, A.; Raphael, E. *Macromolecules* **2004**, *37*, 1067-1075.

(17) Shull, K. R.; Creton, C. *Journal of Polymer Science Part B-Polymer Physics* **2004**, *42*, 4023-4043.

(18) Creton, C.; Roos, A.; Chiche, A. In *Adhesion: Current Research and Applications*; Possart, W. G., Ed.; Wiley-VCH: Weinheim, 2005; pp 337-364.

(19) Good, R. J.; Gupta, R. K. *Journal of Adhesion* **1988**, *26*, 13-36.

(20) Verdier, C.; Piau, J. M. *Journal of Polymer Science Part B-Polymer Physics* **2003**, *41*, 3139-3149.

(21) Roos, A.; Creton, C. *Macromolecules* **2005**, *38*, 7807-7818.

(22) Brandrup, J.; Immergut, E., H.; A., G. E. *Polymer Handbook*, Fourth edition ed.; Wiley & Sons: New-York, 1999.

(23) Brandrup, J.; Immergut, E., H. *Polymer Handbook.*, Third edition ed.; Wiley: New York, 1989.

(24) Mallegol, J.; Dupont, O.; Keddie, J. L. *Langmuir* **2001**, *17*, 7022-7031.

(25) Lakrout, H.; Sergot, P.; Creton, C. *Journal of Adhesion* **1999**, *69*, 307-359.

(26) Carelli, C.; Deplace, F.; Boissonnet, L.; Creton, C. *Journal of Adhesion* **2007**, *83*, 491-505.

(27) Poivet, S.; Nallet, F.; Gay, C.; Teisseire, J.; Fabre, P. *European Physical Journal E* **2004**, *15*, 97-116.
(28) Tobing, S. D.; Klein, A. *Journal of Applied Polymer Science* **2001**, *79*, 2230-2244.
(29) Glassmaker, N. J.; Hui, C. Y.; Yamaguchi, T.; Creton, C. to be published.

5. Role of Particle Interfaces on the Large Strain Behavior

This chapter represents the bulk of this thesis.
The effect of the heterogeneous crosslinking on the adhesive and mechanical properties of soft latex films was investigated with a systematic strategy. We have taken advantage of the core-shell particle morphology to create a heterogeneous network structure without modifying the monomer composition. A more crosslinked shell is localized on the periphery of a softer and less crosslinked core. With such a structure it is possible to achieve a good balance between the adhesion and the cohesion of the material. The adhesion is controlled by the dissipative properties of the less crosslinked phase while the cohesion is controlled by the strength of the network in the shell.
In general, nonlinear properties play an important role during the debonding mechanism of soft and highly deformable adhesives. The present work focuses on the tuning of nonlinear elastic properties by varying the density and localization of the crosslinks.

5.1. Introduction

In order to be effective, a pressure sensitive adhesive (PSA) requires a balance of cohesive strength and dissipative properties. Cohesive strength is normally obtained with a careful control of the degree of crosslinking. However since the material needs to be highly deformable to dissipate energy, a lot of empirical know-how is necessary to obtain an optimal crosslink density and to take advantage of the ability of the polymer chains between crosslinks to dissipate energy and of the presence of crosslinks to restrict the flow of the adhesive.

A precise control of the crosslinking is particularly important in the case of PSA made from acrylate latexes. Indeed, many polymers synthesized by emulsion polymerization are naturally crosslinked inside each particle and some monomers, such as long side-chain acrylates, tend to crosslink, branch and form microgels during emulsion polymerization. This light crosslinking is beneficial to the properties since it is known that an acrylate copolymer which has no crosslinking or is crosslinked only by hydrogen bonds has insufficient cohesiveness and is practically useless as a PSA.

As discussed in chapter 1, PSA made from latexes are formed by the coalescence of individual particles into a film. In order to obtain a macroscopically strong film, the polymer chains must interdiffuse at the interfaces between the particles.

A widely used way of controlling crosslinking in waterborne polymers is to tune the gel content of each particle.[1] In such a case and for all other crosslinking methods occurring during the synthesis process, a homogeneous network is formed inside each particle and a well balance between adhesion and cohesion is nearly impossible to be reached. Indeed the required level of crosslinking to overcome the low shear holding of uncrosslinked polymers has in general a detrimental effect on linear viscoelastic properties of the dried film. The storage modulus G' of a homogeneously crosslinked polymer related the molecular weight of polymer chains between crosslinks is highly affected by a change of the crosslink density.[2,3]As a consequence, a significant decrease in linear dissipation occurring at the crack tip is observed. The importance of this dissipation in controlling adhesion has been discussed by Creton and Lakrout.[4] They showed that evolution of the shape of the cavities during tack experiment plays a crucial role and that the critical energy release rate $\mathcal{G}_c$ affects the vertical and horizontal growth rates of the cavities and the cavity shape changes from spherical to disc-like for lower values. Interfacial crack propagation and thus early debonding is favored when low amount of energy is dissipated within the vicinity of crack tip (Figure 5-1).

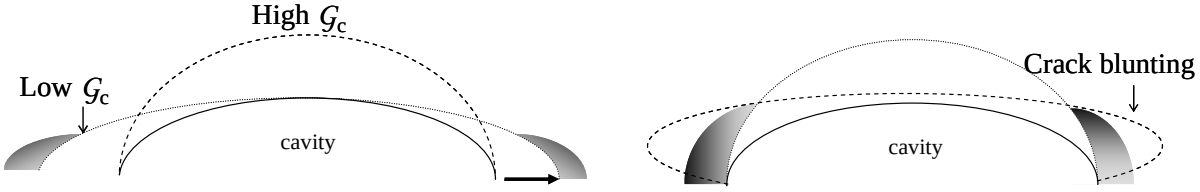

Figure 5-1. Vertical growth of the crack in the case of a dissipative material, horizontal propagation for a less dissipative one. Crack blunting which prevents stress concentration at the crack tip.

In this chapter, we focus on a specific strategy to overcome this limitation through a model system. The cohesion and shear resistance of acrylic emulsion PSA was found to be

significantly enhanced without much trade-off in their peel and tack, by activating a crosslinking reaction occurring at the drying stage, between latex particles as opposed to the crosslinking occurring during the synthesis stage inside each particle. Additionally it is possible to take advantage of the core-shell particle morphology to create a heterogeneously crosslinked structure. A more crosslinked shell is localized on the periphery of a soft less crosslinked core. With such a structure it is possible to achieve a different balance between the adhesion and the cohesion of the material than with a precrosslinked. The peel force is controlled by the dissipative properties of the soft less crosslinked phase while the cohesion, or resistance to creep, is controlled by the strength of the network in the shell. Moreover, the crosslinking reaction is activated through the evaporation during the drying of the film which has the great advantage to strengthen the interfaces of the particles and to make possible the creation of a percolating crosslinked network.

Materials studied are characterized by a low dynamic modulus (between 10 and 100 kPa) and their very viscoelastic behavior. They are highly deformable and the small strain and linear theories cannot be used as tools to describe their adhesive behaviors. Dissipation is not restricted to the area close to the crack tip. Instead a large amount of energy is dissipated within the bulk of the material.

In more microscopic terms, once a cavity nucleates at the interface between the adhesive and the substrate because of the applied tensile stress, its shape does not follow small strain theory but becomes more blunted as shown on Figure 5-1. This blunted crack, which has been studied by Hui and co-workers,[5] is the reason why if cracks can nucleate in soft adhesives they may never propagate to fail catastrophically. Multiple cavities can instead form a foam, which then extends in the tensile direction and forms what is often called a fibril structure. Crack blunting thus appears as a condition to reach high adhesive performance. Moreover, to avoid cohesive fracture of the fibrils leading to deposits on the substrate, the stretched walls between cavities have to strain harden at large strains.

Nonlinear properties have thus to be taken into account and this has led us to focus our work on the relationship between nonlinear deformation properties obtained from tensile experiments and adhesive behavior. We show more specifically how the intermediate strain softening and the ultimate strain hardening are really important in controlling adhesive behavior. We propose two different interpretations of the softening occurring at intermediate strains. From an elastic point of view, the softening should be reversible and could be due to the progressive alignment of entanglements in the direction of traction. This approach describes well the behavior of PSA made from block copolymers, which form a rather elastic entangled network. In our case however, the PSA that we have synthesized are much more viscoelastic and we have attempted to model their behavior using a more physically justified viscoelastic approach. For that, with some assumptions and simplifications, we have constructed a viscoelastic-hardening model based on a combination of the well-known Upper-Convected Maxwell model for the viscoelastic contribution and on the Gent model for the hardening.

We begin with the description of the materials and the crosslinking strategy used. Then, the effect of the activation of the crosslinking between particles is shown. In paragraph 5.3.2 is discussed the effect of the spatial distribution of crosslinks. For that, an adhesive made of homogeneously crosslinked particles is compared to two other PSA made of core-shell

particles where crosslinks are located in the shell only. We end by showing that an independent tuning of cohesion and adhesion is possible taking advantage of the core-shell morphology.

5.2. Experimental sections

5.2.1. Materials

5.2.1.1. Synthesis description

We performed our experiments focusing on a particular class of materials, model soft core-shell pressure-sensitive-adhesives synthesized using a two-stage monomer-starved semi-batch emulsion polymerization (all syntheses were carried out at the University of Manchester by Dr. M. Rabjohns and Dr. A. Foster under the supervision of Prof. P.A. Lovell). The Core and shell are formed directly in sequence using a single preparation. The core was submitted to a "cook-up" resulting in 96-97% conversion of the core monomers before starting polymerization of shell monomers. The blend of monomers used for the syntheses of both the core and the shell was designed to obtain soft acrylic copolymers. The latexes were made of random copolymers of 2-ethyl hexyl acrylate (2-EHA) (glass transition temperature of the homopolymer, T_g = -50°C[6]), butyl acrylate (BA) (T_g = -54°C[6]), ethyl acrylate (EA) (T_g = -24°C[6]), methacrylic acid (MAA) (T_g = 228°C[6]), acrylic acid (AA) (T_g = 106°C[6]) and styrene (S) (T_g = 100°C[6,7]) as the main monomers. The proportion of each monomer in the core and the shell is shown on Table 5-1.

Shells contain some reactive diacetone acrylamide (DAAM) groups as a comonomer. The DAAM containing particles are then able to crosslink and form a network by the reaction of the ketone carboxyl with a water soluble hydrazide during film formation and evaporation at room temperature as shown in Figure 5-2. The density of crosslinking points depends on the concentration of DAAM groups in the shell and also on the amount of adipic acid dihydrazide (ADH) post-added to the latex. The distribution and localization (thickness of the shell) of the crosslinking points are controlled during the synthesis.

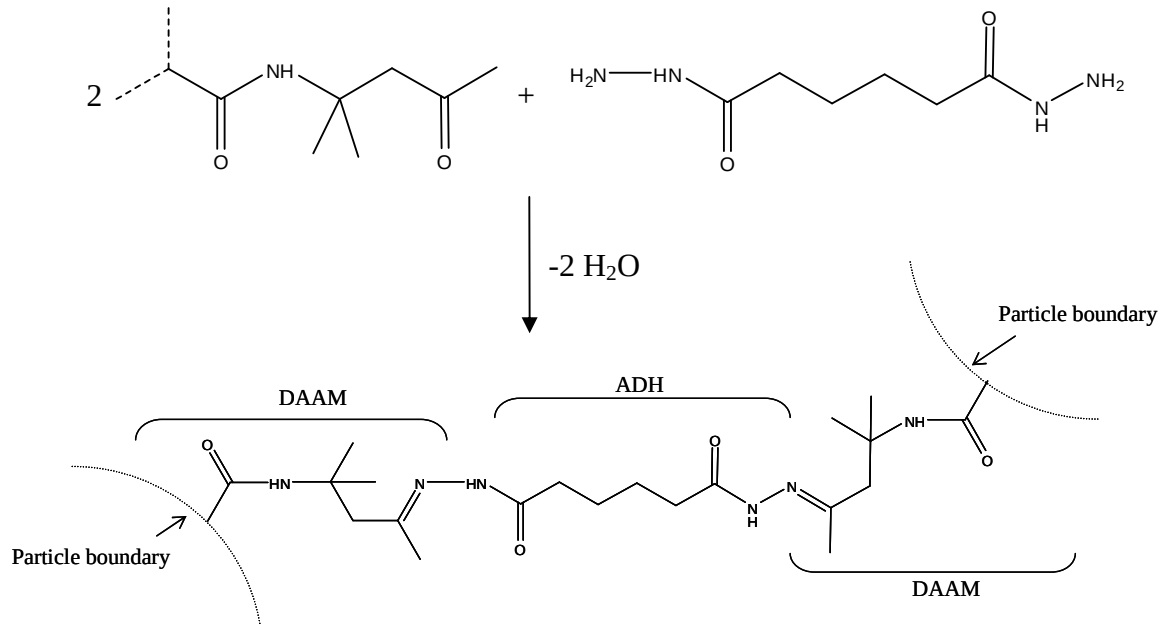

Figure 5-2. Crosslink formation from reaction between DAAM (located in the shell of the particle) and ADH.

5.2.1.2. System for the study of the effect of the crosslinks distribution

The effect of the distribution of DAAM groups on the efficiency of the DAAM-ADH crosslinking reaction and on the final adhesive and deformation properties has been studied on a model system. There are no differences between the core and the shell in terms of composition and the distribution of DAAM is the only variable. This system was specifically designed, to keep a constant total amount of DAAM but to distribute it in shells of different thicknesses. Compositions are summarized in Table 5-1. C0S100 where DAAM groups were distributed homogeneously in the particle was synthesized in only one step. The stoichiometric amount of ADH for a complete reaction was calculated to give 1:2 mole ratio of ADH:DAAM. In these calculations, it was assumed that all DAAM in the outer shell layer was available for reaction with ADH. For this study, the stoichiometric amount of ADH was added in the water phase.

	Model System (wt%)				
Sample name	**C0S100[b]**	**C45S55**		**C80S20**	
Monomer	**Average[c]**	**Core (C45S55)**	**Shell (C45S55)**	**Core (C80S20)**	**Shell (C80S20)**
2-Ethylhexyl Acrylate (2EHA)	66	66.265	65.783	66.265	64.939
Ethyl Acrylate (EA)	15	15.060	14.951	15.060	14.759
Butyl Acrylate (BA)	10	10.040	9.967	10.040	9.839
Styrene (S)	5	5.020	4.984	5.020	4.920
Acrylic Acid (AA)	2	2.008	1.993	2.008	1.967
Sipomer β-CEA	1.2	1.205	1.196	1.205	1.180
Methacrylic Acid (MAA)	0.4	0.402	0.399	0.402	0.394
Diacetone Acrylamide (DAAM)	0.4	-	0.727	-	2
n-Dodecyl Mercaptan (DDM)[a]	0.1	0.1	0.1	0.1	0.1

a - Chain transfer agent, % relative to total monomer in each phase.
b - CxSy: for wt% core = x, wt% shell = y.
c - Shell composition of C0S100.

Table 5-1. Core and shell latex monomer compositions of model system particles.

Figure 5-3 shows schematic representations of the particles. DAAM groups are homogeneously distributed in C0S100 particle (d_z ~ 240 nm) while they are located only in the shells of the two other core-shell particles. From calculations using the core/shell weight ratio, shell thicknesses equal to 28 nm and 9 nm were calculated in C45S55 and C80S20 respectively. In these calculations the seed from which all the polymerizations were started is also taken into account. The seed is a styrene/acrylate copolymer with a slightly different composition than that of the core and with a diameter of 46 nm. This seed is however voluntary not represented on Figure 5-3 for a sake of clarity.

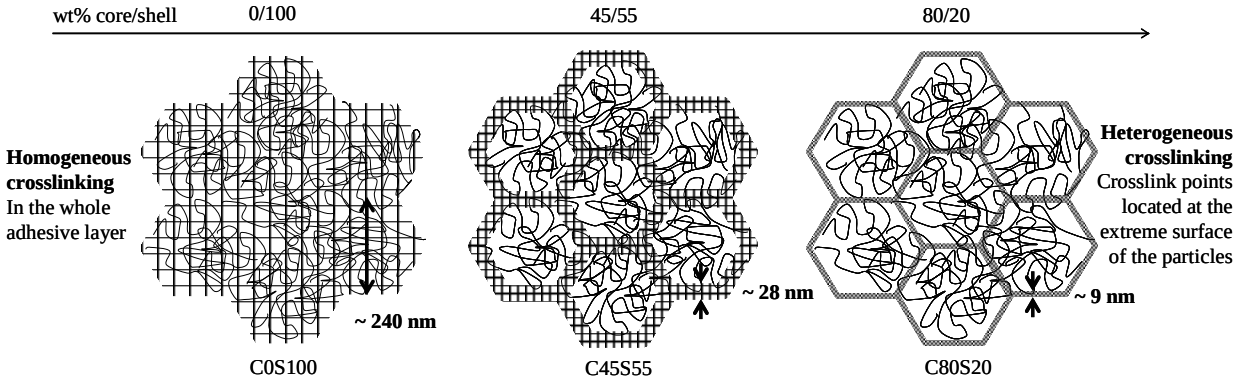

Figure 5-3. Schematics of crosslink distribution of C0S100, C45S55 and C80S20.

The core polymer structure may mainly contain entanglements and branches, some crosslinking is unavoidably created during the synthesis but for these compositions, the gel content stays extremely low. The polymer chains of the shells are basically the same as the core but contain some DAAM groups in their backbone. This enables the formation of non-permanent crosslinks such as hydrogen-bonding and permanent crosslinks when DAAM has reacted with an ADH molecule.

5.2.1.3. System for the study of the effect of an increase in crosslinking density

A second series of latexes designed to vary the initial molecular weight distribution and gel content of the core and shell has been investigated as well. The main monomer composition was the same in the core and in the shell, but the amount of chain transfer agent (CTA) in the shell was lower than in the core. In the series C80dxS20D0.4[(1)], the acidic monomers of the core (acrylic acid AA and Sipomer β-CEA, total 4 wt%) were replaced by 2 wt% of DAAM and 2 wt% of methacrylic acid (MAA). In the series C80d0.1S20D1.1, the amount of DAAM groups was higher and equal to 5.5 wt% of monomers of the shell (1.1 wt% total monomers) (Table 5-2).

(1) "d" has been chosen as an initial letter of DDM while "D" has been chosen as an initial letter of DAAM.

	More Complex System (core/shell = 80/20) (wt%)					
Sample name	**C80dx[a]S20D0.4**			**C80d0.1S20D1.1**		
Monomer	**Average (0.4% DAAM)**	**Core (0.4% DAAM)**	**Shell (0.4% DAAM)**	**Average (1.1% DAAM)**	**Core (1.1% DAAM)**	**Shell (1.1% DAAM)**
2EHA	66	66	66	65.519	66	63.59
EA	15	15	15	14.891	15	14.45
BA	10	10	10	9.927	10	9.64
S	5	5	5	4.963	5	4.82
AA	2	2.5	-	2	2.5	-
Sipomer β-CEA	1.2	1.5	-	1.2	1.5	-
MAA	0.4	-	2	0.4	-	2
DAAM	0.4	-	2	1.1	-	5.5
DDM	0.167-0.087	0.2-0.1	0.037	0.037	0.1	0.037

a -"x" has to be replaced by the amount of chain transfer agent in the core.

Table 5-2. Core and shell latex monomer compositions of the more complex latexes.

Two of these latexes (C80d0.1S20D0.4 and C80d0.15S20D0.4) with a core/shell weight ratio equal to 80/20 and containing 0.4 wt% of DAAM have been used for the evaluation of the effect of the interfacial crosslinking activation on adhesive and linear and nonlinear rheological properties. The crosslinking density in this study was only controlled by the amount of ADH added (various amounts below the stoichiometric one).

5.2.1.4. Additional remarks

For the synthesis of the model system latexes, the reaction temperature was kept fixed at 70°C before the redox stage at 60°C, while it was kept fixed at 80°C for the synthesis of all the other particles. All latexes were treated with NH_4OH (25 wt%) solution to reach pH = 7.0. Servoxyl VLA 2170 surfactant (0.75 g / 100 g latex) was also added to aid coating on to the siliconized release paper during the sample preparation for peel and shear tests. As prepared and formulated latexes were characterized. Particle diameter (measured by light scattering) was typically equal to 240-250 nm, solid content was 54% except for latexes of the model system where the solid content was more around 51%. All glass transition temperatures of the shells calculated using Fox equation were equal to -38°C. T_gs of the latexes of the model system have been measured by DSC. Results are: T_g(C80S20) = -44.8°C, T_g(C45S55) = -41.9°C and T_g(C0S100) = -43.1°C (results at 10K/min).

A molecular weight polydispersity index between 3 and 4 has been found for the soluble fraction (after extraction from the gel fraction) of the selected latex polymers.

The blends of solution of ADH (2wt% in deionized water) with the different latexes were always prepared one day before the sample preparation.

5.2.2. Structure of the films

From AFM images, it is clear that the structure of the adhesive layers after the drying step keeps the memory of the shape of the native particles. Comparing images of C80S20 (core-shell particle) and C0S100 (homogeneous particle) shown in Figure 5-4, the structure seen in the tapping mode AFM image may not be the result of the core-shell particle morphology but rather of the presence of a slightly different (surfactant rich ?[8,9]) composition of the surface layer. It is important to note that, while the existence of a particle structure is clear, the activation of the crosslinking cannot be detected a priori from AFM images of this type. This result was consistently obtained with all latexes.

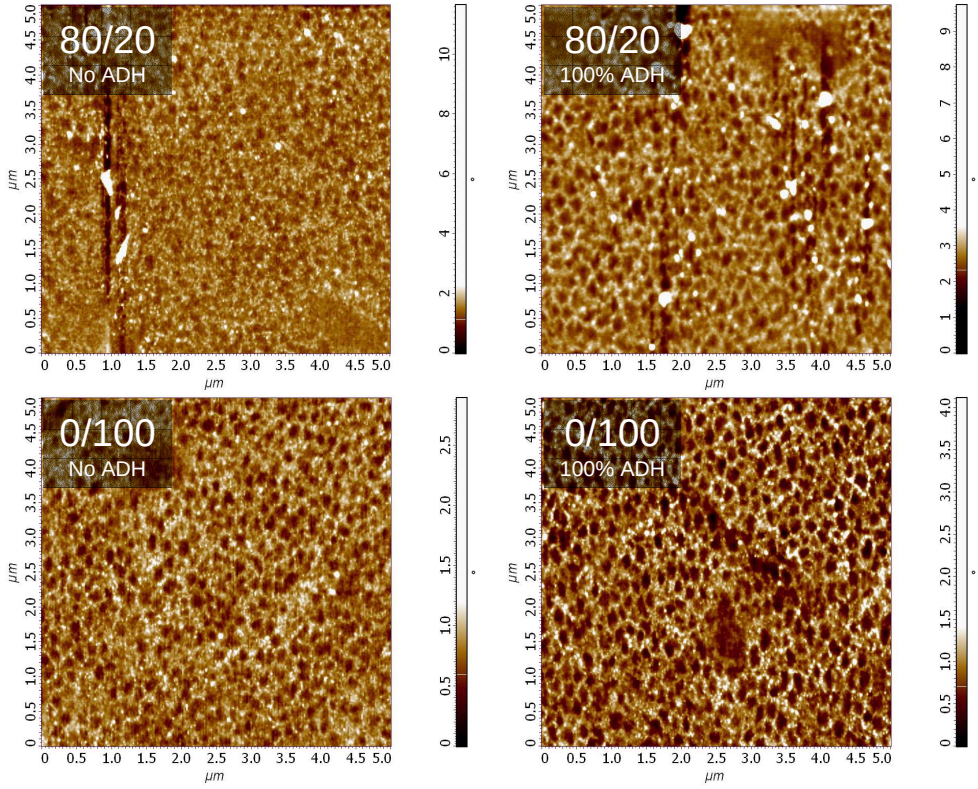

Figure 5-4. Phase contrast AFM images of film cross sections made of C80S20 and C0S100, pristine particles without ADH (left) and interfacially crosslinked particles (right). (AFM images were obtained in the University of Manchester by C. Lei and J.L. Keddie).

5.2.3. Analysis of large strain behavior

There are two possible molecular origins for the softening process occurring at intermediate strains: Within the framework of nonlinear elasticity, the presence of a much higher density of entanglements relative to permanent crosslinks leads to a softening due to the progressive alignment of the entanglements in the tensile direction.[10] Within the framework of viscoelasticity the softening can be due to the relaxation of topological constraints within a time frame commensurable with the inverse of the strain rate.[11] Both approaches have been considered. The methodology used and the definition of relevant parameters within this work are given below.

5.2.3.1. Elastic modeling

As already discussed in chapter 4, one way to explain the softening behavior of PSA is to use the Mooney stress σ_R defined as:

$$\sigma_R = \frac{\sigma_N}{\lambda - 1/\lambda^2} \qquad \textbf{Eq. 5-1}$$

If experimental data is fitted using the empirical Mooney-Rivlin model, the two material's parameters C_1 and C_2 can be approximately interpreted as the contribution due to permanent and temporary crosslinks to the modulus respectively. This molecular interpretation is of course approximate and more detailed molecular elastic models have been developed in particular by Rubinstein and Panyukov for rubber networks. They use a combination of the tube model of Doi and Edwards and of the phantom network model for rubbers.

As already explained in chapter 4, our experimental reduced stress vs. $1/\lambda$ curves cannot be easily fitted using the Mooney-Rivlin elastic model. Thus, in this chapter again C_{hard} and C_{soft} are used as alternatives of C_1 and C_2 respectively.

Using the Mooney representation is equivalent to approximate the softening as an elastic process. Although incorrect, this elastic point of view can then be used even in the case of a viscoelastic PSA to give at a glance a good idea of the degree of softening and hardening of the PSA from tensile results carried out at a given strain rate. It has however the significant disadvantage of neglecting the stress relaxation processes, which must occur in these highly viscoelastic materials.

5.2.3.2. Viscoelastic / Hardening parallel model

Model description

A more accurate viscoelastic description of the behavior of the PSA can also be considered for the description of the relaxation at intermediate strains and of the large strain hardening. In collaboration with Dr. Tetsuo Yamaguchi, post-doc in our laboratory, we have

explored the possibilities of a viscoelastic / hardening parallel model (Figure 5-5) to capture both the viscoelastic relaxation at intermediate strains and the ultimate strain behavior corresponding to the hardening. This model basically consists of a parallel association of a Maxwell branch with a spring in series with a dashpot for the softening description and a nonlinear spring with a finite extensibility to capture the necessary strain hardening at large strains (Figure 5-5). In this study, we have targeted heterogeneous latex based soft adhesives but the methodology used can be generalized to all viscoelastic crosslinked materials.

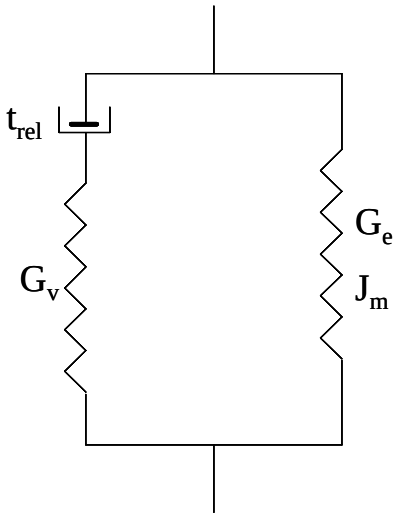

Figure 5-5. Viscoelastic model for the modeling of mechanical properties of viscoelastic and slightly crosslinked materials.

Modeling of the viscoelastic part

The viscoelastic arm is characterized by a neo Hookean spring in series with a dashpot, with a relaxation time t_{rel} and a shear modulus G_v, the hardening arm is a nonlinear neo-Hookean spring with a finite extensibility described by J_m and a shear modulus G_e.
The viscoelastic part of the model is an Upper-Convected Maxwell (UCM) model which is a generalization of the Maxwell model for the case of large deformations of polymers (see chapter 1). The related constitutive equation can be written as:

$$t_{rel}\frac{\delta\underline{\tau}}{\delta t}+\underline{\tau}=2G_v t_{rel}\underline{D} \qquad \textbf{Eq. 5-2}$$

where $\underline{\tau}$ is the stress tensor, t_{rel} the relaxation time, $\frac{\delta\underline{\tau}}{\delta t}$ the upper convected time derivative of $\underline{\tau}$, G_v the shear modulus of the viscoelastic part and $\underline{D}$ the strain rate tensor: $\underline{D}=\frac{1}{2}(\underline{L}+\underline{L}^T)$ where $\underline{L}=\frac{\partial v_j}{\partial x_i}$ is the tensor of velocity derivatives for the fluid.

The upper convected time derivative, also called Oldroyd derivative, is the rate of change of some tensor property of a small element of material written in the Eulerian coordinate system rotating and stretching within the sample. The operator is specified by the following formula:

$$\frac{\delta \underline{A}}{\delta t} = \dot{\underline{A}} - \underline{L}A - A\underline{L}^{T} \qquad \textbf{Eq. 5-3}$$

where $\underline{A}$ is a tensor field, $\dot{\underline{A}}$ the substantive derivative of $\underline{A}$. This upper convected derivative is widely use in polymer rheology for the description of the behavior of a viscoelastic fluid under large deformations.

In the case of a uniaxial elongation and using the coordinate system shown on Figure 5-6, the UCM can be written as the following equation system:

$$\begin{cases} t_{rel}\dot{\tau}_{zz} + (1 - 2t_{rel}\dot{\varepsilon})\tau_{zz} = 2t_{rel}G_v\dot{\varepsilon} \\ t_{rel}\dot{\tau}_{xx} + (1 + t_{rel}\dot{\varepsilon})\tau_{xx} = -t_{rel}G_v\dot{\varepsilon} \\ t_{rel}\dot{\tau}_{yy} + (1 + t_{rel}\dot{\varepsilon})\tau_{yy} = -t_{rel}G_v\dot{\varepsilon} \end{cases} \qquad \textbf{Eq. 5-4}$$

with $\dot{\varepsilon}$ the Hencky's strain rate.

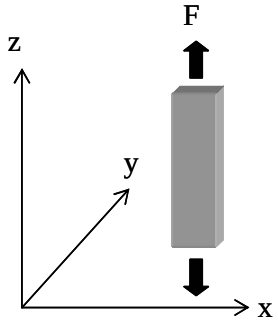

Figure 5-6. Definition of coordinate system used in the case of a uniaxial elongational stretching.

Our tensile experiments are performed at constant crosshead velocity that means at constant nominal strain rate but decreasing Hencky's strain rate. But, to get an analytical solution and to avoid the numerical solving of the differential equations we decided to assume constant the Hencky's strain rate involved in differential equations. At first sight, this has been supported by the fact that the viscoelastic contribution is most important at low strains where the constant Hencky's strain rate approximation should not be bad (an estimation of errors as a consequence of this approximation is discussed in appendix I). Analytical solutions for the stress can thus be written as:

$$\begin{cases} \tau_{zz}(t) = \dfrac{2t_{rel}G_v\dot{\varepsilon}}{1-2t_{rel}\dot{\varepsilon}}\left(1-\exp\left(-(1-2t_{rel}\dot{\varepsilon})\dfrac{t}{t_{rel}}\right)\right) \\ \tau_{xx}(t) = \tau_{yy}(t) = -\dfrac{t_{rel}G_v\dot{\varepsilon}}{1+t_{rel}\dot{\varepsilon}}\left(1-\exp\left(-(1+t_{rel}\dot{\varepsilon})\dfrac{t}{t_{rel}}\right)\right) \end{cases} \qquad \textbf{Eq. 5-5}$$

For $\dot{\varepsilon}$ to be constant, the deformation λ is defined as:

$$\lambda(t) = \exp(\dot{\varepsilon}t) \text{ thus, } t = \frac{\ln\lambda}{\dot{\varepsilon}} \qquad \textbf{Eq. 5-6}$$

The true stress contribution of the viscoelastic part is:

$\sigma_{T,v} = \tau_{zz} - \tau_{xx}$ **Eq. 5-7**

Therefore, the nominal stress evolution as a function of λ can finally be written as:

$$\sigma_{N,v}(\lambda) = \left(\frac{2G_v t_{rel}\dot{\varepsilon}}{1-2t_{rel}\dot{\varepsilon}} \left(1 - \exp\left(-\frac{1-2t_{rel}\dot{\varepsilon}}{\dot{\varepsilon}t_{rel}} \ln\lambda \right) \right) + \frac{G_v t_{rel}\dot{\varepsilon}}{1+t_{rel}\dot{\varepsilon}} \left(1 - \exp\left(-\frac{1+t_{rel}\dot{\varepsilon}}{\dot{\varepsilon}t_{rel}} \ln\lambda \right) \right) \right) .\lambda^{-1}$$

Eq. 5-8

Eq. 5-8 points out the important role played by the $t_{rel}\dot{\varepsilon}$ product. This quantity represents the product of the strain rate and the relevant relaxation time for flow of the polymer and can be viewed as en effective Deborah number called *De*.

$$\sigma_{N,v}(\lambda) = \left(\frac{2G_v D_e}{1-2D_e} \left(1 - \exp\left(-\frac{1-2D_e}{D_e} \ln\lambda \right) \right) + \frac{G_v D_e}{1+D_e} \left(1 - \exp\left(-\frac{1+D_e}{D_e} \ln\lambda \right) \right) \right) .\lambda^{-1}$$

Eq. 5-9

Modeling of the strain hardening part

Let us continue with the strain hardening modeling. It is captured by a nonlinear spring with a finite extensibility added in parallel to the viscoelastic Maxwell model (Figure 5-5). Some limiting chain extensibility constitutive models have been developed on using phenomenological continuum mechanics approaches. One such model, the Gent model for incompressible hyperelastic materials, is particularly simple and has been chosen within the present work. In this model, the strain energy density depends only on the first strain invariant I_1 of the Cauchy-Green strain tensor, is a simple logarithmic function of I_1 and involves just two material parameters, the shear modulus G_e and a parameter J_m which measures a limiting value for $I_1-3 = J_1$ reflecting limiting chain extensibility.[12]

The strain energy density has been proposed to be as:

$$W = \frac{-G_e}{2} J_m \ln\left(1 - \frac{J_1}{J_m} \right)$$

Eq. 5-10

In the case of a uniaxial elongation, $J_1 = \lambda^2 + 2/\lambda - 3$. Thus the nominal stress contribution from the elastic part can be written as:

$$\sigma_{N,e}(\lambda) = \left(\frac{G_e}{1 - \frac{\lambda^2 + 2/\lambda - 3}{J_m}} (\lambda^2 - 1/\lambda) \right) .\lambda^{-1}$$

Eq. 5-11

Finally, the overall nominal stress of the system can be written as:

$$\sigma_N(\lambda) = \sigma_{N,v}(\lambda) + \sigma_{N,e}(\lambda)$$

Eq. 5-12

Some mechanical meanings of the fitting parameters

The decomposition of nominal stress vs. lambda tensile curves into its viscoelastic and hardening parts as shown on Figure 5-7 will be used as a help to well understand the meaning of each adjustable parameter involved in the fitting equation. Obviously, behavior at small and intermediate strains is mainly governed by viscoelastic properties while at larger strains the elastic contribution dominates. With such a representation a rapid estimation of the balance between viscoelasticity and elasticity (or hardening) is possible.

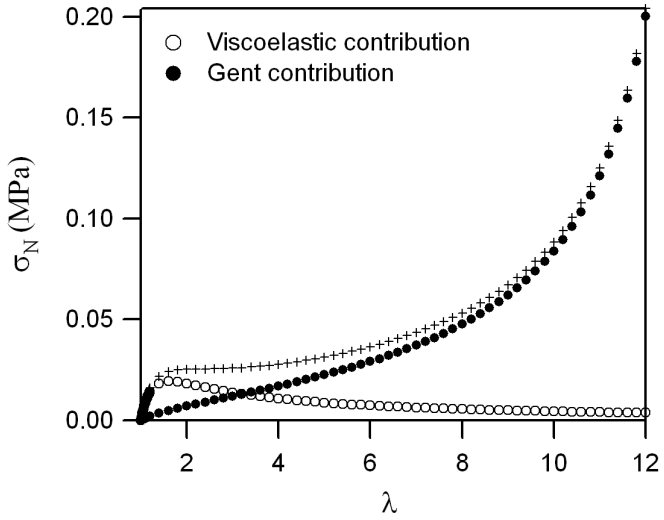

Figure 5-7. Example of the decomposition of a nominal stress vs. lambda tensile curve into its viscoelastic and hardening contributions.

As shown on Figure 5-8, deformation at which the softening starts depends on *De*. Concerning J_m, main effect is observed at high strains where the viscoelastic contribution is no more very important. J_m evolves mainly as the deformability of the material.

The construction of the viscoelastic / hardening model has been induced for a part in the objective to make possible a quantification of the softening occurring at intermediate strains. This will be possible through an estimation of the viscoelastic contribution to the elastic one. So, another important parameter to look at is the ratio G_v/G_e. Higher is G_v/G_e, more pronounced is the softening (Figure 5-8).

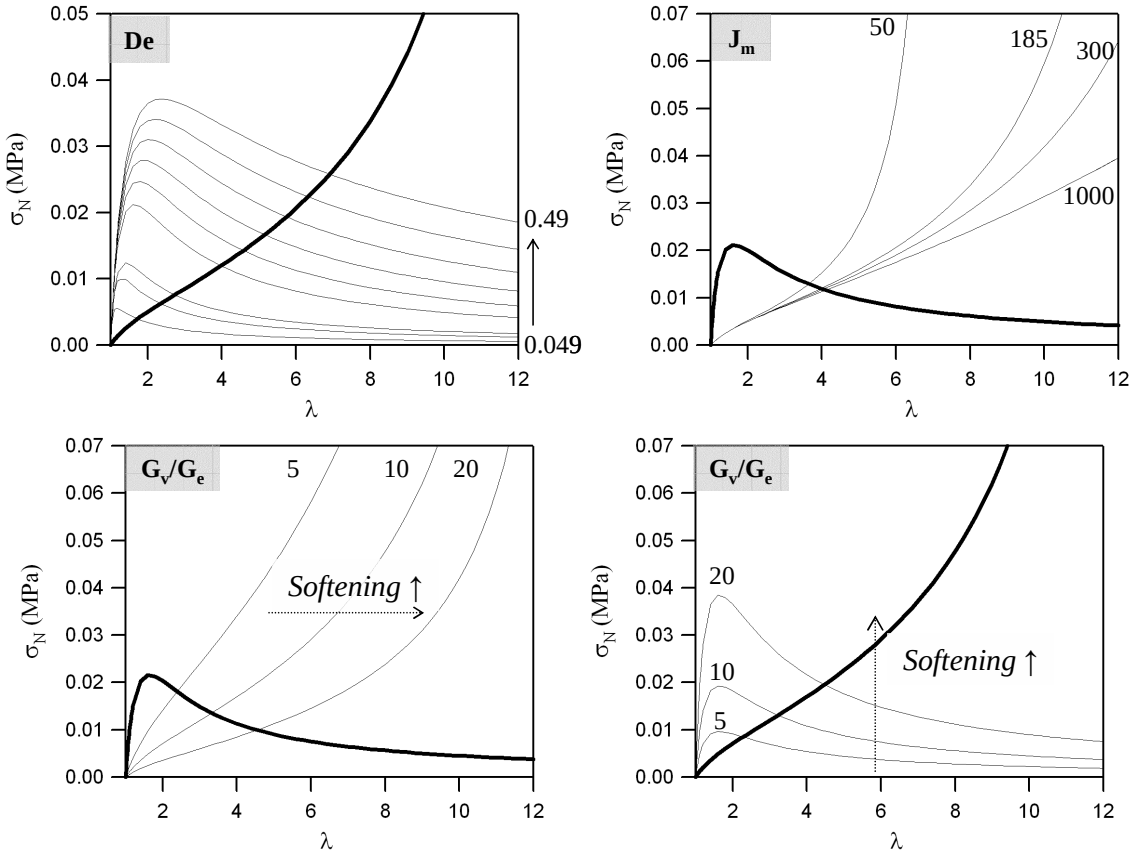

Figure 5-8. Visual estimation of the weight of each contribution, viscoelastic and hardening as fitting parameters vary. And qualitative prediction of the importance of the softening.

Predictions of the model for extreme values of G_v/G_e , λ and *De*.

- When G_v/G_e tends to infinity, the model predicts a viscoelastic liquid behavior while when it tends to zero, it predicts an elastic behavior (no dissipation) ending up by a hardening.

- The model predicts that $\sigma(\lambda) \sim 3(G_v+G_e)(\lambda-1)$ when λ tends to be equal to one. This means that $3(G_v+G_e)$ would represent the linear Young's modulus of the material. In the opposite case, when λ tends to its maximal value λ_m, an infinite increase in the Gent stress is expected while the contribution of the viscoelastic part completely vanishes.

- When *De* is very low, the viscoelastic stress tends rapidly to zero. The viscoelastic part acts mainly as a liquid with a very low viscosity. Main contribution of the overall stress comes from the hardening part which is not affected by *De*.
  In the opposite case, when *De* tends to infinity, a neo-hookean behavior is retrieved and the viscoelastic nominal stress evolves as the following:

  $$\sigma_{N,v} \approx G_v(\lambda - 1/\lambda^2) \text{ when } De \to \infty. \qquad \textbf{Eq. 5-13}$$

  Figure 5-9 shows some theoretical curves obtained using Eq. 5-9 for different values of *De*. The curve corresponding to *De* = 100 is nearly superimposed to the neo-hookean curve.

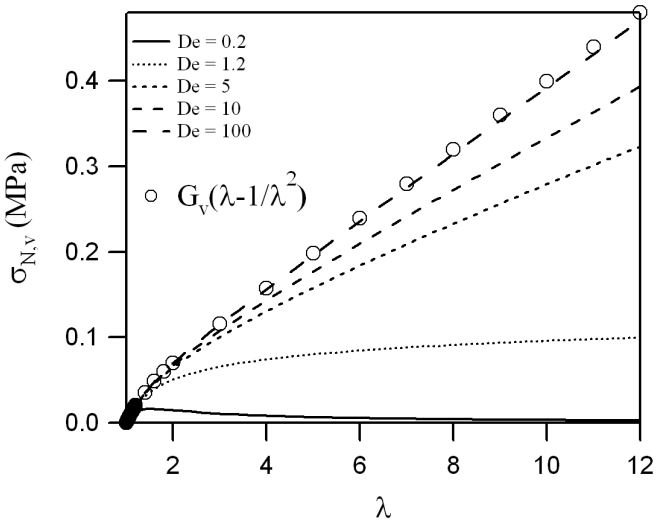

Figure 5-9. Theoretical viscoelastic nominal stress as a function of strain curves obtained with various values of *De*.

Summary of mechanical and molecular interpretation of fitting parameters

To each fitting parameter, one can attribute a meaning in the sense of continuum mechanics. For some, it is also possible to suggest a molecular interpretation.

- G_v, represents the unrelaxed shear modulus of the viscoelastic part. Because this shear modulus relaxes to zero at long times, it is logical to attribute them to the volume density of entanglements.

- G_e, is the small strain modulus of the elastic component. For a homogenously crosslinked network it should not be independent from J_m the strain hardening parameter. However here it can be seen as the volume density of crosslink points that will not relax at long times probably due to the presence of chemical permanent crosslinks ($G_e \propto M_c$).

- $3(G_v+G_e)$ represents the Young's modulus and the cohesion of the material at small strains.

- G_v/G_e gives an indication of how viscoelastic is the material and can quantify the softening observed at intermediate strains.

- For a given strain rate, *De* i.e. the product of strain rate and main relaxation time, indicates how fast the relaxation occurs in the sample. In the case of a polymer with a unique relaxation time it would have been possible to relate it to a molecular characteristic of the polymer such as molecular weight. Materials studied in the present work are PSA characterized by a broad distribution of relaxation times. In such a case, it appears non realistic to attribute a molecular significance to *De*.

- J_m is related to the finite extensibility of polymer chains between crosslinks. In uniaxial extension, $J_m \propto \lambda_m^2$, with λ_m the maximal deformation. If the network were homogeneous, J_m should be nearly proportional to M_c, the average molecular weight between crosslinks.

In the case of a perfectly homogeneous and connected network without defects, both G_e and J_m would predict the same value for M_c. But real networks are not homogeneous and the construction of the Gent model itself is based on the fact that is not the case for the majority of the polymers.

5.2.3.3. Intermediate strain energy dissipation

During uniaxial stretching, part of the energy supplied by the operator is instantaneously dissipated and part is stored. The more energy is dissipated the more pronounced is the softening. A simple estimate of the energy dissipated at intermediate strains can thus be used as another characterization of the softening. Dissipation is due to stress relaxation and a general expression of the relaxation modulus $G(\lambda)$ can be written as:

$$G(\lambda) = G.\Phi(\lambda) \qquad \textbf{Eq. 5-14}$$

where $\Phi(\lambda)$ represents the non relaxed global fraction of the polymer at a given deformation λ. It evolves from 1 to 0.

A very rough estimate of the dissipated energy W_{diss} when the sample is deformed from $\lambda = 1$ to $\lambda = 3$ can be given by the difference between the work performed to deform the material and the energy to deform an elastic material from $\lambda = 1$ to $\lambda = 3$. This is represented by the dotted area of Figure 5-10. The limit of $\lambda = 3$ has been chosen in part arbitrarily but it lies probably in the range of deformations sustained by a crack during tack experiments.

$$W_{diss} = \int_1^3 \sigma(\lambda)d\lambda - \sigma(3) \qquad \textbf{Eq. 5-15}$$

An extension of the dissipation as defined in the linear regime by $\tan(\delta) = G''/G'$ to the nonlinear intermediate strain regime can be obtained normalizing this dissipated energy by the stored elastic one W_e: $\Delta W = W_{diss}/W_e$.

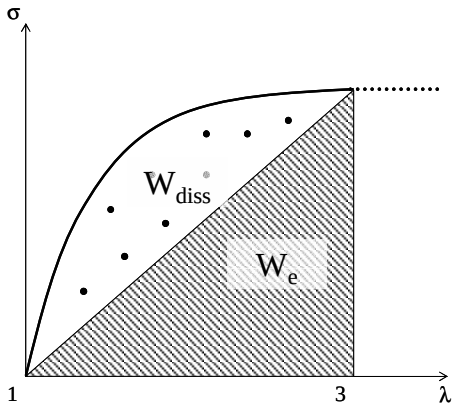

Figure 5-10. Definition of dissipated and elastic energies at intermediate strains during a tensile experiment.

5.3. Results and discussion

5.3.1. Activation of the crosslinking reaction

The key process developed in our study is the interparticle crosslinking and it is logical to start our result section with the effect of the activation of the interfacial crosslinking. Adhesive and linear rheological properties have been studied on C80d0.15S20D0.4 while adhesive properties and nonlinear elongational properties have been studied on a slightly different material, i.e. C80d0.1S20D0.4. In each case, increasing amounts of ADH were added to the latexes. The comparison between these two materials, which differ by their amount of CTA in the core, is outside the scope of this section and is the subject of the part 5.3.3.2 focusing on the effect of an increase in the gel content of the core. For both these materials, the shells of the particles are very thin (typically 9 nm compared to the whole diameter of the particle of about 250 nm), thus it is reasonable to assume that the crosslinking reaction occurs at or near the interface between particles and creates some chemical connections between two neighboring particles.

5.3.1.1. Adhesive performance

Tack results

Tack experiments have been performed on C80d0.1S20D0.4 and C80d0.15S20D0.4 latexes to which various ADH amounts were post-added. Probe tests were carried out on stainless steel probes and on PE coated probes at debonding velocities of 10, 100 and 1000 $\mu m.s^{-1}$. Only results on C80d0.1S20D0.4 at 100 $\mu m.s^{-1}$ are shown on Figure 5-11 since the overall shape of the curves was the same for C80d0.15S20D0.4 and at the other two speeds. Regardless of the crosslinking density a well defined stress plateau is observed at intermediate strains and this is the signature of the fibrillating structure created from the elongation of the microfoam. The peak stress is unchanged with the increasing crosslinking density. Evolution of the adhesive energies as a function of the crosslinking density (Figure 5-11-b) (adhesive energies have been calculated only in cases where an adhesive debonding occurred) show that there is probably an optimum in the amount of ADH added to reach best adhesive performance. In the present case, it seems to correspond to 50% of ADH.

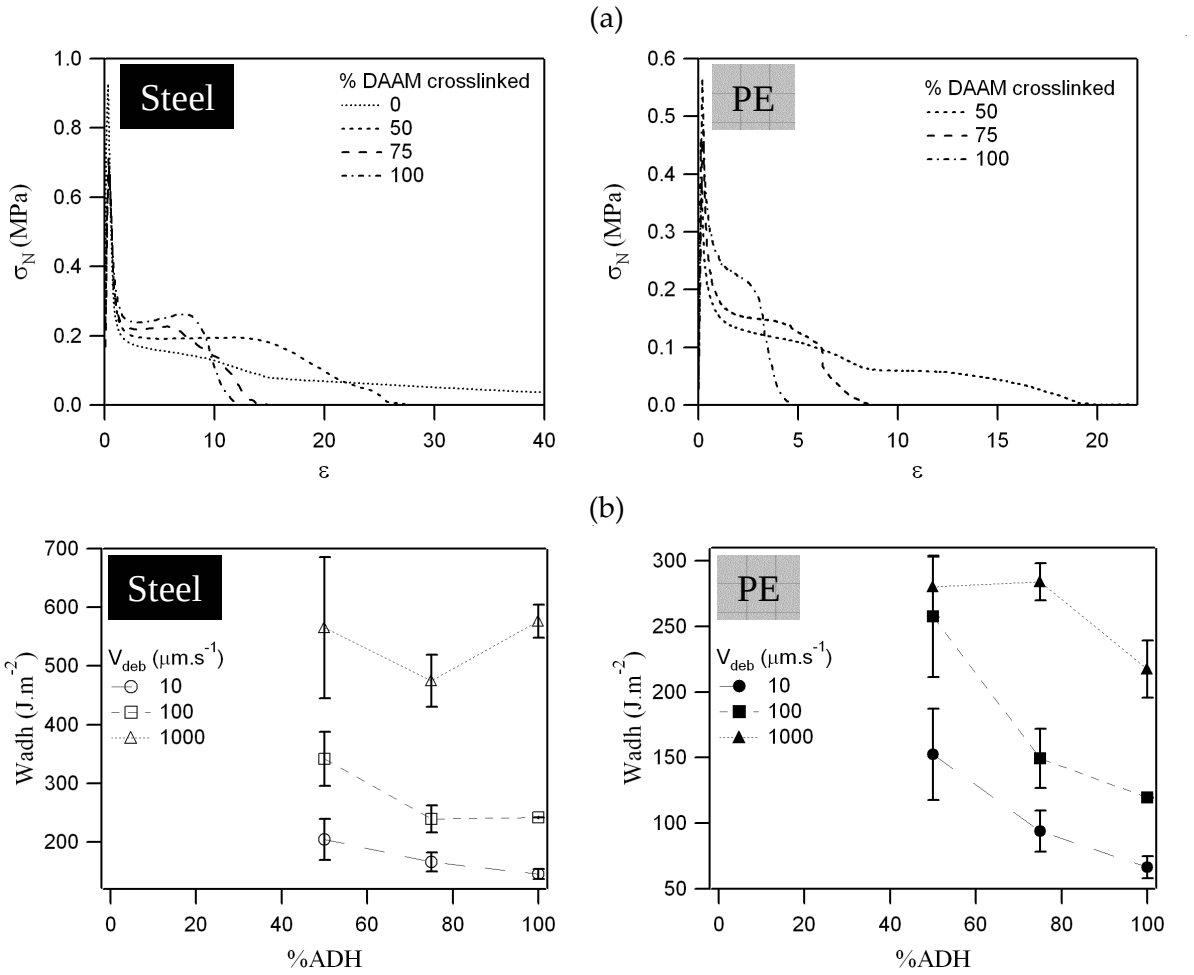

Figure 5-11. (a) Stress vs. strain tack curves of C80d0.1S20D0.4 where 0%, 50%, 75% and 100% of ADH is added compared to the stoichiometric amount. Tests were performed on stainless steel at 100 µm.s^{-1} (figure on the left) and on PE at 10 µm.s^{-1} (figure on the right). (b) Adhesive energies obtained at 10, 100 and 1000 µm.s^{-1} on stainless steel (figure on the left) and on PE (figure on the right). (Tack experiments on C80d0.1S20D0.4 have been performed by Clara Carelli and Aude Langenfeld).

The debonding mechanism is also considerably influenced by the activation of the interparticle crosslinking. An adhesive made of uncrosslinked particles is characterized by a double fibrillation plateau at intermediate strains (Figure 5-12). The decrease in the stress of about 0.1 MPa at a strain of 6 is due to the air penetration in the middle of the adhesive layer.[13] The force then plateaus at a non zero and constant value until the end of the test. This is a typical "liquid-like" debonding also called "cohesive" debonding where some residues of adhesive are left on the probe at the end of the test (Figure 5-13). A systematic observation of the videos recorded during debonding shows growth of fingers from the outside.

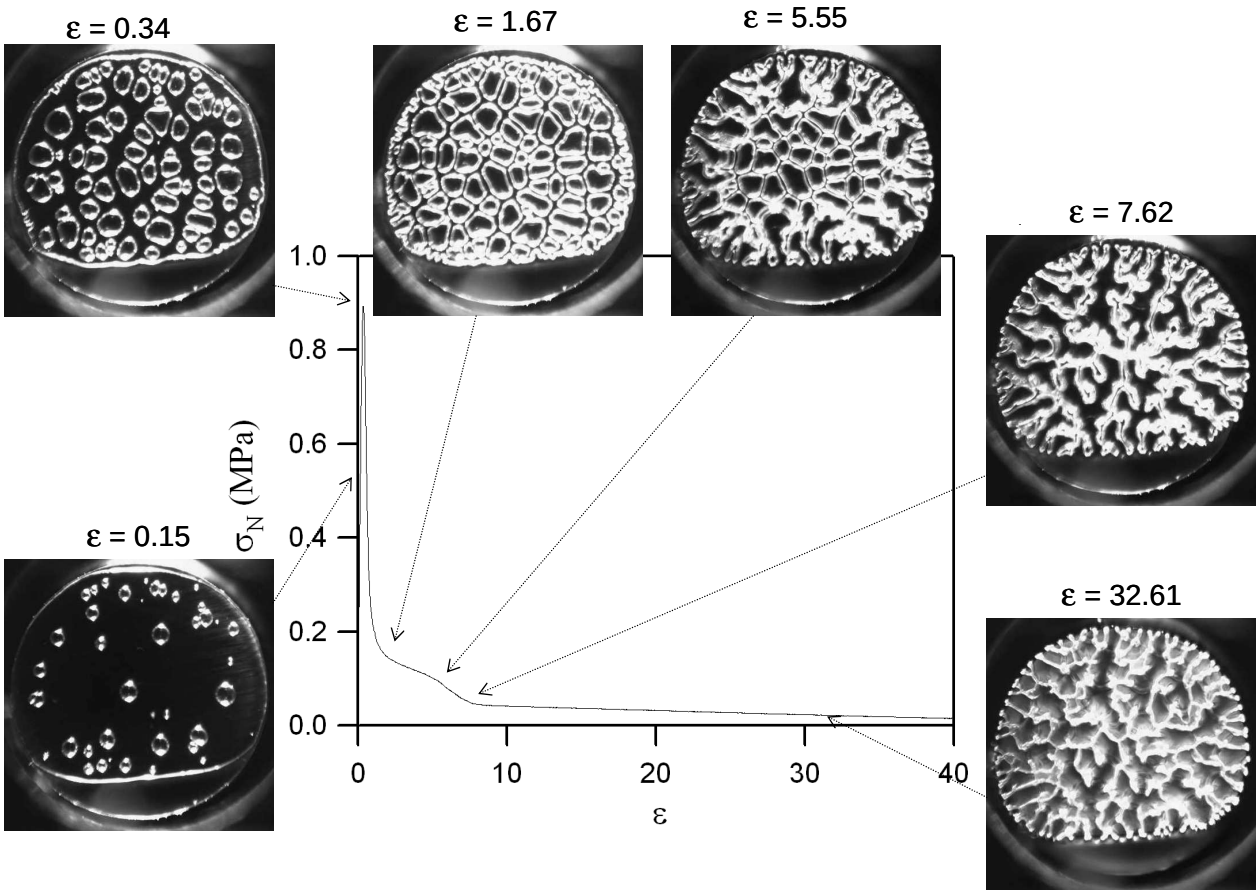

Figure 5-12. Snapshots of an adhesive made of uncrosslinked soft core-shell particles. Example of a liquid-like debonding behavior with fingering. The adhesive layer debonds cohesively from the probe. Test is performed on stainless steel at a debonding velocity of 100 μm.s^{-1}.

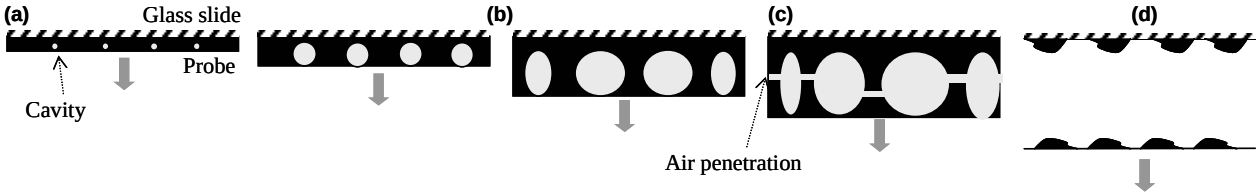

Figure 5-13. Schematic of a side view of the adhesive layer between the probe and the glass slide in the case of a PSA made of uncrosslinked latex particles. (a): cavitation, (b): cavities expansion, (c): air penetration, (d): cohesive debonding.

For an adhesive made of more crosslinked particles, air penetration does not occur anymore. Walls of the cavities tend to extend vertically until the final detachment of the feet of the fibrils from the probe (Figure 5-14 and Figure 5-15). Against a stainless steel surface and at a high enough debonding velocity, fibrils are actually highly extended in a regime where the strain hardening is important. And the increase of the nominal stress during the fibrillation regime is a signature of this hardening.

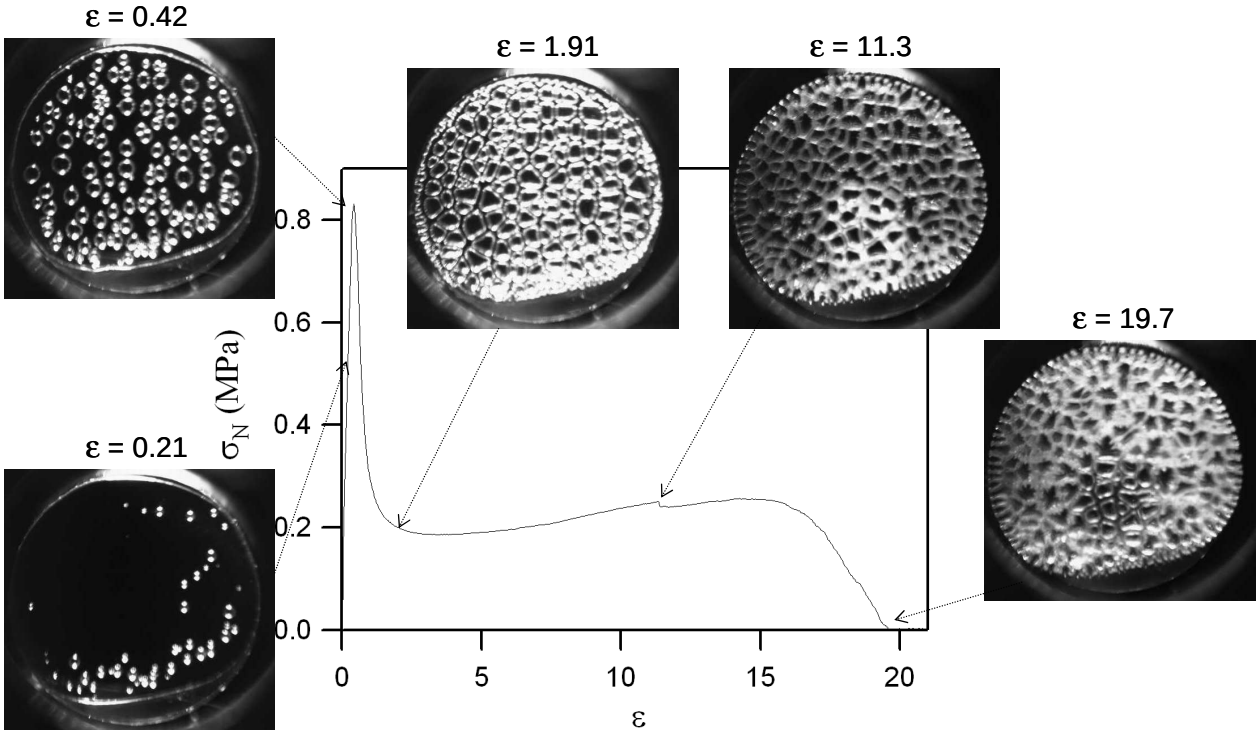

Figure 5-14. Snapshots of an adhesive made of soft core-shell particles crosslinked with 100% ADH (compared to the stoichiometric amount). Example of a solid-like debonding characterized by the strain hardening during the fibrillation process. The adhesive layer debonds adhesively from the probe. Test is performed on stainless steel at a debonding velocity of 100 µm.s^{-1}.

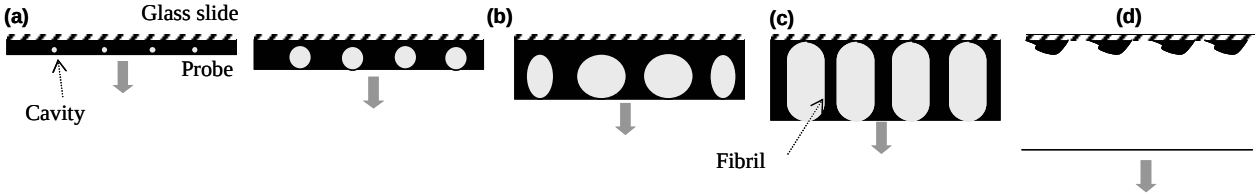

Figure 5-15. Schematic of a side view of the adhesive layer between the probe and the glass slide in the case of a PSA made of crosslinked latex particles. (a): cavitation, (b): cavities expansion, (c): fibrillation, (d): adhesive debonding.

This result is very similar to the situation where the degree the crosslinking is changed by varying the amount of gel content in each particle rather than between particles[1,2] as shown on Figure 5-16.

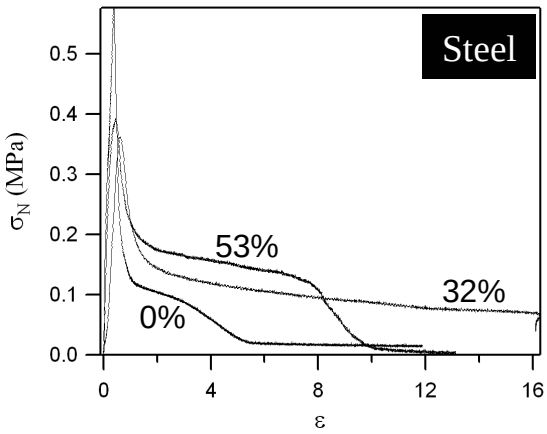

Figure 5-16. Nominal stress vs. strain tack curves of PnBA latexes differing by their gel contents. Tests were performed on stainless steel at 1000 µm.s^{-1} (after [1]).

Standard adhesive test results

It is also interesting to discuss briefly how these PSA based on interfacially crosslinked particles behave in more standard adhesive tests such as peel performance and shear resistance. Crosslinking is known as a tool to improve shear resistance of PSA but the effect on peel adhesion is generally detrimental even at low crosslinking densities[14]. The activation of an interfacial crosslinking during drying of soft and viscoelastic particles can however be an exception. As can be seen on Figure 5-17, a significant increase in the shear resistance is observed and it is accompanied with only a slight decrease in peel performance (only results on PE are shown here but trend is the same on stainless steel). This shows that cohesion of the shell at large strains plays a fundamental role in controlling shear resistance and that peel performance is governed by intermediate strains dissipation of the core.

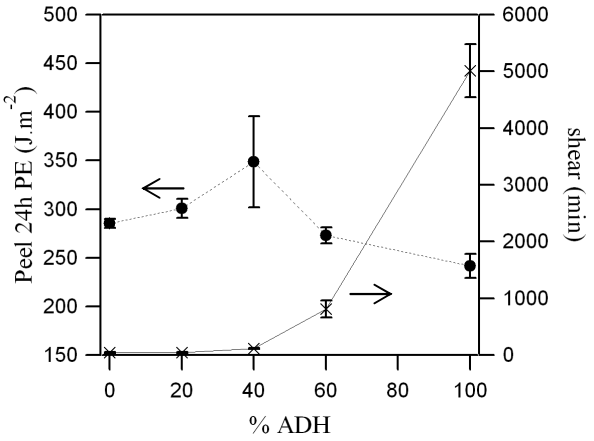

Figure 5-17. Shear resistance and peel performance of C80d0.1S20D0.4 as a function of the amount of ADH added (Results of peel and shear resistance have been obtained in the University of Manchester by A. Foster and P.A. Lovell).

If the PSA is made by traditional emulsion polymerization, the same balance is not generally possible and any increase in shear resistance typically leads to a decrease in peel force. This different behavior led us to investigate the viscoelastic properties of our materials

with the hope to find a revealing sign explaining the peculiar adhesive behavior. Linear viscoelastic measurements have been performed on the microrheometer whose principle has been extensively described in chapter 3.

5.3.1.2. Linear viscoelastic properties

Linear viscoelastic results were obtained on adhesive films made of C80d0.15S20D0.4 where 0%, 23%, 59% and 100% of DAAM groups were crosslinked. Evolutions of elastic, G′, and viscous, G″, moduli and of tan(δ) = G″/G′ with frequency are displayed on Figure 5-18 and Figure 5-19 respectively.

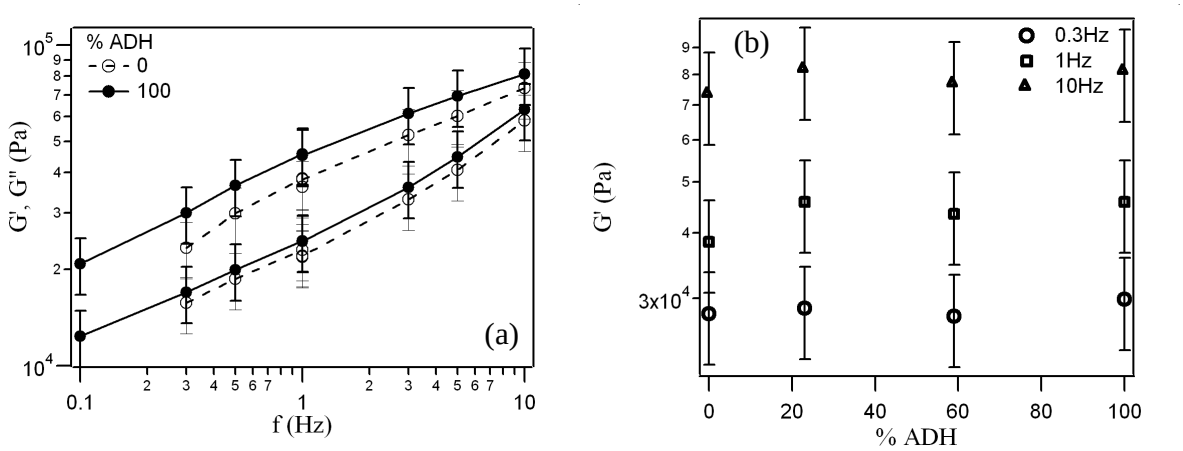

Figure 5-18. Linear rheological results of C80d0.15S20D0.4. (a): Evolution of the elastic (G′) and viscous (G″) moduli as a function of frequency (○: uncrosslinked DAAM groups, ●: 100% of ADH added compared to the stoichiometric amount). (b): Evolution of the shear elastic modulus as a function of the percentage of ADH added to the latex at f = 0.3Hz, f = 1Hz and f = 10Hz.

From Figure 5-18, it is clear that the crosslinking density has not much effect on G′ and G″. What is also important to notice is that in all cases, the shear modulus lies well below 0.1 MPa. The so-called Dahlquist criterion, which stipulates that the shear elastic modulus at the bonding frequency must be lower than 0.1 MPa for the layer to be able to form a good contact within the contact time, is thus always fulfilled. The constant value of G′ also explains why no differences were observed on the peak stress values σ_{max} of the tack curves.

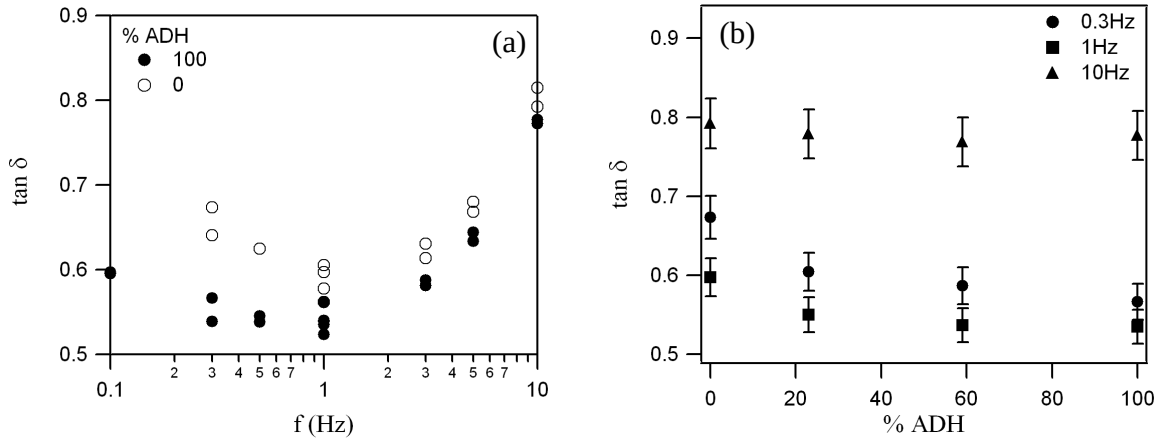

Figure 5-19. Linear rheological results of C80d0.15S20D0.4 (continued). (a): Evolution of tan(δ) as a function of the frequency (○: uncrosslinked DAAM groups, ●: 100% of ADH added compared to the stoichiometric amount). (b): Evolution of tan(δ) as a function of the percentage of ADH added to the latex at f = 0.3 Hz, f = 1 Hz and f = 10 Hz.

Figure 5-19 shows that the activation of the crosslinking reaction and further increases in the crosslink density have no effect on tan(δ) at high frequencies while a slight decrease in tan(δ) with an increasing crosslink density is observed at lower frequencies. This can be explained by the fact that short-range configurational changes which occur at high frequencies should be insensitive of the presence of cross-links while long-range motions at low frequencies are affected.[15]

Despite its decrease with crosslinking density, tan(δ) values always stay above 0.5, which is a signature of a quite dissipative material regardless of the degree of crosslinking. The combination of high dissipative properties in the linear regime with a low modulus gives a high value of the elastic length $\mathcal{G}_c/E$ and is an ideal condition for the evolution of individual expanded cavities into an elongated microfoam structure on a low adhesion substrate such as PE. This is the starting point of the fibrillating structure formation which is one of the conditions required for high adhesive energy.[16]

These results are in direct contrast to the situation where the degree of crosslinking is changed by varying the amount of crosslinking in each particle rather than between particles.[1,2] An increase in G′ was observed leading to a significant decrease in dissipation measured by tan(δ) (Figure 5-20). Increasing gel content within the particles has been found to be detrimental to adhesion especially on low energy surfaces.

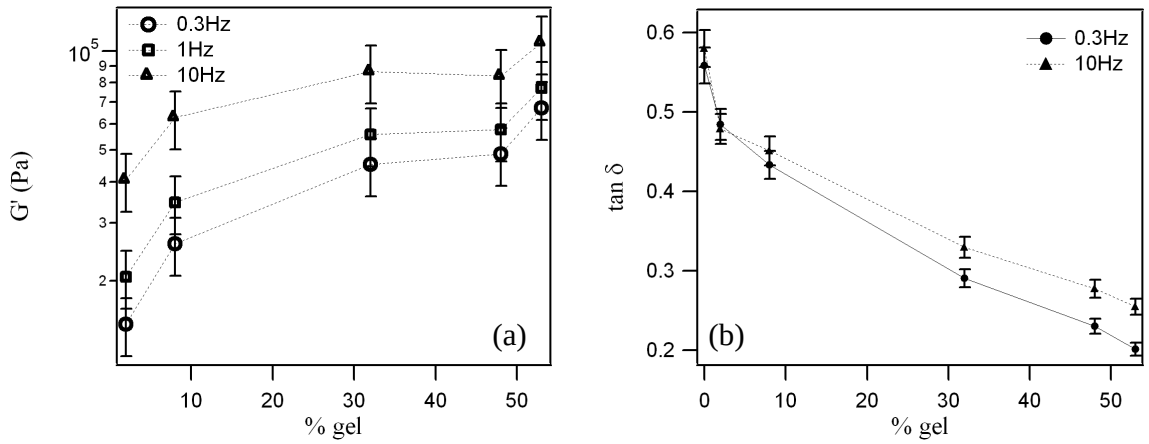

Figure 5-20. Linear rheological results of PnBA latexes differing by their gel contents. (a): Evolution of the elastic modulus G' as a function of the gel content at three frequencies (f = 0.3 Hz, f = 1 Hz and f = 10 Hz). (b): Evolution of tan (δ) as a function of the gel content (f = 0.3 Hz and f = 10 Hz). (after [1]).

5.3.1.3. Extension to large strains

We have shown that viscoelastic properties in the linear regime and adhesive properties at small strains of latexes made of particles with a thin shell are not much influenced by the degree of interfacial crosslinking. The following part will focus on tensile results at intermediate and high strains. These will be used as a tool to interpret adhesive properties afterwards.

Nominal stress vs. strain tensile curves and their corresponding Mooney-Rivlin representations are shown on Figure 5-21. The effect on tensile results of the activation of the crosslinking and of further increases in crosslinking density is considerable and has to be related to the large differences also observed on tack curves after the peak stress. First, the transition from the liquid-like behavior of uncrosslinked particles to a more viscoelastic solid-like behavior of crosslinked particles is observed both on tack and tensile curves. A lack of cohesion of the uncrosslinked sample accounts for the double fibrillation plateau ending with a non zero stress on the tack curves (sample fails by a cohesive debonding letting some residues on the probe) and for the absence of the hardening described by the sharp increase in the reduced stress at ultimate strains (range of low values of $1/\lambda$).

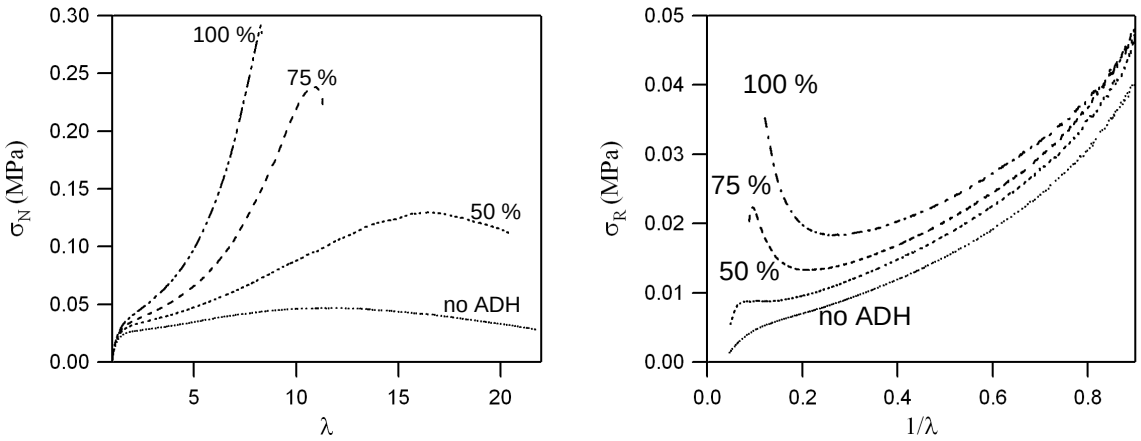

Figure 5-21. Tensile results of C80d0.1S20D0.4 where 0%, 50%, 75% and 100% of DAAM groups are crosslinked. Left: nominal stress vs. strain curves. Right: Corresponding Mooney-Rivlin representations.

To quantitatively compare the nonlinear deformation properties of different adhesives it is important to define a clear methodology. As discussed in chapters 1 and 4, the representation of the data in terms of Mooney stress is a quick and easy way to identify the main features of the large strain behavior of the material at a glance while a full viscoelastic model can give access to a more microstructural and molecular interpretation.

a. Elastic Mooney representation

As shown on Figure 5-21, when the initial particle is fully uncrosslinked and no ADH is added, C_{hard} is not defined. The same result is observed for 50% ADH indicating that the network of crosslink points at that level of crosslinking may not be fully percolating.

C_{hard} and C_{soft} values of C80d0.10S20D0.4 with various amounts of added ADH are shown on Figure 5-22. For all materials C_{soft} is much larger than C_{hard} which means that the modulus at small strains is more governed by entanglements than by chemical crosslinks. However, while C_{soft} appears to be roughly independent of ADH content, C_{hard} increases markedly. This clearly demonstrates the effect of the addition of ADH on the creation of non relaxing permanent crosslinks. Moreover, the linear increase of C_{hard} as a function of crosslinking density suggests a linear increase in active elastic segments created by the crosslinking reaction. Thus, even though values stay relatively low, C_{hard} is an important parameter controlling the large strain properties of the material. This behavior is similar to what has been found for the large strain behavior of block copolymers blends containing both triblocks and diblocks.[17] From the microscopic standpoint, we can interpret this behavior in the following way: the majority component of the core-shell material is the viscoelastic core and its entangled (and branched) structure controls the small and intermediate strain behavior, while the more permanently crosslinked shell structure controls the large strain hardening behavior of the material through the finite extensibility of the crosslinked chains.

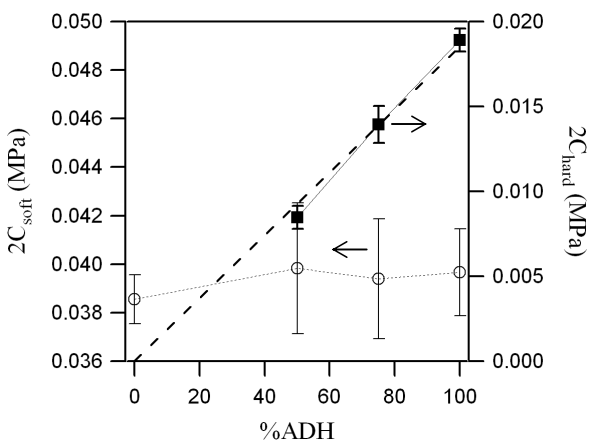

Figure 5-22. $2C_{soft}$ (empty circles) and $2C_{hard}$ (filled squares) of C80d0.1S20D0.4 as a function of the quantity of ADH added compared to the stoichiometric amount. (dashed line corresponds to a linear fit of C_{hard} = f(%DAH)).

While the Mooney stress is very useful to have a quick assessment of the nonlinear properties of the PSA at a given tensile velocity, one has to keep in mind that acrylic PSA in particular are markedly strain rate dependent. This rate dependence is supported by the fact that the maximal deformation of the fibrils is significantly influenced by the debonding velocity during tack experiments as observed on Figure 5-23, where results of C80d15S20D0.4 with 100 % of ADH compared to the stoichiometric amount and of C80d1S20D0.4 with 75 % of ADH are shown.

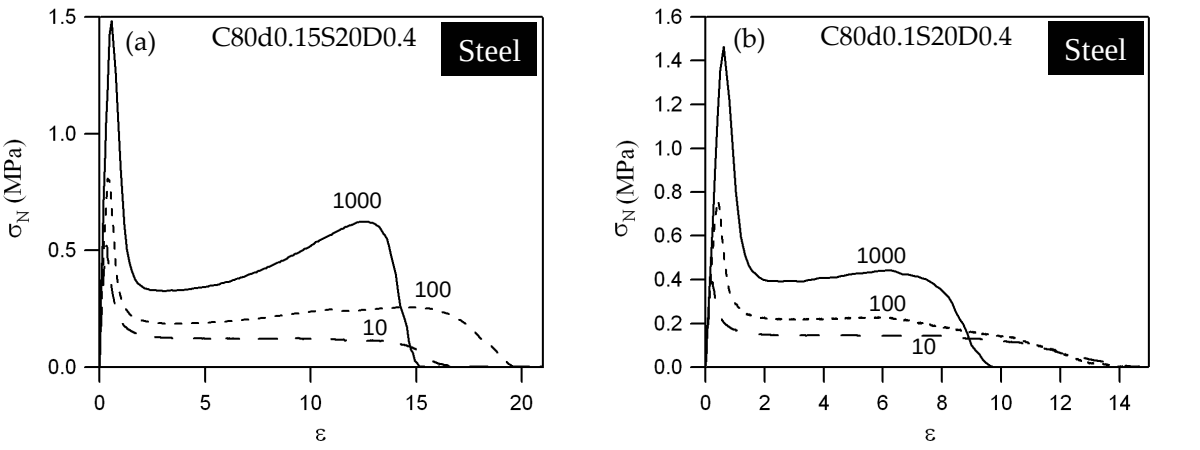

Figure 5-23. Stress vs. strain tack curves (a) of C80d15S20D0.4 with 100 % of ADH compared to the stoichiometric amount, (b) of C80d1S20D0.4 with 75 % of ADH compared to the stoichiometric amount. Tests were performed on stainless steel at 10, 100 and 1000 µm.s^{-1}.

In order to fully account for the viscoelastic nature of the material without sacrificing the large strain description, we have to use a viscoelastic model suitable for the large strain behavior of polymers as has been presented in section 5.2.3.2.

b. Viscoelastic-hardening description

Two fitted tensile curves of C80d0.1S20D0.4 with 50% and 100% of ADH are shown on Figure 5-24. With only 50% of ADH, the tensile specimen tends to flow and neck a little before breaking. That is why the ultimate strain part of the curve has not been fitted. From magnifications of the curve given on the right, the intermediate strain behavior, which is of important interest in controlling adhesion, seems to be correctly described by the model.

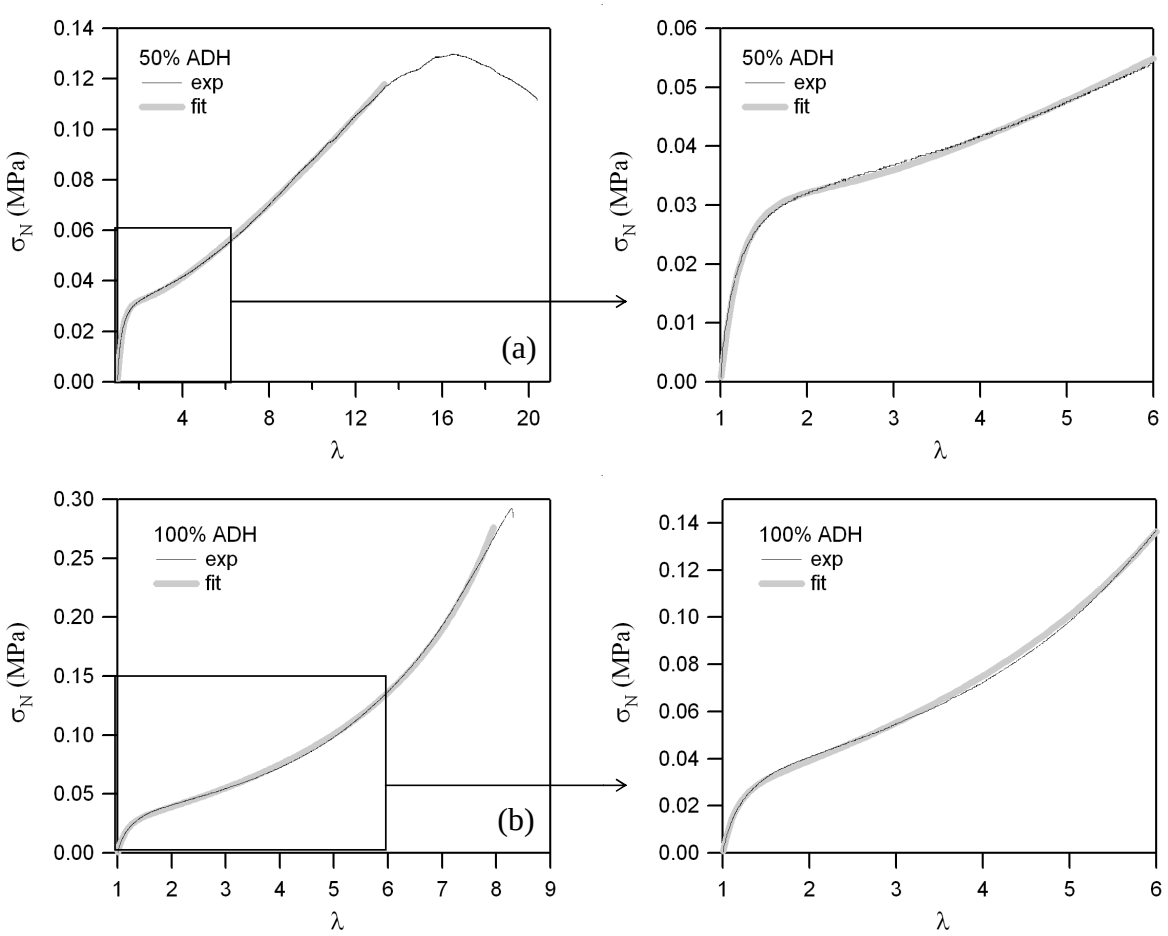

Figure 5-24. Two examples of C80d0.1S20D0.4 tensile curves fitted with the viscoelastic-hardening model. (a) 50% of ADH (compared to the stoichiometric amount) is added. (b) 100% of ADH is added. Magnifications of the curves in the intermediate range of deformations are given on the right. (An example of a fitted tensile curve of C80d0.1S20D0.4 with 75% of ADH is shown in appendix II).

Table 5-3 shows the relevant parameters obtained from the fits of the tensile curves of C80d0.1S20D0.4. Each experimental tensile curve was fitted separately and Table 5-3 shows average values and standard deviations of the fit parameters.

An interesting result is the low values of G_e compared to G_v even at the highest crosslinking density. This means that the network is only slightly crosslinked and does not much participate in the increase in the linear elastic modulus.

A value as high as $J_m = 3000$ obtained when 50% of ADH has been added indicates that the crosslinked network is very extensible. This means that an amount of ADH larger than 50% is required for the creation of a percolating network. Then, the decrease in J_m from 75% to 100% could be related to the decrease in M_c as the crosslinking density increases.

What is also interesting to note is that, while a slight but meaningless increase of G_v is observed, G_e is significantly increased. Dissipated energy at intermediate strains is nearly independent on the crosslinking density but a decrease in the viscoelastic contribution compared to the elastic one is predicted by the decrease of G_v/G_e. Since values of G_e stay low, the linear modulus $3(G_e+G_v)$ tends to increase but only slightly.

C80d0.1S20D0.4	G_v (kPa)	G_e (kPa)	J_m	De	G_v/G_e	$3(G_e+G_v)$ (kPa)
no ADH	30.6 (± 2.11)	4.20 (± 0.398)	10^6 imposed [a]	0.382 (± 0.052)	7.30 (± 0.284)	104 (± 7.47)
50% ADH	47.4 (± 9.73)	7.76 (± 0.946)	3170 (± 748)	0.211 (± 0.068)	6.07 (± 0.581)	165 (± 31.9)
75% ADH	59.6 (± 6.96)	11.9 (± 1.01)	211 (± 21.5)	0.126 (± 0.030)	5.02 (± 0.322)	215 (± 23.5)
100% ADH	58.8 (± 4.01)	16.0 (± 0.507)	111 (± 4.60)	0.114 (± 0.021)	3.68 (± 0.204)	224 (± 13.0)

a- For uncrosslinked liquid-like materials, the model cannot describe fully the behavior unless J_m is set to infinity ($J_m = 10^6$ has been chosen for the fits).

Table 5-3. Fitting parameters obtained in the case of C80d0.1S20D0.4 without ADH and with 50, 75 and 100% of ADH.

The interpretation of *De* is complex in this model. Since we performed all tests at the same initial strain rate, the *De* represents here the average of the relaxation times spectrum of the material in the nonlinear regime. Yet when we crosslink the material, we effectively preferentially crosslink the high molecular weight or branched fraction of the polymer. Because the material is heterogeneous, as a result the uncrosslinked fraction is deprived of its slowly relaxing fraction and relaxes faster. This explains why the *De* effectively decreases with increasing interfacial crosslinking: we are in fact separating the population into an elastic non relaxing one (G_e increases) and a fast relaxing viscoelastic one.

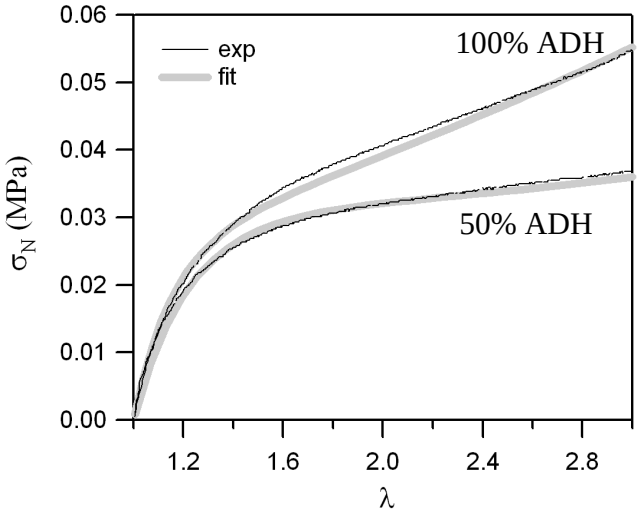

Figure 5-25. Comparison between experimental data and viscoelastic model fit. Visualization of the error made for the prediction of *De*. C80d0.1S20D0.4 (a): with 50% of ADH and (b): with 100% of ADH.

c. Intermediate strain dissipation

C80d0.1S20d0.4	W_{diss} ($J.m^{-3}$)	W_{diss}/W_e
no ADH	19800 (± 1021)	0.667 (± 0.010)
50% ADH	22400 (± 435)	0.615 (± 0.009)
75% ADH	22400 (± 435)	0.509 (± 0.027)
100% ADH	22500 (± 913)	0.398 (± 0.007)

Table 5-4. Intermediate strain dissipated energy for C80d0.1S20D0.4 with various amounts of ADH.

The amount of the dissipated energy at intermediate strains W_{diss} seems nearly independent on the crosslinking density. On the other hand, when compared to the stored elastic energy, the ratio W_{diss}/W_e decreases as the number of crosslinks increases. This indicates an increase in elastically active segments without really reducing the viscoelastic dissipation. Exactly the desired effect, due to the separation of fast relaxing and dissipating chains and permanent crosslinks.

d. Comments on elastic vs. viscoelastic-hardening descriptions and intermediate strain dissipation

Three different tools have been used for the study of the nonlinear properties: a nonlinear elastic representation or a nonlinear viscoelastic modeling. We also showed how the energy dissipated at intermediate strains can be estimated in a quite simple way. Results obtained with the different methods are consistent with each other.

Besides, a few additional remarks can be made:

- Results from elastic and viscoelastic approaches show that for this type of core-shell architecture and polymer, the percentage of ADH needed for the creation of a connected network is higher than 50%.
- Comparison between Figure 5-22 and Figure 5-26 emphasizes the possible analogy between $2C_{hard}$ and G_e. Both values tend to linearly increase as long as the material is enough crosslinked, C_{hard} is not defined for uncrosslinked materials and the observed high value of G_e for 0% of ADH may be attributed to a poor quality of the fits in this case.

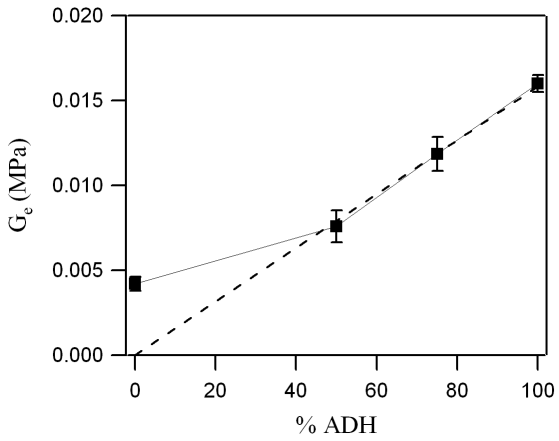

Figure 5-26. G_e of C80d0.1S20D0.4 as a function of the quantity of ADH added compared to the stoichiometric amount. (dashed line corresponds to a linear fit of G_e= f(%ADH)).

- Moreover, from both models one can estimate the dissipation compared to the elasticity using C_{soft}/C_{hard} when the reduced stress representation is chosen and G_v/G_e when the viscoelastic model is preferred. Nearly the same decrease is observed as the amount of ADH added increases (Figure 5-27-a).

W_{diss}/W_e could also be used as a simple way to estimate the nonlinear viscoelastic character in the same way with the advantage that no curve fitting is needed (Figure 5-27-b). However if experiments are performed at different rates, only the viscoelastic model will provide meaningful interpretations of the differences.

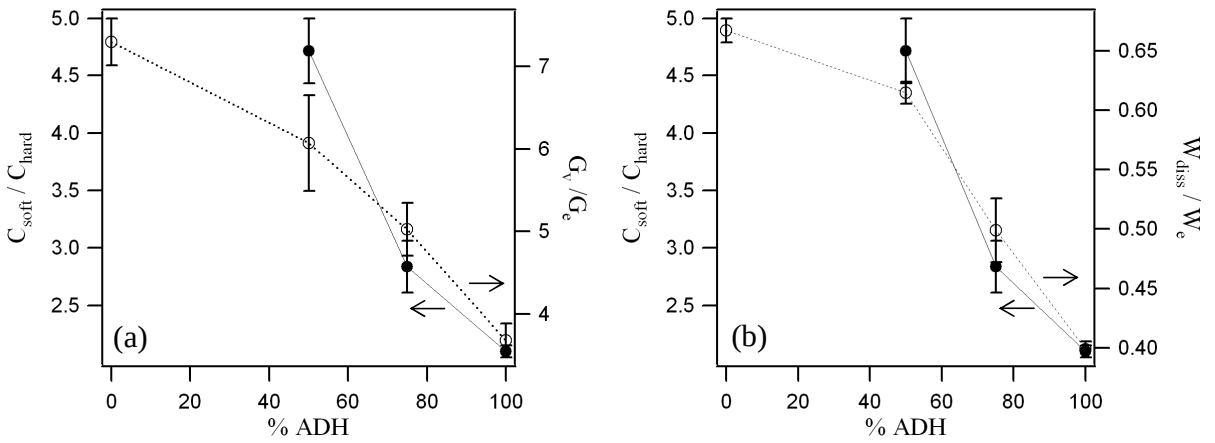

Figure 5-27. C_{soft}/C_{hard} of C80d0.1S20d0.4 as a function of the quantity of ADH added compared to G_v/G_e (a) and to W_{diss}/W_e (b).

- The viscoelastic hardening model includes explicitly a hardening parameter J_m which is a clear indication of the finite extensibility of the connected network of permanently crosslinked chains. Since this parameter was not included in the elastic description, it could only be inferred qualitatively.

5.3.1.4. Rheological properties vs. adhesion

We have analyzed in detail the rheological properties of a series of model PSA where the interfacial crosslinking was activated. The conventionally measured viscoelastic properties have shown very few changes due to the crosslinking process, within the range of frequencies relevant for a tack or peel test. Yet the nonlinear rheological properties characterized in uniaxial tension have proven to be very sensitive to changes in interfacial crosslinking. It is now interesting to discuss the effect that these changes have on the adhesive properties shown on Figure 5-11 and Figure 5-17.

In the probe tests, increasing the shell crosslinking density leads both to an increase in the fibrillation plateau stress and to a decrease in its extension both on stainless steel and on PE. The increase in stress with increasing crosslinking density is also clearly observed in the tensile curves. What is more interesting to notice is that for higher levels of crosslinking, increasing the crosslinking density leads to a decrease in the maximal extension of the fibrils before debonding. This effect is much more pronounced on the low adhesion surface of PE than on the stainless steel surface (Figure 5-11).

There are two possible views for the description of the debonding of a fibrillar structure of an adhesive layer. In order to separate cleanly from the surface the interface between the foot of the fibril and the surface must break. Previous authors have proposed that debonding of the fibrils should occur, either when a critical stress is reached[18] or alternatively when enough elastic energy is released upon detachment to overcome the adhesive energy of the feet of the fibrils[4,19-22]. Increasing the crosslinking density of the material leads most probably to an increase in the amount of stored elastic energy at large strains. We have seen that energy dissipation at intermediate strains is nearly constant as a function of crosslinking density (from values of C_{soft} and W_{diss}) so the increase in stored elastic energy could be mainly due to the increase in the stiffness of the shell.

From a more practical point of view (Figure 5-17), to reach an acceptable shear resistance an increase in the cohesion at ultimate strains is obviously needed. At low levels of ADH, G_e seems sensitive to the presence of additional crosslinks while J_m remains very high and this means that the crosslinking network is being created (adding elastic strands to the small strain modulus) but probably not entirely connected. And this results in very low shear resistance.

The dramatic increase in shear resistance observed between 60% and 100% ADH reflects the formation of a percolating network. Note that this percolating threshold is visible on J_m and on the maximum extension of the plateau between 50% and 75% ADH. On the other hand increasing crosslinking density leads to a continuous increase in G_e. Based on these results, an optimal amount of ADH should be right at the percolation threshold to take advantage of the increase in the cohesion leading to an improvement of the shear resistance without damaging peel performance highly sensitive to the deformability of the polymer chains between crosslinks.

Given these very promising results, the next obvious question is the role played by the localization of the crosslinks. The core-shell architecture of the particle allows some degree of control on the localization of the crosslinkable DAAM groups and given the very high molecular weight and the slight degree of branching it is likely that only a very limited diffusion takes place within the particle.

5.3.2. Effect of the distribution of the crosslinking points

To study the effect of the distribution of the crosslinking points, the Manchester group designed and we investigated the properties of a model system (see *Materials section*, Table 5-1) where DAAM reactive groups could be either incorporated all along the polymerization (giving a homogeneous particle) or only incorporated at the end (DAAM in the shell as in the previous example). The particles in all the three latexes had therefore exactly the same monomer composition in the core and in the shell with the exception of the presence of DAAM groups in the shell. The stoichiometric amount of ADH, i.e. 100% of crosslinking, has been always added for this study.

5.3.2.1. Experimental results

a. Adhesive performance

Tack results

In this section we show nominal stress vs. strain curves and adhesive energies from probe tests performed on PE and stainless steel surfaces and at three debonding velocities. Most attention will be paid to the intermediate and high strain behavior.

The nominal stress as a function of strain is represented for C80S20, C45S55 and C0S100 in Figure 5-28 showing the effect of DAAM distribution on adhesion on PE. Regardless of the type of particles and of the debonding velocity, fibrils detach from the probe always adhesively. At low debonding velocity (V_{deb} = 10 μm.s^{-1}) one clearly observes a decrease in ε_{max} with increasing shell thickness while the fibrillation plateau stress level stays unchanged. This evolution is strain rate dependent. Differences between ε_{max} of C80S20 and C45S55 decrease with increasing debonding velocity until becoming identical at 1000 μm.s^{-1}. Even at high strain rates, ε_{max} of the homogeneously crosslinked particle is lower. Moreover, one can note the marked strain rate dependence of ε_{max} for the heterogeneous particles which indicates a more viscoelastic behavior of the fibrils and supports our choice of a viscoelastic model to predict and interpret the nonlinear behavior of the materials. This strain rate is less pronounced when crosslinks are distributed homogenously in the whole volume of the particle.

Similar σ_{max} values have been found for the three adhesives.

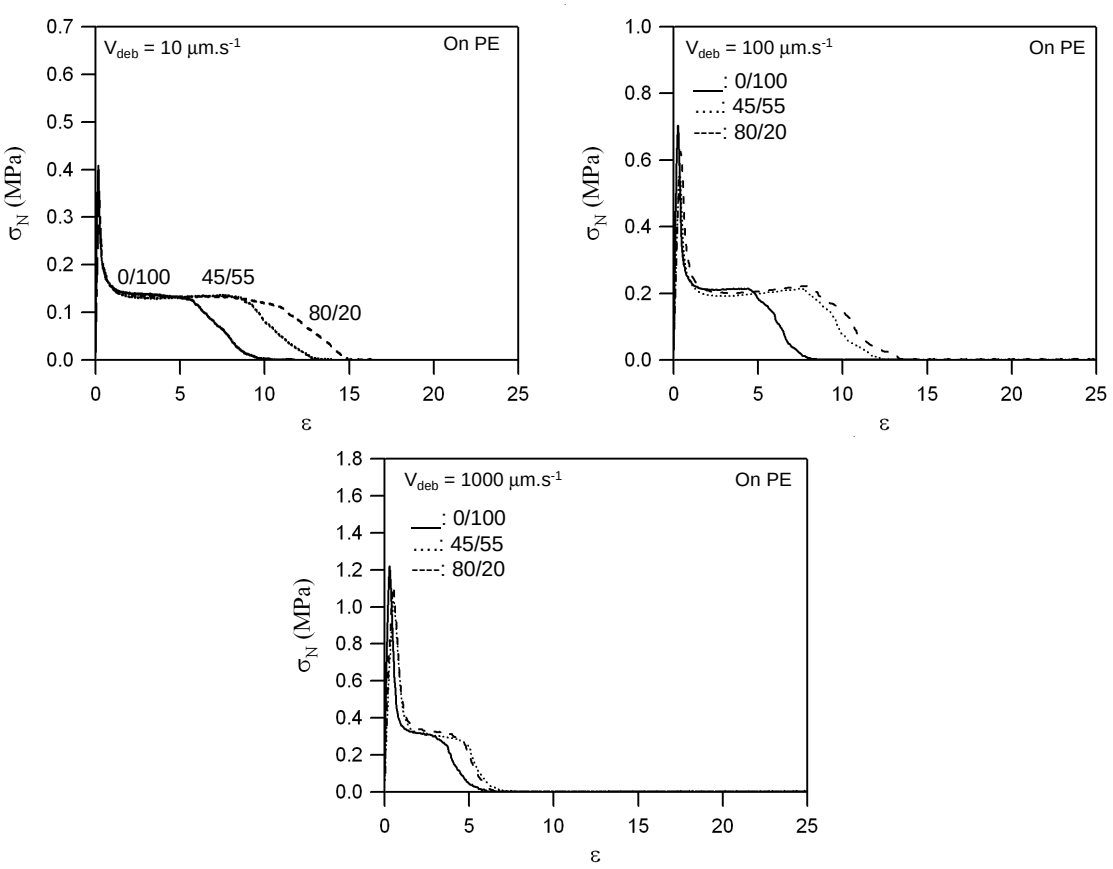

Figure 5-28. Stress vs. strain tack curves of C0S100, C45S55 and C80S20. Tests were performed on PE at debonding velocities of 10, 100 and 1000 µm.s^{-1}.

Adhesive performance of a PSA is generally evaluated by its adhesive energy. To avoid the effect of debonding velocity on the peak stress (an increase in V_{deb} leads to a significant increase in σ_{max} due to viscoelastic cavity expansion) and to be more focused on intermediate and high strains, we decided to look at the fibrillation energy (area under the curve from the beginning of the fibrillation plateau to the debonding) instead of the global adhesive energy. Results (Figure 5-29) confirm that at low velocities, increasing the shell thickness leads to a decrease in fibrillation energy, while at higher velocities, no significant differences are observed. At 1000 µm.s^{-1}, the fibrillation energy seems to become insensitive to the DAAM distribution. Moreover, one can notice the higher strain rate dependence of fibrillation energies of the core-shell particles. And finally, regardless of the thickness of the shell, the highest fibrillation energy is reached at 100 µm.s^{-1}. This means that, on the one hand, from 10 to 100 µm.s^{-1}, the increase in fibril formation stress dominates compared to the decrease in fibril extension, while on the other hand, from 100 to 1000 µm.s^{-1} the decrease in extension at detachment dominates.

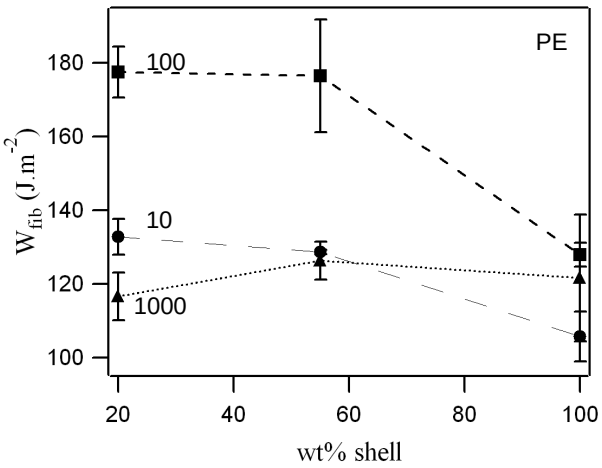

Figure 5-29. Fibrillation energies on PE as a function of the shell thickness at debonding velocities of 10, 100 and 1000 µm.s^{-1}.

Let us continue with results of adhesion on stainless steel. Stress versus strain tack curves of experiments performed at 10, 100 and 1000 µm.s^{-1} are shown on Figure 5-30.

At 10 µm.s^{-1}, no significant differences are observed between the two core-shell latexes C80S20 and C45S55 except the slightly lower plateau stress level of C45S55 (the observed lower value of ε_{max} of C45S55 is not very meaningful and most probably comes from the fact that adhesive layer of C45S55 is slightly higher than that of C80S20, h_{C80S20} ~ 82 µm and h_{C45S55} ~ 94 µm). At 100 µm.s^{-1}, ε_{max} of C80S20 is higher and the final debonding is characterized by a sharper drop in stress. ε_{max} of C45S55 is increased compared to 10 µm.s^{-1} in an even more significant way. With a further increase in debonding velocity, curves of heterogeneous particles draw nearer to that of the homogeneous one through a decrease in ε_{max}. The maximum extensions of the heterogeneous particles vary strongly with debonding velocity and goes through a maximum between 10 and 1000 µm.s^{-1}. This may correspond to the critical Deborah number defined by Lakrout et al.[23] at which the transition from cohesive fracture to adhesive fracture occurs. Indeed, some traces of residue are left on the probe surface at 10 µm.s^{-1} in both cases and at 100 µm.s^{-1} only in the case of the particle with the thicker shell C45S55. This means that this critical Deborah number is reached between 10 and 100 µm.s^{-1} for C80S20 and between 100 and 1000 µm.s^{-1} in the case of C45S55.

C0S100 differentiates oneself from core-shell particles from its higher and shorter fibrillation plateau at 10 µm.s^{-1} and from the constancy of values of ε_{max} as debonding velocity increases. Therefore one finds again a distinctly more viscoelastic behavior for the films made from heterogeneous particles.

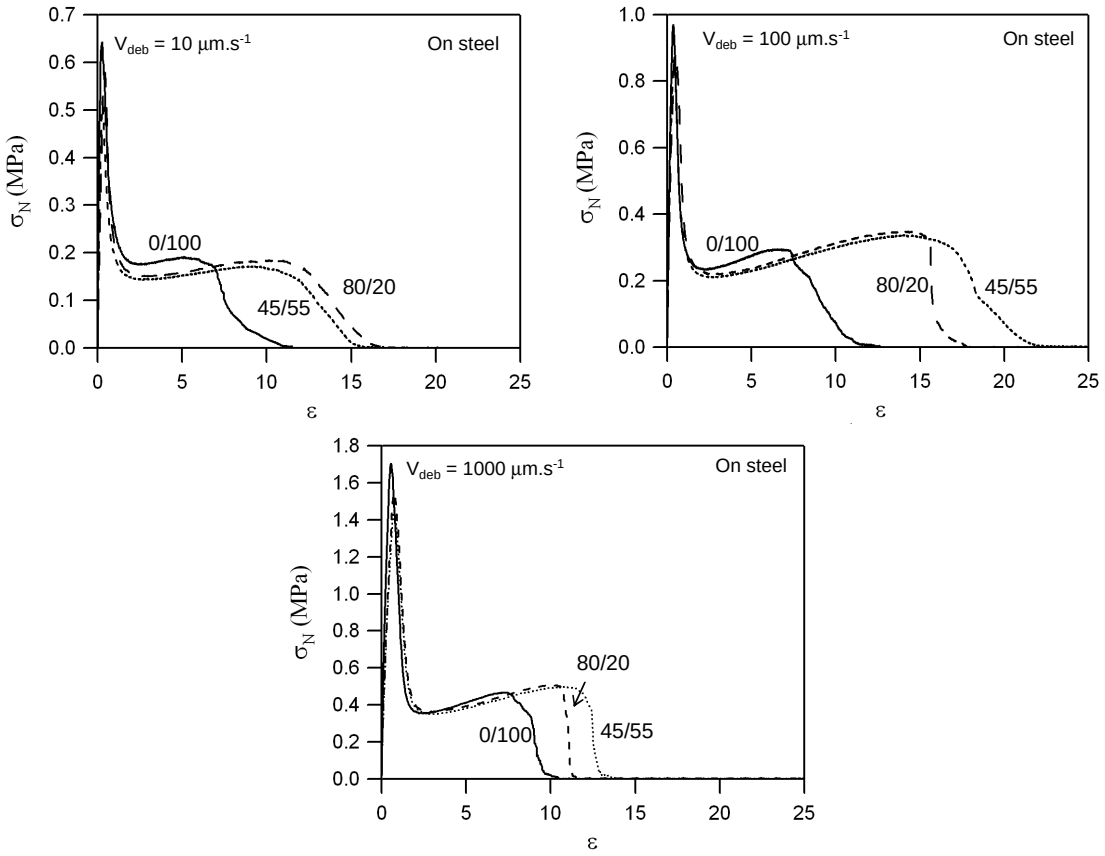

Figure 5-30. Stress vs. strain tack curves of C0S100 (solid line), C45S55 (dotted line) and C80S20 (dashed line). Tests were performed on stainless steel at debonding velocities of 10, 100 and 1000 µm.s^{-1}.

The values of the fibrillation energies as a function of shell thickness are shown on Figure 5-31. What is probably the most important to note is that C45S55 has the highest fibrillation energy as a consequence of a longer fibrillation plateau (as already said difference on ε_{max} between C80S20 and C45S55 observed at 10 µm.s^{-1} is not very meaningful).

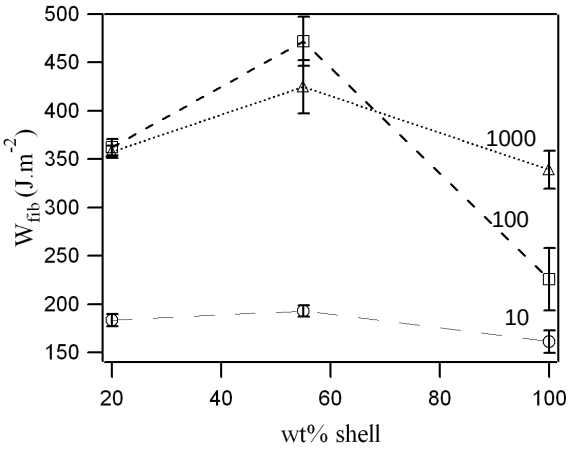

Figure 5-31. Fibrillation energies of C0S100, C45S55 and C80S20 on stainless steel at debonding velocities of 10, 100 and 1000 µm.s^{-1}.

Standard adhesive tests results

As before, it is interesting to show how adhesive properties evolve with a change in the shell thickness. Standard PSA tests have been carried out by Andrew Foster at the University of Manchester for a wider series of particles than that for tack tests and for the sake of clarity, results of C0S100, C45S55 and C80S20 have been encircled in Figure 5-32. Peel performance is not influenced much by the distribution of DAAM groups and this is consistent with adhesion energies obtained at high debonding velocity (Figure 5-32-(a)). The latexes on the other hand exhibit rather different shear resistances. But what gives the most information is probably the comparison between C80S20 and C45S55. In the case of the thinner shell, there is a potentially higher DAAM concentration in its shell which will contribute to a higher crosslinking density on film formation. Moreover, localization of crosslinks at the extreme surface of the particles is probably at the origin of a better reinforcement of the interfaces. Shear resistance would reflect these assumptions. One can also notice that in the case of an extremely thin shell (%wt shell = 10%) the effectiveness of the crosslinking in improving shear resistance is lost. The C0S100 has the best shear resistance and does not lose much peel force. However the probe tests reveal that it is performing significantly less well than the C80S20 and C45S55 at low debonding velocity both on stainless steel and on PE. It is likely therefore that it will not perform very well in applications where slow debonding is involved. This example reveals the better sensitivity of the probe tests relative to the standard PSA tests.

Finally, the best balance between adhesion on stainless steel and PE and cohesion seems to be obtained in the case of a relatively thin shell (20wt% in the present study). The crosslinking strategy where crosslink points are localized at the interface between particles was proved to be effective in producing systems in which significant increases in shear could be obtained while retaining high values of peel adhesion. And this effectiveness is believed to be due mainly to the connectivity of the crosslinked domains and enhanced by the presence of a very viscoelastic core.

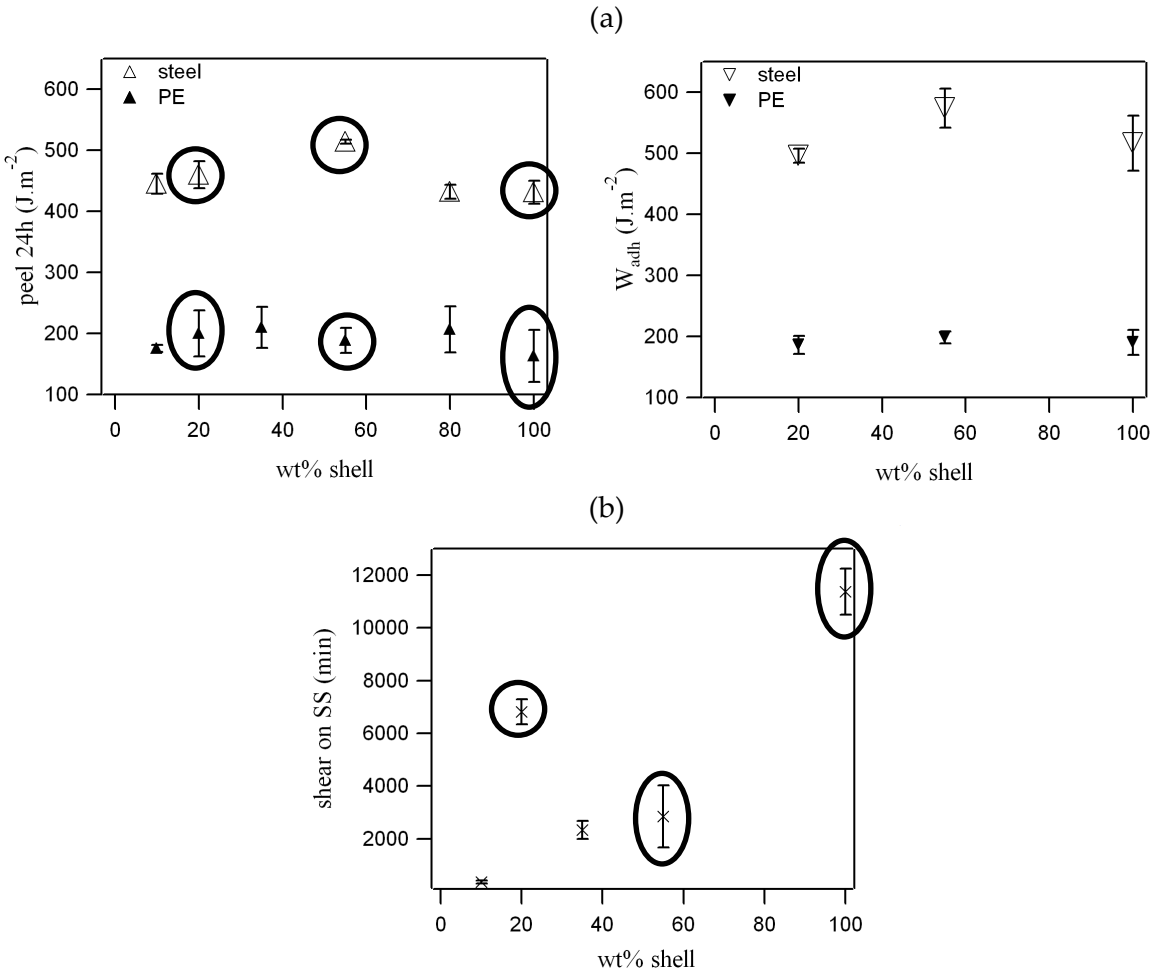

Figure 5-32. (a) 24h peel performance on stainless steel and PE, adhesion energies from tack experiments performed on stainless steel and PE and at V_{deb} = 1000 µm.s^{-1}. (b) Shear resistance on stainless steel. Encircled values are obtained on particles whose tack and nonlinear properties have also been investigated.

b. Tensile results

Tensile results are shown on Figure 5-33. Slight but not significant differences are observed in the Young's modulus, this will be however discussed in more detail later. More interestingly, the magnification of the tensile curves (Figure 5-33-right) clearly shows that the stress-strain curve starts to be significantly different in the intermediate strain regime: the homogeneously crosslinked particles has a less pronounced strain softening compared to the two core-shell particles. This means that the sample where crosslinks are distributed more homogeneously behaves more elastically than that from core-shell particles where crosslinks are only located in a thin shell.

Moreover, some differences in behavior are also observed at larger strains. These should be mainly due to some differences in finite extensibility of polymer chains between permanent crosslinks. The thin-shell material is locally more tightly crosslinked and reached its finite extensibility sooner. Comparison between deformability of C0S100 and C45S55 may be a bit more subtle and will be discussed in more detail in the section 5.3.2.2 about the molecular interpretation of deformation behavior.

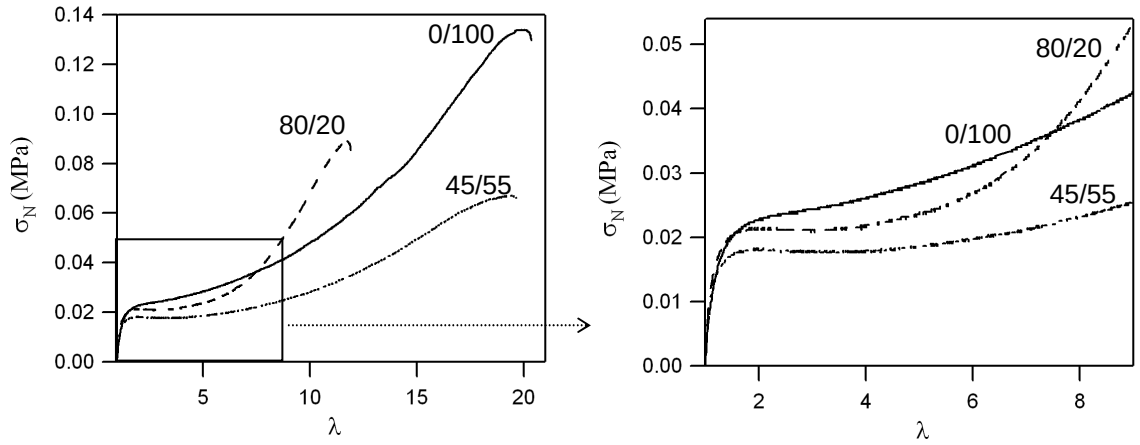

Figure 5-33. Nominal stress vs. strain tensile curves of C0S100, C45S55 and C80S20. Left: entire curves until the rupture of the tensile specimen. Right: magnification of the curves in the range of small and intermediate strains.

Reduced stress vs. 1/λ curves of the above tensile results (Figure 5-34) have similar shapes characterized by a softening at intermediate strains and an increase in the Mooney stress at ultimate strains. No large differences are observed between the three materials and the reduced stress vs. 1/λ representation does not appear very useful in that case.

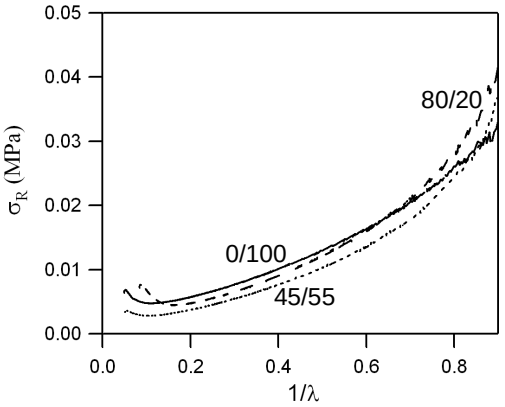

Figure 5-34. Reduced stress vs. 1/λ curves of C0S100, C45S55 and C80S20.

Results of the fits with the viscoelastic hardening model are shown on Table 5-5. (Examples of fitted tensile curves are shown in appendix II).

	G_v (kPa)	G_e (kPa)	J_m	De	G_v/G_e	$3(G_e+G_v)$ (kPa)	W_{diss} ($J.m^{-3}$)	W_{diss}/W_e
C80S20	39.7 (± 3.10)	2.74 (± 0.212)	174 (± 12.7)	0.220 (± 0.021)	14.5 (± 0.418)	127 (± 9.91)	17400 (±702)	0.831 (±0.029)
C45S55	31.1 (± 1.84)	2.11 (± 0.080)	710 (± 153)	0.254 (± 0.006)	14.7 (± 0.467)	99.8 (± 5.72)	15900 (±1070)	0.886 (±0.035)
C0S100	35.6 (± 3.32)	3.85 (± 0.105)	694 (± 131)	0.221 (± 0.048)	9.26 (± 1.12)	118 (± 9.65)	16700 (±686)	0.738 (±0.044)

Table 5-5. Fitting parameters and dissipated energy obtained for C80S20, C45S55 and C0S100.

It is interesting to examine some of the parameters obtained from the fits. First of all the initial modulus (measured by $3(G_e+G_v)$) does not vary much and remains around 100 kPa, a relatively high but reasonable value for a PSA. However the very pronounced softening that is observed for all the three materials is obvious from the high values of W_{diss}/W_e which are close to one and from the values of G_v/G_e which are close to 10. This is typical of a viscoelastic material where most of the stress but not all can relax after about 200% deformation.

Comparing now the three materials with each other, one notes that while values of G_v/G_e (Table 5-5) of C80S20 and C45S55 are similar, C0S100 seems more elastic as it was expected from the less pronounced softening observed on the tensile curves. The highest amount of dissipated energy is obtained in the case of the core-shell particle with the thinner shell but the highest dissipation relative to elasticity estimated through W_{diss}/W_e is reached in the case of the core-shell particle with the thicker shell.

Absolute values of some parameters of Table 5-5 will be discussed in the following section in more detail. This requires first an interpretation of each parameter. This interpretation has already been given in the case of a homogeneous polymer network (see the section 5.2.3.2 concerning the *Analysis of large strain behavior*). This is a bit more complicated in the case of materials based on core-shell particles. In the previous section, the crosslinking density was the only molecular change. In this section, the volume of the shell and its crosslinking density are modified simultaneously, crosslinking density being inversely proportional to the shell volume fraction. This is relevant when interpreting G_v and G_e and one of the objectives of the following section is to understand how this can be taken into account.

5.3.2.2. Discussion

The points to discuss here are twofold:

- Molecular interpretation of the tensile tests.
- Refinement of the relationship between adhesive behavior, a rather complex property including interfacial interactions, and nonlinear deformation properties

a. Molecular interpretations of the deformation behavior

A suitable molecular structure for tacky materials could be described as a nearly uncrosslinked network which will lead not only to the necessary high compliance of the layer for a good contact but also to the viscoelastic losses during the fibrillation. Crosslinks and/or entanglements are also necessary, first to avoid creep and poor shear resistance and second to give the desired fibril cohesive strength and to avoid fibril flow (cohesive debonding) at large strains. In the present work, the balance of these properties has been studied using the core-shell morphology. Viscoelasticity and dissipation are mainly controlled by the core while the necessary cohesion for an adhesive debonding (no residue

on the probe at the end of tack experiments) is governed by the more elastic and crosslinked shell. Keeping in mind this structure, some molecular interpretations of the differences between the three core-shell latexes, differing by their shell thicknesses, can be proposed.

- *Possible adaptation of the viscoelastic-hardening model to core-shell particles*

One can schematically represent the adhesive layer made of core-shell latex particles as a parallel cubic network where the core acts mechanically in parallel with the shell. (Figure 5-35). While the walls are made of the shells, the interior can represent the cores of the particles.

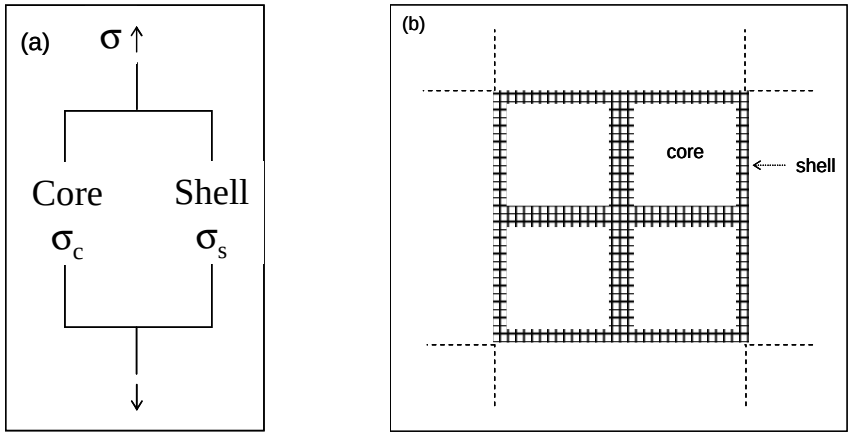

Figure 5-35. (a) Parallel model proposed for the study of deformation behavior of materials made of core-shell particles. (b) 2D schematics of the heterogeneous crosslinked network made of core-shell particles.

From the tensile results, the measured stress or modulus come from both the shell and the core and contributions of each part depends on its "local stress" (σ_c and σ_s) and on its surface fraction (if the surface fraction of the core is called μ_c, $(1-\mu_c)$ is the surface fraction of the shell). In the following, "c" and "s" indexes will be used for core and shell respectively. This model can be written as:

$$\sigma = \mu_c\sigma_c + (1-\mu_c)\,\sigma_s$$

$$G = G_v + G_e = \mu_c G_c + (1-\mu_s)\,G_s \qquad \textbf{Eq. 5-16}$$

where σ stands for the stress and G for the shear modulus of the overall structure.

Note that a simple calculation of the global modulus of our heterogeneous structures from the modulus of each phase is proposed here even though some more complex physical models of polymer composites can be found in the literature.[24,25] This choice has been made because the actual polymer microstructures of latexes studied in the present work are obviously highly complex and probably not as precisely designed as what could be theoretically predicted. Hence, behaviors of the macroscopic samples are most probably not better described with more complex equations.

The question is not how to relate the values of G_c and G_s of this physically based model with the values of G_v and G_e obtained with the fits of the viscoelastic-hardening model. G_v represents the unrelaxed modulus of the fraction of the material which indeed can relax. It is governed by both entanglements (both in the actual shell and in the core) and hydrogen bondings (only in the shell) one can write:

$$G_v = \mu_c G_c + (1-\mu_c) G_{s,v} = G_{ent} + (1-\mu_c) G_{s,H}$$

$$G_e = (1-\mu_c) G_{s,e} \qquad \textbf{Eq. 5-17}$$

where $G_{s,v}$ is the effective modulus of the viscoelastic part of the shell, G_{ent} represents the effective modulus of the uncrosslinked network made of entanglements, $G_{s,H}$ is the effective modulus of the network made of non permanent hydrogen bondings and $G_{s,e}$ the effective modulus made of the permanent chemical crosslinks of the shell. Viscoelasticity and dissipation comes from both the core and the shell. Values of G_v obtained from the best fits of the tensile curves are however not so simple to interpret since our viscoelastic-hardening model has only one relaxation time while characteristic times of entanglements and hydrogen bonds between free DAAM groups are different.

The interpretation of J_m is more intuitive since it should be exclusively influenced by the presence of permanent chemical crosslinks created through the reaction between ADH and DAAM.

A possible modification of the viscoelastic-hardening model is proposed on Figure 5-36. This is mainly targeted at showing how complex the system can become when taking into account all its molecular features. In the following, we will merely point out the most interesting points; to give a detailed molecular interpretation is beyond our reach at this point.

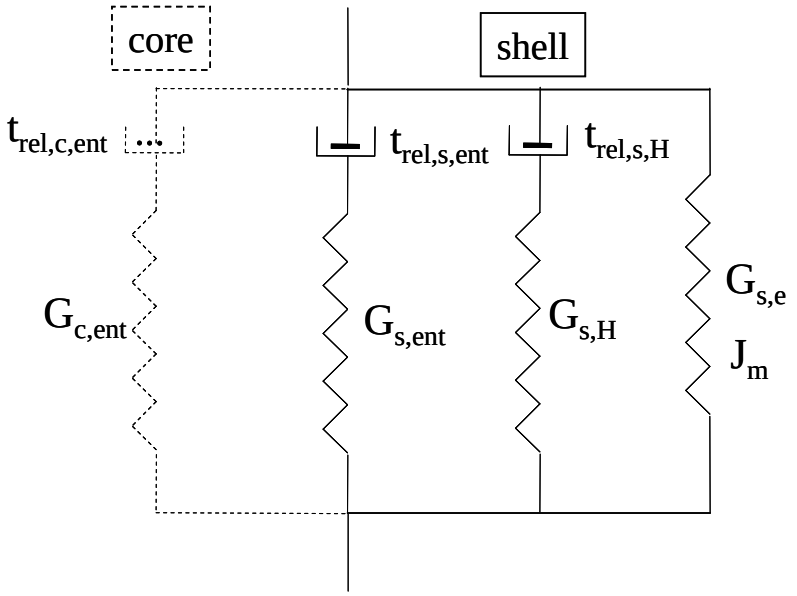

Figure 5-36. Adaptation of the viscoelastic-hardening model in the case of a core-shell particle.

Figure 5-37 is aimed at showing how each fitting parameter can be related to a molecular feature.

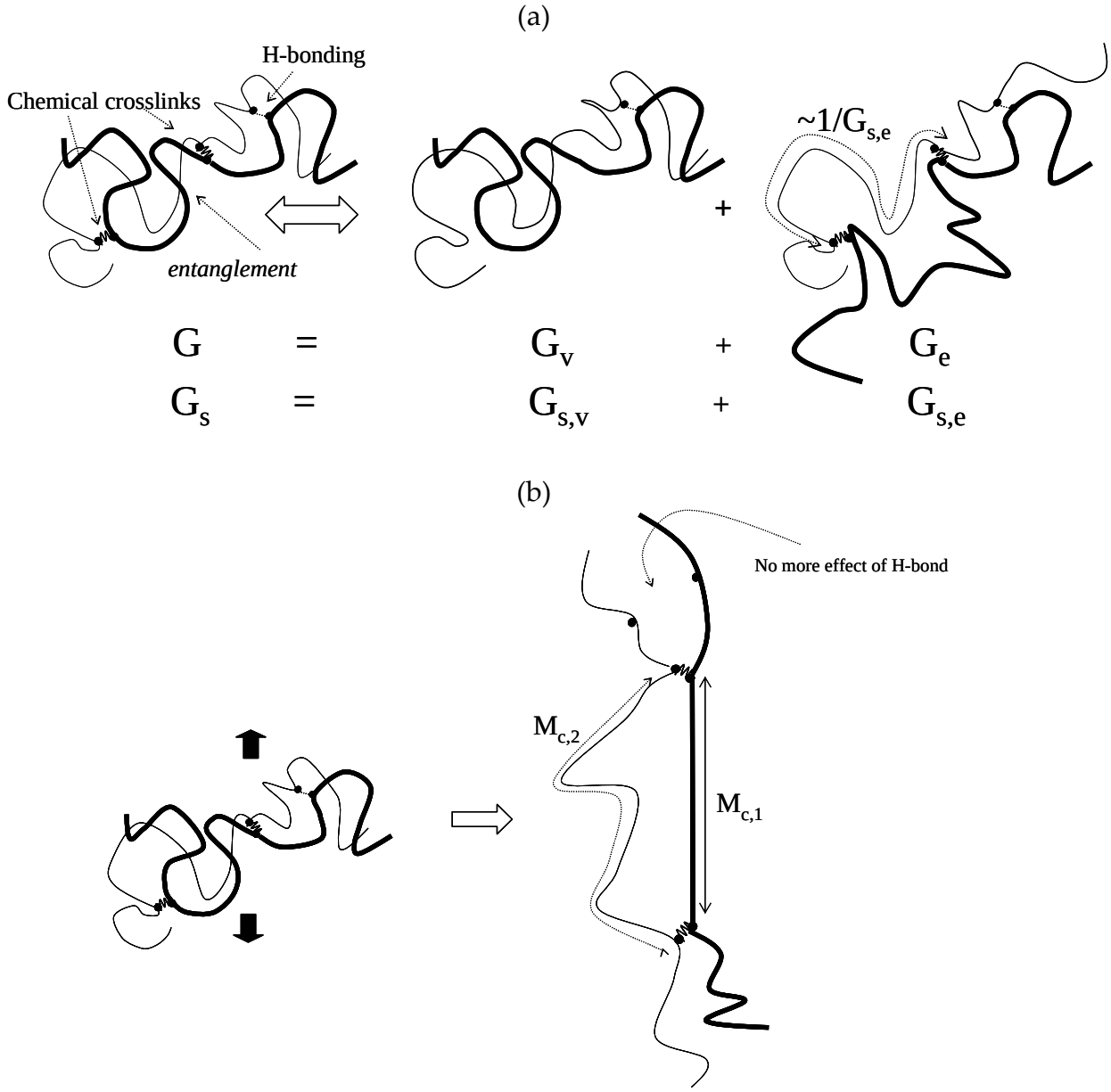

Figure 5-37. (a) Relationship between G G, G_v and G_e (or alternatively to G_s, $G_{s,v}$ and $G_{s,e}$) and molecular features of the structure. (b) Schematics showing how J_m can be interpreted.

- *Behavior in the linear regime*

Let us come back to the experimental results. A first test of our interpretation is the evolution of the Young's modulus as a function of the shell thickness. A value of the linear modulus is also obtained from our viscoelastic-hardening model by $3(G_v+G_e)$. Comparison between both results is shown on Figure 5-38. Even if differences between the three materials are low, a minimum is observed for C45S55.

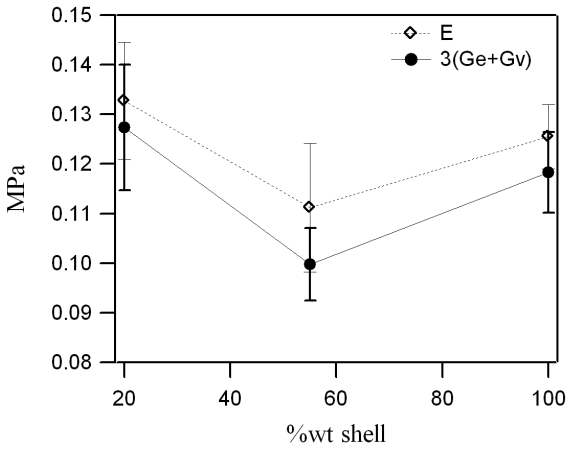

Figure 5-38. Triangles: E measured directly on tensile curves, circles: $3(G_v+G_e)$ from the viscoelastic-hardening modeling.

One could be naturally tempted to think that such an evolution is the result of the simultaneous decrease in the volume fraction of the crosslinked phase (leading to an increase in the effective modulus of the more densely chemically crosslinked domain) with the decrease in its surface fraction (leading to a lower contribution of the shell in the overall shear modulus of the structure). Indeed, evolution of the modulus of a heterogeneous structure (called E) as a function of the volume fraction (X_v) of the crosslinked phase is not obviously predicted. Depending on how much the highly crosslinked phase is stiffer than the less crosslinked one (characterized by its modulus E_c), the evolution of the overall modulus can be completely different. Two examples are displayed in Figure 5-39. Empty circles correspond to the situation where E/E_c of the particle equal 4.7. In that case, the modulus of the overall structure tends to decrease for volume fractions of the crosslinked phase between 0% and 40% and to increase after. In the other hand, if calculations are made considering a homogeneous particle with a lower crosslinking density (squares of Figure 5-39), the modulus starts to decrease significantly between 0% and 60% and tends to increase a little after.

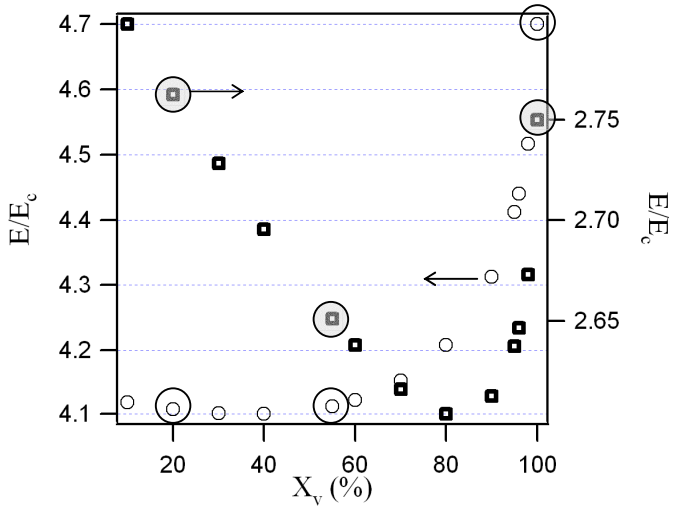

Figure 5-39. Evolution of the theoretical Young's modulus E of a heterogeneous structure made of a slightly crosslinked phase (characterized by its modulus E_c) and a more crosslinked one as a function of the volume fraction of the more crosslinked phase. The total number of crosslink points is independent of the structure of the particle. Number of crosslinks is given by the ratio E/Ec which is equal to 4.7 for the circles and to 2.75 for the squares.

In our case, from $(G_e+G_v)/G_v$, an estimate of the increase in the modulus of C0S100 due to the presence of the crosslinks is equal to 1.13, and a continuous decrease in the modulus would be expected when $E/E_c = 1.13$.

However, our situation is much more complicated since only the part of the modulus due to the presence of DAAM groups ($G_{s,e}$ and $G_{s,H}$) is changed when decreasing the volume fraction of the shell while the major part which comes from the topological constraints induced by the entanglements and branches is not affected. And finally a very slight increase in the modulus is found.

So, simple predictions of the evolution of the unrelaxed Young's modulus of a heterogeneous structure can not explain the experimentally observed evolution. In this study small strain behavior is most probably mainly controlled by the cores. The lower value observed in the case of C45S55 could thus appear surprising but is probably the consequence of some interdiffusion between shell and core before crosslinking which may result in a structure different from the theoretically predicted one. This can probably also explain why C45S55 seems softer also at intermediate strains.

- *Properties of the crosslinked network*

$G_{s,e}$ and J_m are both related to the presence of chemical crosslinks. While $G_{s,e}$ depends on small strain behavior, J_m is only governed by the ultimate strains properties. An estimate of an average molecular weight between crosslinks is possible, either from $G_{s,e}$ or from J_m. It can be written as:

$$M_{cG} = \rho RT / G_{s,e} \qquad \textbf{Eq. 5-18}$$

$$M_{cJ} \cong J_m M_{mono} \qquad \textbf{Eq. 5-19}$$

where ρ is the mass per volume of the adhesive, R is the gas constant, T the temperature and M_{mono} the average molecular weight of monomers (M_{mono}~159g/mol for our system).

If we assume that a connected network is formed, M_{cG} would represent an average value of M_c, while M_{cJ} would be more representative of the lowest value of M_c. The evolution of these M_c as a function of the thickness of the shell is shown on Figure 5-40. A quasi linear increase in M_{cG} as a function of the shell thickness is obtained. Values obtained from J_m are significantly lower.

Two possible reasons can explain that. Either this discrepancy comes from an artifact of the model which underestimates the contribution in the value of $G_{s,e}$ or it is due to a migration of the hydrophilic DAAM groups towards the surface of the particle. This migration tends to decreases the thickness of the shell where crosslinks are effectively localized. This assumption is supported by the fact that such a difference between $\rho RT/G_{s,e}$ and $J_m M_{mono}$ has not been found when the shell had a higher gel content (in the case of C80d0.1S20D0.4 for example, results are not shown here.)

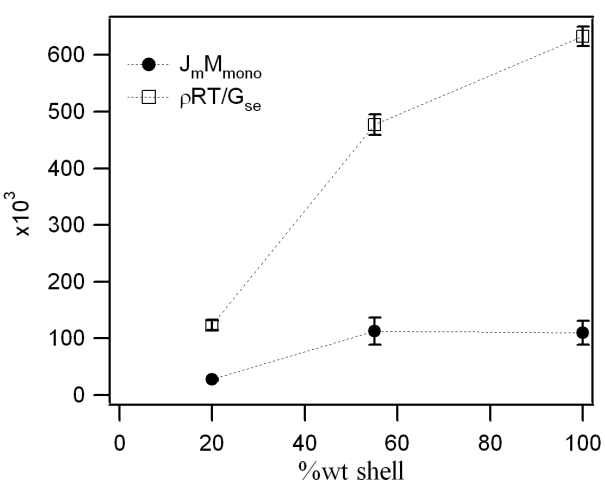

Figure 5-40. Filled circles: Evolution of the molecular weight between crosslinks as a function of the thickness of the shell predicted from J_m. Empty squares: Evolution of the molecular weight between crosslinks predicted from $G_{s,e}$ as a function of the thickness of the shell.

What is also to note is the lower predicted value of M_{cJ} for C0S100 than that of C45S55. This clearly means that the lowest value of M_c is higher for C45S55. However, again this is ambiguous to explain. Either it could be due to a more efficient crosslinking reaction for C0S100 or it is due to the fact that the crosslinked network of C0S100 is more heterogeneous leading to a high polydispersity in the distribution of M_c.

Finally, we have shown that caution needs to be taken when interpreting mechanical results from the molecular point of view. This is mainly due to the fact that while we draw our particles as perfect core-shell structures, in reality the interplay of thermodynamics during and after the synthesis causes certainly some interdiffusion between the core and the shell and some migration of polar components toward the outside of the particle. As a consequence, C45S55 is softer and C0S100 is more crosslinked than what would be theoretically predicted from our simplified models.

b. Effect of rheology on adhesive properties

Let us now continue with the effect of the rheology on adhesive properties. Regardless of the DAAM distribution, probe surface and debonding velocities, the debonding mechanism was similar and could be divided into the following stages: cavitation, lateral propagation, fibril extension and final detachment of the adhesive from the probe. Cavity nucleation and growth is mostly controlled by linear rheological properties and in the absence of quantitative local measures of stress, it is difficult to differentiate the three materials. Then, when fibrillation starts, the nonlinear regime kicks in. Since the stress-strain curve before the peak stress is similar for the three materials, we will concentrate on the behavior at intermediate and high strains. Ideally, one would like to interpret tack curves from simpler deformation properties obtained from tensile experiments.

Tensile experiments were performed at a crosshead velocity of 50 mm.min^{-1}. This corresponds to an initial strain rate of about 0.05 s^{-1}, nearly the same strain rate is experienced by the material during tack experiments at 10 µm.s^{-1} when it begins to form a fibril structure. Thus, let us starts with result at 10 µm.s^{-1}.

Uniaxial elongation results emphasized the more elastic behavior of the homogeneously crosslinked particle (C0S100) and the more viscoelastic and dissipative behavior of the heterogeneously crosslinked core-shell particles (C80S20 and C45S55). On PE, the adhesive energy (or alternatively fibrillation energy) is nearly the same for the two-core shell particles while it is significantly lower for the homogeneous particle. Thus it seems that the more the adhesive is viscoelastic the higher is the fibrillation energy on PE. G_v/G_e seems a good predictor of adhesion on PE (Figure 5-41-a). It is interesting to note that G_v/G_e which is sensitive to the finite extensibility J_m is a better predictor than W_{diss}/W_e which is purely an intermediate strain measure of dissipation.

On stainless steel, the increase in the thermodynamic work of adhesion leads to an increase in the critical energy release rate $\mathcal{G}_c$. Interfacial interactions are stronger, more energy is needed to propagate cracks at the interface and the bulk material is thus allowed to experience greater stress and strain upon pull-off. Bulk high strains properties are in that case really important in controlling adhesion. ε_{max} is not only governed by dissipation and viscoelasticity but depends also on the cohesion and deformability of the material. The earlier detachment of C0S100 can be attributed to its more elastic behavior. But when comparing C80S20 and C45S55, the higher fibrillation energy obtained for the core-shell with the thicker shell can be explained by its lower cohesion (measured by G_v+G_e). Evolutions of W_{adh} or W_{fib} on stainless steel seem better described by the ratio between G_v/G_e and $3(G_v+G_e)$ as can be seen on (Figure 5-41-b). This parameter is analogous in spirit to the G''/G'^2 defined in chapter 4 for linear rheology.

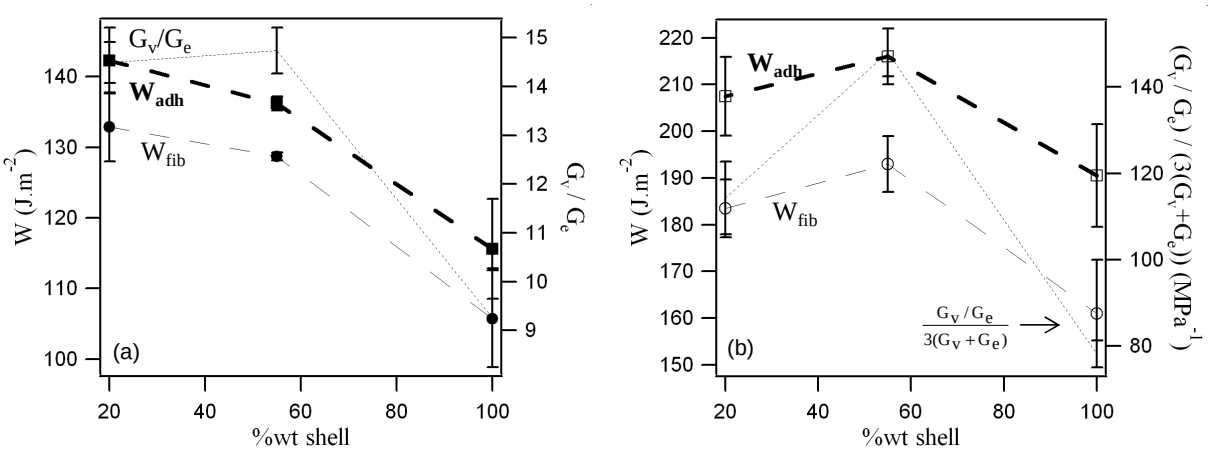

Figure 5-41. (a) Comparison between W_{adh} and W_{fib} on PE at 10 µm.s^{-1} and G_v/G_e. (b) Comparison between W_{adh} and W_{fib} on stainless steel at 10 µm.s^{-1} and $(G_v/G_e)/(3(G_v+G_e))$.

On PE, increasing the debonding velocity leads to a decrease in the difference between the three materials. If dissipation at intermediate strains is due to viscous relaxation of the polymer chains, the higher the strain rate the shorter the length scale where movements are allowed. Thus, at 1000 µm.s^{-1} adhesion on PE becomes independent on crosslink distribution.

On stainless steel, as the debonding velocity increases, the nonlinear strain hardening brought about by the finite extensibility of the polymer chains between chemical crosslinks becomes important in controlling adhesion. Sensitiveness of tack curves on hardening is indeed clearly shown by the stress increase during the fibrillation stage (Figure 5-30). At 100 and 1000 $\mu m.s^{-1}$, the longer fibrillation plateaus of C45S55 compared to that of C80S20 could be explained by its higher deformability measured by J_m. The crosslinked network of the core-shell with the thicker shell is probably not as well connected. As a result, a cohesive debonding (leaving traces of residues on the probe surface) has been even observed at 100 $\mu m.s^{-1}$.

On both surfaces stainless steel and PE, the more elastic behavior of the homogeneous particle is also evident through its nearly constant ε_{max} values as the debonding velocity increases.

To conclude we have shown how adhesive performance can be predicted or interpreted using tensile results. On PE, best performance is reached in the case of the core-shell particle with the thinner shell. This is mainly attributed to its high ability to dissipate energy in the intermediate strain regime. On stainless steel, on the other hand, performance seems governed by a balance between dissipation, cohesion and deformability and the best performance has been obtained in the case of the core-shell particle with the thicker shell. The cohesive debonding observed at 100 $\mu m.s^{-1}$ demonstrated however a lack of cohesion of this material, and this is consistent with its low shear resistance (Figure 5-32- (b)).

Carelli et al.[26] recently showed that adhesion on low energy surfaces is mainly governed by the ability of the adhesive layer to dissipate energy in the linear regime while adhesion on stainless steel is mainly governed by the ability of the material to deform. Results we obtained are in accordance with these observations and can be viewed as a possible extension of them in the nonlinear regime.

5.3.3. How to further improve adhesive performance: results on more complex systems

In the case of interfacially crosslinked particles made of soft core and a soft shell, previous results led to a clear conclusion that the optimum adhesive performance should be achieved through a combination of a highly viscoelastic and dissipative majority phase (for the deformability) and a lightly crosslinked one (for the cohesion). It could be tempting to further improve this performance through an optimization of the latex synthesis parameters. The strategy retained is to independently tune cohesion (decreasing the amount of CTA in shell) and adhesion (increasing the amount of CTA in the core). This study has been performed on particles of the more complex series (Table 5-2). All these particles have a thin shell with a weight core:shell ratio equals to 80:20.

5.3.3.1. Increase in the gel content of the shell (less CTA in the shell)

Let us start with the effect of a decrease in the amount of CTA in the shell as a tool to increase the cohesion. Results are obtained on latexes at which 100% of ADH (compared to the stoichiometric amount) has been added. Stress vs. strain tack curves obtained on stainless steel probe at debonding velocities of 10 and 1000 µm.s^{-1} are shown on Figure 5-42. Decreasing the amount of CTA in the shell leads to an earlier detachment at 10 µm.s^{-1}. But what is more interesting to note is that it also leads to a slight increase in the stress level in the fibrillation stage which suggests a better shear resistance and has nearly no influence on W_{adh} at 1000 µm.s^{-1} (from the area under the curves, the exact values are not given here) which suggests not much change in peel performance.

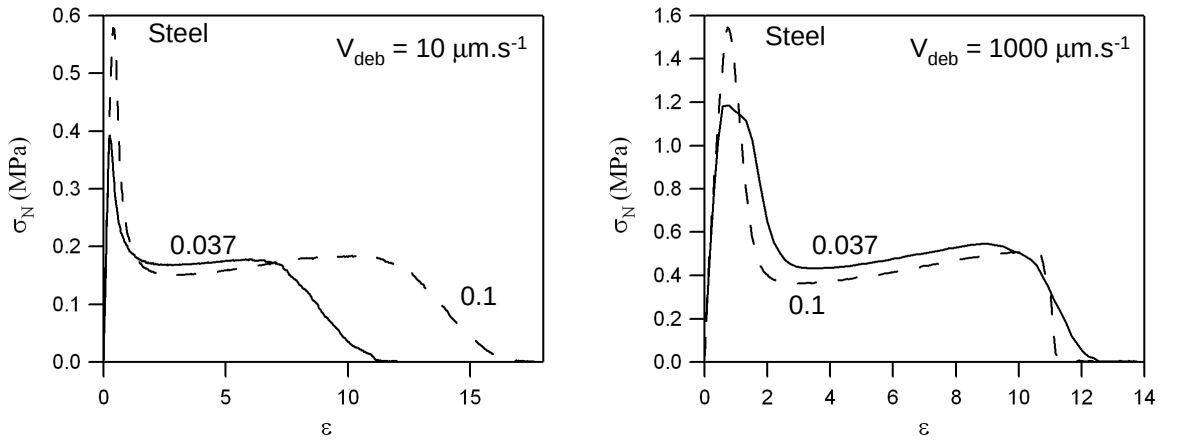

Figure 5-42. Stress vs. strain tack curves of two particles which differ by their amount of CTA in the shell. Tests were performed on stainless steel at debonding velocities of 10 and 1000 µm.s^{-1}.

Looking either at raw tensile curves or at the corresponding reduced stress representations (Figure 5-43), decreasing the amount of CTA leads to a significant increase in stress levels and the effect is even more pronounced at large strains. This is directly visible at intermediate and high strains and Young's modulus or $3(G_v+G_e)$ indicates that this is also the case in the linear regime (an increase in E from 0.13 MPa to 0.17 MPa was obtained).

While the viscoelastic modulus G_v is nearly unchanged (Table 5-6) (the difference observed may be attributed to a slight change in the overall structure of the core as what has been already discussed), both C_{hard} and G_e, related to properties of the crosslinked network, are significantly increased. As a consequence G_v/G_e is significantly reduced. Similarly, while W_{diss} is nearly the same, W_{diss}/W_e decreases significantly. All these observations mean that in one hand, as the amount of CTA in the shell decreases, local viscoelasticity of the core is kept intact, and in the other hand, a more tightly crosslinked shell network is created decreasing the overall viscoelasticity of the adhesive through an increase in its elasticity. And the observed decrease in W_{adh} at low debonding velocities (Figure 5-44) may be the consequence of this loss of viscoelasticity.

If the network is really more tightly crosslinked, the observed decrease in J_m (Table 5-6) was expected. But an interesting result is that this reduction is only relatively low and has not much influence on ε_{max} at 1000 $\mu m.s^{-1}$ (Figure 5-42) and is not detrimental to adhesive energy. On the contrary, through a decrease in the amount of CTA in the shell, an increase in adhesive energy at high debonding velocities has been obtained. This is the result of the slight increase in the fibrillation plateau level. Relative to the 0.1% CTA sample this is probably due to the shorter relaxation time seen in the value of the *De*.

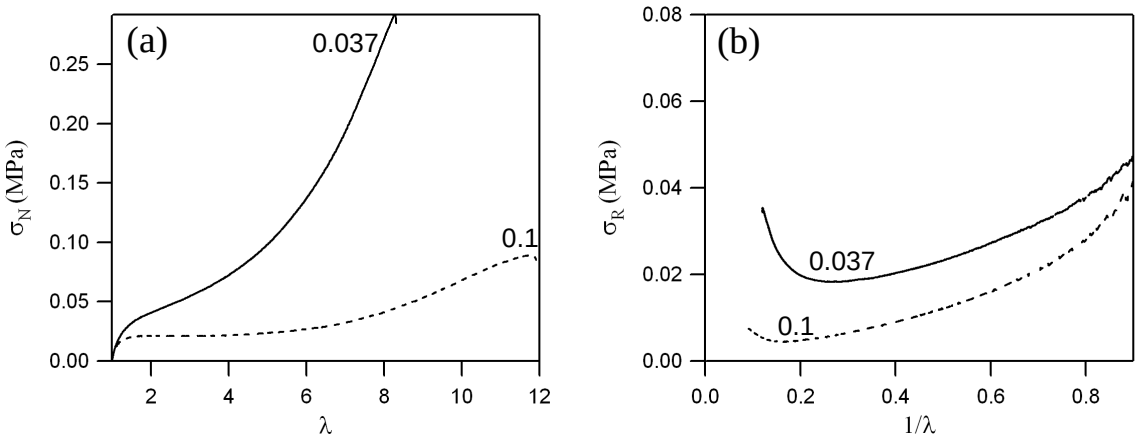

Figure 5-43. Tensile results of C80S20 (%CTA_{shell} = 0.1%) (dashed line) and C80d0.1S20D0.4 (%CTA_{shell} = 0.037%) (solid line). (a): Nominal stress vs. strain tensile curves. (b): The corresponding Mooney-Rivlin representations.

wt% CTA in the shell	G_v (kPa)	G_e (kPa)	J_m	De	G_v/G_e	$3(G_e+G_v)$ (kPa)	W_{diss} ($J.m^{-3}$)	W_{diss}/W_e
0.1	39.7 (± 3.10)	2.74 (± 0.212)	174 (± 12.7)	0.220 (± 0.021)	14.5 (± 0.418)	127 (± 9.91)	17400 (±702)	0.831 (±0.029)
0.037	58.8 (± 4.01)	16.0 (± 0.507)	111 (± 4.60)	0.114 (± 0.021)	3.68 (± 0.204)	224 (± 13.0)	22500 (± 913)	0.398 (± 0.007)

Table 5-6. Fitting parameters and dissipated energy obtained for C80S20 and C80d0.1S20D0.4.

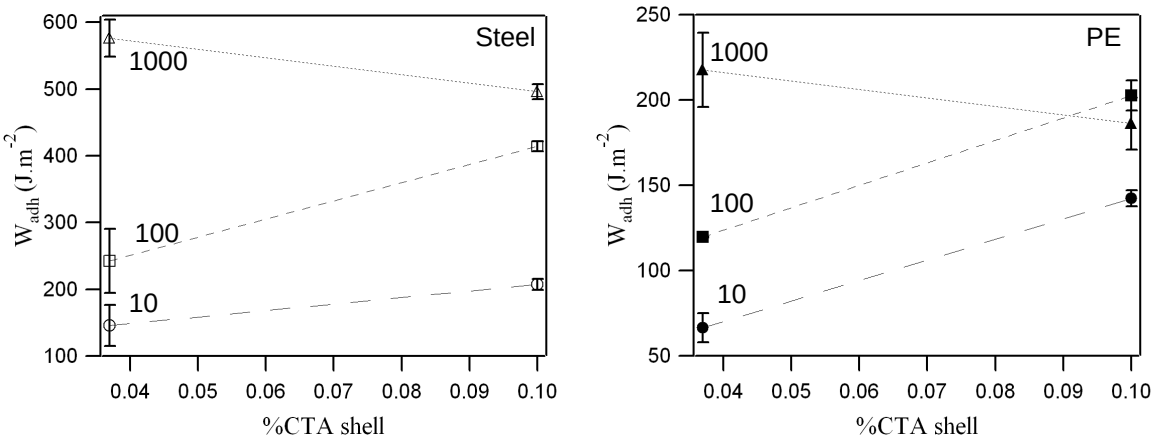

Figure 5-44. Adhesive energy on stainless steel (left) and PE (right) as a function of the amount of CTA in the shell at debonding velocities of 10, 100 and 1000 µm.s^{-1}

From this example, decreasing the amount of CTA in the shell seems to be a good tool to improve cohesion through the creation of a stiffer interfacial crosslinked network. What is even more interesting is that, although it is a little bit detrimental to adhesion at low and intermediate debonding velocities, it leads to a slight increase in adhesion energy at higher velocities which suggests that peel performance is also increased.

5.3.3.2. Increase in the gel content of the core (less CTA in the core)

After successfully showing that shear performance could be enhanced through a decrease in the amount of CTA in the shell, we focused on the possibilities to optimize adhesion. For that, the strategy consisting in the reduction in CTA content of the core has been investigated.

Since viscoelastic properties are mainly governed by the core and since the major part of the particles is made of core polymer chains, a change in viscoelastic behavior in the linear regime could be expected. Evolutions of tan(δ) as a function of the frequency for three adhesives, differing by their amount of CTA in the core, are shown in Figure 5-45 (the core/shell ratio of all the three particles is equal to 80/20, their amount of CTA in the shell is 0.037 wt% and results are obtained on uncrosslinked particles with ADH). As expected, a decrease in the gel of the core leads to a non negligible increase in dissipative properties in the linear regime even at high frequencies. In all cases, tan(δ) is relatively high (always superior to 0.5 in the range of frequencies between 0.1 and 10 Hz) which suggests that a fibrillation structure will always be created during the debonding process. The increase means essentially that the ability for this structure to form is enhanced by a raise of the CTA content of the core.

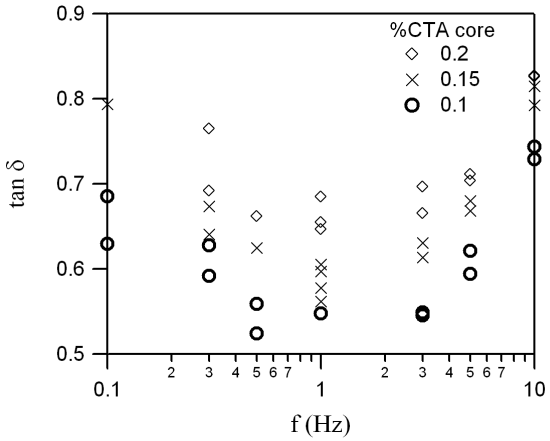

Figure 5-45. Evolution of tan(δ) as a function of the frequency in the linear regime. Rheological measurements have been performed on particles which differ by their amount of CTA in the core.

On Figure 5-46 are shown tack results obtained on stainless steel at 10 and 1000 µm.s^{-1} on fully crosslinked films (formulations are the same as that of Figure 5-45 to which ADH has been added in stoichiometric amounts). Increasing the amount of CTA in the core leads interestingly to a significant increase in the length of the fibrillation plateau. This is however accompanied by a large decrease in its stress level. This means that the adhesive containing the highest level of CTA in the core is more dissipative but also globally softer.

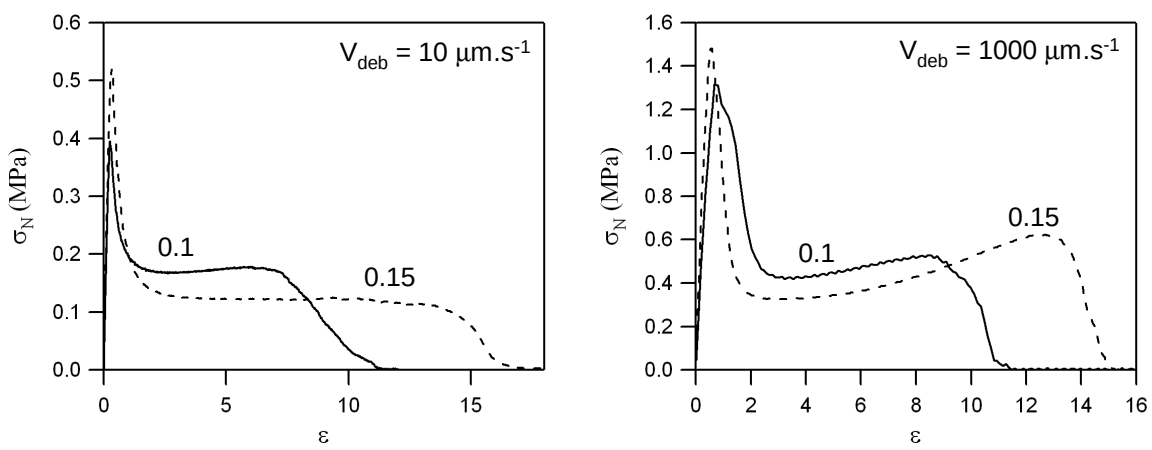

Figure 5-46. Stress vs. strain tack curves of two particles which differ by their amount of CTA in the core. Tests were performed on stainless steel at debonding velocities of 10 and 1000 µm.s^{-1}.

On stainless steel as on PE, the adhesive energy increases as a function of the CTA amount, and this trend is the same at all debonding velocities (Figure 5-47). The most interesting is perhaps the observed improvement at 1000 µm.s^{-1}. This is due to an increase in the fibrillation plateau length as it is shown in Figure 5-46, and this could be due to higher dissipative properties of core macromolecules even at high debonding velocities. An improvement of peel performance is thus reasonably predictable.

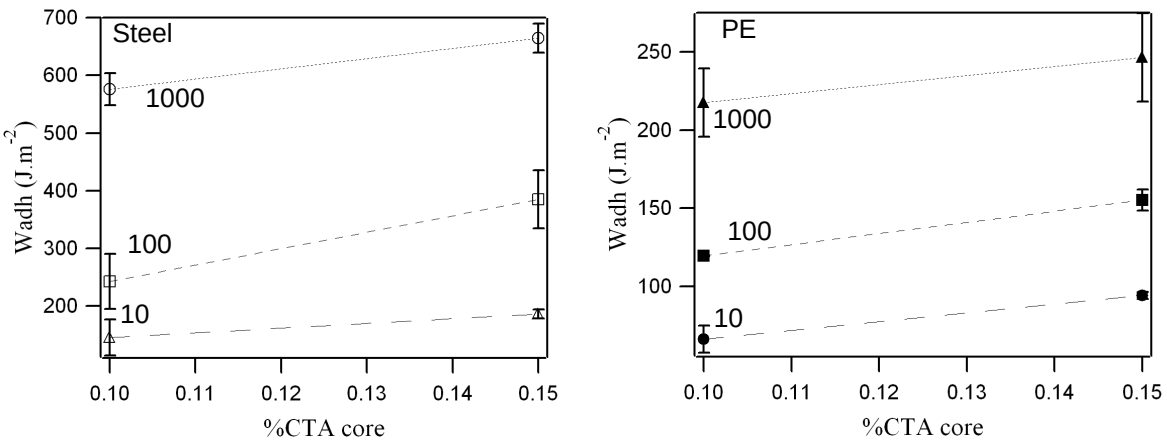

Figure 5-47. Adhesive energy on stainless steel (left) and PE (right) as a function of the amount of CTA in the shell at debonding velocities of 10, 100 and 1000 µm.s^{-1}

Tensile results are shown on Figure 5-48. The decrease in stress values as the amount of CTA in the core increases is consistent with the observed lower fibrillation plateau. Young's modulus is also significantly decreased (from 0.17MPa to 0.09MPa). Not much change is observed on the overall shape of the curve. When comparing Figure 5-43-(b) and Figure 5-48-(b) and looking at stress levels, one observes that the effect of the amount of CTA in the shell increases as the deformation increases. On the contrary, the effect of the amount of CTA in the core seems more pronounced at lower strains. It is also interesting to note that even though 80 wt% of the particle is made of the core, a change in the CTA amount in the core has a similar effect on cohesion as when a similar change is made in the shell below $\lambda = 5$ and much lower effect on cohesion at larger strains.

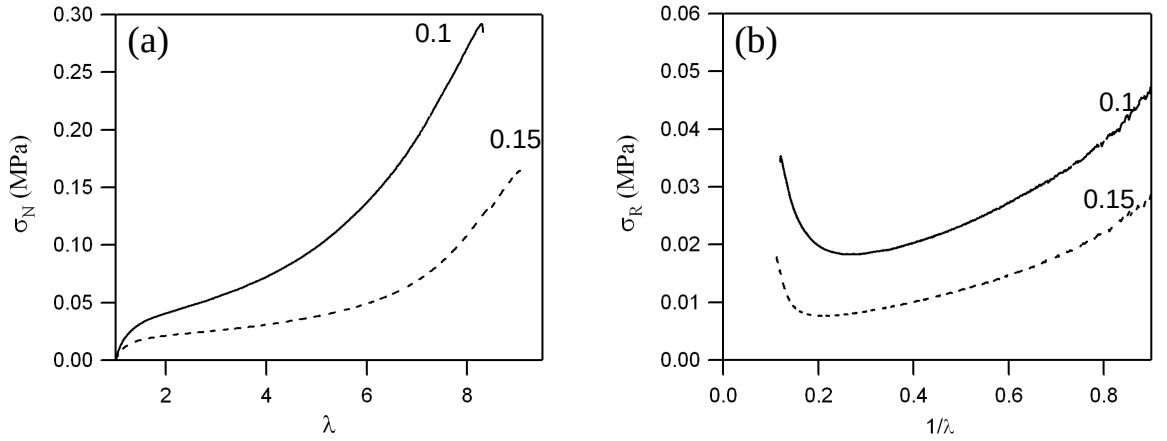

Figure 5-48. Tensile results of C80d0.15S20D0.4 (%CTA$_{core}$ = 0.15%) (dashed line) and C80d0.1S20D0.4 (%CTA$_{core}$ = 0.1%) (solid line). (a): Nominal stress vs. strain tensile curves. (b): The corresponding Mooney-Rivlin representations.

Results of tensile fitting are shown on Table 5-7. Both G_v and G_e are affected by a change in the amount of CTA in the core. While decreasing the amount of CTA in the shell had not much effect on G_v and led to a significant increase in G_e, increasing the amount of CTA in the core tends to significantly decrease both G_v and G_e. A decrease in C_{hard} is also easily observable (Figure 5-48-(b)). This results in a slight increase in the ratio G_v/G_e. Similar trends are observed for W_{diss} and W_e and the result is a slight increase in W_{diss}/W_e.

wt% CTA in the core	G_v (kPa)	G_e (kPa)	J_m	De	G_v/G_e	$3(G_e+G_v)$ (kPa)	W_{diss} ($J.m^{-3}$)	W_{diss}/W_e
0.1	58.8 (± 4.01)	16.0 (± 0.507)	111 (± 4.60)	0.114 (± 0.021)	3.68 (± 0.204)	224 (± 13.0)	22500 (± 913)	0.398 (± 0.007)
0.15	28.0 (± 2.27)	5.04 (± 0.301)	103 (± 7.62)	0.267 (± 0.032)	5.56 (± 0.282)	99.2 (± 7.52)	14900 (± 914)	0.547 (± 0.014)

Table 5-7. Fitting parameters and dissipated energy obtained for C80d0.15S20D0.4 and C80d0.1S20D0.4. (An example of a fitted tensile curve of C80d0.15S20D0.4 is shown in appendix II).

The decrease of G_v lets us thinking that the amount of CTA in the core highly affects the overall cohesion of the material through a significant decrease in the shear modulus of the core. Moreover, the decrease in G_e and C_{hard} suggests that the amount of CTA in the core influences the efficiency of the interfacial crosslinking reaction occurring in the shell. This last point is however not supported by values of J_m which predicts an unchanged molecular weight between crosslinks. This also means that a highly connected crosslinked network is formed in both materials.

Finally, an increase in the CTA amount in the core is an effective way to improve adhesion while retaining an acceptable cohesion. This is confirmed by shear and peel results shown on Table 5-8. The core-shell with a large amount of CTA in the core based adhesive is better suited for PE applications while lower amount of CTA in the core is required to avoid a cohesive debonding on stainless steel.

		%CTA core	
		0.1	**0.15**
Peel 24h 180° (FTM1) (N/25mm)	**Stainless steel**	11.97 (± 0.50)	19.61(± 0.17)ct[1]
	HDPE plate	6.04(± 0.31)	7.63(± 1.15)
Shear (FTM8) (min)	**Stainless steel (1kg, 1 inch^2)**	5013(± 469)	1487(± 396)

[1] Cohesive transfer

Table 5-8. Standard adhesive tests results of C80d0.1S20D0.4 ($\%CTA_{shell}$ = 0.1%) and C80d0.15S20D0.4 ($\%CTA_{shell}$ = 0.15%).

5.3.3.3. Effect of DAAM content in the shell

All adhesives studied up to now were made of particles containing 0.4 wt% of DAAM groups distributed only in the shell of the particles. Optimization of both the amount of the CTA in the shell and in the core led to some promising adhesive results. But it is important to specify that these performances are also in part due to an optimization of the amount of crosslinkable DAAM groups. The following section is aimed at comparing results of adhesives made of particles which differ from their amount of DAAM groups (C80d0.1S20D0.4 and C80d0.1S20D1.1 of Table 5-2) but with equal number of chemical crosslinks (the same quantity of ADH in moles is added). More precisely, C80d0.1S20D0.4 with 100 % of ADH films (0.400 wt% DAAM activated) is compared to C80d0.1S20D1.1 with

36.4 % of ADH films (0.400 wt% DAAM activated + 0.700 wt% uncrosslinked DAAM groups). This means that there are some free DAAM groups in C80d0.1S20D1.1.

Tack results (Figure 5-49) showed that regardless of the debonding velocity, an increase in the amount of DAAM groups leads to a decrease in the length of the fibrillation plateau. An increase in the stress level of the fibrillation plateau is also observed and this is even more pronounced as the debonding velocity increases. An earlier debonding is also obtained on PE (results are no shown here) without any increase in the fibrillation plateau level.

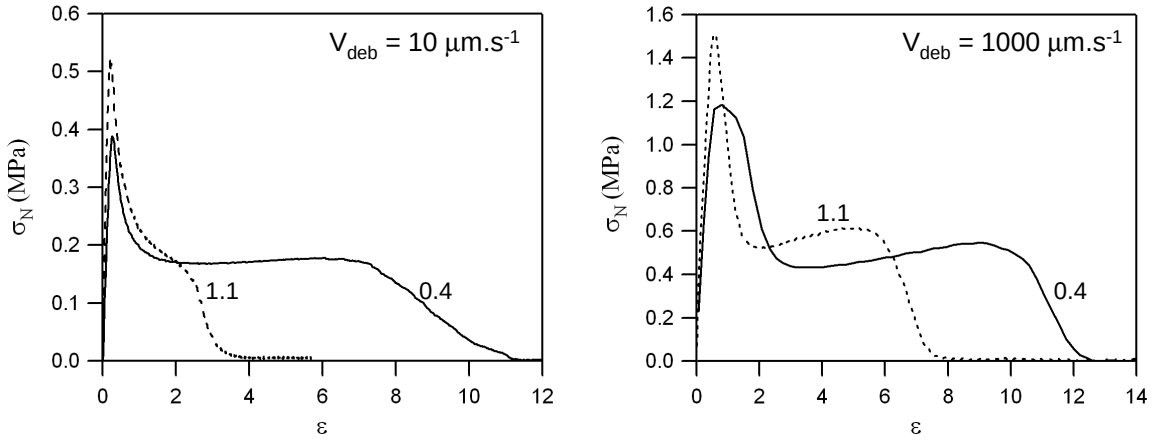

Figure 5-49. Stress vs. strain tack curves of two particles which differ by their amount of DAAM groups (solid line: C80d0.1S20D0.4 with wt% DAAM = 0.4%, dashed line: C80d0.1S20D1.1 with wt% DAAM = 1.1%). Tests were performed on stainless steel at debonding velocities of 10 and 1000 µm.s^{-1}.

Both on stainless steel and on PE probes and at all debonding velocities, a decrease in the adhesive energy has been found. This is the result of the early detachment of the fibrils from the probe. Even if the fibrillation stress level is sometimes increased, it is shadowed by the significant decrease in ε_{max} (on stainless steel at 1000 µm.s^{-1} adhesive energy is found to be the same for the two materials).

Nonlinear tensile results are shown on Figure 5-50. Similar stress levels are obtained. But the most interesting thing to note is the significant change of the shape of the nominal stress vs. strain curve. The pronounced softening at intermediate strains obtained with %wt DAAM = 0.4%, nearly disappears when wt% DAAM = 1.1%.

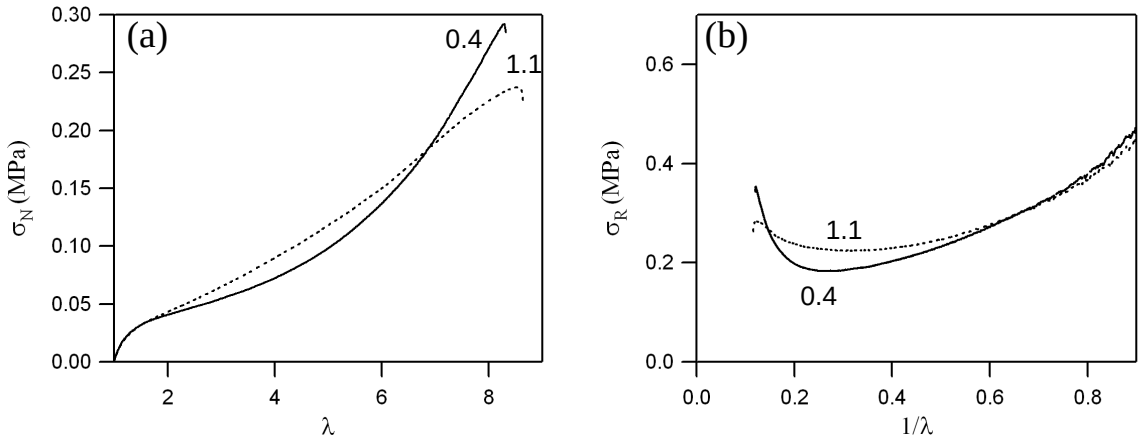

Figure 5-50. Tensile results of C80d0.1S20D0.4 (%DAAM = 0.4%) (solid line) and C80d0.1S20D1.1 (%DAAM = 1.1%) (dashed line). (a): Nominal stress vs. strain tensile curves. (b): The corresponding Mooney-Rivlin representations.

Since stress levels are similar for both materials, W_{diss} can be directly used as a tool for comparison of energy dissipated at intermediate strains. Results show that an increase in the amount of free crosslinkable groups leads to a decrease in dissipation (Table 5-9). The dissipation contribution compared to the more elastic one is also decreased (see G_v/G_e and W_{diss}/W_e).

wt% DAAM groups	G_v (kPa)	G_e (kPa)	J_m	De	G_v/G_e	$3(G_e+G_v)$ (kPa)	W_{diss} (J.m^{-3})	W_{diss}/W_e
0.4	58.8 (± 4.01)	16.0 (± 0.507)	111 (± 4.60)	0.114 (± 0.021)	3.68 (± 0.204)	224 (± 13.0)	22500 (± 913)	0.398 (± 0.007)
1.1	44.8 (± 5.53)	20.5 (± 0.415)	203 (± 16.9)	0.087 (± 0.014)	2.19 (± 0.246)	203 (± 16.9)	18000 (± 1150)	0.281 (± 0.018)

Table 5-9. Fitting parameters and dissipated energy obtained for C80d0.1S20D0.4 and C80d0.1S20d1.1. (An example of a fitted tensile curve of C80d0.1S20D1.1 is shown in appendix II).

Concerning properties of the crosslinked network, when looking at G_e, it seems that the presence of DAAM groups uncrosslinked with ADH participates to the increase in G_e. This could be explained by the ability of DAAM groups to form hydrogen-bonds. This leads to the formation of additional nonpermanent crosslinks. But no increase in G_v has been observed (on the contrary G_v tends to decrease a little). The observed increase in G_e is retrieved when looking at C_{hard} (Figure 5-50-(b)). The characteristic time of hydrogen-bonds is most probably higher than that of disentanglements. This finally results in an increase in the elastic behavior of the material leading to a less pronounced softening. This example shows how difficult it is to choose an optimal methodology for the measurement of the dissipation when using reduced stress representation. Since between $1/\lambda = 1$ to $1/\lambda = 0.5$ slopes of the curves are identical one could have been tempting to predict a similar ability to dissipate energy for both materials.

At ultimate strains, however, the effect of free DAAM groups in increasing cohesion is no more observed and an increase in J_m is even obtained. This means that the shell is less tightly crosslinked as the amount of free DAAM groups increases.

Moreover, it is interesting to note that from tensile results obtained at a strain rate nearly equal to 0.05 s^{-1}, a decrease in the overall cohesion is obtained (measured by $3(G_e+G_v)$ and also evidenced by the decrease in the stress at break) when the amount of free DAAM groups increases while from tack results at significantly higher strain rates (strain rate is about 3 s^{-1} at the beginning of the fibrillation plateau when the tack test is performed at 1000 $\mu m.s^{-1}$) an increase in the cohesion is expected. This may be due to the fact that at low strain rates, hydrogen-bonds do not participate in the increase in cohesion while they play the role of permanent crosslinks and are effective in increasing cohesion at higher strain rates. This is consistent with results of shear resistance which show a decrease as the amount of free DAAM increases.

The simultaneous decrease in adhesion and cohesion resulting from an increase in DAAM group content has been explained as follows:

(i) The change in dissipation at intermediate strain and elastic behavior could be the result of the formation of non permanent hydrogen-bonds between free DAAM groups.

(ii) The increased DAAM concentration in the shell may make crosslinking reaction within the particles statistically more probable than between DAAM belonging to two different particles. And this could lead to a decrease in the cohesion of the structure of the dried film at ultimate strains and at low strain rates.

To conclude concerning the effect of DAAM content in the shell, there is probably a critical value above which the discussed benefit of the interfacial crosslinking is lost as a consequence of a more favorable crosslinking reaction within the particles themselves. Non permanent interactions between the uncrosslinked DAAM groups have also probably a detrimental effect on dissipative properties of core macromolecules at intermediate strains.

5.4. Conclusion

In essence we have shown that an interfacial crosslinking during drying of latex provides a mean to have a very light level of crosslinking which is however entirely connected through the material. This is in contrast to the classical type of crosslinking which takes place within the particle. This low level of crosslinking does not modify significantly the small-strain modulus but significantly enhances the large strain strength and allows to keep a very soft and viscoelastic core. In traditional emulsion polymerization, the same balance is very difficult to achieve because any increase in level of chain transfer agent leads to a modification of small and large strain properties at the same time and does not influence the softening.

We also have demonstrated the possibility to independently tune cohesion and adhesion taking advantage of the possibility to structure particle using emulsion polymerization. Cohesion can be enhanced playing with properties of the shell while adhesion can be improved adjusting core properties.

Accounting for high strain results of highly viscoelastic materials, we also went beyond the simpler use of either linear viscoelasticity or nonlinear elastic properties. We showed that deformation behaviors could be well described using a viscoelastic-hardening model. We have seen that best performances are obtained with a pronounced softening at intermediate strain followed by a well defined hardening and the model have made possible a quantification of them.

APPENDICES

I. Constant Hencky strain rate vs. constant nominal strain rate solutions

It could be interesting to compare numerical (modeling developed by Yamaguchi) and analytical solutions obtained considering a constant Hencky strain rate and a constant nominal strain rate respectively. In one hand nominal stress evolution has been obtained putting given values of G_v and t_{rel} in a numerical program, in the other hand, stress vs. strain curves have been obtained putting the same values of G_v and t_{rel} in the preceding analytical equation (Eq. 5-8). Some results obtained are shown on Figure 5-51. One can note that the analytical solution tends to predict that the maximum is reached a bit later and at a lower level of stress. This means that the analytical solution underestimates t_{rel} and overestimates G_v. The discrepancy between both solutions seems to be linear with G_v and t_{rel}. To get an idea of the numerical value of t_{rel}, analytical fitting result should be multiplied by 1.9 while for G_v it should be divided by 1.7.

Those differences are however shadowed when the hardening contribution is added for the calculation of global nominal stress. Moreover, since the main objective is to compare materials and not to get the exact molecular parameters, it makes sense to keep raw values of t_{rel} and G_v obtained from the analytical equation as tools for comparisons.

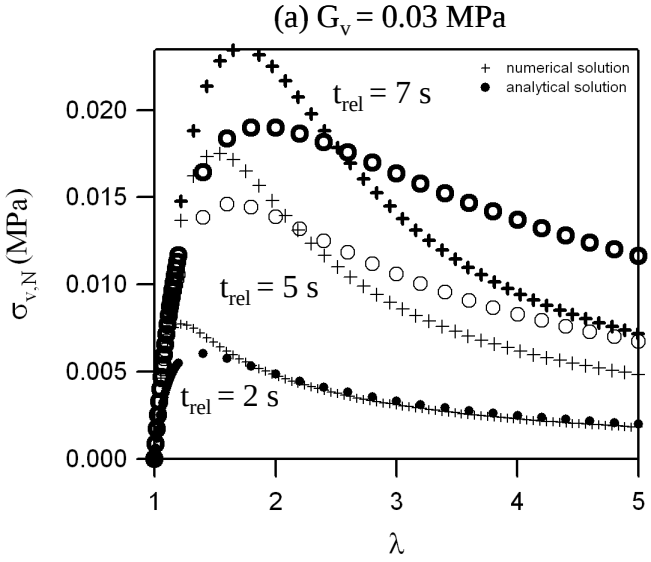

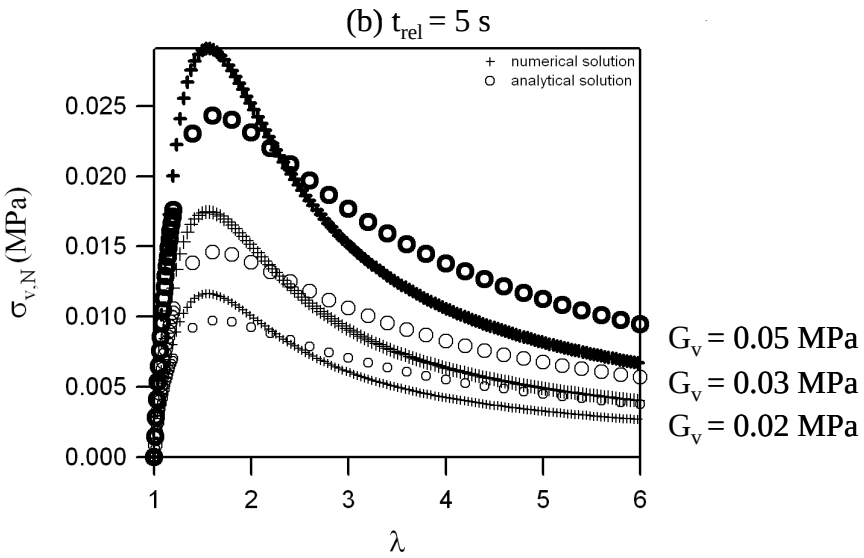

Figure 5-51. Comparison between analytical solution considering a constant nominal strain rate (crosses) and numerical solution obtained considering a constant Hencky's strain rate (circles). (a) Results obtained with three different relaxation times and a fixed value of G_v = 0.03 MPa (t_{rel} = 2 s, 5 s and 7 s). (b) Results shown are obtained with three different shear modulus G_v = 0.02 MPa, 0.03 MPa and 0.05 MPa (t_{rel} = 5 s).

II. Examples of fitted tensile curves

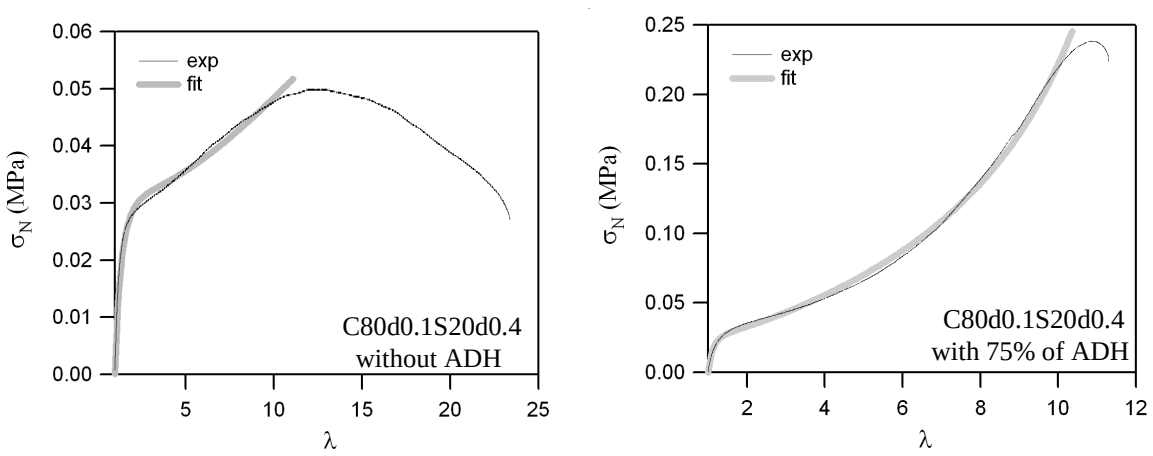

(Figure Continued)

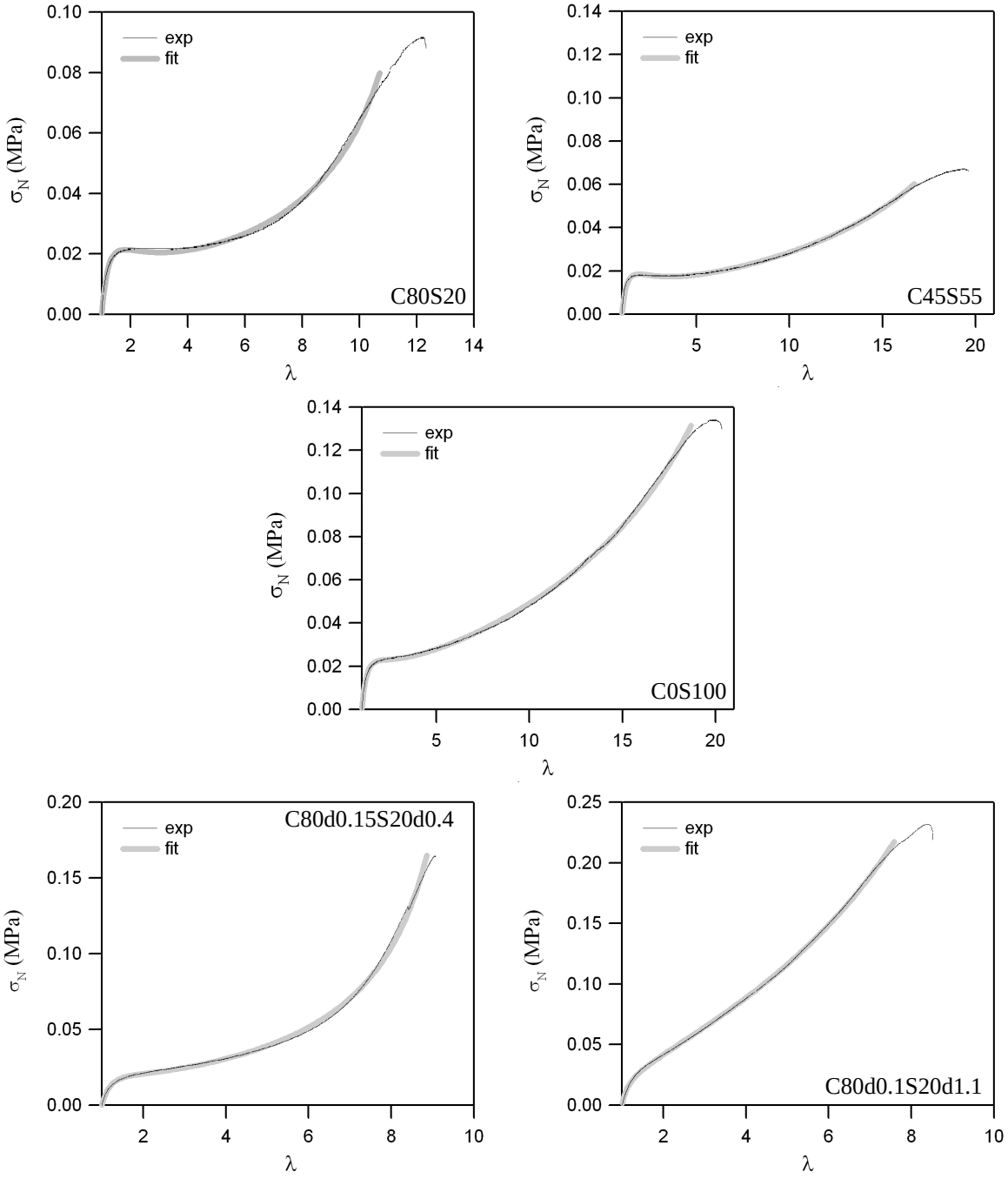

Figure 5-52. Example of fitted tensile curves. One curve is shown per type of material tested and has been selected from series of two to five tests.

References

(1) Josse, G.; Université Paris VI, 2001.
(2) Zosel, A.; Ley, G. *Macromolecules* **1993**, *26*, 2222-2227.
(3) Josse, G.; Sergot, P.; Creton, C.; Dorget, M. *Journal of Adhesion* **2004**, *80*, 87-118.
(4) Creton, C.; Lakrout, H. *Journal of Polymer Science Part B-Polymer Physics* **2000**, *38*, 965-979.
(5) Hui, C. Y.; Jagota, A.; Bennison, S. J.; Londono, J. D. *Proceedings of the Royal Society of London Series a-Mathematical Physical and Engineering Sciences* **2003**, *459*, 1489-1516.
(6) Brandrup, J.; Immergut, E., H.; A., G. E. *Polymer Handbook*, Fourth edition ed.; Wiley & Sons: New-York, 1999.
(7) Brandrup, J.; Immergut, E., H. *Polymer Handbook.*, Third edition ed.; Wiley: New York, 1989.
(8) Mallégol, J.; Gorce, J. P.; Dupont, O.; Jeynes, C.; McDonald, P. J.; Keddie, J. L. *Langmuir* **2002**, *18*, 4478-4487.
(9) Mallégol, J.; Bennett, G.; McDonald, P. J.; Keddie, J. L.; Dupont, O. *Journal of Adhesion* **2006**, *82*, 217-238.
(10) Rubinstein, M.; Panyukov, S. *Macromolecules* **1997**, *30*, 8036-8044.
(11) Verdier, C.; Piau, J. M. *Journal of Polymer Science Part B-Polymer Physics* **2003**, *41*, 3139-3149.
(12) Gent, A. N. *Rubber Chemistry and Technology* **1996**, *69*, 59-61.
(13) Poivet, S.; Nallet, F.; Gay, C.; Fabre, P. *Europhysics Letters* **2003**, *62*, 244-250.
(14) Satas, D. In *Handbook of pressure sensitive adhesive technology*, 2nd ed.; Satas, D., Ed.; Van Nostrand Reinhold: New York, 1989; Vol. 1, pp 396-456.
(15) Ferry, J. D. *Viscoelastic Properties of Polymers*, 1970.
(16) Shull, K. R.; Creton, C. *Journal of Polymer Science Part B-Polymer Physics* **2004**, *42*, 4023-4043.
(17) Roos, A.; Creton, C. *Macromolecules* **2005**, *38*, 7807-7818.
(18) Kaelble, D. H. *Transactions of the Society of Rheology* **1965**, *9*, 135-163.
(19) Lakrout, H.; Sergot, P.; Creton, C. *Journal of Adhesion* **1999**, *69*, 307-359.
(20) Crosby, A. J.; Shull, K. R. *Journal of Polymer Science Part B-Polymer Physics* **1999**, *37*, 3455-3472.
(21) Drzal, P. L.; Shull, K. R. *Journal of Adhesion* **2005**, *81*, 397-415.
(22) Crosby, A. J.; Shull, K. R.; Lakrout, H.; Creton, C. *Journal of Applied Physics* **2000**, *88*, 2956-2966.
(23) Lakrout, H.; Creton, C.; Ahn, D. C.; Shull, K. R. *Macromolecules* **2001**, *34*, 7448-7458.
(24) Dickie, R. A. *Journal of Applied Polymer Science* **1973**, *17*, 45-63.
(25) Kerner, E. H. *Proceedings of the Physical Society of London Section B* **1956**, *69*, 808-813.
(26) Carelli, C.; Deplace, F.; Boissonnet, L.; Creton, C. *Journal of Adhesion* **2007**, *83*, 491-505.

6. Tackified wb-PSA Synthesized by Miniemulsion

In this last chapter are presented results obtained on tackified waterborne PSA. The synthesis process selected to incorporate the hydrophobic tackifying resin inside latex particles is the miniemulsion polymerization.
After a screening and an optimization stage which consisted in the study of their mechanical and adhesive properties, some in situ tackified wb-PSA with promising adhesive performance have been selected by Cytec. In a second step, the materials developed in the lab have been successfully reproduced at the pilot scale in 80kg batches.
This chapter shows how the fundamental concepts developed in the previous two chapters have been used to develop new industrial adhesives which have led to the filing of a patent.

6.1. Introduction

6.1.1. Brief state of the art of tackifier in PSA formulations

The viscoelastic properties is a major factor affecting adhesive performances. In a PSA formulation with a diene elastomer as the major component, the highly entangled polymer generally provides the elastic component, while a low molecular weight tackifying resin is added to increase viscoelastic dissipation at the usage temperature and soften the material so that the resulting composition has the properties of a pressure sensitive adhesive. The role of a tackifier is to adjust the rheological behavior of the system.

A number of studies already exist on PSA made of tackifier resins blended with rubbers[1-7] or block copolymers[8,9]. The major effect of the resin in such systems is to increase the glass transition temperature and to dilute entanglements. Since acrylic copolymers used for PSA, have a much lower plateau modulus (they are much less entangled than their diene counterparts), there is no need to add resins to dilute the entanglement network. Nevertheless, it is common practice and, in fact, quite advisable to incorporate resins as tackifiers in acrylic formulations to enhance viscoelastic dissipation at room temperature and boost the peel force.[10,11] However, even for solution acrylics, few studies on tackified acrylic systems have been reported. Kim et al. have extensively investigated the influence of miscibility of acrylic copolymers and tackifier resins upon PSA performance[12-15] but the actual effect of resin in acrylic systems is poorly described theoretically.

Adding a tackifying resin to a dispersion poses specific challenges since solvents cannot be used, the only option currently available is the use of a simple physical blend between a dispersion of the resin and the base polymer dispersion. The incorporation of the resin occurs then during the drying stage and relies on a very good solubility of the resin in the base polymer. In practice this strategy does not work very well and leads to a poor incorporation of the resin.

6.1.2. Tackified waterborne PSA

Some of the main effects that should be considered when adding resin dispersions to an acrylic dispersion have been reviewed by Zettl.[10]

First, the compatibility of resin-polymer emulsifier systems with the acrylic emulsion systems must be checked. When blending a resin dispersion with a polymer latex, it is advantageous to use products having similar emulsifiers and pH. But this is not a rule and the specific components in the blend must have to be checked for compatibility. The resin dispersion has to be ion tolerant to be stable when mixed with acidic latexes. The relative viscosities of the resin dispersion and of the blended adhesive are also important in the mixing and coating processes.

Another concern specific to resin dispersion/polymer latex systems is that of mixing and particle fusion. In solution adhesives, the adhesive components are mixed on a molecular basis in a common solvent. Therefore, when the solvent is evaporated the adhesive components are as finely mixed as possible in the dried film. In an aqueous adhesive mixture of resin dispersion and polymer latex, each component is present in individual 300 nm particles. On evaporation of the water, the particles coalesce. However, some combination of

additional time and temperature is needed to fuse these particles to the same intimate molecular mixture. The ease of achieving this interdiffusion is dependent on the T_g of the resin, the mutual solubility of the resin and polymer, and the relative particle size distribution of the resin dispersion and polymer latex.

Even after adjusting resin dispersion properties so that all the above requirements for good resin solubility are fulfilled, some problems still persist. These are thought[16] to be inherent to the emulsion system. Tobing et al. proposed a molecular explanation for the understanding on the role of tackifier in a waterborne PSA formulation. They compared results of a tackified emulsion PSA (based on 50/32/15/3 poly(2-ethyl hexyl acrylate-*co*-vinyl acetate-*co*-dioctyl maleate-*co*-acrylic acid) blended with a tackifier dispersion based on glycerol ester abietic acid) to that of high performance solvent-borne and hot melt PSA (tackified SIS block copolymer) and tried to elucidate the problem inherent to the blending of the resin dispersion. They speculated that discrete networks of the microgels localized inside latex particles in the acrylic dispersion would hinder resin diffusion and they supposed that since microgels are present prior to film formation, the tackifiers would not be able to tackify the networks, the micro-networks remained unplasticized, which resulted in only weak improvement in adhesion on low energy substrates. Schematic morphologies of neat and tackified emulsion acrylic PSA are shown in Figure 6-1.

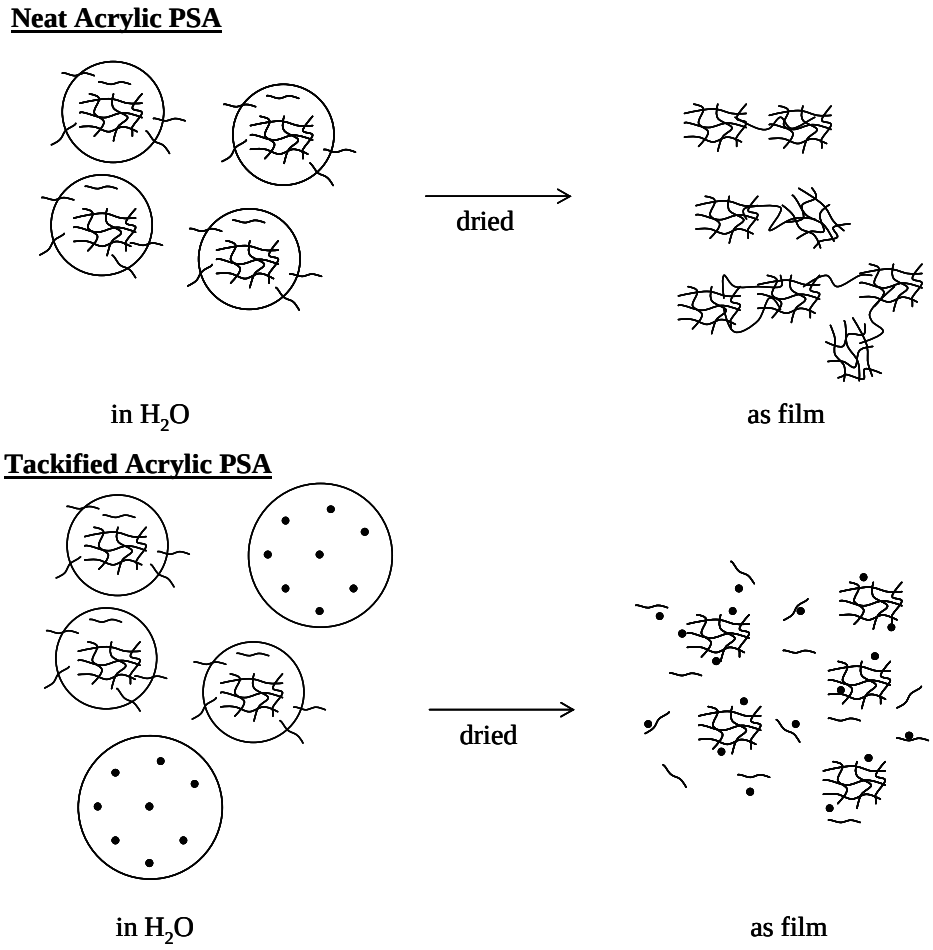

Figure 6-1. Schematic morphology of waterborne PSA films (after [16]).

Besides the problem of resin solubility, substantial problems associated with the use of tackifier dispersion occur. Water resistance is a property of concern since it is largely determined by the emulsifier system used in producing emulsions of the resin and polymer. Stability and rheology of the formulation may be also affected by the substantial amount of unknown surfactant agents added upon blending the resin dispersion to an acrylic latex.

The large number of requirements which a resin must fulfill to act as a tackifier in waterborne PSA and the incomplete mixing of the resin inside the microgels could explain their restricted use compare to solvent borne system. We tried here to overcome some of these limitations using miniemulsion as a preferential process to encapsulate the hydrophobic tackifying resin prior to polymerization. In this research, materials are in situ tackified which means that microgels form in the presence of tackifying resin (Figure 6-2).

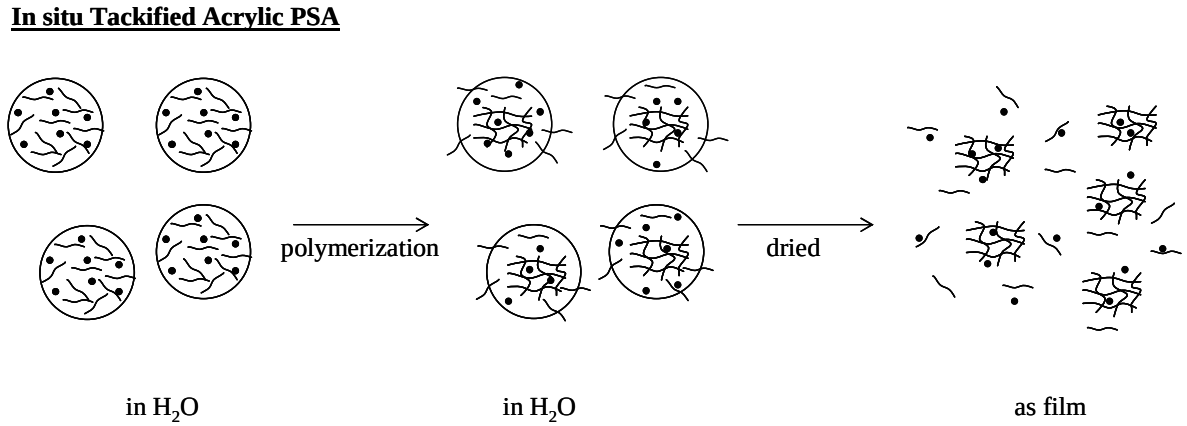

Figure 6-2. Schematic morphology of in situ tackified waterborne PSA films.

This strategy allows us to obtain:

- A better compatibility and solubility with the primary latex.
- A better control over the particle size distribution.

In this chapter, after the presentation of chemicals and synthesis processes used to produce heterogeneous in situ tackified PSA, we will show results of the characterization of the latex formulations obtained from analytical techniques namely differential scanning calorimetry (DSC), gel permeation chromatography (GPC), quasi-elastic light scattering (QELS), liquid chromatography-mass spectroscopy (LC-MS) and size exclusion chromatography (SEC). The specific nanostructure of dried adhesive layers and diluted latex particles are then investigated using atomic force microscopy (AFM).

After that, we used the probe tack experiment to test the adhesive performances of the tackified waterborne PSA, and the home made microrheometer to obtain their linear rheological properties. The deformation behavior of one of the materials studied obtained from tensile experiments is also presented. The aim of this section is not to classify the materials as a function of their adhesive performances, but to gain a fundamental understanding of the effect of the tackification on rheological properties and on the mechanisms of debonding.

The last section is more focused on the long-term commercial aims of the NsHAPe research program. We will present results of the evaluation of technical feasibility of the new synthesis process and show adhesive performances (obtained from standard adhesive techniques) of two commercial prototypes.

The great importance of this chapter lies in the fact that, to our knowledge, this is the first time that some adhesive results of in situ tackified waterborne PSA produced using miniemulsion are let out and the company Cytec has actually patented this process.

It must be emphasized that as in the previous chapter, all syntheses were performed outside the ESPCI, in this case by Cytec Surface Specialties under the supervision of Dr. Keltoum Ouzineb, who initiated this synthesis project.

6.2. Tackifying resins

Various tackifying resins can be used in adhesives and the choice depends upon the base polymer characteristics and the target application. There are two major classes of tackifying resins. There are the rosin ester, terpene phenolic, and hydrocarbon resins.[17] One of the main obstacles for the use of the first two ones is the yellowing after ultraviolet exposure. Whereas hydrocarbon resin types offer good color stability and excellent adhesion to low energy surfaces. Therefore, hydrocarbon resins have been selected as the preferred resin in this work.

6.2.1. Monomers and polymerization processes

Hydrocarbon resins consist of low molecular weight polymers produced from a wide variety of monomers derived primarily from petrochemical sources. They are made from the polymerization of petroleum-derived feedstocks. Steam Cracked Naphta is the source of the monomers and polymerization is performed after separation and purification (Figure 6-3).

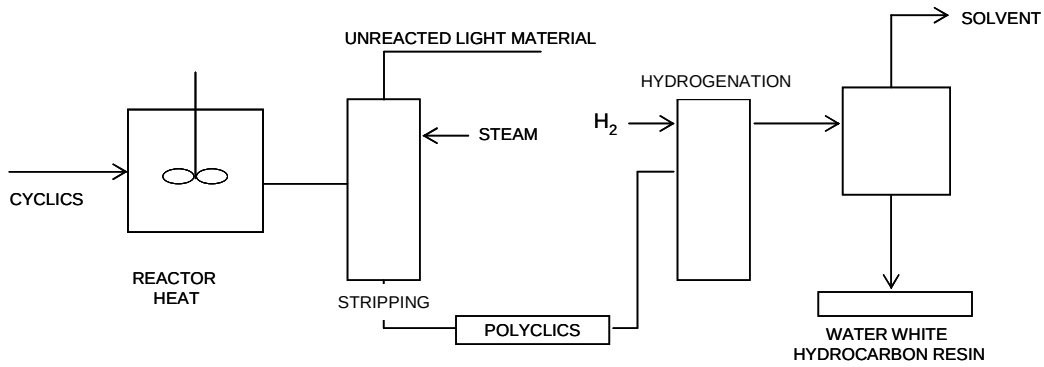

Figure 6-3. Process flow in a plant for the production of tackifying resins.

Two classes of resins have been selected for our study: aliphatic / aromatic hydrocarbon resins and a polyterpene resin. Monomers and polymerization processes used for the production of these types of tackifying resins are presented below.

6.2.1.1. Aliphatic / aromatic hydrocarbon resins

Aliphatic resins are produced from light, so-called C-5 petroleum fractions. The principal monomers are *cis*- and *trans*-piperylene (Figure 6-4). Also found in these streams are varying amounts of isoprene, 2-methylbutene-2, and in some cases, dicyclopentadiene. These streams are polymerized using aluminium chloride, and the T_g is controlled by adjusting the composition of the diluents or monomers (Figure 6-4).

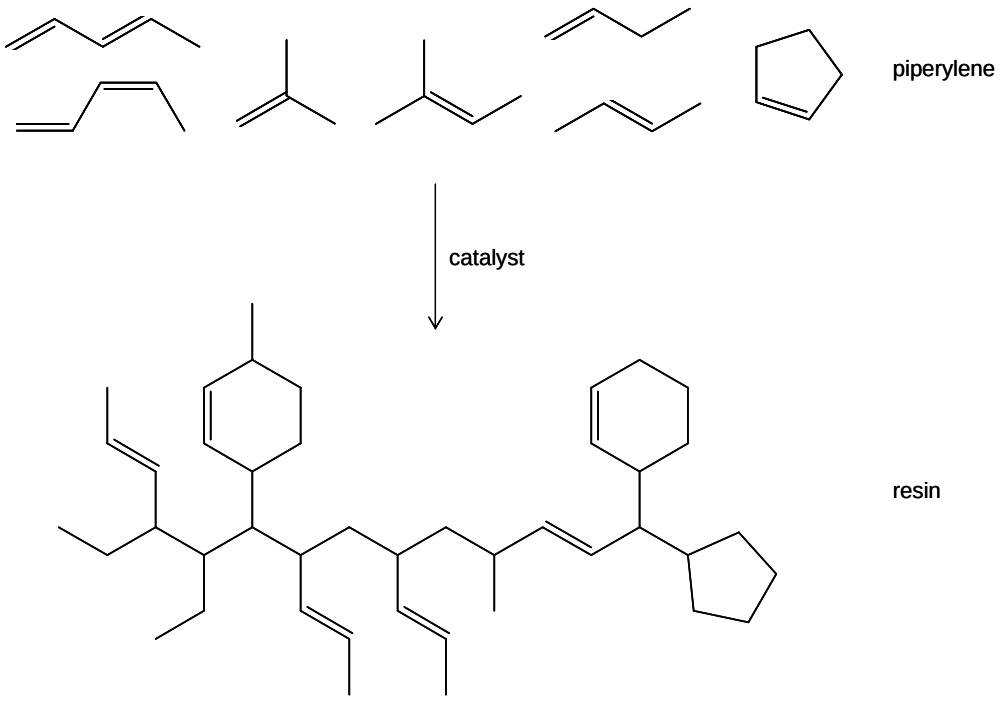

Figure 6-4. C-5 hydrocarbon resin oil polymerization.

The aliphatic or C-5 resins have been available for many years. They possess excellent stability and very light colors. They are outstanding tackifiers for natural rubber, *cis*-polyisoprene and styrene-isoprene block copolymers.

The mixed aliphatic / aromatic resins are hybrid resins produced by blending C-5 and C-9 streams in varying proportions and then polymerizing.

6.2.1.2. Polyterpene resins

The polyterpene resins may be classified as diene or $(C\text{-}5)_2$ resins, since the monomers used in their production may be considered to be dimers of isoprene. Terpene resins are produced by cationic solution polymerization of raw materials obtained from turpentine and other natural sources, including citrus peels. The actual monomers are usually one or a combination of the terpenes: α-pinene, β-pinene, and dipentene or limonene (Figure 6-5). The catalyst is usually the $AlCl_3$, although other Lewis acids can de used.

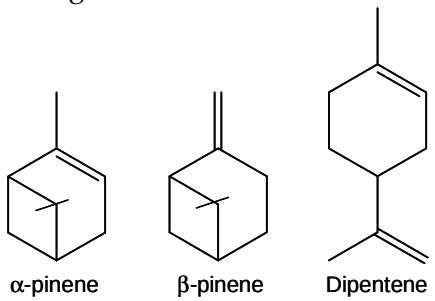

Figure 6-5. Monomers used for the production of terpene resins.

Terpene resins were the resins of choice in the production of PSA for many years. They have outstanding tackifying abilities when used with natural rubber

6.2.2. Role of a tackifying resin in PSA formulations

The preceding section has presented monomers and polymerization processes used for the production of two types of hydrocarbon resins. These are important in determining the compatibility with the tackified polymer matrix. These are the glass transition temperature (T_g) and molecular weight of each resin which in turn define the ability of the resin to act as a tackifying resin.

A tackifying resin must possess three basic properties. It must be compatible with the base elastomer in the adhesive system. It must have a T_g that is significantly higher than that of the elastomer (T_g increases with molecular weight and cyclization, it increases faster with cyclization). And it must have a low molecular weight relative to the base polymer.

The main role of a tackifying resin is to modify viscoelastic properties of the adhesive mass[6,18-20]. At long times, corresponding to the bonding time, the addition of resin causes a reduction in the elastic modulus G' as a result of entanglement dilution. This reduced G' will give a faster and more intimate wetting of the adherent and the resulting increased bond area will lead to higher tack values. This effect occurs until the effect of the resin is to raise T_g above room temperature. At this resin concentration, the adhesive is glassy and unable to wet the adherent, and thus the tack value falls rapidly to zero.

At short times, G'' is increased over that of the elastomer due to the increase in T_g. This results in the increase in dissipative properties.

The effect on G' of blending a resin to an elastomer is schematically shown on Figure 6-6.

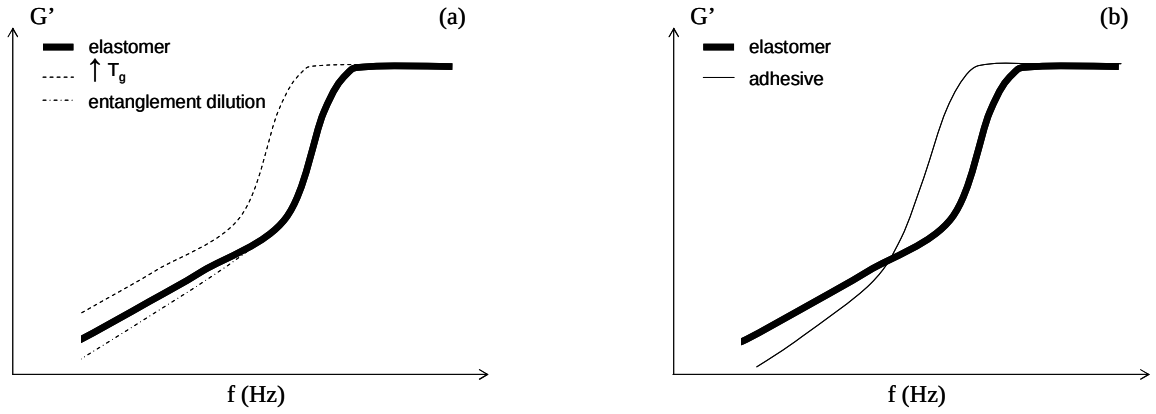

Figure 6-6. Schematic of the effect of the tackification on the evolution of G' as a function of the frequency. (a) Effects of the increase in T_g and of the entanglement dilution. (b) Combination of both these effects.

Use of tackifying resin to achieve a pressure sensitive bond to high energy substrate such as stainless steel is essentially a viscoelastically driven phenomenon. A resin with proper solubility and T_g is needed to affect the flow of the adhesive at low rates of deformation and its resistance to stress at high rates of deformation.

Although the proper viscoelasticity is a prerequisite for adhesion to low-energy substrates, such as polyethylene, it is not the only factor that affects adhesion. For adhesion to PE, the surface energy of the adhesive layer becomes important. And generally, tackifying resins have also the effect of modifying adhesive surface energy.

6.3. Tackified wb-PSA: the materials

Latex syntheses have been carried at Cytec Surface Specialties in Drogenbos (Belgium). They were conducted under the supervision of Dr. Keltoum Ouzineb.

6.3.1. One stage in-situ miniemulsion tackification

6.3.1.1. Synthesis process

Miniemulsion has been used as a process to encapsulate the tackifying resin. The monomer miniemulsions are prepared by dissolving the surfactants in deionised-water, and tackifying resin (hydrophobe) in the monomer. The oil and aqueous solutions are mixed with a mechanical agitator for a few minutes and then in a high intensity mixer (ultrasonifier, 500 mL during five minutes). The aim of this step is to down size monomer droplets to the actual size of the polymer particles. This step allows a control over the particle size distribution.

The resultant miniemulsion is then polymerized 24 hours later with a water soluble free radical initiator as in conventional emulsion systems. All latexes are polymerized under a semi-continuous process. A schematic of the one-stage in-situ miniemulsion tackification process is given on Figure 6-7 and the operating conditions for the miniemulsion polymerization are summarized on Figure 6-8.

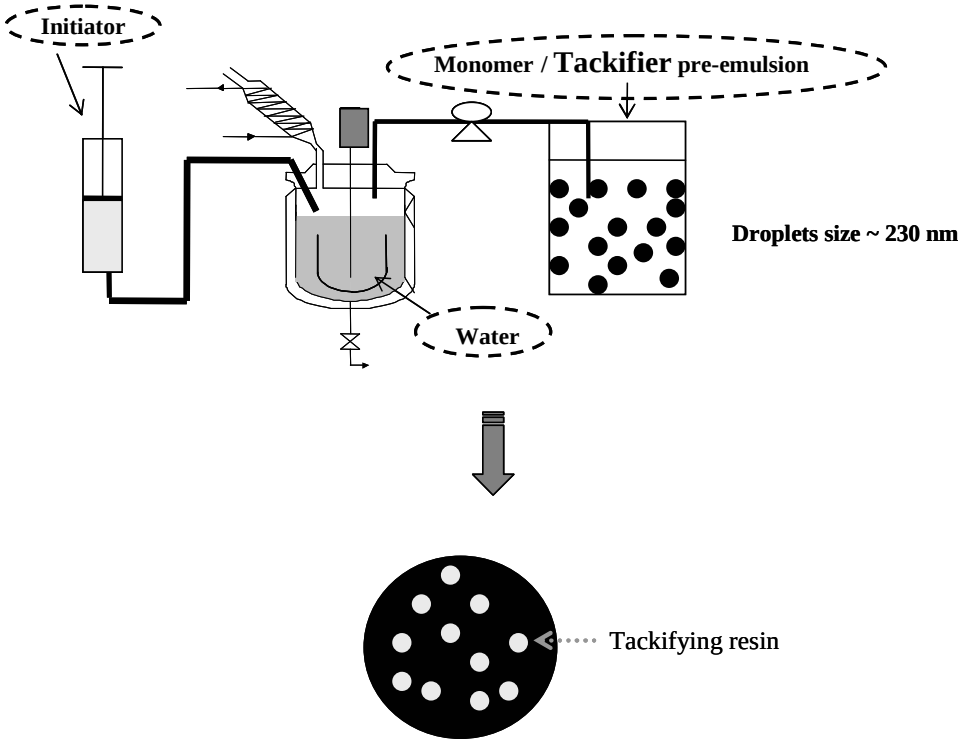

Figure 6-7. Schematic of the one stage in-situ miniemulsion tackification process.

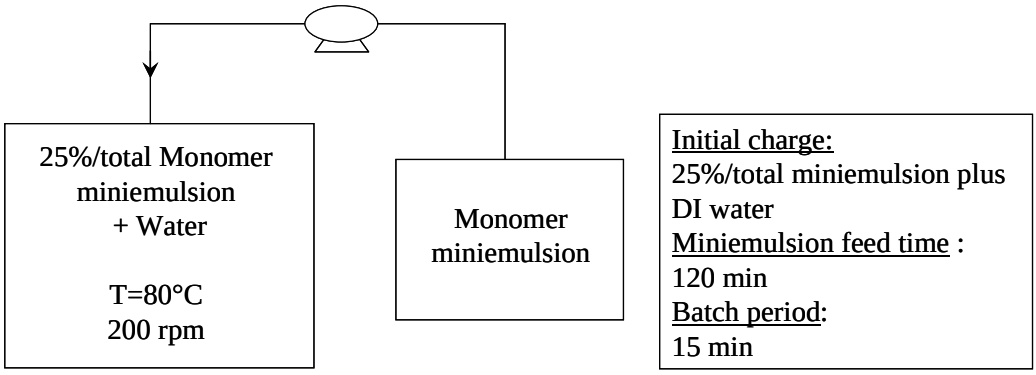

Figure 6-8. Operating conditions for the miniemulsion polymerization.

6.3.1.2. Latexes monomer composition

The polymerization process is initiated by ammonium persulfate. Latex particle stability is controlled by a mixture of anionic surfactants (2 wt% of the total monomer charge). Na_2CO_3 is used as a buffer. The amount of surfactant is adjusted so as to avoid droplets coalescence and micellar nucleation. In order to prevent Ostwald-ripening (see the section about miniemulsion polymerization in chapter 1) a hydrophobic compound (stearyl methacrylate) is added. The tackifier resin dissolved in the monomer phase is also acting to a lower extend as hydrophobic compound.

Miniemulsions will be compared to a latex called "latex IB". Latex IB is not tackified and is synthesized using a conventional emulsion polymerization process. We decided to call the composition of main monomers of IB "composition IB". It is made from a random copolymer of 2-ethyl hexyl acrylate (2-EHA) (glass transition temperature, T_g = -50°C[21]), ethyl acrylate (EA) (T_g = -24°C[21]), methyl methacrylate (MMA) (T_g = 105°C, for the atactic[21]), acrylic acid (AA) (T_g = 106°C[21]) and styrene (S) (T_g = 100°C[21,22]) as the main monomers. The theoretical T_g of this copolymer is -50°C (calculated using the Fox equation and measured by DSC at 20K/min). Composition IB is characterized by a low T_g and a high gel content (gel ~ 64%).

The miniemulsions have the same monomer and surfactant compositions as latex IB, but in these materials, a tackifying resin is used as a hydrophobic compound. Furthermore the synthesis conditions are of course totally different from those of the latex IB.

Three different tackifier resins have been added to the base latexes.

- Dercolyte A115 (supplier DRT) is a polyterpene resin. It is obtained from the polymerization of the α-pinene.
- Piccotac 1095-N and Piccotac 6095-E (supplier Eastman) are hydrocarbon resins.

These three resins are well known to improve adhesion of hot melt adhesives like PSA made of styrene-isoprene-styrene block copolymers.

6.3.1.3. Material characterization

a. Selection of the type of tackifier resin

Some analytical characteristics of tackifier resins used for this study can be found in Table 6-1. One can note that they have the required properties already discussed in section 6.2.2. They are characterized by a much higher T_g than the base latexes and a much lower molecular weight and by relatively narrow molecular weight distributions, typically about 2. This is desirable to improve the compatibilities.

Tackifying resins	Softening point (°C)	T_g[a] (°C)	M_z (g.mol^{-1})	M_w (g.mol^{-1})	M_n (g.mol^{-1})
Dercolyte A115	115	68	-	900	-
Piccotac 1095-N	94	44	3500	1700	800
Piccotac 6095-E	98	44	4000	1700	800

a-DSC (Differential Scanning Calorimetry) results at 20K/min

Table 6-1. Some analytical characteristics of tackifier resins used in this study.

Latexes in situ tackified with Dercolyte A115, Piccotac 1095-N and Piccotac 6095-E are called D, P1 and P6 respectively. Some analytical characteristics of these latexes can be found in Table 6-2.

Similar particle sizes (dp ~160 nm) are obtained for the Piccotac based latexes. Smaller particle size is achieved using Dercolyte as the tackifier resin.

One can note the lower gel content and higher molecular weight of the miniemulsions compared to the IB latex (not tackified latex) synthesized using the conventional emulsion process. This can be explained by the fact that in miniemulsion the droplets are the main loci of polymerization, they act as an individual batch reactor.[23] Some comparisons between batch and semi-continuous starved emulsion polymerizations can be found chapter 1. However, the significantly lower gel content obtained can not be only attributed to the decrease in the total volume fraction of polymer. Depending on the type of tackifier, the decrease in the gel content can be very significant (Dercolyte A115 and Piccotac 6095-E). Comparing the results obtained with Piccotac 6095-E and Piccotac 1095-N, we can see that miniemulsion employing the Piccotac 6095-E shows very low gel content. We suspect that some chain transfer is taking place between the tackifier resin and the acrylic polymer. An ^{1}H-NMR analyze did not allow us to conclude on the mechanism taking place during the miniemulsion polymerization with Piccotac 6095-E but revealed that Piccotac 6095-E contains aromatic compounds while this is not the case for Piccotac 1095-N.

Additionally, compared to IB one can remark that in situ tackified miniemulsions have a much lower solid content. This has to be pointed out since high-solids (above 50 %), low viscosity latexes are of growing interest for many reasons (product transport in the reactor is more efficient and less costly, and film formation and drying times are reduced) and making this type of product entails many difficulties when conventional emulsion polymerization is not used as the synthesis process[24]. We can see that the viscosity follows the same trend i.e. a decrease when using the miniemulsion process. The viscosity depends on solid content and the solid content at which the viscosity becomes significant depends on the particle size distribution.

Adhesives	Tackifier	% tack	$d_{droplets}$ (nm)	d_p[b] (nm)	gel (%)	M_w/M_n[c]	Viscosity @50rpm, mPa.s	SC (%)	T_g[d] (°C)
IB[a]	**-**	0	-	226	58.3	151865/21845	220	55	-50
D	**Dercolyte A115**	19	214	143	1.5	323835/53925	136	47	-42
P1	**Piccotac 1095-N**	19	223	157	29.7	269135/60450	104	47	-40
P6	**Piccotac 6095-E**	19	204	168	1.3	287655/44745	84	47	-41

a- Benchmark without tackifier resin obtained from classical emulsion.
b- QELS (Quasi-elastic light scattering) (Nicomp™, 380 ZLS).
c- GPC (Gel Permeation Chromatography).
d- DSC (Differential Scanning Calorimetry) results at 20 K/min.

Table 6-2. Analytical characteristics of latexes prepared using miniemulsion and containing three different types of tackifying resin.

b. Tackifier resin content

A series of syntheses were carried out employing increasing concentration of tackifier (0% - 20%, wt%/total monomer). The acrylic monomer composition and surfactant systems were kept constant.

- Evolution of T_g

The evolution of the T_g of the latex as a function of the amount of tackifier (Piccotac 1095-N) has been followed by DSC (20 K/min). A single T_g was observed for all the samples. The adhesives prepared from the miniemulsion latexes show an increase in T_g as the resin content increases (Figure 6-9). For a miscible blend, T_g can roughly be estimated with Fox equation. For P1 (19 wt% of tackifier), a T_g of -36°C was calculated from the composition and the T_g of the individual compounds. For another blend containing 9 wt% of tackifier, T_g from DSC measurement and from Fox equation are both equal to -44°C.

This means that the tackifier is compatible with the base polymer and that there is no evidence of phase separation and this reflects the partial or even total miscibility of the tackifier with the copolymer.

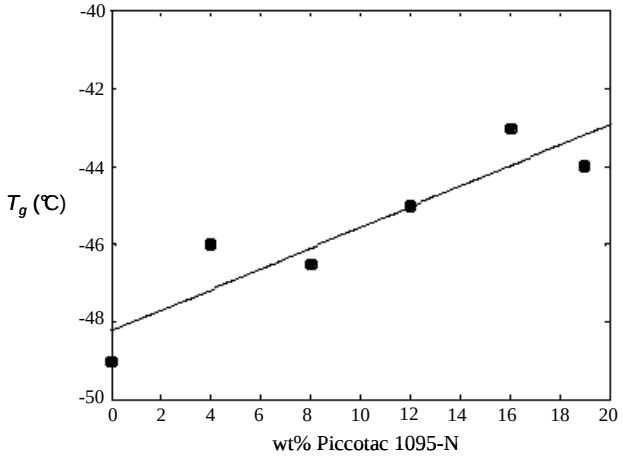

Figure 6-9. T_g versus Piccotac 1095-N content.

- Evolution of the gel content

Gel content measurements were also performed on this series (Figure 6-10). We can see that gel content decreases as the tackifier content is increased. This indicates that the tackifier is interacting with the polymer chain growth. As no evidence of grafting from gel permeation chromatography results[25] has been observed we can reasonably suspect that this aliphatic hydrocarbon resin is acting as a transfer agent.

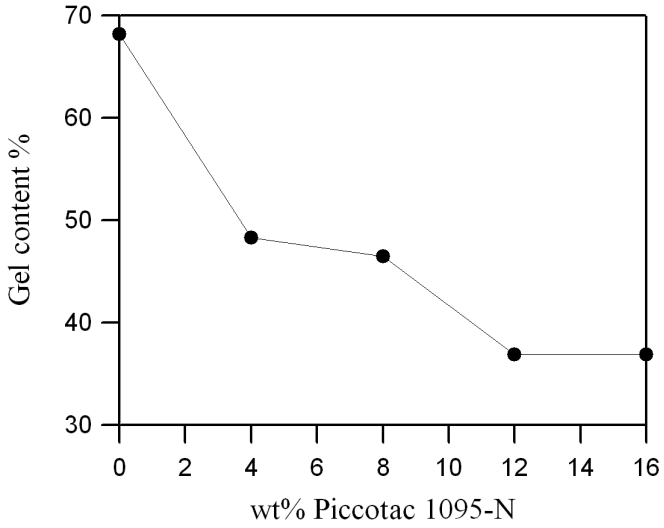

Figure 6-10. Gel content as a function of tackifier content.

c. Further remarks

- Molecular weight distribution

The molecular weight distribution (*MWD*) characterization showed that two distinct populations are present. The bimodal *MWD* is made of M_{w1} ~ 2000 g.mol^{-1} and

M_{w2} ~ 110 000 g.mol^{-1} (Figure 6-11). And as the tackifying resin concentration is increased the lower M_w population is increased. As already discussed in chapter 2, the *MWD* is a key parameter in the control of the final adhesive properties. The low population may contribute to the adhesion level while the larger may ensure the cohesion level. Therefore, one can predict an increase in the adhesion and a decrease in the cohesion with an increasing amount of tackifier.

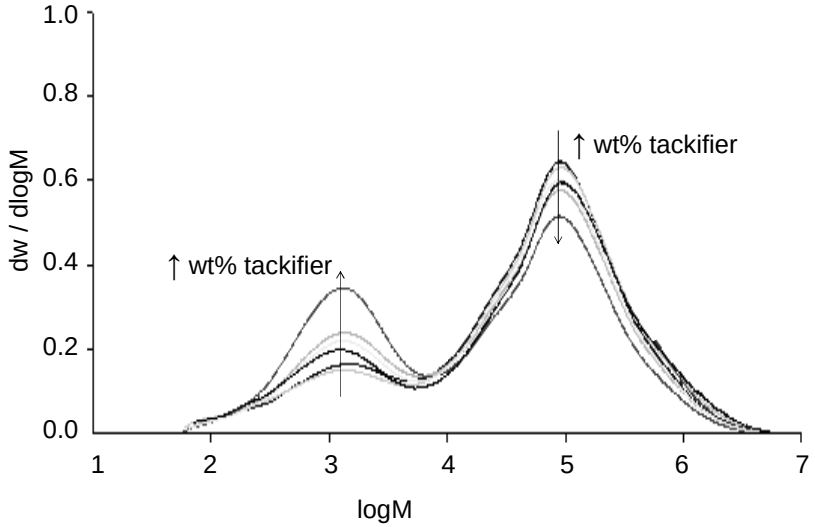

Figure 6-11. Molecular weight distribution of miniemulsions. Effect of the tackifier content.

- Tackifier location

To address the tackifier location (liquid phase / polymer phase), some liquid chromatography–mass spectroscopy (LC-MS) measurements have been performed. The goal was to determine if tackifier resin can be detected in the aqueous phase of the miniemulsion (this study has been made only in the case of Piccotac 1095-N). The conclusion is that no Piccotac 1095-N was detected in the aqueous phase. When comparing the SEC (Size Exclusion Chromatography) chromatograms of a pristine miniemulsion containing Piccotac 1095-N and the same miniemulsion but cleaned, the peak corresponding to the resin is present in both samples. This could be an indication that the Piccotac 1095-N is incorporated in the polymer particles.

In summary, based on results obtained from various analytical characterization techniques:

- Depending on its type, the effect of tackifier resin on gel is very different. Grafting is suspected in the case of Dercolyte A115 and Piccotac 6095-E.
- Results on Piccotac 1095-N showed that:
    - It is partially or even totally miscible with the copolymer.
    - It probably acts as chain transfer agent.
    - A bimodal *MWD* is obtained.
    - It is incorporated in the polymer particles.

6.3.2. In-situ tackified core-shell latexes

6.3.2.1. Synthesis process

The addition of a second stage polymer around the tackified miniemulsions has been motivated by two major reasons. The first one is to use the second stage as a tool to increase the solid content of the latexes. Two-stage or multistage polymerizations are the most common techniques for the preparation of high-solid latexes.[26-29] The second one is the possibility to adjust adhesive properties with a polymer shell. For that, the polymer shell can have a different monomer composition than that of the core or functionalized polymers. The addition of a polymer shell that can be crosslinked during the drying of the adhesive film can also be envisaged (see chapter 5) but this has not been investigated in the present study.

The synthesis process for the preparation of in situ tackified core-shell latexes is divided in two stages. The first stage corresponds to the synthesis of the tackified core using the process described in the previous section (for these materials, Piccotac 1095-N has been selected as the tackifier resin). This is followed by a second step for the addition of the shell. The polymer particles generated during the first stage are acting as seed particles during the second stage. A classical pre-emulsion is added semi-continuously in order to create a polymer shell surrounding the previous polymer particles (Figure 6-12).

For the first series, the shell has the same monomer composition as the one used for the first stage miniemulsion process. For another series, some slight changes have been voluntarily introduced and they will be discussed later. The thickness of the shell is controlled by the amount of monomers added during the second step. Thus core/shell weight ratio can be varied.

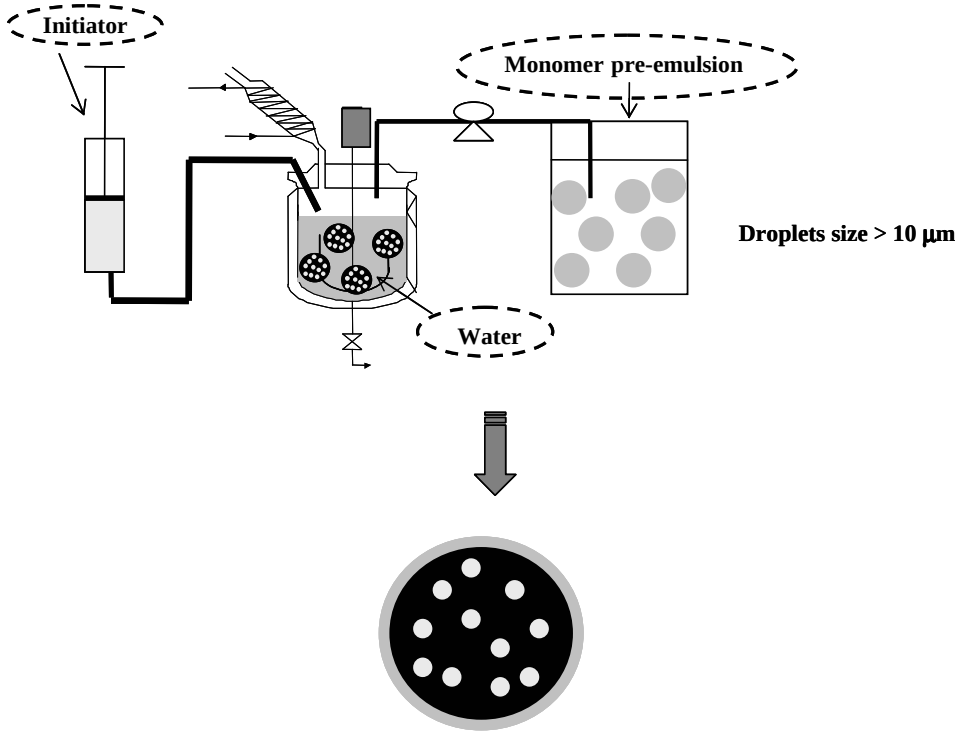

Figure 6-12. Schematic of the second step of the process for the synthesis of core-shell latexes in situ tackified.

At the end of the polymerization, a monomer chasing is used to remove all monomer residues. (TBHP (tert butyl hydroperoxide) / SFS (sodium formaldehyde sulfoxylate) red/ox reaction is used for this monomer chasing step).

A representation of the structure of the dried adhesive film in the case where shell polymer is different from that of the core is given on Figure 6-13.

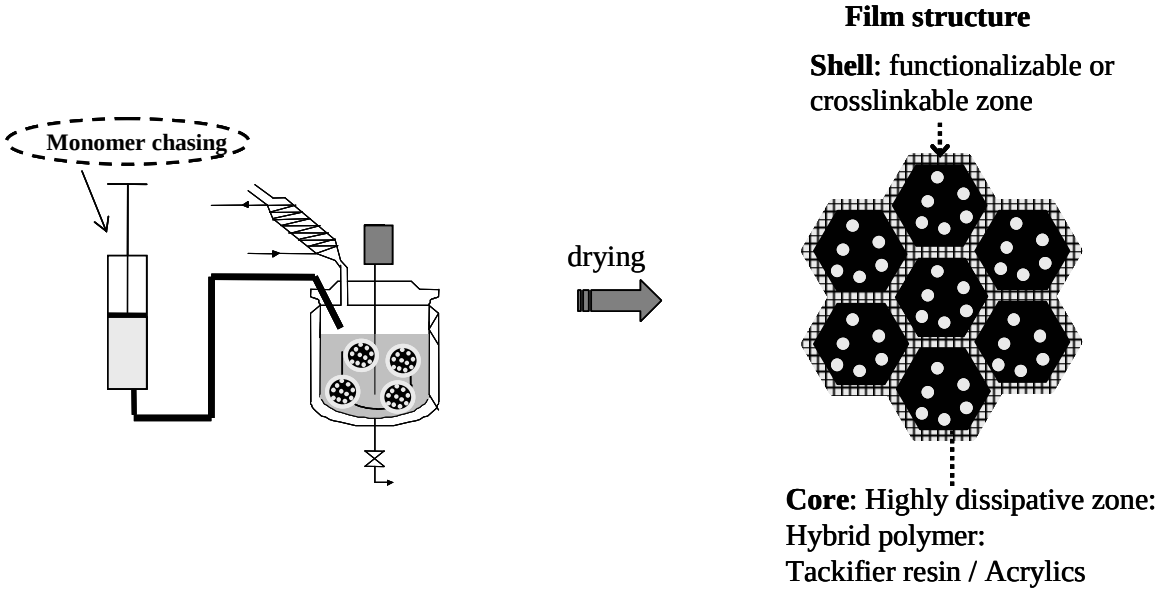

Figure 6-13. Schematic of the final stage of the process for the synthesis of core-shell latexes in situ tackified.

One can also add that even when the monomer composition is the same in the core and in the shell, the polymer structure is with no doubt totally different since

- The processes used for their synthesis are different.
- The core is tackified and not the shell.
- The amount of transfer agent is lower in the shell than in the core.

6.3.2.2. Latexes monomer composition

Cores of the particles are made of miniemulsions containing Piccotac 1095-N as a tackifying resin. Their composition is the same as P1, but the tackifying resin content is varied. In some cases, the effect of the elimination of the transfer agent has also been investigated.

Two types of shells have been studied. A first series of adhesives is made of shells with the composition IB. Composition IB contains some crosslinkable monomers and the crosslinking reaction occurs during the final stage of the synthesis.

One of the adhesives studied is made of core-shell particles with a different shell composition. This composition will be called "composition B". It is made from a random copolymer of 2-EHA, BA and styrene as the main monomers. The theoretical T_g of this

copolymer (calculated using the Fox equation) is -45.5°C. Composition B contains also some polar monomers (4 wt% total monomers) and it is a softer composition than IB.

6.3.2.3. Material characterization

"Two-stage latexes" have been characterized. Some analytical characteristics can be found in Table 6-3.

- The first interesting think to note is the increase in the solid content compared to the one-stage materials. One of the motivations to add a shell was to increase the solid content and this objective has been achieved.
- One can see that particle sizes are higher than that of "one-stage particles". Particle size has been followed during the synthesis and it has been shown that it increases during the second stage of the synthesis.
- Viscosity is slightly increased but values stay acceptable for industrial applications.
- Again a significant impact on the final gel content is observed (compared to IB) and this indicates that tackifier resin is indeed acting as a transfer agent.
- T_gs are a bit lower but this change is not significant.

Adhesives	IB87[4.85]-IB13[a]	IB90[9]-IB10	IB70[8.4]-B30
% tack[b]	4.85	9	8.4
$d_{droplets}$ (nm)	218	223	223
d_p (nm)	196	224	217
Gel (wt%)	42.4	-	-
Viscosity @50rpm, mPas	300	249	212
SC (%)	58	53	52.4
[TA] core (wt%) [c]	X1	0.05	0
[TA] shell (wt%) [d]	X2	0.005	0
T_g (°C) [e]	-46	-50	-45

a- The notation chosen is: Ax[α]-By with A: core composition, x: weight fraction of the core, α: tackifier content, B: shell composition and y: weight fraction of the shell.
b- Tackifier content: wt% / total monomers of the particle.
c- Amount of transfer agent in the core. wt% / total monomer of the core.
d- Amount of transfer agent in the shell. wt% / total monomer of the shell.
e- DSC result at 20 K/min.

Table 6-3. Some analytical characteristics of the two-stage latexes.

6.4. Optical quality and nanostructure of adhesive films

6.4.1. Adhesive film optical quality

In general, one of the drawbacks of adding resins is that it impairs the transparency of the film. But interestingly, using miniemulsion as a tool for the incorporation of the tackifying resin, transparent films are obtained. Some reactions have been carried out under identical experimental conditions in miniemulsion and conventional emulsion. Transparent films are obtained in miniemulsion polymerization whereas an opaque one is observed with conventional emulsion process (Figure 6-14).

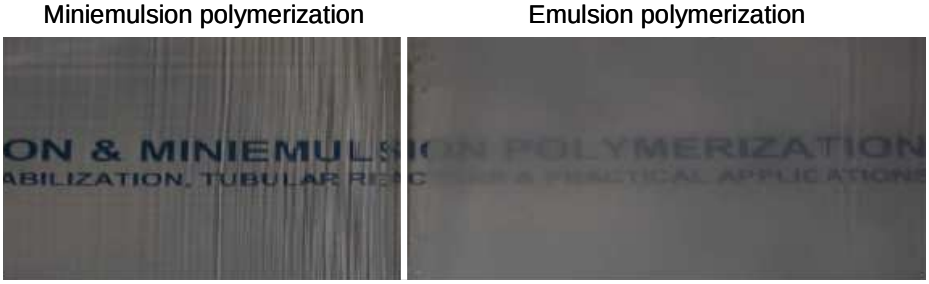

Figure 6-14. Pictures of dried films obtained in miniemulsion (left) and conventional emulsion polymerization (right).

In addition, a high level of scraps is obtained in conventional emulsion. This can be explained by the limitation of tackifier transport through the aqueous phase (high hydrophobic compound) during the semi-continuous process. This results in non negligible defects in the film formation.

6.4.2. AFM characterization

AFM analyses have been carried out on in situ tackified latexes by C. Lei and J. L. Keddie in the University of Surrey (United Kingdom).

6.4.2.1. One stage tackified latexes

One stage tackified latexes have been characterized. To determine the structure of individual particles, latexes were diluted and spin-coated onto poly(ethyleneimide) (PEI)-modified mica surface.

Comparing images obtained on IB and that of a tackified miniemulsion (Figure 6-15), one can observe that when tackifier is added, there are some small hard solid particles, which are attributed to being the aggregated tackifier. Images of individual particles also show that there are few examples of tackifier particles being fully encapsulated by the polymer particle. The majority of the tackifier particles, however, appear isolated in the images with an average size of approximately 200 nm. It appears that a significant fraction of the tackifier was not retained within the latex particles during the miniemulsion polymerization.

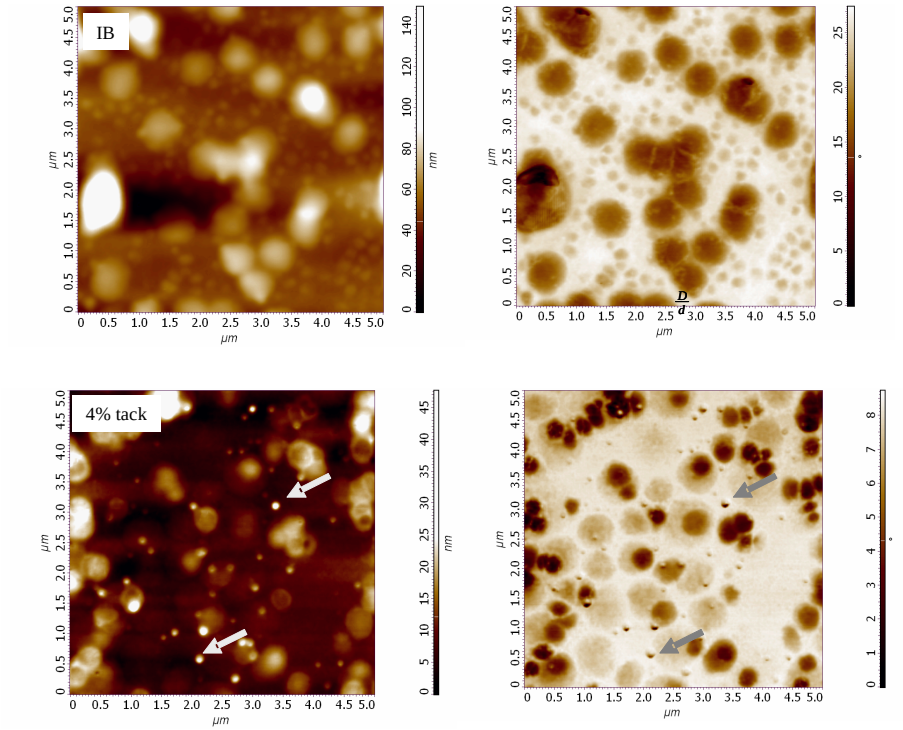

Figure 6-15. Height and phase AFM images of diluted IB (the presence of two distinctive particle sizes is the signature of a bimodal particle size distribution) and diluted in situ tackified miniemuslion based latex containing 4 wt% of tackifier. (arrows: small hard solid particles). Height images are shown on the left, phase images on the right.

Some AFM analyses have also been performed on dried adhesive films. For that, the latex dispersions were cast onto PET (Polyethylene terephthalate) sheet using a 30 µm coating bar. Films were dried at 110°C in an oven during 3 min. AFM images were obtained from the air-interface. Examples are given on Figure 6-16 and Figure 6-17.

Comparing IB and miniemulsion latexes, when the tackifier was added, there are some non continuous patchy hard zones (bright zones to be distinguished from other bright zones corresponding to surfactant rich regions). It seems that tackifier is finely and uniformly dispersed in the films and that the size of the corresponding bright zones increases with increasing tackifier concentration.

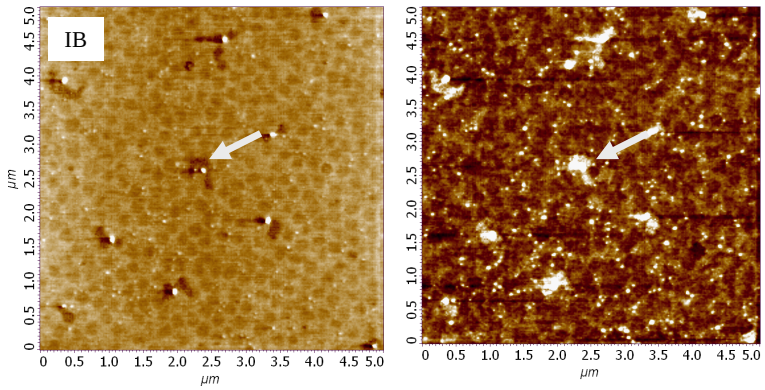

Figure 6-16. Height and phase images of IB the untackifed latex produced with a classical emulsion polymerization. Arrows: surfactant rich region. Height images are shown on the left, phase images on the right.

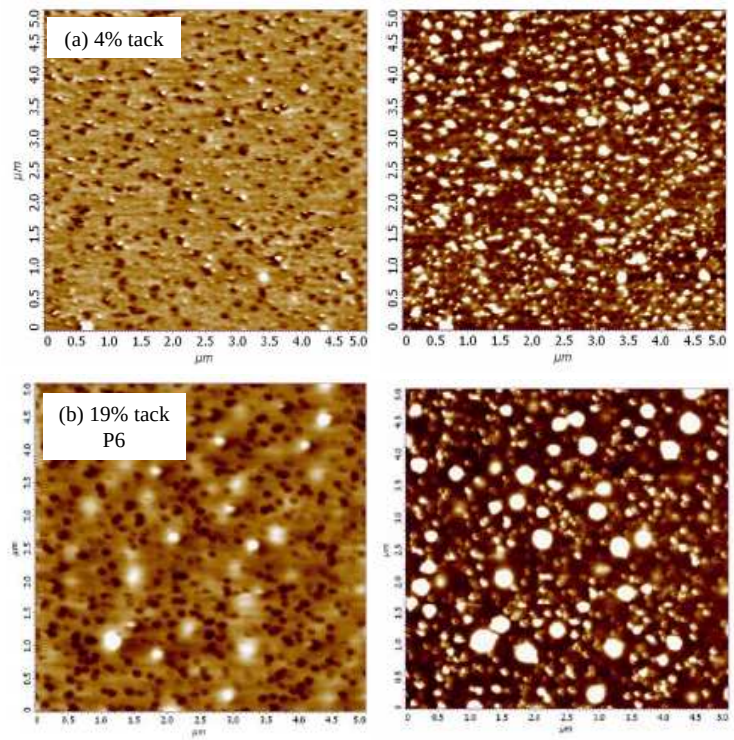

Figure 6-17. Height and phase images of in situ tackified miniemulsions based adhesive films. (a) wt% tack = 4 wt%, (b) wt% tack = 19 wt%. Height images are shown on the left, phase images on the right.

6.4.2.2. Two stage tackified latexes

The structures of individual particles of two-stage tackified latexes were explored through AFM analysis as shown in Figure 6-18. No well defined core-shell structure has been found either in the case of a shell with the composition IB or in the case of a shell with the composition B.

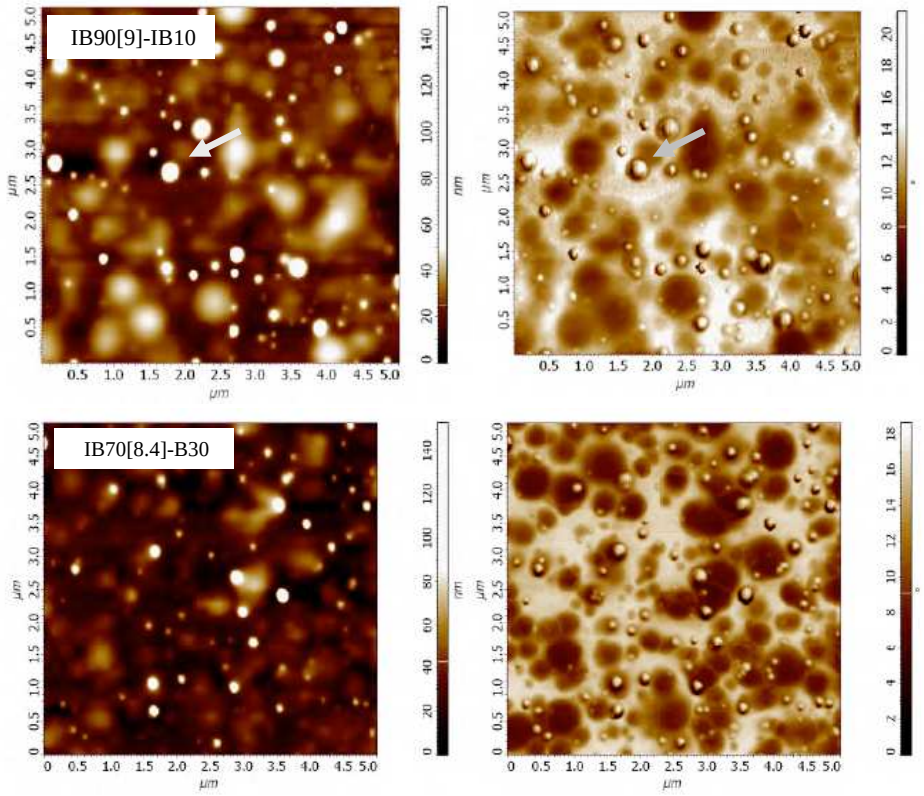

Figure 6-18. Height and phase AFM images of diluted IB90[9]-IB10 and diluted IB70[8.4]-B30. Height images are shown on the left, phase images on the right.

The structure of two-stage latexes based adhesive films (Figure 6-19) is similar to that of one stage materials. There is no obvious effect of the addition of a shell on the film structure. Here the increase in tackifier content is especially quite visible on height images. The higher the tackifier content the more numerous are the bright spots.

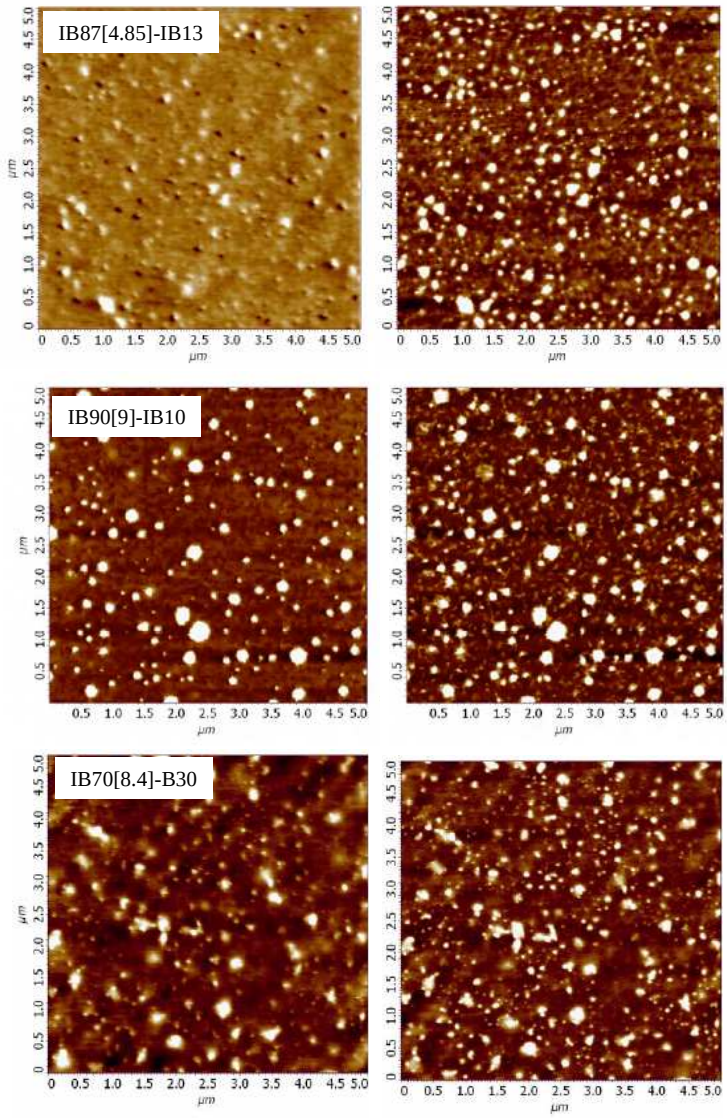

Figure 6-19. Height and phase images of two-stage based adhesive films. From the top to the bottom, one can see IB87[4.85]-IB13, IB90[9]-IB10 and IB70[8.4]-B30. Height images are shown on the left, phase images on the right.

Air-interface surfaces of layers made of tackified latexes have also been previously studied by Mallégol et al. using the AFM technique.[30] The effect the addition of a tackifying resin to an acrylic latex was different than what has been observed in the present work. In their study, PSA latexes were blended with tackifying resin dispersions. In one hand they found that the addition of the tackifier at low concentrations promotes a better coalescence of the acrylic particles since it forms a continuous phase with the serum solid phase. On the other hand, for tackifier concentrations of 25 wt% or more, the miscibility between acrylic and the tackifying resin has enabled the formation of a fully coalesced layer at the PSA surface leading to the creation of a dry skin layer.

The film formation process observed by Mallégol et al. is different from ours. But is that due to the tackification process (blend instead of situ tackification) or to the type of tackifier resin (rosin ester instead of hydrocarbon resin) or to more subtle parameters such as the

drying conditions (temperature and relative humidity)? This has not been elucidated but this example demonstrates how different can be the surface structure of films made of latexes prepared from similar formulations.

6.5. Adhesive and Rheological Results

6.5.1. Influence of the type of tackifying resin on tack results

The effect of the tackifying resin type (wt% resin = 19 wt%) on adhesive behavior, on stainless steel at debonding velocities of 10 and 1000 µm.s^{-1}, is clearly shown on Figure 6-20.

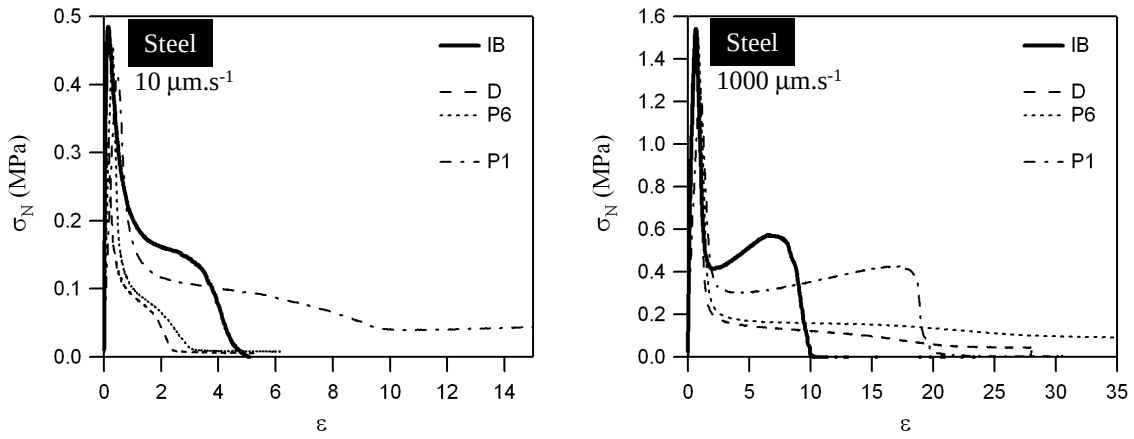

Figure 6-20. Nominal stress vs. strain of IB, D, P6 and P1 on stainless steel at debonding velocitis of 10 and 1000 µm.s^{-1}. Influence of the type of tackifying resin.

The adhesive made from latex without tackifying resin, IB, (bold solid line on Figure 6-20) is characterized by an adhesive debonding regardless of the debonding velocity. This is directly visible on tack curves from the drop of the stress to zero after the fibrillation plateau. During the debonding of the adhesive layer from a stainless steel probe, some cavities are formed; they grow laterally until reaching a maximal size. Then walls between these cavities are stretched vertically as long as the foot stay attached to the probe. The end of the test is characterized by the detachment of all the feet without leaving any residues on the probe. A sequence of images taken during the debonding is shown on Figure 6-21.

When tackifier is added, the debonding mechanism is different. All tackified latexes are characterized by a cohesive debonding at 10 µm.s^{-1}. At 1000 µm.s^{-1}, depending on the type of resin, debonding is either adhesive (P1) or cohesive (D and P6). These differences could have been expected from gel content measurements which revealed that different polymerization mechanisms are taking place according to the tackifier resin.

D and P6 have similar debonding behavior. Regardless of the speed of debonding, the debonding mechanism has the characteristic behavior of a viscoelastic fluid. It is characterized by the air penetration and a final cohesive debonding. This mechanism may be not easily predicted from the shape of the curve at 10 µm.s^{-1}, but looking at the sequence of images of Figure 6-21, there is no longer any doubt about it. Such fingers which evolve from the outer to the center are characteristic of a liquid behavior.

Concerning P1, at low debonding velocities the debonding mechanism has the characteristic behavior of a weakly crosslinked PSA. We can observe the air penetration from

the drop of the stress of 0.1 MPa which ends at a deformation of about 10. As for D and P6, some fingers are observed (Figure 6-21) and ε = 10 corresponds to the deformation at which the fingers have reached the center of the contact area between the probe and the adhesive layer. But, one can note that while the shapes of D and P6 fingers are similar, the shape of P1 fingers is a bit different.

At higher debonding velocity (1000 µm.s^{-1} on Figure 6-20), the debonding mechanism of P1 resembles more that of a crosslinked PSA. And the hardening during the fibrillation plateau is a signature of the limited extensibility of chains in the crosslinked network.

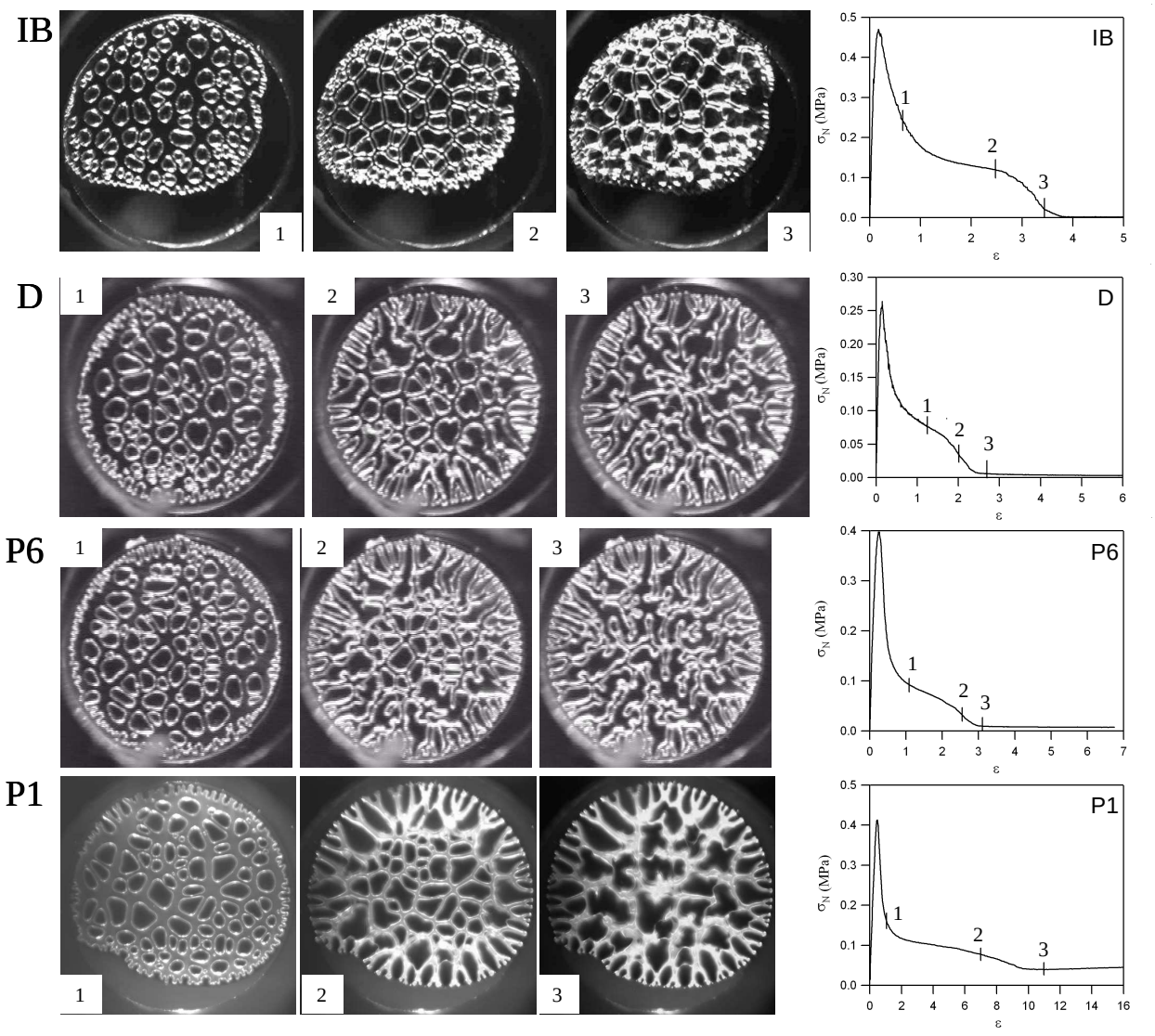

Figure 6-21. Sequences of debonding on stainless steel for the three miniemulsions D, P1 and P6 and for latex IB at a debonding velocity of 10 µm.s^{-1}.

Adhesives made of Dercolyte A115 or Piccotac 6095-E are too liquid to be used as PSA. Thus, Piccotac 1095-N has been selected as the preferred tackifying resin. Results already obtained suggest that a promising performance could be reached with this type of resin. An increase in adhesive energy at 1000 µm.s^{-1} from W_{adh} ~ 470 J.m^{-2} in the case of IB to W_{adh} ~ 600 J.m^{-2} for adhesive layer made of P1 is indeed observed.

Therefore, from now on, results shown are exclusively obtained on materials containing Piccotac 1095-N as the tackifying resin.

6.5.2. Further results of miniemulsion with Piccotac 1095-N

6.5.2.1. Linear viscoelastic properties

The rheological responses in the linear regime of IB and P1 have been measured. Results (Figure 6-22-a) show that, with the addition of resin, the storage modulus G′ decreases. Similar values of G″ are obtained. One can also observe that the slope of the G′ curve of P1 is a little bit higher and this may be a consequence of the higher T_g of the resin compared to that of the base latex.

From the higher tan(δ) values of P1 (Figure 6-22-b), the addition of resin results in a significant increase in dissipative properties. Moreover, in the range of low frequencies one can observe a slight increase in tan(δ) of P1 as the frequency decreases. This is not observed in the case of IB and this is the typical behavior of a very slightly or uncrosslinked polymer.

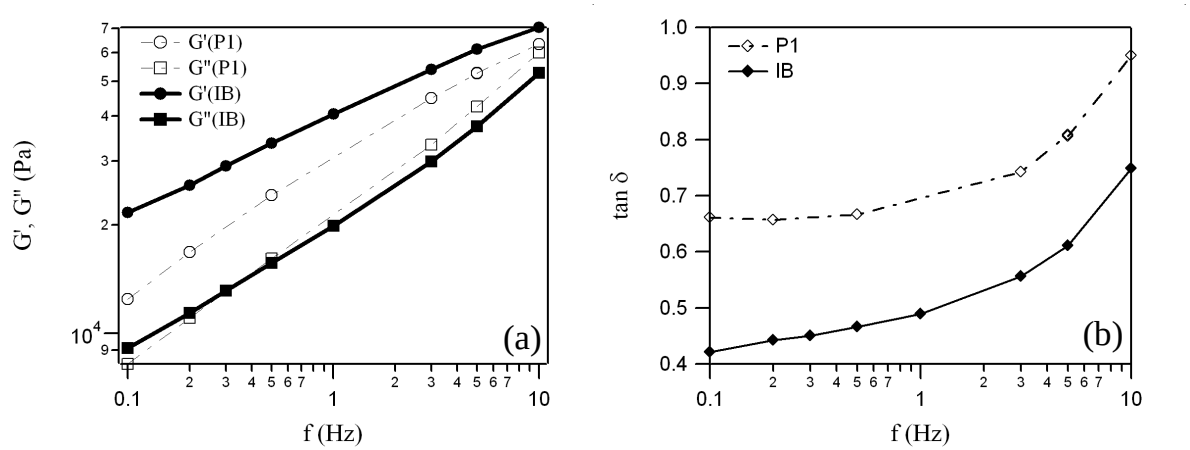

Figure 6-22. Rheological results over a range of frequencies from 0.1 Hz to 10 Hz. (a) Evolutions of G′ and G″. (b) Evolutions of tan(δ). Bold line: IB, thin dashed line: P1. Tests were performed on the microrheometer.

Adhesive results on P1 have been already shown on Figure 6-20 and the decrease in G′ is consistent with the observed decrease in σ_{max} of nominal stress vs. strain tack curves[31] (Figure 6-23). The increase in dissipation is responsible for the liquid-like behavior at 10 µm.s^{-1} and for the increase in the length of the fibrillation plateau at 1000 µm.s^{-1} (Figure 6-20).

Magnification of the early stages of the debonding of Figure 6-23 also clearly shows reproducibly that the tackified films have a lower and more nonlinear slope, characteristic of significant formation of cavities and/or fingers at an early stage.

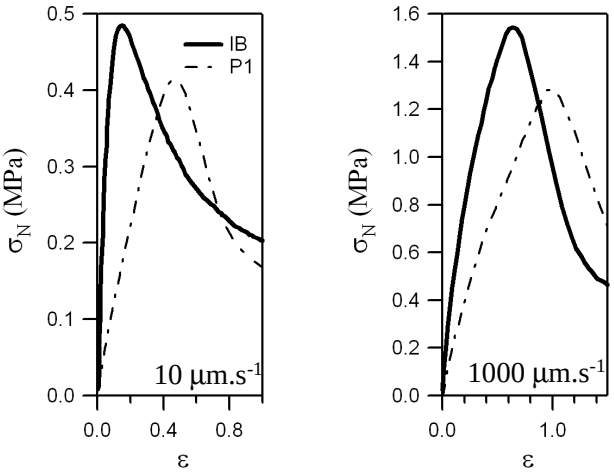

Figure 6-23. Magnifications of nominal stress vs. strain tack curves of IB and P1 in the range of small strains. Tests were performed on stainless steel at debonding velocitis of 10 and 1000 µm.s^{-1}.

Therefore, one can conclude that P1 is softer and more dissipative than IB and that its behavior is similar to that of a weakly crosslinked PSA.

6.5.2.2. Influence of tackifier content on tack results

The influence of tackifying resin content has been investigated in the case of tackified miniemulsions containing Piccotac 1095-N. (The adhesive sample containing 19 wt% of tackifying resin corresponds to the PSA called P1 in the previous section).

From Figure 6-24, at 10 µm.s^{-1}, the tackifying resin content has an effect on the debonding mechanism on stainless steel. A decrease from 19 wt% to 4 wt% leads to a progressive transition from a liquid-like behavior characterized by the air penetration (double fibrillation plateau) and a final cohesive debonding to a solid-like behavior characterized by a final adhesive debonding. The hardening during the fibrillation plateau observed when only 4 wt% is added is the signature of a crosslinked network. Between these two extremes, an intermediate behavior is observed with the adhesive made of the tackified miniemulsion containing 16 wt% of resin. It is characterized by a double fibrillation plateau and an adhesive debonding.

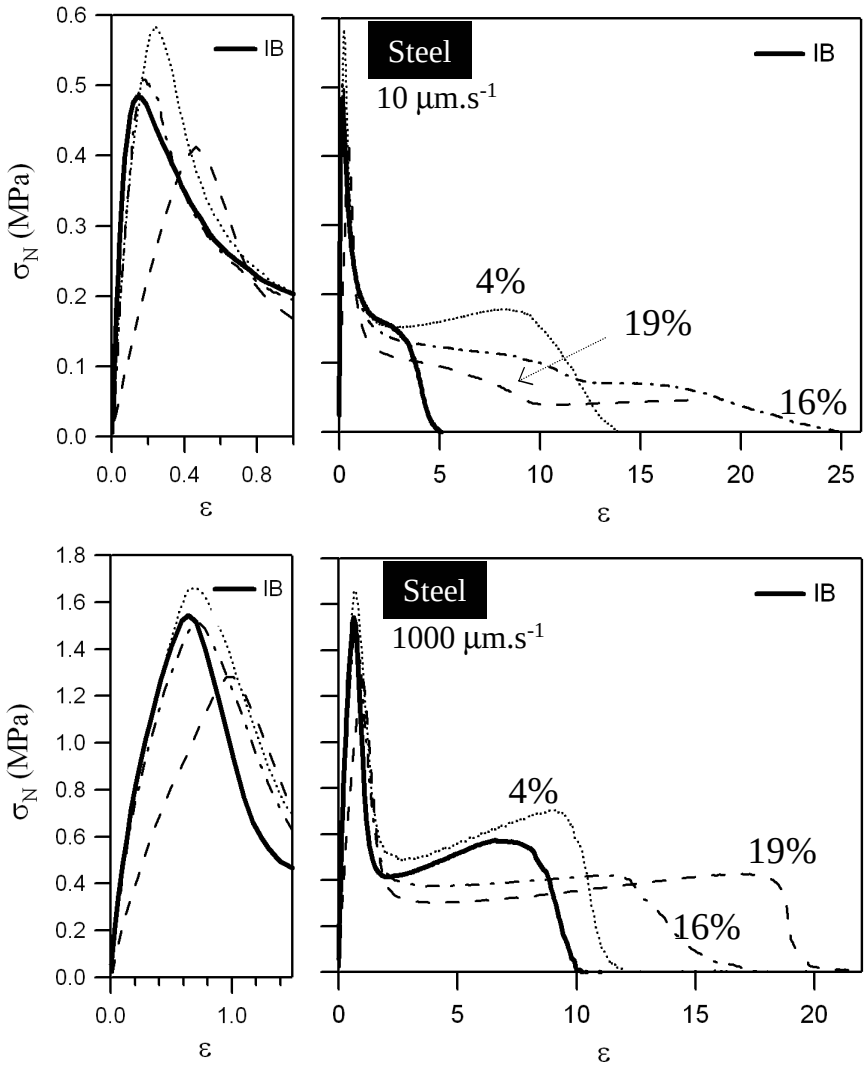

Figure 6-24. Nominal stress vs. strain tack curves of three miniemulsions with various tackifying resin content. Comparison with IB. Tests were performed on stainless steel at 10 and 1000 µm.s^{-1}. Magnifications of the peak stress are shown on the left part.

At 1000 µm.s^{-1}, on the contrary, the same debonding mechanism is observed for all the three adhesives tested. All curves are characterized by a well defined fibrillation plateau followed by a sharp final drop of the stress to zero. One can however notice that the fibril hardening tends to disappear as the resin content increases. Moreover, at high debonding velocity, addition of resin tends to simultaneously increase the fibrillation plateau length and decrease its stress level. These combined effects make adhesive energy at 1000 µm.s^{-1} nearly unchanged (Figure 6-25). This is interesting since, depending on application and substrate, either a soft and deformable material is required or a more cohesive and more rigid material is favorable.

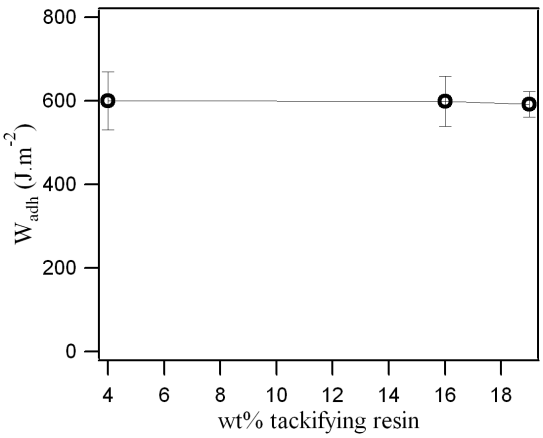

Figure 6-25. Evolution of the adhesive energy on stainless steel at a debonding velocity of 1000 µm.s^{-1} as a function of the tackifying resin content.

Magnifications of the curves in the small strain region (Figure 6-24) also show that increasing the tackifying resin content leads to a slight decrease in the peak stress σ_{max}. Thus one can reasonably expect that an increase in the tackifying resin content leads to a decrease in G′.

6.5.3. In-situ tackified core-shell latexes

In the following section will be presented results obtained on some in situ tackified core-shell latex based PSA.

6.5.3.1. In-situ tackified core-shell latexes vs. non tackified latex

a. Linear rheological properties

Some rheological measurements in the linear regime have been performed on IB87[4.85]-IB13. This is one of adhesives made of tackified core-shell particles. Both shell and core have the same IB monomer composition. IB87[4.85]-IB13 latex particles contain 4.85 wt% of tackifying resin (wt%/total monomers in the particle).

From results shown on Figure 6-26, values of the elastic modulus of IB87[4.85]-IB13 are nearly the same as that of IB until 1 Hz. Beyond, it is a little bit higher. As what has been observed for P1, the slope of G′ curve of IB87[4.85]-IB13 is higher than that of IB and this may be the consequence of the increase in T_g due to the presence of the tackifying resin. Values of G″ are significantly higher in the case of the tackified core-shell particle and this leads to higher dissipative properties measured by tan(δ) and shown on Figure 6-26-(b).

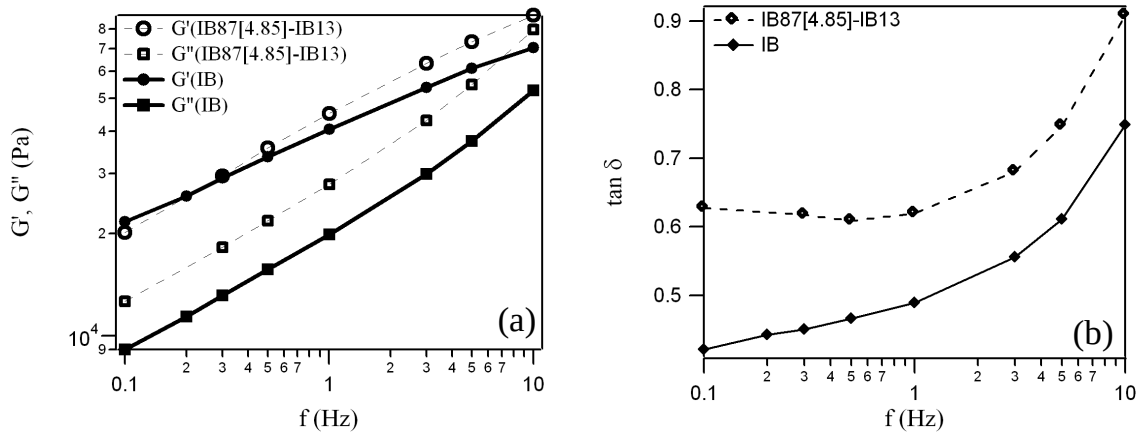

Figure 6-26. Rheological results over a range of frequencies from 0.1 Hz to 10 Hz. (a) Evolutions of G′ and G″. (b) Evolutions of tan(δ). Bold line: IB, thin dashed line: IB87[4.85]-IB13. Tests were performed on the microrheometer.

b. Tack results

Tack results are consistent with rheological measurements. Similar values of elastic modulus are confirmed by similar values of σ_{max} (Figure 6-27). And the higher dissipative properties of the tackified core-shell based adhesive film improve its ability to create a fibril structure; the final detachment is delayed.

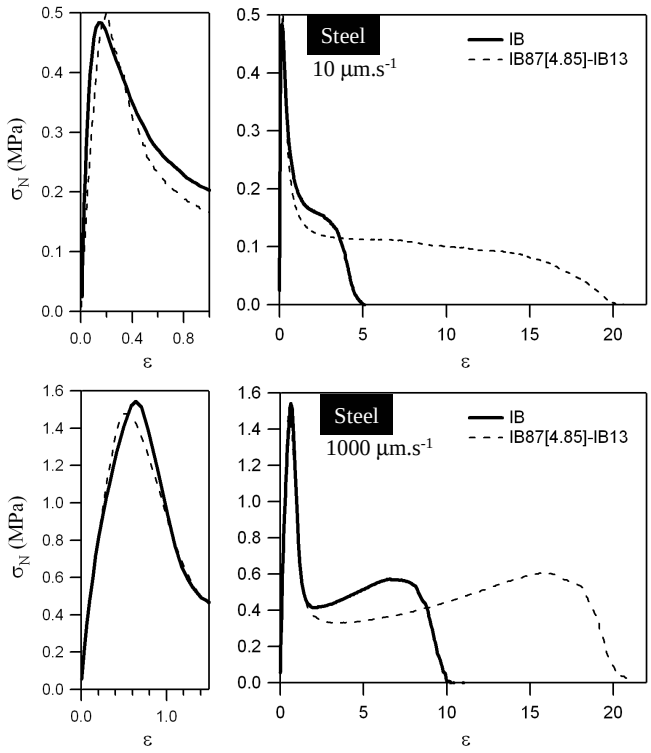

Figure 6-27. Nominal stress vs. strain tack curves of IB and IB87[4.85]-IB13 based adhesive films. Tests were performed on stainless steel at 10 and 1000 µm.s^{-1}. Magnifications of the peak stress are shown on the left part.

6.5.3.2. Homogeneous vs. core-shell tackified latexes

a. Linear rheological properties

It seems now logical to continue with a comparison between results obtained on PSA made of homogeneously tackified miniemulsions and on PSA made of tackified core-shell latexes. We will start with rheological measurements. These have been performed only on the core-shell containing 4.85 wt% of tackifying resin (comparison with IB has been already discussed) and in the one stage miniemulsion containing 19 wt% of resin.

Even though resin content is much lower in the tackified core-shell than in the tackified miniemulsion, a large increase in dissipation compared to IB is obtained in both cases (Figure 6-28-a).

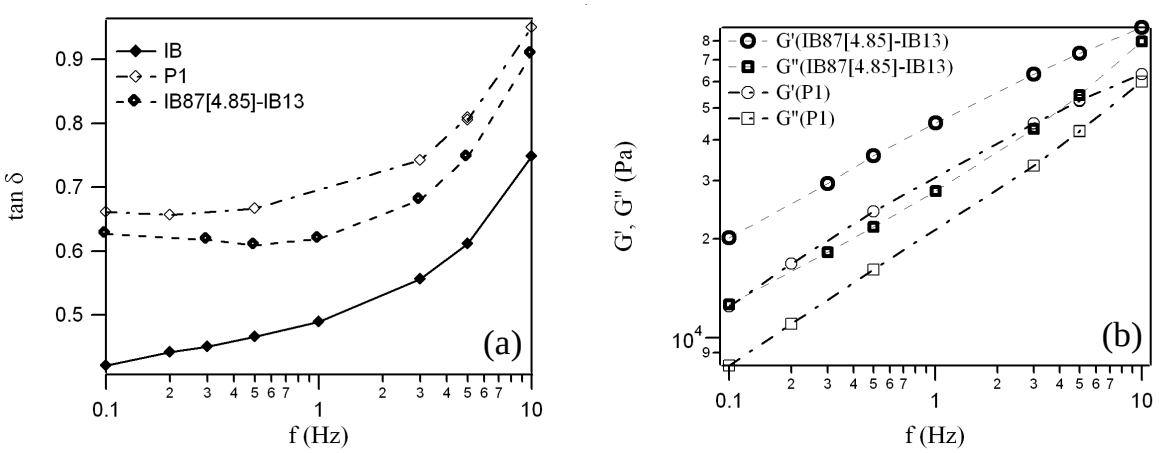

Figure 6-28. (a) Evolution of tan(δ) of IB, P1 and IB87[4.85]-IB13 as a function of the frequency. (b) Evolution of G′ and G″ of IB, P1 and IB87[4.85]-IB13 as a function of the frequency. Tests were performed on the microrheometer.

However, contrary to what has been observed for the homogeneously tackified PSA, the increase of this dissipation is not the result of a decrease in the elastic modulus G′ (Figure 6-22-a), but more that of an increase in the viscous modulus G″ (Figure 6-26-a).

G′ and G″ values of IB87[4.85]-IB13 are both higher than that of P1 and G′ and G″ curves of IB87[4.85]-IB13 can be viewed as the vertical translation of P1 curves towards the higher values (Figure 6-28-b). This could mean that the addition of the shell tends to increase the complex shear modulus G^* of the tackified core. Cautions must be however taken when interpreting these results since tackifier amounts are also different in these two materials. Comparison of debonding mechanism of materials having the same tackifier content is the scope of the second part of the following section but unfortunately linear rheological properties of core-shell with 19 wt% of tackifier or homogeneously tackified particles with 4.85 wt% of resin have not been characterized.

b. Tack results

In the previous section, we have compared IB87[4.85]-IB13 and P1 in terms of rheological properties in the linear regime. We will continue with a comparison of their adhesive results. Results are shown on Figure 6-29. At 10 µm.s^{-1}, while P1 has a liquid-like behavior, IB87[4.85]-IB13 is more solid like and characterized by an adhesive debonding.

At 1000 µm.s^{-1}, the increase in cohesion leads to a much more pronounced strain hardening during the fibrillation stage. This is a signature of a more crosslinked PSA. What is unusual but interesting to note is that this hardening does not induce an earlier detachment of the fibrils. ε_{max} of both materials is nearly the same.

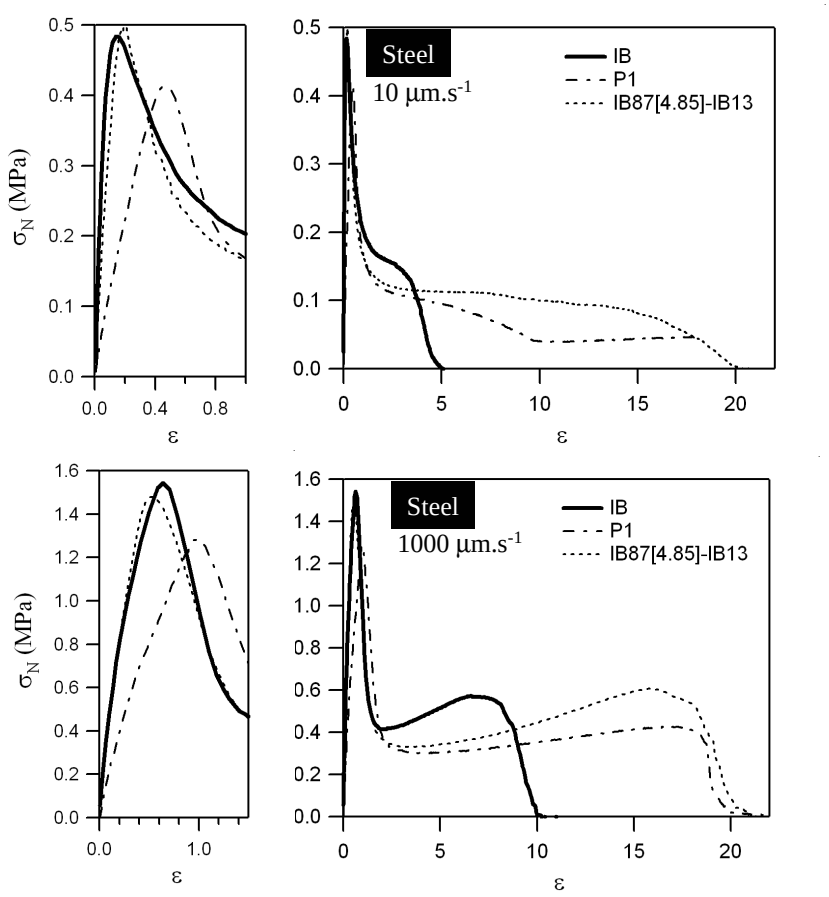

Figure 6-29. Nominal stress vs. strain tack curves. Bold solid line: IB, thin dashed line: P1, thin dotted line: IB87[4.85]-IB13. Tests were performed on stainless steel at 10 and 1000 µm.s^{-1}. Magnifications of the peak stress are shown on the left part.

Tack results are consistent with rheological results. Both materials are soft and highly dissipative and thus characterized by a long fibrillation plateau. The increase in cohesion due to the decrease in tackifier content and the addition of the shell is favorable since it increases the adhesive energy at 1000 µm.s^{-1} from a more pronounced strain hardening. However since both parameters have been changed, it is difficult conclude on the respective role of each.

More interesting is the comparison of tack results on two tackified materials containing the same amount of tackifying resin. Tack results are shown on Figure 6-30. This comparison

has been made on latexes containing about 4 wt% of resin. A homogeneously tackified material called IB100[4]-0 is compared to IB87[4.85]-IB13.

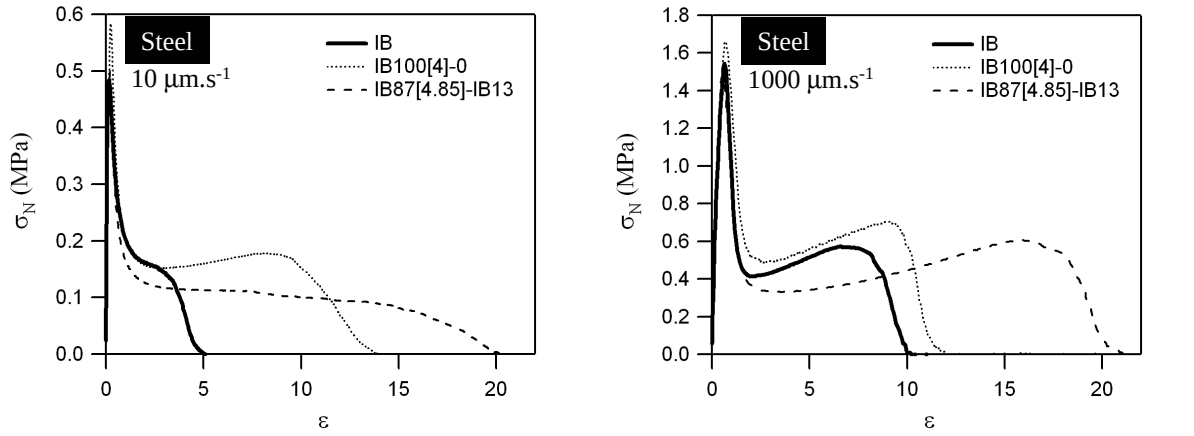

Figure 6-30. Comparison of tack results obtained on homogeneously tackified miniemulsion based PSA and tackified core-shell latexes based PSA. Dotted lines: homogeneously tackified miniemulsion containing 4 wt% of tackifying resin, dashed lines: tackified core-shell based PSA with 4.85 wt% of resin. Tests were performed on stainless steel at 10 and 1000 µm.s^{-1}.

We can see (Figure 6-30) that the addition of a shell around a tackified core with about 4 wt% of tackifier has a significant effect on the adhesive behavior. One can observe a significant decrease in the fibrillation plateau level. This is accompanied with an increase in its length. The increase in dissipation obtained has a detrimental effect on the cohesion but an increase in adhesive energy is nevertheless finally obtained (from about 600 J.m^{-2} for IB100[4]-0 to about 800 J.m^{-2} for IB87[4.85]-IB13).

It seems that the addition of a second stage results in a significant decrease in the cohesion of the material and to a large increase in dissipative properties. A slight crosslinking however remains and is responsible for the final detachment of the adhesive layer from the probe. This decrease in the cohesion is unexpected and not yet well understood.

One would have expected that the behavior of the two-stage latex based adhesive behaves like a more crosslinked and cohesive material due to the presence of the shell which is in principle not affected by the presence of the tackifier resin and characterized by a higher gel content. But it is highly possible that the change of the synthesis process has additional and not well understood effects.

6.5.3.3. Influence of the tackifier content of two stage latexes

The influence of the tackifying resin content has been studied in the case of core-shell particles. IB87[4.85]-IB13 is compared to IB90[9]-IB10. While the former latex contains 4.85 wt% of resin, the latter one has 9 wt%. As before, tack results have been obtained at various debonding velocities, what is new is that some tests have also been made on polyethylene (PE) probes.

Regardless of the tackifier amount, of the probe surface and of the debonding velocity, tested PSA debond always adhesively from the probes. Moreover, regardless of test

conditions, the fibrillation plateau of IB90[9]-IB10 is slightly lower than that of IB87[4.85]-IB13.

At 10 µm.s^{-1}, on stainless steel as on PE, an increase in the tackifier amount leads to the appearance of a double fibrillation plateau, characteristic of a more liquid-like behavior. The differences between the two materials are a bit more pronounced on PE. Everything can however readily be explained by the viscoelastic properties of the adhesives. The softer and more liquid IB90[9]-IB10 is rather insensitive to the change in surface while the harder and more solid-like IB87[4.85]-IB13 becomes much more sensitive to the interfacial interactions and in particular at high debonding velocity where the stainless steel and PE results are very different.

On stainless steel, increasing the resin content makes the strain hardening disappear. What is more surprising is the decrease in the maximal deformation (ε_{max}) and no similar trend has been observed in the case of homogeneously tackified particles (Figure 6-24). This is also not observed on PE. In general, the longer fibrillation plateau has been obtained for the higher amount of resin.

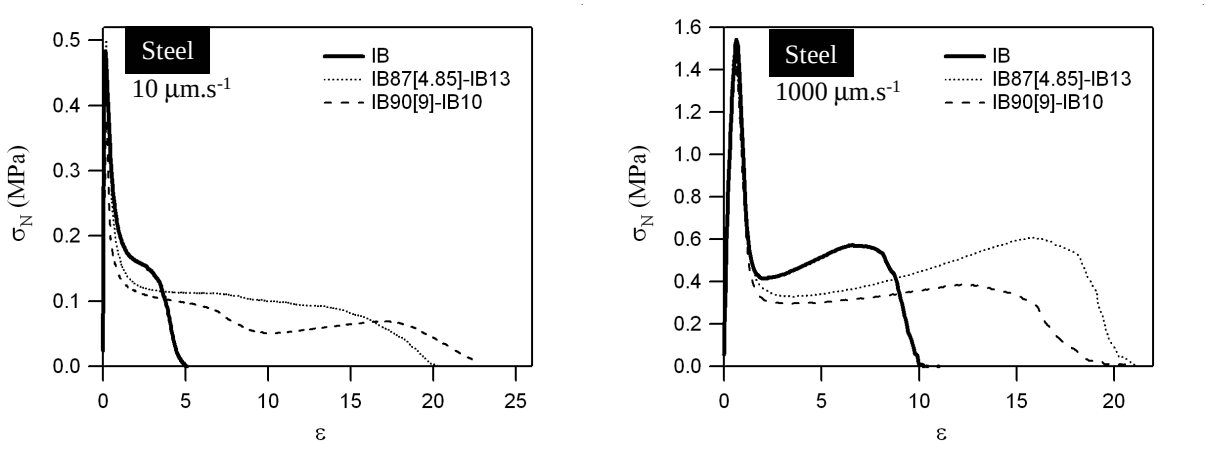

Figure 6-31. Influence of resin content on tack results of tackified core-shell based PSA. Comparison between IB87[4.85]-IB13 and IB90[9]-IB10. Tests were performed on stainless steel at 10 and 1000 µm.s^{-1}.

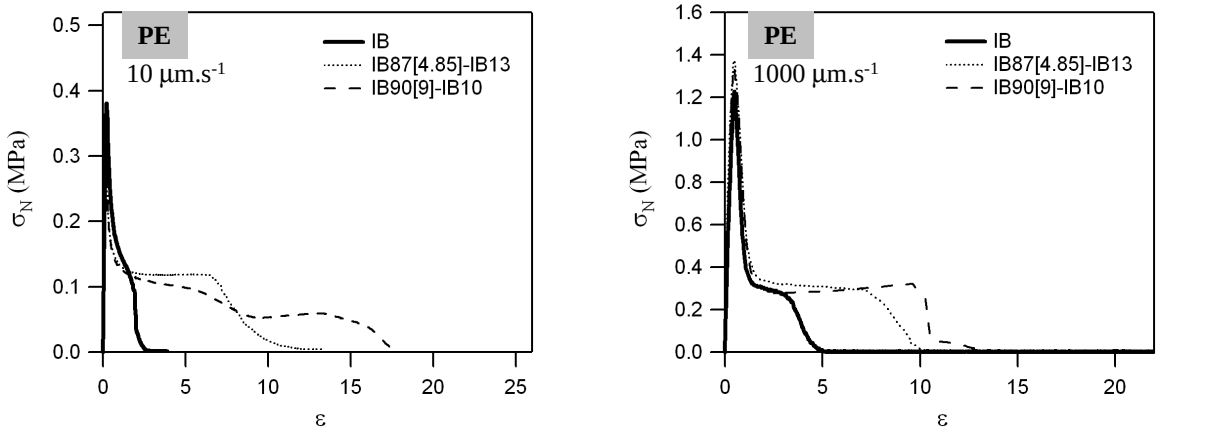

Figure 6-32. Influence of resin content on tack results of tackified core-shell based PSA. Comparison of nominal stress vs. strain tack curves obtained with IB87[4.85]-IB13 and IB90[9]-IB10. Tests were performed on PE at 10 and 1000 µm.s^{-1}.

From an industrial prospective, one can note that adhesive performance of the non tackified IB latex based PSA (bold solid line of Figure 6-32) has been significantly improved. On stainless steel, this improvement of adhesion is to the prejudice of the cohesion of the materials and a significant decrease in the fibrillation plateau level is observed. This decrease however completely disappears when tests are performed on a PE surface which was the goal set out by the industrial partner in adding the resin.

From these results, adhesion on stainless steel seems better with 4.85 wt% of tackifying resin while performance on PE is better with 9 wt%. Moreover, the strategy which consists in the incorporation of a tackifying resin to a latex seems very well adapted for applications on PE.

6.5.3.4. Nonlinear deformation behavior

We have seen that in situ tackified core-shell latexes based PSA show much better adhesive properties than the non tackified IB latex. In chapter 5, we showed that better adhesive performance could be explained by a more pronounced softening at intermediate strains. Thus, it is interesting to examine the nonlinear behavior of the present materials.

Tensile curves of IB and IB90[9]-IB10 are shown on Figure 6-33. The nominal stress vs. strain curve as well as the reduced stress vs. $1/\lambda$ curve of the tackified core-shell latex is characterized by a very low level of stress during nearly all the elongation process. This is thought to be the result of the presence of the tackifier resin which probably acts as a chain transfer agent.

Nominal stress vs. strain curves have been fitted using the viscoelastic-hardening model presented in chapter 5. Data resulted from the fit are shown on Table 6-4. A decrease in the level of stress has been clearly observed at intermediate and high strains and is retrieved at small strains from the fit. From the homogeneous untackified based PSA to the tackified core-shell based PSA, a decrease of $3(G_v+G_e)$ from 170 kPa to 75 kPa (Table 6-4) is indeed obtained. What is also interesting to note is that this decrease is for a large part due to a significant decrease in the more elastic shear modulus G_e of the model. The viscoelastic contribution quantifies by G_v is also reduced but to a lower extend. This confirms that the tackifying resin has the effect to reduce the crosslink density of the crosslinked network.

This is in agreement with the delayed strain hardening of the reduced stress curve and with the increase in J_m. Nevertheless, a value as low as J_m = 400 indicates that a percolating network is created and is responsible for the adhesive debonding of the fibrils at the end of the tack experiments.

Nominal stress vs. strain fitted curves depicted on Figure 6-34 clearly show that the tackified core-shell based PSA is characterized by a much more pronounced softening at intermediate strains than IB. This softening is quantified by the ratio G_v/G_e (Table 6-4) and a large increase from about 2 to 10 is indeed observed from IB to IB90[9]-IB10. This increase in the dissipation thus explains the higher ability of the tackified PSA to fibrillate during tack experiments leading to higher maximal deformations both on stainless steel and PE surfaces.

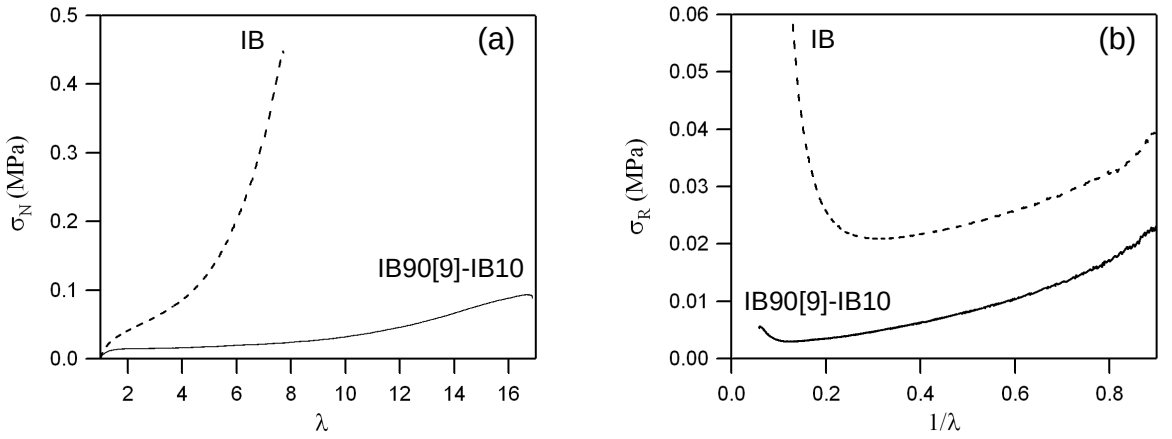

Figure 6-33. Tensile results of IB90[9]-IB10 (solid line) and IB (dashed line) (a) Nominal stress vs. strain curves. (b) The corresponding Mooney representations. Tests were performed at 50 $mm.min^{-1}$.

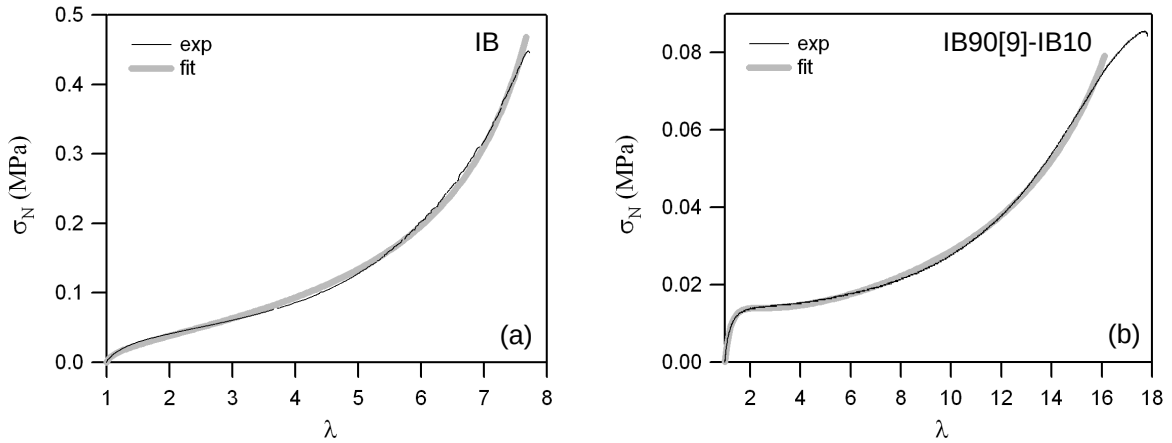

Figure 6-34. Examples of nominal stress vs. strain tensile curves fitted using the viscoelastic-hardening model. (a) tensile curve of IB and (b) tensile curve of IB90[9]-IB10.

	G_v (kPa)	G_e (kPa)	J_m	De	G_v/G_e	$3(G_e+G_v)$ (kPa)
IB	38.7 (± 6.89)	17.4 (± 1.69)	71.0 (± 8.46)	0.092 (± 0.013)	2.21 (± 0.226)	169 (± 25.3)
IB90[9]-IB10	23.1 (± 2.00)	2.27 (± 0.18)	419.1 (± 29.4)	0.240 (± 0.022)	10.2 (± 0.386)	76.2 (± 6.52)

Table 6-4. Fitting parameters obtained for IB and IB90[9]-IB10.

To conclude, better adhesive performance of tackified material can indeed be related to a more pronounced softening observed at intermediate strains during tensile experiments. Additionally, the low level of stress accompanied with a final strain hardening are ideal conditions for good adhesive performance on PE.

6.5.3.5. Core and shell optimization

One of the advantages of the two-stage process is the possibility to independently tune properties of both stages which we will call for simplicity core and shell. Both core and shell of IB90[9]-IB10 have been modified.

- Chain transfer agent has been removed from both the core and the shell. This has been done in the objective of increasing the cohesion.
- The monomer composition of the shell was changed from composition IB to composition B which contains some polar monomers (see section 6.3.2.2) in order to improve adhesion on polar substrates (like stainless steel or glass).
- The thickness of the shell has also been slightly increased so that the effect of the change in shell composition is more visible.

Tack experiments have been performed on stainless steel and PE. Some of results shown here has been obtained by Jeanne Marchal, post-doc in our laboratory. Regardless of the debonding velocity, results on stainless steel (Figure 6-35) show that the fibrillation plateau level of the modified tackified core-shell latex based PSA is higher. This means that the modifications had the expected effect of increasing the cohesion of the material. This increase in the cohesion has however a detrimental effect on the adhesion. Adhesive energy at 1000 $\mu m.s^{-1}$ is indeed decreased from about 640 $J.m^{-2}$ to about 400 $J.m^{-2}$.

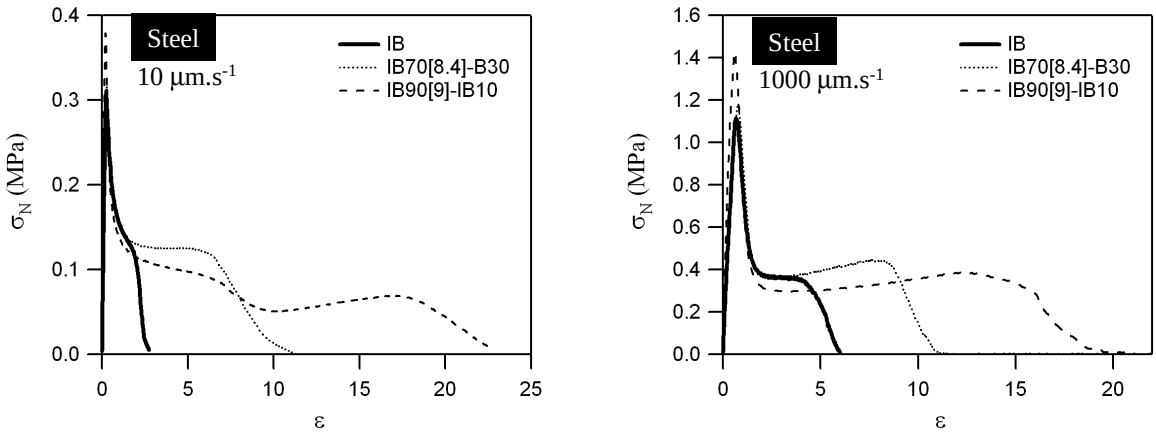

Figure 6-35. Nominal stress vs. strain tack curves obtained with IB90[9]-IB10 and IB70[8.4]-B30. Tests were performed on stainless steel at 10 and 1000 $\mu m.s^{-1}$. (Tack experiments on IB70[8.4]-B30 have been performed by Jeanne Marchal).

The increase in cohesion accompanied with a decrease in adhesion is also observable on PE (Figure 6-36). However, performance of the modified PSA becomes very low. This may due to the fact that the more elastic composition B is not well adapted for applications on substrates with weak adhesive interactions like PE.

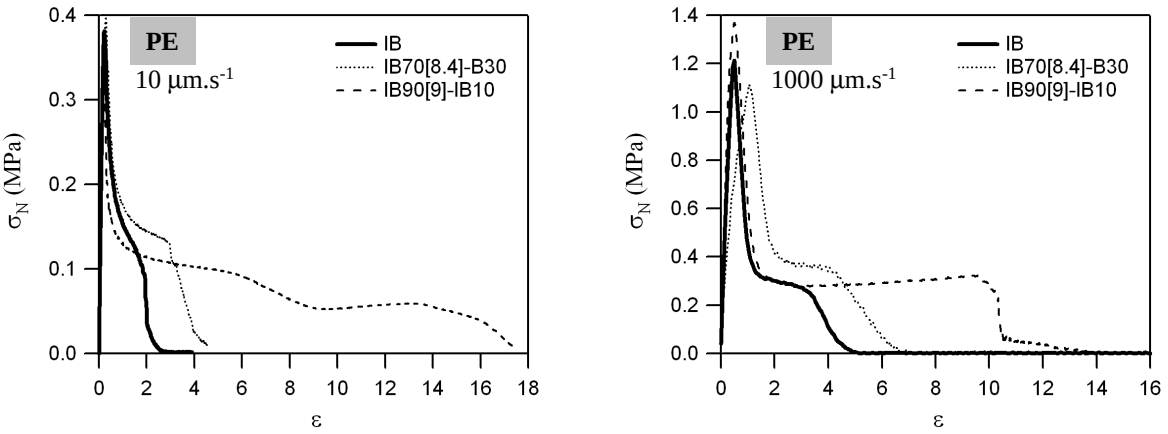

Figure 6-36. Nominal stress vs. strain tack curves obtained with IB90[9]-IB10 and IB70[8.4]-B30. Tests were performed on PE at 10 and 1000 µm.s^{-1}.

Finally, these results show that the modification of core-shell composition leads to the expected increase in the cohesion and to a significant loss of adhesive performance on PE.

It seems that IB70[8.4]-B30 is well adapted for applications on stainless steel which requires a high cohesion level while IB90[9]-IB10 is more suitable for applications on PE. These conclusions in terms of better or worse performance will be discussed in more detail in the following section.

6.6. Technical feasibility

A part of the NsHAPe research program was dedicated to establishing the technical feasibility for commercial implementation of new concepts identified in the laboratories for designing PSA with enhanced performances. Implementation of the selected approach i.e. miniemulsion as an industrial process at pilot scale, and production of 80-kg pilot batch(es) of the selected prototypes has been made by Cytec Surface Specialties in Drogenbos in Belgium under the supervision of K. Ouzineb. Machine coating tests and film's final application properties evaluation have been done in Raflatac in Tempere in Finland under the supervision of I. Pietari and T. Helin.

The last two materials studied (IB70[8.4]-B30 and IB90[9]-IB10) have been selected as promising candidates and have been scaled up. Pilot samples have been developed and evaluated.

The best pilot trials are obtained after optimizing the runnability and coating. For that, it is necessary to pay attention on both wetting and foaming problems. For the first prototype (called "proto 1") and based on IB90[9]-IB10, best film performance was obtained adding 0.2 part by weight of anti foam agent and 0.2 part by weight of wetting agent per hundred parts by weight of latex. The runnability of the second prototype (called "proto 2") based on IB70[8.4]-B30 was better when compared to "proto 1". But higher amounts of wetting agent and anti foam agent were required (0.3 parts for each agent) since there was still foaming.

From a practical point of view, it appears that there is no major obstacle which would prevent the implementation of the selected miniemulsion tackified core-shell polymerization process in an industrial context. Feasibilities of both up-scaling of polymerization process and coating on machine have been demonstrated.

Materials have been characterized using analytical techniques. Results obtained indicate that latex features, including particle size and particle morphology, are not affected in the transfer from lab to pilot plant. The only significant difference noticed between pilot and lab batch is the lower viscosity of the former one. Nonetheless, this will have no impact for the machine-coating trials. Indeed, the coating formulation recipe can be adapted accordingly.

AFM pictures (Figure 6-37 and Figure 6-38) indicate that the morphologies of particles and of lab-coated films of pilot latexes are comparable to the ones observed previously on corresponding lab scale samples.

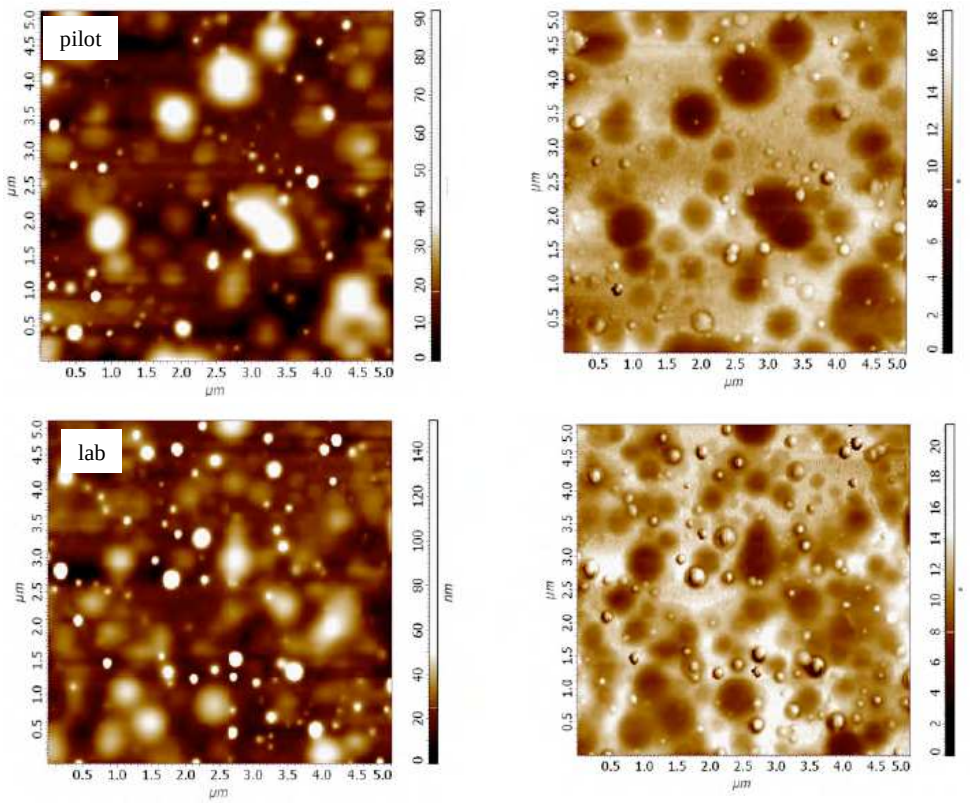

Figure 6-37. Height and phase AFM images of diluted IB90[9]-IB10 pilot and lab samples. Height images are shown on the left, phase images on the right.

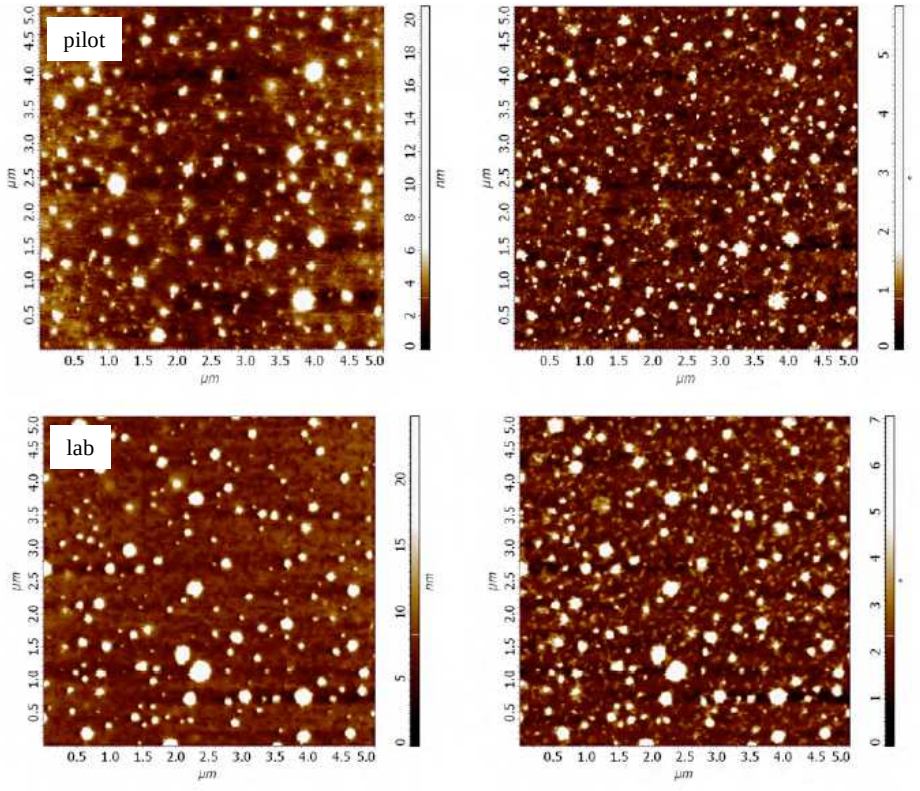

Figure 6-38. Height and phase images IB90[9]-IB10 pilot and lab latexes based adhesive films. Height images are shown on the left, phase images on the right.

Adhesive and deformation results already shown in the previous section were performed on the pilot samples. A comparison between lab and pilot samples of IB70[8.4]-B30 is given on Figure 6-39. Results show that the sample prepared in the laboratory seems a bit more cohesive (slightly higher fibrillation plateau) and less dissipative (earlier debonding). The same trend has been observed on the IB non tackified material (results are not shown here). The decrease in the cohesion is confirmed by a decrease in the shear resistance for the transfer from the lab to pilot scale. Nonetheless, one can conclude that both materials have similar adhesive behaviors.

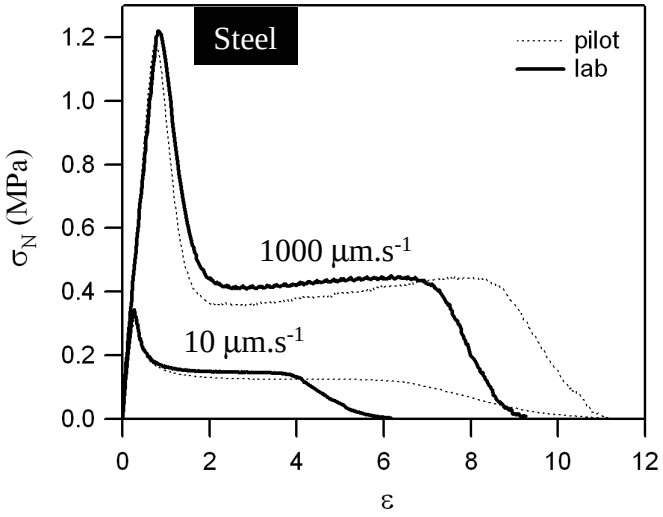

Figure 6-39. Nominal stress vs. strain tack curves obtained with IB70[8.4]-B30 pilot (dotted line) and lab (solid line) samples. Tests were performed on stainless steel at 10 and 1000 µm.s^{-1}.

Adhesive results obtained from standard adhesive tests of the pilot runs are shown on Table 6-5. They have to be compared to results on IB and to adhesive targets. Adhesive performance targets have been set in relation to current industry expectations. They are in line with expectations of a potential customer for high performance transparent plastic label applications. A new pilot run of IB is produced again and retested whenever a new sample is produced. That is why two different columns correspond to IB results.

Although shear values of proto 1 were below the target, adhesion properties were quite good and much better than IB. Concerning proto 2, shear resistance has been significantly improved compared to proto 1. And even though some target values were not reached, when compared to IB, it is clearly better in all aspects.

			Target	IB[a]	Proto 1 IB90[9]-IB10	IB[b]	Proto 2 IB70[8.4]-B30
Peel 24h 180° (FTM1) (N/25mm)	**glass**		> 17	4.0	12.9 PCF[c]	3.3	6.0
	HDPE plate		11	2.3	4.7	2.5	4.2
Peel 24h 90° (FTM2) (N/25mm)	**glass**		> 15	6.3	10.9	4.4	6.8
	HDPE plate		10	4.5	6.0	3.2	7.6
Looptack (FTM9) (N/25mm)	**glass**		> 20	8.7	15.5	7.6	11.4
	HDPE plate		10	3.6	7.4	3.2	6.4
Shear (FTM8) (min)	**Stainless steel (1kg, 1 inch^2)**		> 1500	10000	698	> 11490	2481
Water resistance	**Glass**	**One day[d] (N)**		3.8	4.2	2.1	4.6
		Whitening (mm)		0.5	1.0	0-0.5	0-0.5
	HDPE	**One day (N)**		3.1	10.1	4.3	5.2
		Whitening (mm)		1.0	0.5	0	0-0.5
UV-tack (N/25mm)			10.0	8.6	12.0	5.1	7.8

a- To be compared to proto 1.
b- To be compared to proto 2.
c- PCF: Partly cohesive failure.
d- Measurement is performed after a 24h immersion in water.

Table 6-5. Standard adhesive tests results of pilot runs.

Additional results of water resistance and ultraviolet stability are shown in Table 6-5. These properties are both enhanced compared to the untackified latex. This is an interesting result when we know that UV stability and water resistance are some factors of importance in selecting a resin.

From this work, the key challenges in further development of miniemulsion tackified core-shell type adhesives have been identified. The needed improvement of the coatability could be reached through an optimized selection of different wetting agent/defoamer and the drying of the film during the pilot coating may be improved with an increase in the final solids.

The technical feasibility for commercial implementation of a new concept for designing wb-PSA with enhanced performance has been established.

6.7. Discussion

The addition of Piccotac 1095-N as a tackifying resin to our latex formulations seems to have qualitatively the same effect as the addition of a tackifying resin to styrene-isoprene-styrene PSA formulations in that increasing the resin content leads to higher values of the maximal extension ε_{max} and lower values of stress during the fibrillation plateau (Figure 6-40). However the amounts added are vastly different. In SIS PSA, the main role of the resin is to dilute the entanglement network, while in the acrylic PSA's the resin is only added in much smaller amounts and increases the viscoelastic dissipation.

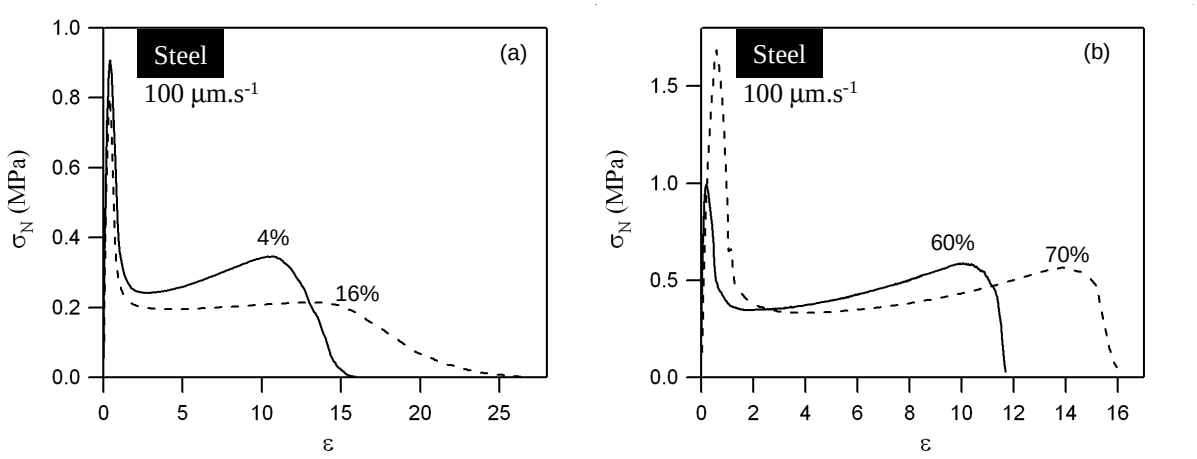

Figure 6-40. Influence of the tackifier content on stress vs. strain tack curves. (a) Comparison between a homogeneously tackified latex containing 4% of resin (solid line) and a homogeneously tackified latex containing 16% of resin (dashed line). (b) Comparison between two SIS formulations with 42 wt% of SI containing 60 wt% (solid line) and 70 wt% (dashed line) of tackifying resin (a hydrogenated hydrocarbon resin) (after[32]). Tests were performed on stainless steel at 100 µm.s^{-1}.

In our system, a liquid like behavior characterized by a low level of cohesion is very rapidly obtained when the debonding velocity is decreased (for tackified wb-PSA with 16% of tackifier resin) and the origin of such an effect is not yet completely elucidated. Much is known about the action of a tackifier in rubber or hot-melt block copolymer formulations. But this is the first research carried out on in situ tackified waterborne formulations produced with miniemulsion.

These results clearly point to the fact that the resin interacts with the polymer growing chains during the polymerization.

Nonetheless, this work clearly shows that resin interacts with the polymer growing chains during the polymerization. While no evidence of grafting has been observed, it seems that resin acts like a chain transfer agent in regulating the gel content of the emulsion latexes. This has the combined effect of increasing adhesion (increase in the peel strength) and decreasing cohesion (decrease in the shear resistance). But is the effect of a tackifying resin exactly the same as a conventional chain transfer agent? This is still unclear.

Apart from the fact that the resin probably acts as a chain transfer agent, it seems to have the most important characteristics which must be fulfilled by a resin to be considered as a tackifier. Its solubility in the polymer has been demonstrated from the increase in T_g as the

resin content increases and from SEC measurements which show that the resin is incorporated in the polymer particle. Its ability to modify the viscoelastic properties of the polymer has also been demonstrated from linear rheological measurements. Finally, the resin has the desired properties to enhance adhesion of the non tackified PSA. Additionally, the adjustment of the resin content can be a promising tool to modulate adhesion of the PSA depending on the type of adherent used. While a low resin content may be preferred for applications on high surface energy substrates like stainless steel, high contents is more favorable for applications on low energy substrates like polyethylene.

A second question which we have to address is the effect of the addition of the shell around the core. Interestingly, this has revealed itself to be a promising strategy to increase the final solid content of the latex. Results on adhesive and rheological properties are however still unclear. We still wonder why two stage materials exhibit a much lower cohesion and higher dissipation than the homogeneously tackified materials.

6.8. Conclusion

In situ tackified waterborne PSA have been synthesized using miniemulsion polymerization which is not yet known as a process used at industrial scale. Large differences in viscoelastic and adhesive properties are observed between these tackified adhesives and a non tackified benchmark PSA synthesized using a conventional emulsion polymerization process. An improvement of adhesive performance has been obtained. More importantly from an industrial prospective, the films are transparent, the resin does not macroscopically phase separate and seems to be incorporated homogeneously in the base polymer.

To our knowledge this is the first systematic study demonstrating the potential of miniemulsion polymerization to design the structure of pressure-sensitive-adhesives and while many aspects remain poorly understood and will need to be addressed with a better model system, this first study is clearly encouraging.

Furthermore the use of probe tack, combined to the rheological characterization and to the large strain tensile tests has proved to be a powerful and sensitive analytical tool to guide chemists toward the required synthesis changes.

Finally, we also showed that the industrial implementation of the new synthesis process is possible. And two stage in situ tackified miniemulsion waterborne PSA could become the next generation of high performance environmental friendly commercial PSA as originally proposed in the N-sHAPe project.

References

(1) FerrandizGomez, T. D.; FernandezGarcia, J. C.; OrgilesBarcelo, A. C.; MartinMartinez, J. M. *Journal of Adhesion Science and Technology* **1996**, *10*, 833-845.

(2) Aubrey, D. W.; Sherriff, M. *Journal of Polymer Science Part a-Polymer Chemistry* **1980**, *18*, 2597-2608.

(3) Class, J. B.; Chu, S. G. *Journal of Applied Polymer Science* **1985**, *30*, 805-814.

(4) Class, J. B.; Chu, S. G. *Journal of Applied Polymer Science* **1985**, *30*, 815-824.

(5) Class, J. B.; Chu, S. G. *Journal of Applied Polymer Science* **1985**, *30*, 825-842.

(6) Aubrey, D. W.; Sherriff, M. *Journal of Polymer Science Part a-Polymer Chemistry* **1978**, *16*, 2631-2643.

(7) FerrandizGomez, T. D.; FernandezGarcia, J. C.; OrgilesBarcelo, A. C.; MartinMartinez, J. M. *Journal of Adhesion Science and Technology* **1996**, *10*, 1383-1399.

(8) Nakajima, N.; Babrowicz, R.; Harrell, E. R. *Journal of Applied Polymer Science* **1992**, *44*, 1437-1456.

(9) Tse, M. F.; Jacob, L. *Journal of Adhesion* **1996**, *56*, 79-95.

(10) Satas, D. *Handbook of Pressure Sensitive Adhesive Technology*; Van Nostrand Reinhold Book: New York, 1989.

(11) Mallegol, J.; Bennett, G.; McDonald, P. J.; Keddie, J. L.; Dupont, O. *Journal of Adhesion* **2006**, *82*, 217-238.

(12) Kim, H. J.; Mizumachi, H. *Journal of Adhesion* **1995**, *49*, 113-132.

(13) Kim, H. J.; Hayashi, S.; Mizumachi, H. *Journal of Applied Polymer Science* **1998**, *69*, 581-587.

(14) Kim, H. J.; Mizumachi, H. *Journal of Applied Polymer Science* **1995**, *57*, 175-185.

(15) Kim, H. J.; Mizumachi, H. *Journal of Applied Polymer Science* **1995**, *56*, 201-209.

(16) Tobing, S. D.; Klein, A. *Journal of Applied Polymer Science* **2000**, *76*, 1965-1976.

(17) Schlademan, J. A. In *Handbook of pressure sensitive adhesive technology*, 2nd ed.; Satas, D., Ed.; Van Nostrand Reinhold: New York, 1989; Vol. 1, pp 527-544.

(18) Sherriff, M.; Knibbs, R. W.; Langley, P. G. *Journal of Applied Polymer Science* **1973**, *17*, 3423-3438.

(19) Gibert, F. X.; Marin, G.; Derail, C.; Allal, A.; Lechat, J. *Journal of Adhesion* **2003**, *79*, 825-852.

(20) Yang, H. W. H. *Journal of Applied Polymer Science* **1995**, *55*, 645-652.

(21) Brandrup, J.; Immergut, E., H.; A., G. E. *Polymer Handbook*, Fourth edition ed.; Wiley & Sons: New-York, 1999.

(22) Brandrup, J.; Immergut, E., H. *Polymer Handbook.*, Third edition ed.; Wiley: New York, 1989.

(23) Arzamendi, G.; Asua, J. M. *Macromolecules* **1995**, *28*, 7479-7490.

(24) Guyot, A.; Chu, F.; Schneider, M.; Graillat, C.; McKenna, T. F. *Progress in Polymer Science* **2002**, *27*, 1573-1615.

(25) Huang, N. J.; Sundberg, D. C. *Polymer* **1994**, *35*, 5693-5698.

(26) Chu, F. X.; Graillat, C.; Guyot, A. *Journal of Applied Polymer Science* **1998**, *70*, 2667-2677.

(27) Ouzineb, K.; Graillat, C.; McKenna, T. F. *Journal of Applied Polymer Science* **2005**, *97*, 745-752.

(28) Tang, C. B.; Chu, F. X. *Journal of Applied Polymer Science* **2001**, *82*, 2352-2356.

(29) Leiza, J. R.; Sudoi, E. D.; ElAasser, M. S. *Journal of Applied Polymer Science* **1997**, *64*, 1797-1809.
(30) Mallégol, J.; Bennett, G.; McDonald, P. J.; Keddie, J. L.; Dupont, O. *Journal of Adhesion* **2006**, *82*, 217-238.
(31) Lakrout, H.; Sergot, P.; Creton, C. *Journal of Adhesion* **1999**, *69*, 307-359.
(32) Roos, A.; Université Paris VI, 2004.

Conclusion Générale

Dans le cadre de cette thèse nous avons étudié les propriétés d'adhésion de films adhésifs mous préparés à partir de particules de latex. L'objectif de ce travail était de mieux comprendre les mécanismes mis en jeu lors du décollement de ces films de manière à guider les chimistes en vue d'obtenir des PSA préparés par polymérisation en émulsion ayant des propriétés adhésives aussi bonnes que les PSA hot-melt ou en phase solvant notamment sur des surfaces de faible énergie comme le polyéthylène.

Nous avons dans un premier temps proposé une méthodologie pour l'optimisation des propriétés adhésives des PSA. Elle repose sur les relations qui existent entre les propriétés d'adhésion et les propriétés rhéologiques. Nous avons proposé deux critères pour prédire les performances adhésives. Le premier a été construit à partir de propriétés viscoélastiques linéaires facilement caractérisables. Nous avons montré que le mode de décollement peut être prédit grâce au rapport G''/G'^2. Un décollement de type interfacial caractérisé par une énergie d'adhésion faible est attendu sur PE pour des valeurs de ce rapport inférieures à 10^{-5} Pa^{-1}. Sur des surfaces d'énergie un peu plus élevée comme l'acier, cette limite semble pouvoir être diminuée à $0{,}5.10^{-5}$ Pa^{-1}.
L'ajustement de ce ratio permet la création d'une structure fibrillaire entre le film adhésif et le poinçon lors du processus de décollement. Ensuite, plus les fibrilles sont déformables plus l'énergie d'adhésion est élevée. Il existe néanmoins une limite : trop liquide le matériau se décolle de manière cohésive laissant des résidus sur le poinçon. Nous avons alors montré qu'il était possible de rendre compte du comportement observé au cours de la fibrillation en utilisant les résultats de tests de traction. Nous avons utilisé la représentation de Mooney-Rivlin et défini deux paramètres caractéristiques du matériau : C_{soft} et C_{hard}. C_{soft} permet de quantifier les processus dissipatifs à déformations intermédiaires alors que C_{hard} donne une idée de la cohésion apportée par les points de réticulations permanents. Nous avons alors montré que l'extension des fibrilles est d'autant plus favorisée que le ramollissement à déformation intermédiaires est prononcé, i.e que le rapport C_{soft}/C_{hard} est grand. De bonnes propriétés adhésives semblent obtenues pour des valeurs de ce rapport supérieures à 3 pour des applications sur PE et pour des valeurs supérieures à 2 pour des

applications sur acier. Ici, en utilisant la représentation de Mooney-Rivlin nous avons adopté une approche élastique pour décrire le ramollissement.
Les courbes représentant la contrainte réduite en fonction de 1/λ sont également utiles dans le sens où une simple observation de la forme de ces courbes dans le domaine des grandes déformations permet de prédire le mode de décollement final. Le décollement est cohésif lorsque le matériau ne rhéodurcit mais au contraire s'écoule à la fin des tests de traction, il est adhésif lorsqu'une remontée de la contrainte réduite est observée en fin de test.
Cette étude sur les relations entre les propriétés rhéologiques et adhésives a été menée dans le but particulier d'améliorer les performances adhésives de films préparés à partir de particules de latex ayant une morphologie cœur-écorce. La méthodologie utilisée peut être néanmoins reproduite pour n'importe quel type de PSA, aussi bien hot-melt qu'en solution ou que préparé par polymérisation en émulsion.

Nous avons ensuite étudié l'effet de l'activation d'une réaction de réticulation pendant la formation du film adhésif, i.e. lors de l'évaporation de l'eau de la dispersion colloïdale. Ce procédé de post réticulation présente l'avantage de ne pas affecter la structure moléculaire des polymères formés pendant l'étape de synthèse ce qui n'est évidemment pas le cas lorsque que la réticulation est ajustée par ajout d'agents réticulant ou d'agents de transfert au cours de la synthèse. Nous avons aussi tiré bénéfice du procédé de synthèse par polymérisation en émulsion et contrôlé à façon la localisation et la densité des points de réticulation.
Nous avons choisi de créer une réticulation hétérogène localisée uniquement dans l'écorce des particules. Nous avons montré qu'il était possible de modifier la cohésion du matériau en jouant avec la densité de réticulation sans que cela n'ait d'effets néfastes sur les propriétés adhésives qui sont elles principalement contrôlées par les propriétés viscoélastiques du cœur mou et dissipatif des particules. Ce résultat est d'autant plus intéressant qu'il est difficilement réalisable avec des méthodes plus traditionnelles qui consistent à réticuler l'ensemble de la particule de manière homogène.
Une large part de ce chapitre a été consacrée à l'étude des propriétés des matériaux en grandes déformations. Nous avons vu que les propriétés en grandes déformations jouaient un rôle important lors du décollement d'un film adhésif mou et nous avons montré l'effet remarquable de la réticulation interparticulaire sur ces propriétés. Les tests de probe tack ont confirmé qu'un ajustement de la densité de réticulation permettait l'obtention de films PSA très déformables ayant de bonnes propriétés d'adhésion et capables de se détacher du poinçon sans laisser de résidu à sa surface.
Nous sommes aussi allés au-delà des propriétés de viscoélasticité linéaires et d'élasticité non-linéaires utilisées dans le chapitre précédent. Nous avons montré que le comportement de nos matériaux caractérisé par des propriétés viscoélastiques non-linéaires, gouvernées principalement par le cœur mou et dissipatif, et par un rhéodurcissement, résultant de la réticulation de l'écorce, était assez bien décrit par un modèle construit à partir d'une combinaison du modèle de Maxwell sur-convecté et du modèle de Gent. Ce modèle a notamment rendu possible la quantification du ramollissement observé aux déformations intermédiaires d'un point de vue viscoélastique cette fois, et celle du rhéodurcissement intervenant à grandes déformations. De l'analyse des courbes de traction est ressorti le fait que les matériaux ayant les meilleures propriétés adhésives étaient caractérisés par un net ramollissement suivi d'un durcissement. Nous avons montré que les films adhésifs préparés

à partir de particules de latex hétérogènes, c'est à dire ayant une fine écorce assez réticulée et un cœur très mou, possédaient ces bonnes propriétés.
De nombreuses questions restent néanmoins encore ouvertes notamment au niveau de la structure moléculaire qui est beaucoup trop complexe pour pouvoir être caractérisée de manière fine. Des hypothèses ont été faites quant à la localisation des points de réticulation mais il est fort probable que la structure réelle ne soit pas exactement celle prédite par la théorie, on peut par exemple facilement envisager la migration d'une partie des groupements hydrophiles DAAM à la périphérie de particules.
Les propriétés de viscoélasticité non-linéaires des matériaux ont été observées grâce à des tests de tack réalisés à différentes vitesses. Il serait aussi intéressant de les étudier par des tests de traction à différentes vitesses où l'on s'affranchirait dans ce cas des processus complexes mis en jeu lors du processus de cavitation qui intervient au cours du décollement.
Nous avons proposé d'étudier le ramollissement en utilisant soit le point de vue viscoélastique et le modèle de Maxwell sur-convecté, soit un point de vue plus élastique avec la représentation de Mooney-Rivlin. Cependant, la question de l'origine exacte du ramollissement se pose encore. Il est fort probable que les deux types de processus (i.e. les processus de relaxation d'une part et l'orientation des chaînes à l'origine des désenchevêtrements d'autre part) interviennent en même temps. L'origine dominante de ce ramollissement pourrait être mise en évidence par des tests d'hystérèse en traction et cela nous permettrait de nous orienter plus facilement vers une approche plutôt que vers l'autre. Une description encore plus correcte serait aussi obtenue en combinant ces deux approches.

Nous avons enfin présenté des résultats obtenus sur des latex tackifiés. Le procédé de synthèse sélectionné pour permettre l'incorporation in situ de la résine tackifiante hydrophobe à l'intérieur des particules de latex est celui de la polymérisation en miniémulsion. L'étude des propriétés d'adhésion et de déformation a permis l'obtention d'échantillons de laboratoire aux propriétés adhésives optimisées. Ces matériaux ont ensuite été reproduits avec succès à l'échelle industrielle et nous avons montré que les prototypes industriels avaient les mêmes propriétés que les échantillons de laboratoire. Ces résultats sont d'autant plus intéressants que la polymérisation en miniémulsion n'est pas encore reconnue comme procédé couramment utilisé par les industriels. Ce procédé de synthèse a néanmoins été décrit dans la demande de brevet déposée par Cytec Surface Specialties en 2007 et il serait tout a fait envisageable que la prochaine génération de PSA commerciaux à base aqueuse soient préparés à partir de latex tackifiés in situ synthétisés par polymérisation en miniémulsion.
Là encore, tout n'est aujourd'hui pas compris. Nous avons montré que la résine sélectionnée pour cette étude avait bien les propriétés requises pour jouer le rôle de tackifiant. Néanmoins, son effet sur la structure des chaînes de polymères acryliques reste encore assez flou.
Ce travail sur les latex tackifiés a été repris par deux post doctorantes : Jeanne Marchal dans notre laboratoire à l'ESPCI et Elisabetta Canetta à l'université de Surrey. L'objectif est de comparer les propriétés d'adhésion de latex tackifiés in situ, comme cela a été réalisé dans le cadre de cette thèse, à celles de latex tackifiés préparés par mélange du latex avec une dispersion de résine tackifiante. Les propriétés adhésives sont caractérisées à l'échelle macroscopique à l'aide du test de probe tack et à l'échelle des particules à l'aide de la technique de l'AFM.

Extended Abstract in French

Dans le cadre de cette thèse nous avons étudié les propriétés d'adhésion de films adhésifs mous préparés à partir de particules de latex. L'objectif de ce travail est de mieux comprendre les mécanismes mis en jeu lors du décollement de ces films de manière à guider les chimistes en vue d'obtenir des adhésifs sensibles à la pression (pressure sensitive adhesive ou PSA en anglais) préparés par polymérisation en émulsion ayant des propriétés adhésives aussi bonnes que les PSA hot-melt ou en phase solvant notamment sur des surfaces de faible énergie comme le polyéthylène.

Ce résumé commence par une présentation des matériaux ainsi que du procédé utilisé pour leur synthèse. D'après une revue des travaux reportés dans la littérature sur l'adhésion des PSA en voie émulsion, nous montrons comment les paramètres de synthèse ont une influence sur l'architecture macromoléculaire et finalement sur les performances adhésives. Nous présentons ensuite les techniques expérimentales utilisées. La dernière partie est consacrée aux résultats expérimentaux et aux principales conclusions qui ressortent de notre étude.

Matériaux

Les matériaux étudiés sont synthétisés par *polymérisation radicalaire en chaîne*. La cinétique d'une polymérisation radicalaire comporte trois étapes : l'amorçage, la propagation et la terminaison. Outre ces réactions se produisent également des *réactions de transfert*. Selon la nature des monomères ajoutés au milieu réactif et des polymères synthétisés ces réactions se produisent naturellement plus ou moins facilement. Elles peuvent également être activées par ajout d'agents de transfert de chaîne (chain transfer agent ou CTA en anglais). Les réactions de transfert au polymère donnent lieu à la formation de branchements puis de gel lorsqu'une réaction de terminaison vient à se produire entre deux branches libres. Tout polymère synthétisé par polymérisation radicalaire comprend donc une partie non réticulée soluble aussi appelée *sol* et une partie réticulée insoluble communément connue sous le nom

de *gel* et se caractérise par son taux de gel et par la masse moléculaire moyenne (M_w) des chaînes du sol. Le taux de gel et la M_w du sol sont en général contrôlés par ajout de CTA au cours de la polymérisation. Il tend à limiter le taux de gel et à diminuer la M_w du sol.

Notre étude s'inscrit dans le courant actuel qui pousse les industriels à se tourner préférentiellement vers les technologies sans solvant et le procédé de polymérisation sélectionné est celui de la *polymérisation en émulsion*. Les films adhésifs sont obtenus par séchage de dispersions colloïdales de particules de latex dont le diamètre est de l'ordre de quelques centaines de nanomètres et dont la composition en monomères et les structures interne et de surface peuvent être contrôlées à l'échelle nanométrique pendant la synthèse. Dans ce procédé le milieu réactif comporte essentiellement de l'eau (milieu continu), un ou des monomères (en général insolubles dans l'eau) dispersés sous forme de gouttelettes maintenues en émulsion grâce à un tensioactif (émulsifiant) amphiphile, et un amorceur. Des agents de transfert peuvent également être ajoutés pour contrôler les masses molaires.
Un cas particulier de polymérisation en émulsion est celui du processus de polymérisation en *miniémulsion.* Dans ce type de procédé la taille des gouttelettes de monomères est largement réduite par forte agitation et/ou utilisation d'ultrasons. Les gouttelettes produites dont la surface est suffisamment grande pour participer à la capture des oligomères radicalaires servent de sites de polymérisation. Ce procédé est idéal pour des réactifs insolubles en phase aqueuse ou pour l'encapsulation de composés hydrophobes à l'intérieur des particules car il ne nécessite aucun transport de ces espèces dans la phase aqueuse. Nous l'avons utilisé comme procédé d'incorporation in situ de résine tackifiante hydrophobe.

Il existe différents types de procédés de polymérisation en émulsion. Pour la synthèse de nos matériaux nous avons choisi le procédé *semi-continu*. Dans ce cas, après introduction d'une charge initiale (ou seed en anglais) qui est destinée à maîtriser le processus de nucléation, l'essentiel des monomères est introduit de manière continue. Les synthèses ont également été conduites en régime *affamé* ce qui signifie que les particules ne sont pas gonflées en monomères à saturation. Dans de telles conditions, la composition des copolymères est pratiquement constante et égale à celle du mélange de monomères ajouté en continu.
Nous avons tiré bénéfice de la possibilité qu'offre le procédé semi-continu de produire des particules à structure hétérogène. Dans le cas particulier d'une morphologie cœur-écorce, il est possible de contrôler de manière relativement fine la composition en monomères de chaque phase ainsi que l'épaisseur de l'écorce. On utilise pour cela une polymérisation en deux étapes avec à chaque étape une composition différente du mélange en monomères.

Les polymères constituant les adhésifs étudiés sont des copolymères acryliques aléatoires composés en majeur partie de monomères mous i.e. de faible température de transition vitreuse (T_g) comme l'acrylate d'éthyle hexyle (T_g = -50°C), l'acrylate de butyle (T_g = -54°C) et l'acrylate d'éthyle (T_g = -24°C). La T_g des copolymères est ajustée par ajout de monomères plus durs i.e. de plus haute T_g comme le styrène (T_g = 100°C) ou le méthacrylate de méthyle (T_g = 106°C). De l'acide acrylique ou méthacrylique a systématiquement été ajouté comme monomère fonctionnel pour contrôler la nature de la surface des particules.

L'adhésion des PSA en voie émulsion

Selon Jovanovic et Dubé la polymérisation en émulsion est utilisée comme procédé de synthèse de PSA depuis les années 70.[1] Cependant c'est seulement depuis quelques années que l'on a commencé à étudier de manière assez systématique les propriétés obtenues et à essayer de mieux comprendre les origines des différences observées entre des PSA préparés par polymérisation en solution et ceux préparés en voie émulsion (sous entendu à même composition en monomères). De nombreuses difficultés inhérentes au procédé de l'émulsion sont à prendre en compte. Le contrôle fin de la structure moléculaire des polymères à l'intérieur de chaque particule est beaucoup plus difficile qu'en solution. Les tensioactifs nécessaires à la stabilisation des particules en milieux aqueux se retrouvent dans les films secs est leur effet sur les propriétés macroscopiques est encore assez mal compris. Une des difficultés réside aussi dans le fait que le film adhésif est obtenu après séchage et coalescence des particules de latex. Par conséquent, la fragilité des interfaces entre les particules fait qu'il est bien souvent nécessaire de sur-réticuler les particules pour obtenir une cohésion acceptable. Nous nous sommes proposés de surmonter ces limitations.

Nous avons commencé par faire un inventaire des principaux travaux reportés dans la littérature portant sur les propriétés adhésives des PSA en voie émulsion. Les effets d'un certain nombre de paramètres de synthèse sur les propriétés macromoléculaires ont été étudiés et il en ressort que :

- La T_g est fixée par la composition en monomères.
- Le principal facteur ayant une influence sur le taux de gel et la M_w du sol est la quantité de CTA ajoutée. La composition en monomères a également son importance du fait que la formation de gel est largement influencée par la fréquence des réactions de transfert au polymère.
- Les fréquences de branchements et d'enchevêtrements sont eux aussi fortement gouvernées par la composition en monomères.
- La présence d'acide acrylique favoriserait la formation de liaisons hydrogène et augmenterait la cohésion du matériau à faible vitesse de déformation.
- Des films réticulés de manière continue seraient obtenus par activation de réaction de réticulation interparticulaire.

L'architecture macromoléculaire des polymères ainsi que la morphologie des particules sont déterminantes dans le contrôle des performances adhésives. Optimiser les performances adhésives de PSA consiste en général à trouver le meilleur compromis entre les propriétés adhésives (i.e. le pouvoir collant) et cohésives (i.e. la capacité du matériau à ne pas fluer sous l'application d'une charge). Il a notamment été montré que :

- L'adhésion est favorisée lorsque le taux de gel est bas et par la présence de chaînes de faible masse dans le sol.
- La cohésion est quant à elle d'autant meilleure que la M_w des chaînes de polymère du sol est grande et que le taux de gel est élevé.
- La présence de microgels discrets à l'intérieur de chaque particule individuelle conduit à la formation de réseaux réticulés discontinus avec des interfaces entre les particules qui restent assez fragiles et par conséquent à une cohésion globale du film assez médiocre.

Il est donc possible d'améliorer l'adhésion et la cohésion par ajustement des propriétés moléculaires cependant, une amélioration de l'adhésion s'accompagne quasi systématiquement d'une diminution de la cohésion et inversement.

Nous avons essayé de faire face à ce problème en découplant les propriétés de cohésion et d'adhésion au sein même de la particule. Pour cela nous avons choisi d'adopter la morphologie cœur-écorce dans le but de contrôler les propriétés d'adhésion par le cœur mou et dissipatif et les propriétés de cohésion en jouant sur la composition et la structure de l'écorce. L'effet de la structure des particules sur les propriétés adhésives avait déjà été étudié par Aymonier et al.[2,3] et ils avaient conclu que l'introduction d'hétérogénéité ne permettait pas d'améliorer les performances adhésives. Ces résultats peuvent s'expliquer par le fait que la structure des particules a été modifiée sans ajuster en même temps de manière précise le taux de gel et de la distribution des masses molaires du sol.

Peu d'études ont finalement abouti à la production de PSA aux propriétés adhésives optimisées. Cela peut s'expliquer par les difficultés inhérentes au procédé de polymérisation en émulsion mais également sans doute par le manque d'études systématiques des effets des paramètres de synthèse sur les propriétés rhéologiques des matériaux, or propriétés adhésives et rhéologiques sont très fortement liées. Dans le cadre de cette thèse nous leur avons au contraire porté une attention toute particulière et nous les avons largement utilisées comme outils pour mieux comprendre les propriétés d'adhésion.

Techniques expérimentales

Nous avons essentiellement utilisé trois techniques de caractérisation :

- les propriétés d'adhésion ont été caractérisées par des tests de *probe tack*,
- les propriétés viscoélastiques dans le domaine linéaire ont été caractérisées à l'aide d'un *microrhéomètre*,
- les propriétés en grandes déformations ont été caractérisées par des *tests de traction*.

Propriétés d'adhésion

Le test du *probe tack* consiste à mesurer l'adhésion induite entre deux surfaces par leur contact. Il est réalisé grâce à une adaptation d'une machine hydraulique MTS.[4] Le vérin inférieur est mobile et porte le poinçon (en acier ou polyéthylène PE). Le vérin supérieur porte la lame de verre sur laquelle est déposé le film adhésif.

Lors du déroulement d'un test, la vitesse d'approche du poinçon vers le film adhésif est fixée à 30 $\mu m.s^{-1}$. Lorsque la force de compression atteint la valeur de consigne de -70 N, le poinçon est stoppé et maintenu immobile pendant 1 s. Les deux surfaces sont alors séparées à une vitesse de décollement variant de 10 à 1000 $\mu m.s^{-1}$.

Les mécanismes de déformation lors du décollement d'un film adhésif sont relativement complexes.[4]

La couche commence par se déformer de manière homogène jusqu'à ce que des cavités apparaissent à l'interface entre le poinçon et le film adhésif.
Ensuite, soit l'expansion des cavités se fait latéralement et dans ce cas il s'en suit le décollement rapide de l'adhésif du poinçon, soit les cavités préfèrent s'étirer verticalement donnant alors lieu à une structure fibrillaire. On parle de « *décollement adhésif* » lorsque les fibrilles se détachent du poinçon et de « *décollement cohésif* » dans le cas où, par manque de cohésion du matériau, la rupture intervient au milieu des fibrilles laissant des résidus de polymères à la surface du poinçon à la fin du test.

Les tests de tack ont tous été réalisés à température ambiante sur des films séchés pendant une douzaine d'heures à température ambiante puis à 110°C pendant 5 min. L'épaisseur des films secs est d'environ 100 µm.

Propriétés viscoélastiques linéaires

Les propriétés viscoélastiques linéaires ont été caractérisées à l'aide d'un *microrhéomètre* mis au point au laboratoire par Antoine Chateauminois et Philippe Sergot dans l'objectif de caractériser des films séchés dans les mêmes conditions que celles utilisées pour la préparation des échantillons testés par le test du probe tack. Cela sous entend que les films ont la même épaisseur que ceux utilisés pour le tack, i.e. environ 100 µm. Les propriétés rhéologiques de films aussi fins ne peuvent être caractérisées par des rhéomètres traditionnels.

Un test consiste à faire osciller une lentille de saphir sur le film adhésif. Cet hémisphère est activé par un activateur piézoélectrique et la force tangentielle est mesurée par une cellule de force piézoélectrique.
Les composantes en phase, K', et en opposition de phase, K'', de la raideur sont obtenues par transformée de Fourier de la force tangentielle. Les modules élastiques, G', et visqueux, G'', sont ensuite calculés selon:

$$G^* = \frac{K^* h}{\pi a^2}$$

avec h l'épaisseur du film et a le rayon du contact entre la lentille et le film adhésif.

Les tests sont réalisés à très faible amplitude d'oscillation (de l'ordre de quelques microns) de manière à se placer dans le domaine de réponse linéaire du matériau et à éviter tout micro-glissement qui pourrait se produire entre la lentille et le film adhésif. La gamme de fréquences balayée est comprise entre 0.1 et 10 Hz.

Tests de traction

Les propriétés en grandes déformations ont été caractérisées par des tests de traction réalisés à une vitesse de 50 $mm.min^{-1}$.
Les échantillons sont préparés par dépôt d'une certaine quantité de latex dans des moules en silicone. Ils sont séchés à l'air pendant une dizaine de jours puis à 110°C pendant 5 min. Les films sont ensuite décollés à l'aide de talc et déposés entre deux feuilles de papier siliconé.

Des éprouvettes de 4 mm de large sont découpées à l'emporte pièce. L'épaisseur est d'environ 800 µm et la distance initiale entre les mors de la machine de traction est fixée à 17 mm.

Résultats

De la structure des particules de latex aux propriétés adhésives

Nous avons dans un premier temps proposé une méthodologie pour l'optimisation des propriétés adhésives des PSA qui repose sur les relations entre propriétés d'adhésion et les propriétés rhéologiques. Le premier critère rhéologique est celui de Dahlquist et stipule que pour pouvoir être utilisé comme PSA un matériau doit nécessairement avoir un module élastique assez faible (< 0.1 MPa).[5,6] Nous avons proposé deux critères rhéologiques pour prédire les performances adhésives. Le premier part de la description du mécanisme de décollement d'une couche adhésive élastique d'un substrat solide.[7,8] Nous avons étendu cette analyse au régime viscoélastique et nous avons montré que le mode de décollement (i.e. propagation interfaciale des cavités ou fibrillation) peut être prédit grâce au rapport $G''(\omega)/G'^{2}(\omega)$ facilement mesurable par des tests de rhéologie. Un décollement de type interfacial caractérisé par une énergie d'adhésion faible est attendu sur PE pour des valeurs de ce rapport inférieures à 10^{-5} Pa^{-1}. Sur des surfaces d'énergie un peu plus élevée comme l'acier, cette limite semble pouvoir être diminuée à $0{,}5.10^{-5}$ Pa^{-1}.
L'ajustement de ce ratio permet la création d'une structure fibrillaire entre le film adhésif et le poinçon lors du processus de décollement. Ensuite, plus les fibrilles sont déformables plus l'énergie d'adhésion est élevée. Il existe néanmoins une limite : trop liquide le matériau se décolle de manière cohésive laissant des résidus sur le poinçon. Nous avons alors montré qu'il était possible de rendre compte du comportement observé au cours de la fibrillation en utilisant les résultats de tests de traction. Nous avons utilisé la représentation de Mooney-Rivlin et défini deux paramètres caractéristiques du matériau : C_{soft} et C_{hard}. C_{soft} permet de quantifier les processus dissipatifs à déformations intermédiaires alors que C_{hard} donne une idée de la cohésion apportée par les points de réticulations permanents. Nous avons alors montré que l'extension des fibrilles est d'autant plus favorisée que le ramollissement à déformation intermédiaires est prononcé, i.e que le rapport C_{soft}/C_{hard} est grand. De bonnes propriétés adhésives semblent obtenues pour des valeurs de ce rapport supérieures à 3 pour des applications sur PE et pour des valeurs supérieures à 2 pour des applications sur acier. Ici, en utilisant la représentation de Mooney-Rivlin nous avons adopté une approche élastique pour décrire le ramollissement.
Les courbes représentant la contrainte réduite en fonction de $1/\lambda$ sont également utiles dans le sens où une simple observation de la forme de ces courbes dans le domaine des grandes déformations permet de prédire le mode de décollement final. Le décollement est cohésif lorsque le matériau ne rhéodurcit mais au contraire s'écoule à la fin des tests de traction, il est adhésif lorsqu'une remontée de la contrainte réduite est observée en fin de test.
Cette étude sur les relations entre les propriétés rhéologiques et adhésives a été menée dans le but particulier d'améliorer les performances adhésives de films préparés à partir de particules de latex ayant une morphologie cœur-écorce. La méthodologie utilisée peut être

néanmoins reproduite pour n'importe quel type de PSA, aussi bien hot-melt qu'en solution ou que préparé par polymérisation en émulsion.

Rôle des interfaces sur le comportement en grandes déformations

Nous avons ensuite étudié l'effet de l'activation d'une réaction de réticulation pendant la formation du film adhésif, i.e. lors de l'évaporation de l'eau de la dispersion colloïdale. Ce procédé de post réticulation présente l'avantage de ne pas affecter la structure moléculaire des polymères formés pendant l'étape de synthèse ce qui n'est évidemment pas le cas lorsque que la réticulation est ajustée par ajout d'agents réticulant ou d'agents de transfert au cours de la synthèse. Nous avons aussi tiré bénéfice du procédé de synthèse par polymérisation en émulsion et contrôlé à façon la localisation et la densité des points de réticulation.
Nous avons choisi de créer une réticulation hétérogène localisée uniquement dans l'écorce des particules. Nous avons montré qu'il était possible de modifier la cohésion du matériau en jouant avec la densité de réticulation sans que cela n'ait d'effets néfastes sur les propriétés adhésives qui sont elles principalement contrôlées par les propriétés viscoélastiques du cœur mou et dissipatif des particules. Ce résultat est d'autant plus intéressant qu'il est difficilement réalisable avec des méthodes plus traditionnelles qui consistent à réticuler l'ensemble de la particule de manière homogène.
Une large part de ce chapitre a été consacrée à l'étude des propriétés des matériaux en grandes déformations. Nous avons vu que les propriétés en grandes déformations jouaient un rôle important lors du décollement d'un film adhésif mou et nous avons montré l'effet remarquable de la réticulation interparticulaire sur ces propriétés. Les tests de probe tack ont confirmé qu'un ajustement de la densité de réticulation permettait l'obtention de films PSA très déformables ayant de bonnes propriétés d'adhésion et capables de se détacher du poinçon sans laisser de résidu à sa surface.
Nous sommes aussi allés au-delà des propriétés de viscoélasticité linéaires et d'élasticité non-linéaires utilisées dans le chapitre précédent. Nous avons montré que le comportement de nos matériaux caractérisé par des propriétés viscoélastiques non-linéaires, gouvernées principalement par le cœur mou et dissipatif, et par un rhéodurcissement, résultant de la réticulation de l'écorce, était assez bien décrit par un modèle construit à partir d'une combinaison du modèle de Maxwell sur-convecté et du modèle de Gent. Ce modèle a notamment rendu possible la quantification du ramollissement observé aux déformations intermédiaires d'un point de vue viscoélastique cette fois, et celle du rhéodurcissement intervenant à grandes déformations. De l'analyse des courbes de traction est ressorti le fait que les matériaux ayant les meilleures propriétés adhésives étaient caractérisés par un net ramollissement suivi d'un durcissement. Nous avons montré que les films adhésifs préparés à partir de particules de latex hétérogènes, c'est à dire ayant une fine écorce assez réticulée et un cœur très mou, possédaient ces bonnes propriétés.
De nombreuses questions restent néanmoins encore ouvertes notamment au niveau de la structure moléculaire qui est beaucoup trop complexe pour pouvoir être caractérisée de manière fine. Des hypothèses ont été faites quant à la localisation des points de réticulation mais il est fort probable que la structure réelle ne soit pas exactement celle prédite par la théorie, on peut par exemple facilement envisager la migration d'une partie des groupements hydrophiles DAAM à la périphérie de particules.

Les propriétés de viscoélasticité non-linéaires des matériaux ont été observées grâce à des tests de tack réalisés à différentes vitesses. Il serait aussi intéressant de les étudier par des tests de traction à différentes vitesses où l'on s'affranchirait dans ce cas des processus complexes mis en jeu lors du processus de cavitation qui intervient au cours du décollement.
Nous avons proposé d'étudier le ramollissement en utilisant soit le point de vue viscoélastique et le modèle de Maxwell sur-convecté, soit un point de vue plus élastique avec la représentation de Mooney-Rivlin. Cependant, la question de l'origine exacte du ramollissement se pose encore. Il est fort probable que les deux types de processus (i.e. les processus de relaxation d'une part et l'orientation des chaînes à l'origine des désenchevêtrements d'autre part) interviennent en même temps. L'origine dominante de ce ramollissement pourrait être mise en évidence par des tests d'hystérèse en traction et cela nous permettrait de nous orienter plus facilement vers une approche plutôt que vers l'autre. Une description encore plus correcte serait aussi obtenue en combinant ces deux approches.

PSA tackifiés préparés par polymérisation en miniémulsion

Nous avons enfin présenté des résultats obtenus sur des latex tackifiés. Le procédé de synthèse sélectionné pour permettre l'incorporation in situ de la résine tackifiante hydrophobe à l'intérieur des particules de latex est celui de la polymérisation en miniémulsion. L'étude des propriétés d'adhésion et de déformation a permis l'obtention d'échantillons de laboratoire aux propriétés adhésives optimisées. Ces matériaux ont ensuite été reproduits avec succès à l'échelle industrielle et nous avons montré que les prototypes industriels (production de lots de 80 kg) avaient les mêmes propriétés que les échantillons de laboratoire. Ces résultats sont d'autant plus intéressants que la polymérisation en miniémulsion n'est pas encore reconnue comme procédé couramment utilisé par les industriels. Ce procédé de synthèse a néanmoins été décrit dans la demande de brevet déposée par Cytec Surface Specialties en 2007 et il serait tout a fait envisageable que la prochaine génération de PSA commerciaux à base aqueuse soient préparés à partir de latex tackifiés in situ synthétisés par polymérisation en miniémulsion.
Là encore, tout n'est aujourd'hui pas compris. Nous avons montré que la résine sélectionnée pour cette étude avait bien les propriétés requises pour jouer le rôle de tackifiant. Néanmoins, son effet sur la structure des chaînes de polymères acryliques reste encore assez flou.
Ce travail sur les latex tackifiés a été repris par deux post doctorantes : Jeanne Marchal dans notre laboratoire à l'ESPCI et Elisabetta Canetta à l'université de Surrey. L'objectif est de comparer les propriétés d'adhésion de latex tackifiés in situ, comme cela a été réalisé dans le cadre de cette thèse, à celles de latex tackifiés préparés par mélange du latex avec une dispersion de résine tackifiante. Les propriétés adhésives sont caractérisées à l'échelle macroscopique à l'aide du test de probe tack et à l'échelle des particules à l'aide de la technique de l'AFM.

Références

(1) Jovanovic, R.; Dube, M. A. *Journal of Macromolecular Science-Polymer Reviews* **2004**, *C44*, 1-51.
(2) Aymonier, A.; Ledercq, D.; Tordjeman, P.; Papon, E.; Villenave, J. J. *Journal of Applied Polymer Science* **2003**, *89*, 2749-2756.
(3) Aymonier, A.; Papon, E.; Castelein, G.; Brogly, A.; Tordjeman, P. *Journal of Colloid and Interface Science* **2003**, *268*, 341-347.
(4) Lakrout, H.; Sergot, P.; Creton, C. *Journal of Adhesion* **1999**, *69*, 307-359.
(5) Dahlquist, C. A. In *Treatise on Adhesion and Adhesives*; Patrick, R. L., Ed.; Dekker, 1969; pp 219-260.
(6) Creton, C.; Leibler, L. *Journal of Polymer Science Part B-Polymer Physics* **1996**, *34*, 545-554.
(7) Webber, R. E.; Shull, K. R.; Roos, A.; Creton, C. *Physical Review E* **2003**, *68*.
(8) Crosby, A. J.; Shull, K. R.; Lakrout, H.; Creton, C. *Journal of Applied Physics* **2000**, *88*, 2956-2966.

Bibliography

- Ahn, D.; Shull, K. R. *Langmuir* **1998**, 14, 3637-3645.
- Antonietti, M.; Landfester, K. *Progress in Polymer Science* **2002**, 27, 689-757.
- Arzamendi, G.; Asua, J. M. *Journal of Applied Polymer Science* **1989**, 38, 2019-2036.
- Arzamendi, G.; Asua, J. M. *Macromolecules* **1995**, 28, 7479-7490.
- Aubrey, D. W.; Ginosatis, S. *Journal of Adhesion* **1981**, 12, 189-198.
- Aubrey, D. W.; Sherriff, M. *Journal of Polymer Science Part a-Polymer Chemistry* **1980**, 18, 2597-2608.
- Aubrey, D. W.; Sherriff, M. *Journal of Polymer Science Part a-Polymer Chemistry* **1978**, 16, 2631-2643.
- Aymonier, A.; Ledercq, D.; Tordjeman, P.; Papon, E.; Villenave, J. *J. Journal of Applied Polymer Science* **2003**, 89, 2749-2756.
- Aymonier, A.; Papon, E.; Castelein, G.; Brogly, A.; Tordjeman, P. *Journal of Colloid and Interface Science* **2003**, 268, 341-347.
- Aymonier, A.; Papon, E.; Villenave, J. J.; Tordjeman, P.; Pirri, R.; Gerard, P. *Chemistry of Materials* **2001**, 13, 2562-2566.
- Benyahia, L.; Verdier, C.; Piau, J. M. *Journal of Adhesion* **1997**, 62, 45-73.
- Bird, R. B.; Armstrong, R. C.; Hassager, O. *Dynamics of Polymeric Liquids - Fluid Mechanics*; John Wiley & Sons second edition, **1987**; Vol. 1.
- Blackley, D. C. *Emulsion Polymerisation*; Applied Science Publishers LTD: London, **1975**.
- Brandrup, J.; Immergut, E., H.; A., G. E. *Polymer Handbook*, Fourth edition ed.; Wiley & Sons: New-York, **1999**.
- Brandrup, J.; Immergut, E., H. *Polymer Handbook.*, Third edition ed.; Wiley: New York, **1989**.
- Carelli, C.; Deplace, F.; Boissonnet, L.; Creton, C. *Journal of Adhesion* **2007**, 83, 491-505.
- Chan, H. K.; Howard, G. J. *Journal of Adhesion* **1978**, 9, 279-304.
- Charmeau, J. Y.; Berthet, R.; Gringreau, C.; Holl, Y.; Kientz, E. *International Journal of Adhesion and Adhesives* **1997**, 17, 169-176.
- Christensen, S. F.; McKinley, G. H. *International Journal of Adhesion and Adhesives* **1998**, 18, 333-343.

- Chu, F. X.; Graillat, C.; Guyot, A. *Journal of Applied Polymer Science* **1998**, 70, 2667-2677.
- Chu, S. G. In *Handbook of pressure sensitive adhesive technology*, 2nd ed.; Satas, D., Ed.; Van Nostrand Reinhold: New York, **1989**; Vol. 1, pp 158-203.
- Class, J. B.; Chu, S. G. *Journal of Applied Polymer Science* **1985**, 30, 805-814.
- Class, J. B.; Chu, S. G. *Journal of Applied Polymer Science* **1985**, 30, 815-824.
- Class, J. B.; Chu, S. G. *Journal of Applied Polymer Science* **1985**, 30, 825-842.
- Creton, C. *Mrs Bulletin* **2003**, 28, 434-439.
- Creton, C.; Roos, A.; Chiche, A. *In Adhesion: Current Research and Applications*; Possart, W. G., Ed.; Wiley-VCH: Weinheim, **2005**; pp 337-364.
- Creton, C.; Fabre, P. *In The mechanics of adhesion*; Dillard, D. A.; Pocius, A. V., Eds.; Elsevier: Amsterdam, **2002**; Vol. 1, pp 535-576.
- Creton, C.; Lakrout, H. *Journal of Polymer Science Part B-Polymer Physics* **2000**, 38, 965-979.
- Creton, C.; Leibler, L. *Journal of Polymer Science Part B-Polymer Physics* **1996**, 34, 545-554.
- Crosby, A. J.; Shull, K. R.; Lakrout, H.; Creton, C. *Journal of Applied Physics* **2000**, 88, 2956-2966.
- Crosby, A. J.; Shull, K. R. *Journal of Polymer Science Part B-Polymer Physics* **1999**, 37, 3455-3472.
- Dahlquist, C. A. *In Handbook of pressure sensitive adhesive technology*, 2nd ed.; Satas, D., Ed.; Van Nostrand Reinhold: New York, **1989**; Vol. 1, pp 97-114.
- Dahlquist, C. A. *In Treatise on Adhesion and Adhesives*; Patrick, R. L., Ed.; Dekker, **1969**; pp 219-260.
- Degennes, P. G. *Comptes Rendus De L Academie Des Sciences Serie Ii* **1988**, 307, 1949-1953.
- Dehnke, M. K. *Adhesives Age* **1994**, 37, 12-13.
- Derail, C.; Allal, A.; Marin, G.; Tordjeman, P. *Journal of Adhesion* **1997**, 61, 123-157.
- Derail, C.; Allal, A.; Marin, G.; Tordjeman, P. *Journal of Adhesion* **1999**, 68, 203-228.
- Dickie, R. A. *Journal of Applied Polymer Science* **1973**, 17, 45-63.
- Do Amaral, M.; Van Es, S.; Asua, J. M. *Journal of Polymer Science Part a-Polymer Chemistry* **2004**, 42, 3936-3946.
- Do Amaral, M.; Asua, J. M. *Journal of Polymer Science Part a-Polymer Chemistry* **2004**, 42, 4222-4227.
- Donkus, L. J. *Adhesives Age* **1997**, 40, 32-37.
- Dos Santos, F. D.; Leibler, L. *Journal of Polymer Science Part B-Polymer Physics* **2003**, 41, 224-234.
- Drzal, P. L.; Shull, K. R. *Journal of Adhesion* **2005**, 81, 397-415.
- FerrandizGomez, T. D.; FernandezGarcia, J. C.; OrgilesBarcelo, A. C.; MartinMartinez, J. M. *Journal of Adhesion Science and Technology* **1996**, 10, 833-845.
- FerrandizGomez, T. D.; FernandezGarcia, J. C.; OrgilesBarcelo, A. C.; MartinMartinez, J. M. *Journal of Adhesion Science and Technology* **1996**, 10, 1383-1399.
- Ferry, J. D. *Viscoelastic Properties of Polymers*, **1970**.
- FINAT Technical Handbook, 7th ed., 2005.
- Gacoin, E.; Chateauminois, A.; Fretigny, C. *Polymer* **2004**, 45, 3789-3796.
- Gacoin, E.; Fretigny, C.; Chateauminois, A.; Perriot, A.; Barthel, E. *Tribology Letters* **2006**, 21, 245-252.
- Garrett, J.; Lovell, P. A.; Shea, A. J.; Viney, R. D. *Macromolecular Symposia* **2000**, 151, 487-496.
- Gent, A. N. *Journal of Rheology* **2005**, 49, 271-275.
- Gent, A. N. *Rubber Chemistry and Technology* **1996**, 69, 59-61.

- Gibert, F. X.; Marin, G.; Derail, C.; Allal, A.; Lechat, J. *Journal of Adhesion* **2003**, 79, 825-852.
- Glassmaker, N. J.; Hui, C. Y.; Yamaguchi, T.; Creton, C, to be published
- Gooch, J. W.; Dong, H.; Schork, F. J. *Journal of Applied Polymer Science* **2000**, 76, 105-114.
- Good, R. J.; Gupta, R. K. *Journal of Adhesion* **1988**, 26, 13-36.
- Gorce, J. P.; Bovey, D.; McDonald, P. J.; Palasz, P.; Taylor, D.; Keddie, J. L. *European Physical Journal E* **2002**, 8, 421-429.
- Gower, M. D.; Shanks, R. A. *Journal of Applied Polymer Science* **2004**, 93, 2909-2917.
- Gower, M. D.; Shanks, R. A. *Journal of Polymer Science Part B-Polymer Physics* **2006**, 44, 1237-1252.
- Gower, M. D.; Shanks, R. A. *Macromolecular Chemistry and Physics* **2005**, 206, 1015-1027.
- Gower, M. D.; Shanks, R. A. *Macromolecular Chemistry and Physics* **2004**, 205, 2139-2150.
- Guyot, A.; Chu, F.; Schneider, M.; Graillat, C.; McKenna, T. F. *Progress in Polymer Science* **2002**, 27, 1573-1615.
- Hammond, F. H. *In Handbook of pressure sensitive adhesive technology*, 2nd ed.; Satas, D., Ed.; Van Nostrand Reinhold: New York, **1989**; Vol. 1, pp 38-60.
- Horgan, C. O.; Saccomandi, G. *Journal of Elasticity* **2002**, 68, 167-176.
- Horwat, D. W. *Adhesives Age* **1999**, 42, 20-+.
- Huang, N. J.; Sundberg, D. C. *Polymer* **1994**, 35, 5693-5698.
- Hui, C. Y.; Jagota, A.; Bennison, S. J.; Londono, J. D. *Proceedings of the Royal Society of London Series a-Mathematical Physical and Engineering Sciences* **2003**, 459, 1489-1516.
- James, H. M.; Guth, E. *Journal of Polymer Science* **1949**, 4, 153-182.
- Josse, G.; Sergot, P.; Creton, C.; Dorget, M. *Journal of Adhesion* **2004**, 80, 87-118.
- Josse, G.; Université Paris VI, 2001.
- Jovanovic, R.; McKenna, T. F.; Dube, M. A. *Macromolecular Materials and Engineering* **2004**, 289, 467-474.
- Jovanovic, R.; Ouzineb, K.; McKenna, T. F.; Dube, M. A. *Macromolecular Symposia* **2004**, 206, 43-56.
- Jovanovic, R.; Dube, M. A. *Industrial & Engineering Chemistry Research* **2005**, 44, 6668-6675.
- Jovanovic, R.; Dube, M. A. *Journal of Macromolecular Science-Polymer Reviews* **2004**, C44, 1-51.
- Juhue, D.; Lang, J. *Macromolecules* **1995**, 28, 1306-1308.
- Kaelble, D. H. *Transactions of the Society of Rheology* **1965**, 9, 135-163.
- Kamagata, K.; Saito, T.; Toyama, M. *Journal of Adhesion* **1970**, 2, 279-291.
- Keddie, J. L. *Materials Science & Engineering R-Reports* **1997**, 21, 101-170.
- Kerner, E. H. *Proceedings of the Physical Society of London Section B* **1956**, 69, 808-813.
- Kim, H. B.; Winnik, M. A. *Macromolecules* **1995**, 28, 2033-2041.
- Kim, H. J.; Hayashi, S.; Mizumachi, H. *Journal of Applied Polymer Science* **1998**, 69, 581-587.
- Kim, H. J.; Mizumachi, H. *Journal of Adhesion* **1995**, 49, 113-132.
- Kim, H. J.; Mizumachi, H. *Journal of Applied Polymer Science* **1995**, 57, 175-185.
- Kim, H. J.; Mizumachi, H. *Journal of Applied Polymer Science* **1995**, 56, 201-209.
- Lakrout, H.; Creton, C.; Ahn, D. C.; Shull, K. R. *Macromolecules* **2001**, 34, 7448-7458.
- Lakrout, H.; Sergot, P.; Creton, C. *Journal of Adhesion* **1999**, 69, 307-359.
- Landfester, K. *Advanced Materials* **2001**, 13, 765-768.
- Landfester, K. *Macromolecular Rapid Communications* **2001**, 22, 896-936.

- Laureau, C.; Vicente, M.; Barandiaran, M. J.; Leiza, J. R.; Asua, J. M. *Journal of Applied Polymer Science* **2001**, 81, 1258-1265.
- Leiza, J. R.; Sudoi, E. D.; ElAasser, M. S. *Journal of Applied Polymer Science* **1997**, 64, 1797-1809.
- Lindner, A.; Lestriez, B.; Mariot, S.; Creton, C.; Maevis, T.; Luhmann, B.; Brummer, R. *Journal of Adhesion* **2006**, 82, 267-310.
- Mallegol, J.; Bennett, G.; McDonald, P. J.; Keddie, J. L.; Dupont, O. *Journal of Adhesion* **2006**, 82, 217-238.
- Mallegol, J.; Dupont, O.; Keddie, J. L. *Langmuir* **2001**, 17, 7022-7031.
- Mallégol, J.; Gorce, J. P.; Dupont, O.; Jeynes, C.; McDonald, P. J.; Keddie, J. L. *Langmuir* **2002**, 18, 4478-4487.
- Marcais, A.; Papon, E.; Villenave, J. J.; Tordjeman, P.; Pirri, R.; Gerard, P. *Macromolecular Symposia* **2000**, 151, 497-502.
- Marin, G.; Derail, C. *Journal of Adhesion* **2006**, 82, 469-485.
- Maugis, D.; Barquins, M. *Journal of Physics D-Applied Physics* **1978**, 11, 1989-2023.
- Mindlin, R. D.; Deresiewicz, H. *Journal of Applied Mechanics-Transactions of the Asme* **1953**, 20, 327-344.
- Mooney, M. *Journal of Applied Physics* **1940**, 11, 582-592.
- Nakajima, N.; Babrowicz, R.; Harrell, E. R. *Journal of Applied Polymer Science* **1992**, 44, 1437-1456.
- Novikov, M. B.; Roos, A.; Creton, C.; Feldstein, M. M. *Polymer* **2003**, 44, 3561-3578.
- Ouzineb, K.; Graillat, C.; McKenna, T. F. *Journal of Applied Polymer Science* **2005**, 97, 745-752.
- Piau, J. M.; Ravilly, G.; Verdier, C. *Journal of Polymer Science Part B-Polymer Physics* **2005**, 43, 145-157.
- Plessis, C.; Arzamendi, G.; Leiza, J. R.; Alberdi, J. M.; Schoonbrood, H. A. S.; Charmot, D.; Asua, J. M. *Journal of Polymer Science Part a-Polymer Chemistry* **2001**, 39, 1106-1119.
- Plessis, C.; Arzamendi, G.; Leiza, J. R.; Schoonbrood, H. A. S.; Charmot, D.; Asua, J. M. *Macromolecules* **2000**, 33, 5041-5047.
- Plessis, C.; Arzamendi, G.; Leiza, J. R.; Schoonbrood, H. A. S.; Charmot, D.; Asua, J. M. *Macromolecules* **2001**, 34, 5147-5157.
- Plessis, C.; Arzamendi, G.; Leiza, J. R.; Schoonbrood, H. A. S.; Charmot, D.; Asua, J. M. *Macromolecules* **2000**, 33, 5041-5047.
- Poivet, S.; Nallet, F.; Gay, C.; Teisseire, J.; Fabre, P. *European Physical Journal E* **2004**, 15, 97-116.
- Poivet, S.; Nallet, F.; Gay, C.; Fabre, P. *Europhysics Letters* **2003**, 62, 244-250.
- Roos, A.; Creton, C. *Macromolecules* **2005**, 38, 7807-7818.
- Roos, A.; Université Paris VI, **2004**.
- Routh, A. F.; Russel, W. B. *Langmuir* **1999**, 15, 7762-7773.
- Rubinstein, M.; Panyukov, S. *Macromolecules* **1997**, 30, 8036-8044.
- Salamanca, J. M.; Ciampi, E.; Faux, D. A.; Glover, P. M.; McDonald, P. J.; Routh, A. F.; Peters, A.; Satguru, R.; Keddie, J. L. *Langmuir* **2001**, 17, 3202-3207.
- Satas, D. *Handbook of Pressure Sensitive Adhesive Technology*; Van Nostrand Reinhold Book: New York, **1989**.
- Satas, D. *In Handbook of pressure sensitive adhesive technology*, 2nd ed.; Satas, D., Ed.; Van Nostrand Reinhold: New York, **1989**; Vol. 1, pp 396-456.

- Saulnier, F.; Ondarcuhu, T.; Aradian, A.; Raphael, E. *Macromolecules* **2004**, 37, 1067-1075.
- Schellenberg, C.; Tauer, K.; Antonietti, M. *Macromolecular Symposia* **2000**, 151, 465-471.
- Schlademan, J. A. *In Handbook of pressure sensitive adhesive technology*, 2nd ed.; Satas, D., Ed.; Van Nostrand Reinhold: New York, **1989**; Vol. 1, pp 527-544.
- Sherriff, M.; Knibbs, R. W.; Langley, P. G. *Journal of Applied Polymer Science* **1973**, 17, 3423-3438.
- Shull, K. R.; Creton, C. *Journal of Polymer Science Part B-Polymer Physics* **2004**, 42, 4023-4043.
- Smith, W. V.; Ewart, R. H. *Journal of Chemical Physics* **1948**, 16, 592-599.
- Tamai, T.; Pinenq, P.; Winnik, M. A. *Macromolecules* **1999**, 32, 6102-6110.
- Tang, C. B.; Chu, F. X. *Journal of Applied Polymer Science* **2001**, 82, 2352-2356.
- Tobing, S. D.; Klein, A. *Journal of Applied Polymer Science* **2000**, 76, 1965-1976.
- Tobing, S. D.; Klein, A. *Journal of Applied Polymer Science* **2001**, 79, 2230-2244.
- Tobing, S. D.; Klein, A. *Journal of Applied Polymer Science* **2001**, 79, 2558-2564.
- Tobing, S.; Klein, A.; Sperling, L. H.; Petrasko, B. *Journal of Applied Polymer Science* **2001**, 81, 2109-2117.
- Tonck, A.; Sabot, J.; Georges, J. M. *Journal of Tribology-Transactions of the Asme* **1984**, 106, 35-42.
- Tordjeman, P.; Papon, E.; Villenave, J. J. *Journal of Polymer Science Part B-Polymer Physics* **2000**, 38, 1201-1208.
- Treloar, L. R. G. *Transactions of the Faraday Society* **1944**, 40, 0059-0069.
- Tsavalas, J. G.; Gooch, J. W.; Schork, F. J. *Journal of Applied Polymer Science* **2000**, 75, 916-927.
- Tse, M. F.; Jacob, L. *Journal of Adhesion* **1996**, 56, 79-95.
- Urahama, Y. *Journal of Adhesion* **1989**, 31, 47-58.
- Verdier, C.; Piau, J. M.; Benyahia, L. *Journal of Adhesion* **1998**, 68, 93-116.
- Verdier, C.; Piau, J. M. *Journal of Polymer Science Part B-Polymer Physics* **2003**, 41, 3139-3149.
- Verdier, C.; Ravilly, G. *Journal of Polymer Science Part B-Polymer Physics* **2007**, 45, 2113-2122.
- Wang, S. T.; Schork, F. J.; Poehlein, G. W.; Gooch, J. W. *Journal of Applied Polymer Science* **1996**, 60, 2069-2076.
- Wang, Y. C.; Winnik, M. A. *Macromolecules* **1990**, 23, 4731-4732.
- Webber, R. E.; Shull, K. R.; Roos, A.; Creton, C. *Physical Review E* **2003**, 68.
- Yang, H. W. H. *Journal of Applied Polymer Science* **1995**, 55, 645-652.
- Yarusso, D. J. *Journal of Adhesion* **1999**, 70, 299-320.
- Zawilinski, A. *Adhesives Age* **1984**, 27, 29-32.
- Zosel, A. *Adhesives Age* **1989**, 42-47.
- Zosel, A. *Advances in Pressure Sensitive Adhesive Technology* **1992**, 1, 92-127.
- Zosel, A. *Colloid and Polymer Science* **1985**, 263, 541-553.
- Zosel, A. *Journal of Adhesion* **1989**, 30, 135-149.
- Zosel, A. *Journal of Adhesion* **1994**, 44, 1-16.
- Zosel, A.; Ley, G. *Macromolecules* **1993**, 26, 2222-2227.
- Zosel, A.; Schuler, B. *Journal of Adhesion* **1999**, 70, 179-195.